

# **Hydrogen from Urea: A Novel Energy Source**

Andrew Neil Rollinson

Submitted in accordance with the requirements for the degree of  
Doctor of Philosophy

The University of Leeds  
Energy and Resources Research Institute  
School of Process, Environmental, and Materials Engineering

November, 2011

The candidate confirms that the work submitted is his own except where work which has formed part of jointly-authored publications has been included. The contribution of the candidate and the other authors to this work has been explicitly indicated below. The candidate confirms that appropriate credit has been given within the thesis where reference has been made to the work of others.

## Publications

**Rollinson, A.N., Dupont, V., Rickett, G.L., Twigg, M.V. *Hydrogen Production by Catalytic Steam Reforming of Urea*. 5<sup>th</sup> International Energy Symposium and Exhibition, Denizli (Turkey), 27<sup>th</sup> to 30<sup>th</sup> June 2010.**

This publication is based on the work contained in Chapters 2, 3 and 6. The Candidate was principal experimenter and author. Co-authors contributed with the publication's concept and structure. Additionally, Dr Dupont formulated the elemental mass balance, and Dr Rickett assisted with the experimental set up.

**Rollinson, A.N., Jones, J.M., Dupont, V., Twigg, M.V. *Urea as a hydrogen carrier: a perspective on its potential for safe, sustainable and long-term energy supply*. *Energy and Environmental Science*, 2011, 4, pp. 1216-1244.**

This publication is based on the work contained in Chapter 2. The Candidate was principal researcher and author. Co-authors contributed with the concept and structure.

**Rollinson, A.N., Rickett, G.L., Lea-Langton, A., Dupont, V., Twigg, M.V. *Hydrogen from urea-water and ammonia-water solutions*. *Applied Catalysis B: Environmental*, 2011, 106 (3-4), pp. 304-315.**

This publication is based on the work contained in Chapters 2, 3, 6 and 7. The candidate was the principal experimenter and researcher. The elemental mass balance was formulated in collaboration with Dr Dupont and Dr Rickett. In this paper, section 3.3, section 3.4, and the part of section 3.5.2 relating to crystallite sizes are not attributable to the candidate, and consequently they are not explained in this thesis. A footnote reference only is made to this additional work, with a citation to the publication.

**Rollinson, A.N., Jones, J.M., Dupont, V., Twigg, M.V. *Characterisation of Nickel Catalyst used in Urea Steam reforming*. *EuropacatX*, Glasgow (Scotland), 28<sup>th</sup> August to 2<sup>nd</sup> September 2011.**

This publication is based on the work contained in Chapter 7. The Candidate was principal researcher and author. Co-authors contributed with the concept and structure.

This copy has been supplied on the understanding that it is copyright material and that no quotation from the thesis may be published without proper acknowledgement.

The right of Andrew Neil Rollinson to be identified as Author of this work has been asserted by him in accordance with the Copyright, Designs and Patents Act 1988.

© 2011, The University of Leeds, Andrew Neil Rollinson.

## Acknowledgements

I am grateful to the Engineering and Physical Sciences Research Council and Johnson Matthey for this project's financial CASE award, and to The Energy Research Institute at The University of Leeds for hosting me.

I thank the following people for graciously offering their time to assist me: Professor Jenny Jones for my final year's supervision, Mrs Jane Hetherington (Microsoft Word) and Miss Anna Clough (OriginPro) for I.T. Training, staff at the Leeds Engineering Graduate Research Office, Dr Adrian Cunliffe and Stuart Micklethwaite for operation of the Ion Chromatograph, Dr Chunfei Wu for operation of the off-line GC analyser, Dr Leilani Darvell and Dr Xiaomin Baxter for training me to use the TA-MS analyser, Mr Steven Caddick for welded adjustments to the spray reactor, Mr Tarsem Hunjan for advice on purchase of the spray reactor power unit, and Dr Nicole Houndow for operation of the TEM analyser. These people, along with my colleagues Dr Antonia Borissova and Councillor Clive Hudson on the teaching of PEME1000 over the last three years, and all the students I have taught (in particular Miss Emma Young for her care and diligence in assisting me with ion-chromatography sample preparation), have helped to make my working environment an enjoyable one.

Finally, I acknowledge Dr Gavin Rickett for fabrication of spray reactor temperature control unit, and for his collaborative input with the downflow reactor material balance. I also acknowledge Dr Valerie Dupont and Dr Martyn Twigg for assistance with the initial planning of this project.

My love to Karen my wife; to Mary, Joy, and Emily; and to my mother Iris and late father Albert.

## Abstract

This research presents a viability assessment of using urea as an energy vector. Urea is attractive in comparison to the chemicals previously considered for supplying hydrogen since it is non-toxic, non-flammable and stable at room temperature and atmospheric pressure. Urea is cheap to produce and has an existing manufacturing infrastructure, but it also has a huge untapped natural resource, of which this study found that the knowledge to extract was technically attainable. Modelling predicted that when urea is heated with steam, a simple hydrogen-rich synthesis gas is formed, with product concentrations of ca. 60 % H<sub>2</sub>, 20 % CO<sub>2</sub> and 20 % N<sub>2</sub>. Relatively mild temperatures of  $500\text{ }^{\circ}\text{C} \leq T \leq 700\text{ }^{\circ}\text{C}$  were predicted for optimum steam conversion and H<sub>2</sub> yield. Experimental steam reforming in this temperature range using a fixed bed catalytic flow reactor was developed specifically for aqueous urea fuel using a novel drop-feed and passively cooled inlet system. Steady state operation created a hydrogen rich syngas with a composition closely matching that predicted at equilibrium. A nickel catalyst was found to be effective and robust for the process, permitting repeated cycling without observed degradation. Characterisation of the catalyst revealed urea steam reforming to be clean, with no evidence of carbon formation apparent. The experimental study used urea solutions in the steam to urea (S:C) range of 3:1 to 7:1. Preliminary analyses of these mixtures confirmed that the fuel would be unaffected by isomerisation and decomposition prior to reactor input. Further preliminary experimentation of kinetic mechanisms confirmed that thermal urea conversion alone would be at worst 99.9 % within 0.5 seconds at  $T \geq 500\text{ }^{\circ}\text{C}$ . Simultaneous thermal analyses explored a greater than previously reported range of evolved species produced by thermolysis of urea and urea solution in the presence of nickel catalyst.

## Contents

<b>Publications.....</b>	<b>iii</b>
<b>Acknowledgements.....</b>	<b>v</b>
<b>Abstract.....</b>	<b>vi</b>
<b>List of Figures.....</b>	<b>xii</b>
<b>List of Tables.....</b>	<b>xix</b>
<b>Nomenclature.....</b>	<b>xxii</b>
<b>1 Introduction.....</b>	<b>1</b>
1.1 Background.....	1
1.2 Project Aims and Objectives.....	3
1.3 Thesis Structure.....	3
<b>2 Literature Review.....</b>	<b>5</b>
2.1 Aims and Objectives.....	5
2.2 Hydrogen.....	5
2.3 Steam Reforming.....	6
2.3.1 Partial Oxidation.....	7
2.3.2 Autothermal Steam Reforming.....	7
2.3.3 Sorbtion Enhanced Steam Reforming.....	7
2.3.4 Unmixed Steam Reforming.....	8
2.4 Fuel Cells.....	8
2.5 Current Hydrogen Carriers.....	9
2.5.1 Simple Hydrogen-bearing Chemicals.....	10
2.5.1.1 Methanol (CH <sub>3</sub> OH).....	10
2.5.1.2 Ethanol (C <sub>2</sub> H <sub>5</sub> OH).....	11
2.5.1.3 Cycloalkanes.....	12
2.5.1.4 Hydrazine (N <sub>2</sub> H <sub>4</sub> ).....	12
2.5.1.5 Ammonia (NH <sub>3</sub> ).....	13
2.6 Urea ((NH <sub>2</sub> ) <sub>2</sub> CO).....	17
2.6.1 History and Properties.....	17
2.6.2 Occurrence.....	19
2.7 Urea Decomposition and Dehydrogenation.....	19

2.7.1	Enzymatic Decomposition .....	19
2.7.2	Thermal Decomposition.....	19
2.7.3	Spontaneous Decomposition.....	24
2.7.4	Previous Reports of Urea Steam Reforming.....	25
2.7.5	Previous Reports of using Urea for Hydrogen and Energy.....	25
2.8	Production of Urea .....	25
2.8.1	Present Industrial Synthesis .....	25
2.8.2	Production Status and Trends.....	27
2.8.3	Economics of Present Production .....	29
2.9	Environmental Impact of Urea.....	29
2.9.1	Environmental fate of Urea.....	29
2.9.2	Environmental Aspects of Present Production.....	30
2.10	Alternative/Sustainable Routes of Urea Production .....	31
2.10.1	Urea from Urine .....	32
2.10.2	Urea from Bacteria.....	36
2.11	Conclusions.....	37
<b>3</b>	<b>Thermochemical Equilibrium Modelling .....</b>	<b>39</b>
3.1	Objectives.....	39
3.2	Method .....	39
3.2.1	Conditions of Simulation .....	39
3.2.2	Products at Equilibrium .....	40
3.2.3	Thermochemistry .....	41
3.2.3.1	Stoichiometric Calculations .....	41
3.2.3.2	Equilibrium Mol Fraction Calculations.....	44
3.3	Results/Discussion .....	45
3.3.1	Products at Equilibrium .....	46
3.3.1.1	Syngas Composition.....	46
3.3.1.2	Reactant Conversions .....	47
3.3.1.3	Hydrogen Yield .....	48
3.3.1.4	Carbon Selectivity .....	48
3.3.1.5	Ammonia (NH <sub>3</sub> ) in Dry Corrected Syngas.....	51
3.3.1.6	Pressure.....	52



3.3.2	Thermochemistry .....	55
3.3.2.1	Stoichiometric Calculations .....	55
3.3.2.2	Equilibrium Mol Fraction Calculations.....	58
3.3.3	Model Limitations .....	61
3.4	Conclusions .....	62
<b>4</b>	<b>Fuel Characterisation .....</b>	<b>64</b>
4.1	Introduction .....	64
4.1.1	Solubility .....	64
4.1.2	Thermolysis .....	65
4.2	Method .....	66
4.2.1	Urea in Water Solubility .....	66
4.2.2	Ion Chromatography.....	67
4.2.3	Thermal Analysis .....	68
4.2.3.1	Thermogravimetric Analysis .....	69
4.2.3.2	Simultaneous Thermal Analysis.....	70
4.3	Results/Discussion .....	73
4.3.1	Solubility .....	73
4.3.2	Ion Chromatography.....	73
4.3.3	Thermal Analysis .....	75
4.3.3.1	Stanton Redcroft TGH100.....	75
4.3.3.2	Simultaneous Thermal Analysis.....	76
4.3.3.3	Reaction Kinetics.....	92
4.4	Conclusions .....	94
<b>5</b>	<b>Steam Reforming: Quartz Upflow Reactor .....</b>	<b>97</b>
5.1	Introduction .....	97
5.2	Method .....	97
5.3	Data Analysis .....	102
5.4	Results/Discussion .....	103
5.4.1	Residence Times .....	111
5.4.1.1	Rationale.....	111
5.4.1.2	Method.....	112
5.4.1.3	Results/Discussion.....	113

5.5	Conclusions .....	114
<b>6</b>	<b>Steam Reforming: Quartz Downflow Drop-feed Reactor .....</b>	<b>116</b>
6.1	Introduction .....	116
6.2	Method .....	116
6.3	Product Analysis .....	122
6.3.1	Dry Gases Online Analysis .....	122
6.3.2	Condensate Ion Chromatography .....	122
6.4	Data Analysis .....	123
6.4.1	Condensate .....	124
6.4.2	Nitrogen balance .....	124
6.4.3	Carbon balance .....	124
6.4.4	Hydrogen balance .....	125
6.4.5	Products, Conversions, Selectivities, and Hydrogen Yield .....	125
6.5	Results/Discussion .....	126
6.5.1	Steam Reforming .....	126
6.5.2	Condensate ion Chromatography .....	137
6.5.3	Coke Formation .....	140
6.6	Conclusions .....	142
<b>7</b>	<b>Catalyst Characterisation .....</b>	<b>144</b>
7.1	Introduction .....	144
7.2	Method .....	145
7.2.1	Digital microscopy .....	146
7.2.2	Scanning Electron Microscopy .....	146
7.2.3	BET Adsorption/Desorption .....	146
7.2.4	Transmission Electron Microscopy and Energy Dispersive X-ray .....	147
7.2.5	X-ray Diffraction .....	147
7.3	Results and Discussion .....	147
7.3.1	Digital Microscopy .....	147
7.3.2	Scanning Electron Microscopy .....	149
7.3.3	BET Adsorption/Desorption .....	152
7.3.4	Transmission Electron Microscopy and Energy Dispersive X-ray .....	153
7.3.4.1	Sample 1a. Post Steam Reforming Catalyst .....	154

7.3.4.2	Sample 2. Fresh Oxidised Catalyst.....	158
7.3.4.3	Sample 3. Reduced Catalyst.....	159
7.3.5	X-ray Diffraction.....	160
7.4	Conclusions.....	162
<b>8</b>	<b>Conclusions.....</b>	<b>164</b>
	<b>Appendix A: Downflow Reactor Maximum Fuel Feed Test.....</b>	<b>168</b>
	<b>Appendix B: Urea Wire Monolith Spray Reactor.....</b>	<b>169</b>
B.1	Introduction.....	169
B.2	Materials.....	170
B.3	Reactor Design.....	172
B.4	System Tests.....	175
B.5	Conclusions.....	183
	<b>References.....</b>	<b>185</b>

## List of Figures

<b>Figure 1-1.</b> Global CO <sub>2</sub> emissions by region [3].....	2
<b>Figure 2-1.</b> Molecular structure of some urea-derived compounds named in this document [60]. Note that isocyanic acid and cyanic acid are tautomers. Reference books sometimes refer erroneously to cyanic acid as a synonym for isocyanic acid.....	21
<b>Figure 2-2.</b> Potential global urea resource. Human urine resource estimated from average daily production of 35 g [113] multiplied by world population of 6.8 billion...	32
<b>Figure 2-3.</b> Status of technology and process stages necessary for utilising the urea produced by animals and plants in preparation for steam reforming. ....	35
<b>Figure 2-4.</b> Ornithine-urea cycle in ureotelic organisms showing possible in-vitro mechanism for urea production.....	36
<b>Figure 3-1.</b> Dry corrected syngas (excluding water and diluent) with argon diluent to show product nitrogen from reactant mixture of S:C = 7. All significant species are shown. ....	46
<b>Figure 3-2.</b> Steam conversion for urea steam reforming.....	47
<b>Figure 3-3.</b> H <sub>2</sub> Yield per mol of reactant urea with 63 % N <sub>2</sub> dilution.....	48
<b>Figure 3-4.</b> CO in the dry corrected syngas.....	49
<b>Figure 3-5.</b> CO <sub>2</sub> in the dry corrected syngas. ....	50
<b>Figure 3-6.</b> CH <sub>4</sub> in the dry corrected syngas. ....	50
<b>Figure 3-7.</b> NH <sub>3</sub> in dry corrected Syngas. ....	51
<b>Figure 3-8.</b> NH <sub>3</sub> in dry corrected syngas as a function of temperature, with varying pressure. ....	53
<b>Figure 3-9.</b> H <sub>2</sub> in dry corrected syngas as a function of temperature, with varying pressure. ....	54
<b>Figure 3-10.</b> Conversion of H <sub>2</sub> O as a function of temperature, with varying pressure. ....	54
<b>Figure 3-11.</b> CO <sub>2</sub> in dry corrected syngas as a function of temperature, with varying pressure. ....	55

<b>Figure 3-12.</b> Total kJ per mol of H <sub>2</sub> produced at equilibrium.....	56
<b>Figure 3-13.</b> Total kJ per mol of H <sub>2</sub> for 63% diluent urea steam reforming. ....	59
<b>Figure 3-14.</b> Hydrogen product mol fraction in the wet syngas for urea steam reforming with 63% carrier gas dilution. ....	60
<b>Figure 3-15.</b> Comparison between the energy needed to produce one mol of H <sub>2</sub> by steam reforming urea and methane. Both results shown are for reactant mixtures of S:C = 3, and with a 63% dilution of carrier gas. ....	61
<b>Figure 4-1.</b> Ion chromatogram for of 40 ppm cyanate stock dilution used in calibration.....	74
<b>Figure 4-2.</b> Ion chromatogram of S:C = 3 (18.5 M) urea in distilled water. ....	74
<b>Figure 4-3.</b> TGA curve of urea at a heating rate of 3 °C min <sup>-1</sup> . Weight percent mass loss shown as a function of temperature under N <sub>2</sub> flow of 80 cm <sup>3</sup> min <sup>-1</sup> .....	76
<b>Figure 4-4.</b> TGA, DTA, and DTG curves for urea as a function of temperature under a He flow of 80 cm <sup>3</sup> min <sup>-1</sup> . A heating rate of 5 °C min <sup>-1</sup> was applied. ....	77
<b>Figure 4-5.</b> Selected MS multiple ion detection curves for pure urea thermolysis EGA.....	80
<b>Figure 4-6.</b> Evolved gas profiles for HNCO, detected via FTIR absorbance at wavenumber 2271 – 2285 cm <sup>-1</sup> .....	81
<b>Figure 4-7.</b> FTIR transmittance spectrum from STA of pure (anhydrous) urea sample at T = 170 °C. Spectral peaks identified from [137] and [148]. ....	82
<b>Figure 4-8.</b> FTIR transmittance spectrum from STA of S:C = 7 aqueous urea sample at T = 105 °C. Spectral peaks identified from [137].....	82
<b>Figure 4-9.</b> TGA, DTA, and DTG curves for S:C = 7 urea solution as a function of temperature under a He flow of 80 cm <sup>3</sup> min <sup>-1</sup> . A heating rate of 5 °C min <sup>-1</sup> was applied. ....	84
<b>Figure 4-10.</b> Urea in de-ionised water at S:C = 7 MS full ion intensity range curves. ....	85
<b>Figure 4-11.</b> Urea in de-ionised water at S:C = 7 MS multiple ion detection curves (low and medium intensity detection). ....	86

- Figure 4-12.** TGA, DTA, and DTG curves for urea and nickel catalyst as a function of temperature under a He flow of  $80 \text{ cm}^3 \text{ min}^{-1}$ . A heating rate of  $5 \text{ }^\circ\text{C min}^{-1}$  was applied. Marked regions are referred to in text. ....88
- Figure 4-13.** TGA, DTA, and DTG curves for S:C = 7 urea solution and nickel catalyst as a function of temperature under a He flow of  $80 \text{ cm}^3 \text{ min}^{-1}$ . A heating rate of  $5 \text{ }^\circ\text{C min}^{-1}$  was applied. ....88
- Figure 4-14.** Urea and reduced nickel catalyst MS multiple ion detection curves. ....90
- Figure 4-15.** Urea in de-ionised water at S:C = 7 plus reduced nickel catalyst MS selected multiple ion detection curves. ....91
- Figure 5-1.** Schematic diagram of the atmospheric pressure quartz upflow urea steam reforming reactor system. ....99
- Figure 5-2.** Photograph of the quartz upflow urea steam reforming reactor. ....100
- Figure 5-3.** Dry product gas concentrations for S:C = 7 at  $600 \text{ }^\circ\text{C}$  with a  $4 \text{ ml hr}^{-1}$  fuel feed rate, and  $300 \text{ cm}^3 \text{ min}^{-1}$  carrier gas flow rate, shown as scatterpoints as a function of time using 20 % of datapoints for clarity. Also shown are calculated equilibrium values represented by dashed lines for  $\text{H}_2$  and  $\text{CO}_2$ . ....104
- Figure 5-4.** Dry product gas concentrations for S:C = 6, at  $600 \text{ }^\circ\text{C}$  with  $4 \text{ ml hr}^{-1}$  feed rate, and  $300 \text{ cm}^3 \text{ min}^{-1}$  carrier gas flow rate, shown as scatterpoints as a function of time, using 20 % of datapoints for clarity. Also shown are calculated equilibrium values represented by dashed lines. ....106
- Figure 5-5.** Schematic diagram of the fuel line, inlet and lower section of the upflow urea steam reforming reactor showing temperature gradient encountered by the urea solution. ....109
- Figure 5-6.** Dry product gas concentrations for S:C = 4, at  $600 \text{ }^\circ\text{C}$  with  $4 \text{ ml hr}^{-1}$  feed rate, and  $300 \text{ cm}^3 \text{ min}^{-1}$  carrier gas flow rate, shown as scatterpoints as a function of time, using 20 % of datapoints for clarity. Also shown are calculated equilibrium values represented by dashed lines. ....110
- Figure 5-7.** Dry product gas concentrations for S:C = 5, at  $600 \text{ }^\circ\text{C}$  with  $4 \text{ ml hr}^{-1}$  feed rate, and  $300 \text{ cm}^3 \text{ min}^{-1}$  carrier gas flow rate, shown as scatterpoints as a function

of time, using 20 % of datapoints for clarity. Also shown are calculated equilibrium values represented by dashed lines.....110

**Figure 6-1.** Schematic diagram of the experimental setup for atmospheric pressure quartz downflow drop-feed urea steam reforming reactor. ....118

**Figure 6-2.** Photograph of the atmospheric pressure quartz downflow drop-feed urea steam reforming reactor.....119

**Figure 6-3.** Inlet assembly of drop feed quartz urea steam reforming reactor during operation. ....120

**Figure 6-4.** Condensate collection during steam reforming operation. Experiment shown is at 600 °C reactor temperature with an S:C = 6 fuel feed. ....121

**Figure 6-5.** Dry product gas concentrations for S:C = 7, at 600 °C reactor temperature. 20 % datapoints are shown for clarity. Also shown is calculated equilibrium data displayed as dotted lines. Gaseous ammonia (< 0.00 %) at steady state omitted. ....127

**Figure 6-6.** Dry product gas concentrations for S:C = 6, at 600 °C reactor temperature. 20 % datapoints are shown for clarity. Also shown is calculated equilibrium data displayed as dotted lines. Gaseous ammonia (< 0.00 %) at steady state omitted. ....128

**Figure 6-7.** Dry product gas concentrations for S:C = 5, at 600 °C reactor temperature. 20 % datapoints are shown for clarity. Also shown is calculated equilibrium data displayed as dotted lines. Gaseous ammonia (< 0.00 %) at steady state omitted. ....128

**Figure 6-8.** Dry product gas concentrations for S:C = 4, at 600 °C reactor temperature. 20 % datapoints are shown for clarity. Also shown is calculated equilibrium data displayed as dotted lines. Gaseous ammonia (< 0.00 %) at steady state omitted. ....129

**Figure 6-9.** Dry product gas concentrations for S:C = 3, at 600 °C reactor temperature. 20 % datapoints are shown for clarity. Also shown is calculated equilibrium data displayed as dashed lines. Gaseous ammonia (< 0.00 %) at steady state omitted. ....129

<b>Figure 6-10.</b> Mean experimental and calculated equilibrium hydrogen yield (mol H <sub>2</sub> produced per mol of urea in the feed) for S:C = 6 and S:C = 7 at a range of temperatures. ....	134
<b>Figure 6-11.</b> Dry product gas concentrations for S:C = 7, at 700 °C reactor temperature. 20 % datapoints are shown for clarity. Also shown is calculated equilibrium data displayed as dashed lines. Gaseous ammonia (< 0.00 %) at steady state omitted. ....	135
<b>Figure 6-12.</b> Dry product gas concentrations for S:C = 7, at 500 °C reactor temperature. 20 % datapoints are shown for clarity. Also shown is calculated equilibrium data displayed as dashed lines. Gaseous ammonia (< 0.00 %) at steady state omitted. ....	136
<b>Figure 6-13.</b> Ion chromatogram of condensate obtained during downflow reactor urea steam reforming experiment with S:C = 6 fuel at 550 °C reactor temperature. ....	137
<b>Figure 6-14.</b> Mean experimental and calculated equilibrium hydrogen selectivity towards NH <sub>3</sub> for a range of experimental temperatures. Experimental values are steady-state averages from 20 minutes after start of the experiment up to cessation. ....	139
<b>Figure 6-15.</b> Mean experimental and calculated equilibrium hydrogen selectivity towards NH <sub>3</sub> for a range of S:C fuel mixtures at 600 °C reactor temperature. Experimental values are steady-state averages from 20 minutes after start of the experiment up to cessation. Exponential decay curve fit applied. ....	140
<b>Figure 7-1.</b> Digital microscopy image and topography of urea steam reforming catalyst crushed to size used in experiments (0.66 – 1.70 mm). Sample shown is post steam reforming catalyst 1a (see <b>Table 7-1</b> ). ....	148
<b>Figure 7-2.</b> Digital microscopy image of urea steam reforming catalyst. Sample shown is post steam reforming catalyst 1a (see <b>Table 7-1</b> ). ....	149
<b>Figure 7-3.</b> Low magnification SEM image of post steam reforming catalyst Sample 1a (see <b>Table 7-1</b> for sample provenance). ....	150
<b>Figure 7-4.</b> High magnification SEM image of the reduced catalyst Sample 3 (see <b>Table 7-1</b> for sample provenance). ....	151
<b>Figure 7-5.</b> High magnification SEM image of fresh as supplied catalyst Sample 2 (see <b>Table 7-1</b> for sample provenance). ....	151



<b>Figure 7-6.</b> High magnification SEM of catalyst sample 1a post steam reforming (see <b>Table 7-1</b> for sample provenance).....	152
<b>Figure 7-7.</b> TEM image of fresh oxidised catalyst (Sample 2) showing differences in morphology between alumina and nickel.....	154
<b>Figure 7-8.</b> TEM image of post-steam reforming catalyst (Sample 1a) with FFT analysis in boxed region showing structural distances.....	155
<b>Figure 7-9.</b> TEM image of post-steam reforming catalyst (Sample 1a) with FFT analysis in boxed region showing structural distances.....	156
<b>Figure 7-10.</b> TEM image of post-steam reforming catalyst (Sample 1a) with FFT analysis in boxed region showing structural distances.....	157
<b>Figure 7-11.</b> EDX of nickel in post steam reforming catalyst (Sample 1a) showing nickel is in its reduced state. Gold is from the support media, not the catalyst. ....	157
<b>Figure 7-12.</b> EDX of nickel in as supplied catalyst (Sample 2) showing the higher presence of oxygen indicative of nickel in its oxidised state. Copper is from the support media, not the catalyst.....	159
<b>Figure 7-13.</b> Reduced catalyst (Sample 3) EDX of nickel area. Copper comes from support grid.....	160
<b>Figure 7-14.</b> XRD spectrum of nickel in as supplied catalyst (Sample 2) revealing the presence of NiO and the absence of Ni peaks.....	161
<b>Figure 7-15.</b> XRD spectrum of reduced nickel catalyst (Sample 3) revealing the presence of Ni peaks. ....	161
<b>Figure 7-16.</b> XRD spectra of catalyst sample post five-stage steam reforming, showing nickel still in its reduced state (Ni).....	162
<b>Figure A.</b> Dry product gas concentrations for S:C = 7, at 600 °C with 350 cm <sup>3</sup> min <sup>-1</sup> carrier gas flow rate, shown as scatterpoints as a function of time, using 20 % of datapoints for clarity. Fuel feed rate varied, and increased to maximum during late stages of analysis time.....	169
<b>Figure B-1.</b> Ceramic monolith in stainless steel casing with nichrome wire. See text for dimensions.....	170

<b>Figure B-2.</b> Stainless steel casing supplied to house monolith as shown in <b>Figure B-1</b> . Annotated areas “b” to “d” show components that were removed or replaced (see section <b>B.3</b> ). Text refers to annotated areas “a”, “c”, “e”, and “f”.....	171
<b>Figure B-3.</b> Schematic of wire and monolith spray reactor.....	174
<b>Figure B-4.</b> Positions of pyrometer sampling on reactor outer metal casing .....	175
<b>Figure B-5.</b> AL04 (0.088 mm orifice) nozzle spray pattern with $5 \text{ dm}^3 \text{ min}^{-1}$ $\text{N}_2$ flow at 3 – 4 cm from nozzle aperture and fuel flow of $100 \text{ ml hr}^{-1}$ .....	180
<b>Figure B-6.</b> AL04 (0.088 mm orifice) nozzle spray pattern with $4.5 \text{ dm}^3 \text{ min}^{-1}$ , $\text{N}_2$ flow at 3 – 4 cm from nozzle aperture and fuel flow of $200 \text{ ml hr}^{-1}$ .....	180
<b>Figure B-7.</b> AL04 (0.088 mm orifice) nozzle spray pattern with $4 \text{ dm}^3 \text{ min}^{-1}$ , $\text{N}_2$ flow at 3 – 4 cm from nozzle aperture and fuel flow of $200 \text{ ml hr}^{-1}$ .....	181
<b>Figure B-8.</b> AL01 (0.040 mm orifice) nozzle spray pattern with $1.5 \text{ dm}^3 \text{ min}^{-1}$ , $\text{N}_2$ flow at 3 – 4 cm from nozzle aperture and fuel flow of $200 \text{ ml hr}^{-1}$ .....	181
<b>Figure B-9.</b> AL01 (0.040 mm orifice) nozzle spray pattern with $1.8 \text{ dm}^3 \text{ min}^{-1}$ , $\text{N}_2$ flow at 3 – 4 cm from nozzle aperture and fuel flow of $100 \text{ ml hr}^{-1}$ .....	182
<b>Figure B-10.</b> AL01 (0.040 mm orifice) nozzle spray pattern with $2.0 \text{ dm}^3 \text{ min}^{-1}$ , $\text{N}_2$ flow at 3 – 4 cm from nozzle aperture and fuel flow of $500 \text{ ml hr}^{-1}$ .....	182
<b>Figure B-11.</b> AL01 (0.040 mm orifice) nozzle spray pattern with $2.5 \text{ dm}^3 \text{ min}^{-1}$ , $\text{N}_2$ flow at 3 – 4 cm from nozzle aperture and fuel flow of $500 \text{ ml hr}^{-1}$ .....	182

## List of Tables

<b>Table 2-1.</b> Equilibrium ammonia cracking as a function of temperature and pressures of 1 and 10 bar [30].	14
<b>Table 2-2.</b> Comparison of physical properties, hydrogen content, toxicity and safety aspects of hydrogen carriers [40].	16
<b>Table 2-3.</b> Physical Data of Urea [47] <sup>except where stated</sup> .	18
<b>Table 2-4.</b> Properties of Saturated Aqueous Urea Solutions. Columns 1-5 from reference [47] Column 6 calculated from column 2 by division through relative molecular masses of urea (60.06) and water (18).	18
<b>Table 2-5.</b> Solubility of Urea in Alcohol Solvents (wt% of urea) [49].	19
<b>Table 2-6.</b> Urea reagent composition using in experimentation. Purchased from Fisher Scientific (U/P610/50).	27
<b>Table 2-7.</b> Present applications of urea.	28
<b>Table 2-8.</b> Life Cycle Greenhouse Gas Emissions from Urea Production Plant [84].	31
<b>Table 3-1.</b> Values for molecular enthalpy of formation [137].	41
<b>Table 3-2.</b> Values used to calculate urea sensible enthalpy [139].	42
<b>Table 3-3.</b> Values used to calculate reactant and product species $\Delta H_{\text{sens}}$ and $C_p$ [137].	43
<b>Table 3-4.</b> EQUIL modelled reactant mole fraction values for 63% dilution. Diluent = Ar or N <sub>2</sub> .	45
<b>Table 3-5.</b> Values of minimum energy needed to produce 1 mol of H <sub>2</sub> from urea and steam. kJ surplus and power available has been calculated by deducting from the energy content of H <sub>2</sub> (285.83 kJ mol <sup>-1</sup> ).	57
<b>Table 3-6.</b> Calculated enthalpy of different carrier gases at the range of optimum urea steam reforming temperatures.	58
<b>Table 4-1.</b> Concentrations of urea in de-ionised water solution in Molar and S:C terms. * represents the concentration of urea in human urine.	64

<b>Table 4-2.</b> Mass/charge values programmed for detection in QMS. Values obtained from [137] unless otherwise stated.....	72
<b>Table 4-3.</b> Kinetic parameters, and statistical co-efficient of determination calculated from results of urea thermolysis over temperature range $140\text{ }^{\circ}\text{C} \leq T \leq 185\text{ }^{\circ}\text{C}$ . Name of analyser used given in brackets. ....	92
<b>Table 4-4.</b> Residence time (in seconds) for values of urea conversion as a function of temperature based on derived thermal decomposition parameters in the range $140\text{ }^{\circ}\text{C} \leq T \leq 185\text{ }^{\circ}\text{C}$ .....	93
<b>Table 5-1.</b> Urea steam reforming catalyst composition as supplied.....	97
<b>Table 5-2.</b> GC analysis of dry reformat sample obtained immediately following on-line analysis of urea steam reforming with S:C = 6 fuel mixture fed at $4\text{ ml hr}^{-1}$ , $600\text{ }^{\circ}\text{C}$ reactor temperature, and $150\text{ cm}^3\text{ min}^{-1}\text{ N}_2$ carrier gas flow.....	105
<b>Table 5-3.</b> Mean experimental steady state (Exp), and calculated equilibrium (Eq.Calc) reactant conversions and product distribution at $600\text{ }^{\circ}\text{C}$ with $4\text{ ml hr}^{-1}$ fuel feed, and $300\text{ cm}^3\text{ min}^{-1}$ carrier gas flow rate. ....	107
<b>Table 5-4.</b> Calibration gases and experimental residence times through the upflow reactor system at a flow rate of $300\text{ cm}^3\text{ min}^{-1}$ . Time (t) values are in seconds. See text for definition of $t_0$ , $t_{50}$ , and $t_{90}$ . ....	113
<b>Table 6-1.</b> Mean experimental (Exp) and calculated equilibrium (Eq.Calc) reactant conversions and product species distribution at $600\text{ }^{\circ}\text{C}$ for a range of S:C fuel mixtures at steady state operation. ....	132
<b>Table 6-2.</b> Mean experimental (Exp) and calculated equilibrium (Eq.Calc) reactant conversions and product species distribution for S:C = 7 for a range of reactor bed temperatures at steady state operation. ....	132
<b>Table 6-3.</b> Mean experimental (Exp) and calculated equilibrium (Eq.Calc) reactant conversions and product species distribution for S:C = 6 for a range of reactor bed temperatures at steady state operation. ....	133
<b>Table 6-4.</b> $\text{NH}_3$ concentration in the urea steam reforming condensate in gravimetric parts per million (ppm). ....	138
<b>Table 7-1.</b> Provenance of catalyst samples prior to characterisation analyses ....	145

**Table 7-2.** Results of catalyst surface area at different stages of the steam reforming process, obtained by BET adsorption/desorption method.....153

**Table B-1.** Insulating mat composition, used as packing in spray reactor. Purchased from 3M (100 EPP) .....171

**Table B-2.** Results of pyrometry test on reactor and power unit. T/C = thermocouple.....176

## Nomenclature

A = frequency factor, in units of collisions  $\text{sec}^{-1}$  (assuming first order reaction)

A = ampere

atm = atmospheric pressure = 101,325 Pascals

Å = Ångström =  $1 \times 10^{-10}$  metres

BET = Brunauer, Emmett and Teller method

$C_p$  = molar heat capacity at constant pressure

C = Celcius

D = diameter

DMFC = direct methanol fuel cell

DSC = differential scanning calorimetry

DTA = Differential thermal analysis

DTG = Derivative thermogravimetry

$dt$  = small change in time

$dw$  = small change in weight

$\Delta H_{298}^{\circ}$  = standard state enthalpy change

$\Delta H_{\text{sens}}$  = sensible enthalpy

$\Delta H_{\text{total}}$  = total enthalpy

$\Delta H_{\text{sub}}$  = sublimation enthalpy

$\Delta H_r$  = reaction enthalpy

$\Delta H_{\text{vap}}$  = vaporisation enthalpy

$\Delta H_{\text{solv}}$  = solvation enthalpy

$i$  = species

E/D = external diameter

EDX = Energy-dispersive X-ray Spectroscopy

EGA = Evolved Gas Analysis

$E_a$  = activation energy, in  $\text{J mol}^{-1}$

FTIR = Fourier transform infra-red

FID = Flame Ionisation Detector

FEG = Field Emission Gun

GC = Gas Chromatograph

g = gram

g = gaseous state

HTS = High temperature shift

HPLC = high performance liquid chromatography

hr = hour

I/D = internal diameter

J = Joule =  $\text{kg}\cdot\text{m}^2 \text{sec}^{-2}$

K = Kelvin

$k$  = experimental reaction rate constant

LTS = low temperature shift

l = litre

l = liquid state

$M_r$  = relative molecular mass

( $m/z$ ) = mass/charge ratio

min = minimum

max = maximum

m = metre

MID = multiple ion detection

MS = Mass spectrometry

M = molar concentration = mol/litre =  $\text{mol}/\text{dm}^3$

$n$  = number of mols

$N_{\text{out}}$  = total number of moles out

N/K and  $n/k$  = not known

N/A and  $n/a$  = not applicable

0 = initial

OTM = oxygen transfer material

$\Omega$  = Ohm = electrical resistance

P = pressure

PEMFC = poly-electrolyte membrane fuel cell

PSA = pressure swing absorption

ppm = parts per million

QMS = quadruple mass spectrometer

R = universal gas constant =  $8.314472 \text{ J K}^{-1} \text{ mol}^{-1}$

SCR = selective catalytic reduction

S:C = steam to carbon ratio

STA = simultaneous thermal analysis

STP = standard temperature and pressure

$\Sigma$  = summation

SOFC = solid oxide fuel cell

SEL = selectivity

SEM = scanning electron microscopy

s = second

s = solid state

° = standard state

TGA = thermogravimetric analysis

Total<sub>C</sub> = total carbon species

TCD = thermal conductivity detector

TEM = Transmission electron microscopy

TA = Thermal analysis

T = temperature

T/C = thermocouple

t = terminal

[urea] = concentration of fuel

u/k = unknown

V = volt

v = stoichiometric co-efficient

WGSR = water gas shift reaction

wt % = weight percentage



W = Watt = Joule sec<sup>-1</sup>

$w_{\infty}$  = terminal mass

$w_i$  = initial mass

$X_{H_2O}$  = steam conversion

$X_{urea}$  = urea conversion

$x$  = mole fraction

XRD = X-ray Diffraction

$y$  = mole fraction in the vapour phase for a two phase system

### S.I Numeric Prefixes

T = tera =  $10^{12}$

G = giga =  $10^9$

M = mega =  $10^6$

k = kilo =  $10^3$

m = milli =  $10^{-3}$

$\mu$  = micro =  $10^{-6}$

n = nano =  $10^{-9}$

### Overlays

· = rate (per unit time)

— = mean

### Chemical Species

Ar = argon

Au = gold

C = carbon

$C_2H_5N_3O_2$  = biuret

$C_3H_6N_4O_3$  = triuret

$C_3H_3N_3O_3$  = cyanuric acid

$C_3H_4N_2O_2$  = ammelide

$C_3H_5N_5O$  = ammeline

$C_3H_6N_6$  = melamine

$CO_2$  = carbon dioxide

$CO$  = carbon monoxide

$CH_4$  = methane

$Cu$  = copper

$H_2$  = hydrogen

$HCN$  = hydrogen cyanide

$H_2O$  = water or steam

$He$  = helium

$HNCO$  = isocyanic acid

$N_2$  = nitrogen

$NH_3$  = ammonia

$(NH_2)_2CO$  = urea

$NH_4^+$  = ammonium ion

$NH_2COONH_4$  = ammonium carbamate

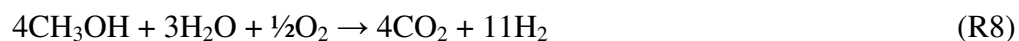
$NH_4^+NCO^-$  = ammonium cyanate

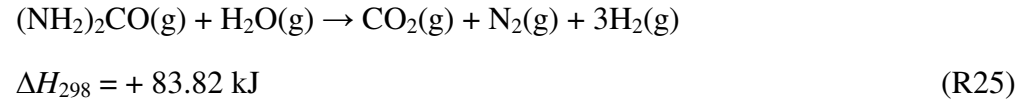
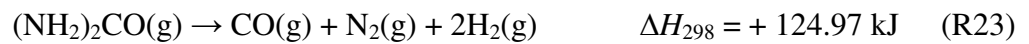
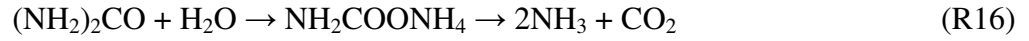
$Ni$  = nickel

$NiO$  = nickel oxide

$NO_x$  = nitrogen oxides

### Chemical Reactions





### Equilibrium Modelling Equations

$$\text{Steam conversion} = \frac{(x_{\text{H}_2\text{O},in})(N_{in}) - (x_{\text{H}_2\text{O},out})(N_{out})}{(x_{\text{H}_2\text{O},in})(N_{in})} \quad (\text{Eq. 1})$$

$$\text{Urea conversion} = \frac{(x_{\text{urea},in})(N_{in}) - (x_{\text{urea},out})(N_{out})}{x_{\text{urea},in}} \quad (\text{Eq. 2})$$

$$\text{Hydrogen yield} = \frac{(x_{\text{H}_2,out})(N_{out})}{(x_{\text{H}_2\text{O},in})(N_{in}) + 2(x_{\text{urea},in})(N_{in})} \quad (\text{Eq. 3})$$

$$\text{Hydrogen yield per reactant urea} = \frac{(x_{H_2,out})(N_{out})}{(x_{urea,in})(N_{in})} \quad (\text{Eq. 4})$$

$$\text{Sel}_{\text{Ceq}} = \frac{x_{i,out}}{x_{CO,out} + x_{CO_2,out} + x_{CH_4,out}} \quad (\text{Eq. 5})$$

$$\text{Sel}_{\text{Heq}} = \frac{x_{i,out}}{x_{H_2,out} + x_{CH_4,out} + x_{NH_3,out} + x_{NH_2,out} + x_{H_2O,out}} \quad (\text{Eq. 6})$$

$$\text{Dry corrected syngas} = \frac{(x_{i,out})(N_{out})}{(N_{out})(1 - x_{H_2O,out}) - (x_{diluent,out})(N_{out})} \quad (\text{Eq. 7})$$

## Formulae

$$\Delta H_{T_2} = \Delta H_{T_1} + \sum_{\text{PRODUCTS}} \nu(\Delta H_{\text{sens}})_{T_2} - \sum_{\text{REACTANTS}} \nu(\Delta H_{\text{sens}})_{T_2} \quad (\text{F1})$$

$$\Delta H_{T_2} = \Delta H_{T_1} + \left( \sum_{\text{PRODUCTS}} \nu(Cp)_{T_2} - \sum_{\text{REACTANTS}} \nu(Cp)_{T_2} \right) (T_2 - T_1) \quad (\text{F2})$$

$$Cp = A + Bt + Ct^2 + Dt^3 + E/t^2, \text{ where } t = T/1000 \quad (\text{F3})$$

$$\Delta H_{\text{sens}} \text{ for urea} = \int_{H_{T_1}}^{H_{T_2}} Cp.dT \quad (\text{F4})$$

$$\Delta H_{\text{sens}} = At + Bt^2/2 + Ct^3/3 + Dt^4/4 - E/t + F - H, \text{ where } t = T/1000 \quad (\text{F5})$$

$$(\Delta H_{\text{total, H}_2\text{O}} = (\Delta H_{\text{lat, H}_2\text{O}} + \Delta H_{\text{sens, H}_2\text{O}})(S:C) \quad (\text{F6})$$

$$\Delta H_{\text{total}} = \Delta H_r + ((\Delta H_{\text{sens, H}_2\text{O}} + (\Delta H_{\text{lat, H}_2\text{O}})(S:C) + \Delta H_{\text{sub, UREA}} \quad (\text{F7})$$

$$\bar{H} = \sum_i^{i_{\text{TOTAL}}} H_i x_i \quad (\text{F8})$$

$$\Delta H_{\text{solv}} = [(3656.308 - 89.9082(M) + 5.54228(M^2) - 0.24071(M^3) + 0.00449022(M^4)] \times 4.186 \text{ J mol}^{-1} \quad (\text{F9})$$

$$S:C = \left( \frac{M_{r(\text{urea})}}{M_{r(\text{water})}} \right) \times \left( \frac{\text{measured\_mass}_{(\text{water})}}{\text{measured\_mass}_{(\text{urea})}} \right) \quad (\text{F10})$$

$$\text{measured mass}_{(\text{urea})} = \left( \frac{\text{measured\_mass}_{(\text{water})}}{S:C} \right) \times \left( \frac{M_{r(\text{urea})}}{M_{r(\text{water})}} \right) \quad (\text{F11})$$

$$k = A \exp\left(-\frac{E_a}{RT}\right) \quad (\text{F12})$$

$$k = -\frac{1}{(w_i - w_\infty)} \times \frac{dw}{dt} \quad (\text{F13})$$

$$\frac{d[\text{urea}]}{dt} = -k[\text{urea}] \quad (\text{F14})$$

$$\text{Residence time (t)} = \frac{-\ln \left[ \frac{[urea_t]}{[urea_0]} \right]}{k} \quad (\text{F15})$$

$$\dot{V}_{STP} = \left( \frac{P_{measured}}{T_{measured}} \right) (\dot{V}_{measured}) \left( \frac{293.15K}{101.328kPa} \right) \quad (\text{F16})$$

$$\text{mean residence time} = \text{Volume of catalyst/Fluid flow rate} \quad (\text{F17})$$

## Experimental Mass Balance Nomenclature

$M_{urea}$  measured mass of fuel loaded into the syringe mix (syringe pump feed) (kg)

$\bar{W}_{urea}$  molar mass of fuel (kg mol<sup>-1</sup>)

$M_{H_2O}$  measured mass of water loaded the syringe mix (syringe pump feed) (kg)

$\bar{W}_{H_2O}$  molar mass of water= 18 ×10<sup>-3</sup> kg mol<sup>-1</sup>

$V_{tot,in}$  volume of mixture in the syringe mix at loading (m<sup>3</sup>)

$\dot{V}_{mix}$  volume flow rate of feed at programmable syringe pump (m<sup>3</sup> s<sup>-1</sup>)

$\dot{V}_{N_2}$  volume flow rate (STP) of nitrogen entering the reactor (m<sup>3</sup> s<sup>-1</sup>)

$t$  duration of experiment (s)

$dt$  sampling interval(s).

$\dot{n}, \dot{n}_i$  total molar flow rate and molar flow rate of species  $i$  at time  $t$ , (mol s<sup>-1</sup>)

$\dot{m}, \dot{m}_i$  Mass flow rates. (kg s<sup>-1</sup>)

$\dot{V}, \dot{V}_i$  Volume flow rates (m<sup>3</sup> s<sup>-1</sup>)

$m_i$  mass of species  $i$  present in reactor at time  $t$ , (kg)

$n_i$  moles of species  $i$  present in reactor at time  $t$ , (mol)

$dn_i$  change in moles of species  $i$  present in reactor during interval of time  $dt$

$W_i$  molar mass of species  $i$ , (kg mol<sup>-1</sup>)

$\rho_t$  liquid density of species  $i$  (kg m<sup>-3</sup>) at lab temperature

$y_i$  mass fraction

## Experimental Mass Balance equations

$$x_{urea} = \frac{\dot{n}_{urea,in} - \dot{n}_{urea,out}}{\dot{n}_{urea,in}} = \frac{(\dot{n}_{dry,out}) (\sum y_{c,out})}{\dot{n}_{urea,in}} \quad (\text{E1})$$

$$\dot{n}_{dry,out} = \frac{\dot{n}_{N_2,in} + \dot{n}_{urea,in}}{y_{N_2,out}} = \frac{\dot{n}_{N_2,in} + \dot{n}_{urea,in}}{\left(1 - \sum_{\text{all dry gas products}} y_i\right)} = \frac{\dot{n}_{N_2,in} + \dot{n}_{urea,in}}{\left(1 - (y_{H_2} + y_{CO_2} + y_{CO} + y_{CH_4})\right)} \quad (E2)$$

$$x_{H_2O} = \frac{\dot{n}_{H_2O,in} - \dot{n}_{H_2O,out}}{\dot{n}_{H_2O,in}} = \frac{2\dot{n}_{H_2O,in} - [\dot{n}_{dry,out} (2y_{H_2} + 4y_{CH_4}) - 4(\dot{n}_{urea,in})(x_{urea})]}{2\dot{n}_{H_2O,in}} \quad (E3)$$

$$H_2, SEL(\%) = \frac{(y_{H_2})(\dot{n}_{out,dry})}{((y_{H_2} + 2y_{CH_4})(\dot{n}_{out,dry}) + \dot{n}_{H_2O,prod})} \times 100 \quad (E4)$$

$$totalC_{MIN} = \dot{n}_{out,dry} (y_{CO_2} + y_{CO} + y_{CH_4}) \quad (E5)$$

$$SEL_{CO,EST}(\%) = 100 \times \frac{y_{CO} \times \dot{n}_{out,dry}}{(totalC_{MIN})} \quad (E6)$$

$$SEL_{CO_2,EST}(\%) = 100 \times \frac{y_{CO_2} \times \dot{n}_{out,dry}}{(totalC_{MIN})} \quad (E7)$$

$$SEL_{CH_4,EST}(\%) = 100 \times \frac{y_{CH_4} \times \dot{n}_{out,dry}}{(totalC_{MIN})} \quad (E8)$$

$$\dot{n}_{N_2,in} = \frac{\dot{V}_{N_2}}{22.5 \times 10^{-3}} \left[ \frac{[m^3 s^{-1}]}{[m^3 mol^{-1} at STP]} \right] \text{ mol. s}^{-1} \quad (E9)$$

$$\dot{n}_{cond} = \dot{n}_{H_2O,out} + \dot{n}_{NH_3,c,out} \quad (E10)$$

$$\dot{n}_{NH_3,c,out} = y'_{NH_3} \times \dot{n}_{cond} \quad (E11)$$

$$\dot{n}_{NH_3,c,out} = \left( \frac{y'_{NH_3}}{1 - y'_{NH_3}} \right) \dot{n}_{H_2O,out} \quad (E12)$$

$$\begin{aligned} & (2y_{N_2} + y_{NH_3}) \times \dot{n}_{out,dry} + \left( \frac{y'_{NH_3}}{1 - y'_{NH_3}} \right) \times \dot{n}_{H_2O,out} + j \times \dot{n}_{CnHmOkNj,out} \\ & = j \times \dot{n}_{CnHmOkNj,in} + 2\dot{n}_{N_2,in} \end{aligned} \quad (E13)$$

$$\left( \frac{(y_{CO} + y_{CO_2} + y_{CH_4})}{n} \times \dot{n}_{out,dry} \right) + 0 + 1 \times \dot{n}_{CnHmOkNj,out} = \dot{n}_{CnHmOkNj,in} \quad (E14)$$

$$\begin{aligned} & \left(4y_{CH_4} + 2y_{H_2} + 3y_{NH_3}\right) \times \dot{n}_{out,dry} + \left(2 + \frac{3y'_{NH_3}}{(1-y'_{NH_3})}\right) \times \dot{n}_{H_2O,out} + m \times \dot{n}_{CnHmOkNj,out} \quad (E15) \\ & = m \times \dot{n}_{CnHmOkNj,in} + 2\dot{n}_{H_2O,in} \end{aligned}$$

$$x_{CnHmOkNj} = \frac{\dot{n}_{CnHmOkNj,in} - \dot{n}_{CnHmOkNj,out}}{\dot{n}_{CnHmOkNj,in}} \quad (E16)$$

$$x_{H_2O} = \frac{(\dot{n}_{H_2O,in} - \dot{n}_{H_2O,out})}{\dot{n}_{H_2O,in}} \quad (E17)$$

$$\dot{n}_{H_2,out} = y_{H_2} \times \dot{n}_{out,dry} \quad (E18)$$

$$\dot{n}_{CO_2,out} = y_{CO_2} \times \dot{n}_{out,dry} \quad (E19)$$

$$\dot{n}_{CO,out} = y_{CO} \times \dot{n}_{out,dry} \quad (E20)$$

$$\dot{n}_{CH_4,out} = y_{CH_4} \times \dot{n}_{out,dry} \quad (E21)$$

$$\dot{n}_{NH_3,out} = y_{NH_3} \times \dot{n}_{out,dry} + \left(\frac{y'_{NH_3}}{1-y'_{NH_3}}\right) \times \dot{n}_{H_2O,out} \quad (E22)$$

$$SEL_{H_2} = 100 \times \frac{\dot{n}_{H_2,out}}{\dot{n}_{H_2,out} + \dot{n}_{NH_3,out} + \dot{n}_{CH_4,out}} \quad (E23)$$

$$SEL_{NH_3} = 100 \times \frac{\dot{n}_{NH_3,out}}{\dot{n}_{H_2,out} + \dot{n}_{NH_3,out} + \dot{n}_{CH_4,out}} \quad (E24)$$

$$SEL_{CH_4} = 100 \times \frac{\dot{n}_{CH_4,out}}{\dot{n}_{H_2,out} + \dot{n}_{NH_3,out} + \dot{n}_{CH_4,out}} \quad (E25)$$

$$SEL_{CO_2} = 100 \times \frac{\dot{n}_{CO_2,out}}{\dot{n}_{CO_2,out} + \dot{n}_{CO,out} + \dot{n}_{CH_4,out}} \quad (E26)$$

$$SEL_{CO} = 100 \times \frac{\dot{n}_{CO,out}}{\dot{n}_{CO_2,out} + \dot{n}_{CO,out} + \dot{n}_{CH_4,out}} \quad (E27)$$

$$SEL_{CH_4} = 100 \times \frac{\dot{n}_{CH_4,out}}{\dot{n}_{CO_2,out} + \dot{n}_{CO,out} + \dot{n}_{CH_4,out}} \quad (\text{E28})$$

$$H_2 \text{ yield} = \frac{\dot{n}_{H_2,out}}{\dot{n}_{CnHmOkNj,in}} \quad (\text{E29})$$



# 1 Introduction

## 1.1 Background.

One hundred and fifty years of large-scale fossil fuel extraction and combustion have led to a scientific consensus that the resultant product gases are forcing observed changes in atmospheric composition [1]. This phenomenon is ‘global warming’ with the combustion products responsible termed ‘greenhouse gases’. The two main combustion greenhouse gases are carbon dioxide (CO<sub>2</sub>) and methane (CH<sub>4</sub>).

Environmental disturbances such as the shrinkage of polar ice-caps and rising sea-levels have been recorded to validate scientific theories of global warming. These had been predicted along with other events that posed a serious threat to humanity and life on earth such as increased frequency of extreme weather events, famine caused by failing crop yields, and ecosystem collapse with resulting species extinctions [2]. Further scientific predictions have identified that the future trend is for an increasing acceleration of climate change due to the longevity of atmospheric greenhouse gases, and resultant positive feedback effects in other systems [3].

Despite these warnings, economic and social preferences in many of the more ‘developed’ countries favour the ease and relative cheapness of fossil fuels for heating and power, particularly with associated individual rather than communal technologies. Additionally, the economic development of some of the other most populated countries has seen them embracing the fossil fuel-driven economic philosophy and tapping the resources that they possessed to support this expansion. This has resulted in a global failure to offset emissions mitigation strategies implemented by European Union and United States governments. Consequently atmospheric greenhouse gases are predicted to increase by 44% (CO<sub>2</sub> equivalent) by 2020 relative to 1990 levels (**Figure 1-1**). Furthermore, deforestation, which had been occurring throughout this time (forests being a known atmospheric carbon sink keeping the global balance in equilibrium) continued [1].

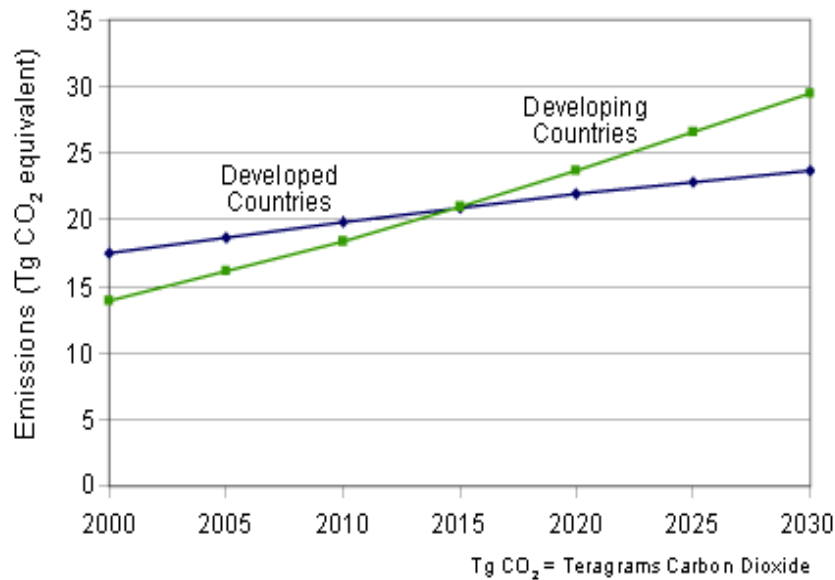


**Figure 1-1.** Global CO<sub>2</sub> emissions by region [3].

World energy consumption decreased by 1.1% in 2009 for the first time in 30 years due to global financial recession. The long term trends however are for increased energy consumption, with electrical energy demand expected to increase by 76% from 2007 to 2030 [4].

Though it is considered that the World's energy resources are adequate to meet projected demands up to 2030 [4] this would have dire consequences for climate change. Furthermore, it takes no account of the social and economic implications of increasing dependence on fossil fuels as these finite resources reach the end of their feasible extraction and supply lifetimes up to and beyond 2030. It is widely accepted that alternative sustainable energy sources are needed.

1.3 billion people (mostly in Africa, Latin America and Asia) presently live in energy poverty without access to electricity [4] and are therefore unable to acquire the most basic services of clean drinking water, communication, improved health services and education. Not only are alternatives to fossil fuels required to meet the global energy demand, but also new power sources that can meet the energy needs of poorer communities. For remote regions, this is likely to require energy creation close to the point of use due to the absence of a supply infrastructure.

Hydrogen powered fuel cells are identified as one attractive option in the search for alternatives to fossil fuels and as a way of supplying energy to remote locations as they offer the potential to be a reliable, mobile, non-polluting technology using an abundant and almost infinite resource. Present obstacles to the large scale application of hydrogen fuel cells include issues with the fuel, namely hydrogen production, storage, and transportation. Numerous compounds have been considered as suitable hydrogen

carriers, but all have inherent disadvantages. This project's aim was to assess the feasibility of using the stable and naturally occurring hydrogenous molecule urea as a hydrogen carrier for fuel cell energy supply.

## 1.2 Project Aims and Objectives

The objectives for achieving the aim of making an adequate and thorough assessment on the feasibility of using urea as a future energy vector are specified in the relevant introductory sections throughout this thesis. A summary list of these objectives is also given below:

- Determine the context in which urea would fit as a hydrogen carrier substance, understanding urea's physical properties in comparison with previously suggested contenders, its resource availability, and environmental impact. Specific focus was given to the identification of sustainable production routes, and long-term global availability of urea.
- Assess the thermodynamics of urea steam reforming by using equilibrium modelling calculations to predict optimum conditions for hydrogen production over a range of temperatures, pressures and reactant mixtures. To also calculate the energy required for the production of hydrogen from urea.
- Design and operate bench-scale steam reforming process systems that produce a hydrogen-rich synthesis gas from a urea feedstock. Emphasis was placed on optimised conditions for steam conversion and steady state operation at thermodynamic equilibrium.
- Characterisation of the urea fuel and of the catalyst used in experimental work to appraise the robustness of the process for scale-up, longer periods of operation, and practical application.

## 1.3 Thesis Structure

Succeeding Chapter 1, which has already provided an introduction to the context of this research and the motivating rationale behind it, Chapter 2 contains the literature survey that presents the status of present knowledge into which urea steam reforming and hydrogen production from urea fits. This Chapter describes how the physical properties, environmental impact, and resource availability of urea relate to the present technological requirements of a hydrogen carrier substance and to those materials which have previously been suggested as vectors for fuel cell feedstock and hydrogen supply.

Chapter 3 contains the results of modelling calculations that reveal predictions of product variations attainable at thermodynamic equilibrium. Calculations that estimate

the energy required to produce one mole of hydrogen gas from urea are also provided in this Chapter. The results from this section continue to be used in Chapter 5 and Chapter 6 in comparison with experimental results.

The central Chapter 5 and Chapter 6 of this thesis report the experimental results of optimised urea steam reforming in catalytic bench-scale reactor process systems, focussing, as per the research objectives, on maximum steam conversion and optimised steady state operation. Chapter 5 describes first attempts at extracting hydrogen from urea, while Chapter 6 reports an extended parametric study using a process system design specific to urea solution fuel, and with an extended range of product analyses. Results of in-situ process characterisation are also provided in these chapters.

Ex-situ characterisation of a urea solution fuel and of the catalyst used in urea steam reforming is discussed in Chapter 4 and Chapter 7 respectively. A range of wet chemistry and instrumental analytical techniques were used to achieve the objectives of exploring the underlying nature of urea thermal decomposition with excess steam in flow reactor conditions, and of the catalyst's ability to achieve and maintain the process of urea steam reforming.

Following the Conclusions provided in Chapter 8 are Appendices. **Appendix A** contains results of a urea steam reforming experiment outside of the parametric study remit. **Appendix B** contains a description of a steam reforming reactor system that was built by the author at the direction of, and utilising a novel reactor component that had been supplied by, the industrial sponsor.

Reference citations within the text are numbered consecutively and contained inside square brackets. A reference list is provided at the end of the thesis.

## 2 Literature Review

### 2.1 Aims and Objectives

No previously reported studies were available for consultation on the subjects of either using urea as a hydrogen carrier, or of extracting hydrogen gas (H<sub>2</sub>) from urea. Consequently, the aim of this literature review was to determine the viability of these processes.

The first objective was to critique the present status of chemical energy supply, fuel cell technology, and steam reforming methodologies in perspective of their adequacy to meet future sustainable energy needs; and, in terms of the chemical energy carriers presently identified, by comparison with the physical properties of urea. The second objective was to determine the knowledge of urea decomposition with a focus on possible pathways for H<sub>2</sub> release, release conditions, and the chemical reactions involved. Focus was also given to urea decomposition by-products that could be considered either beneficial or detrimental to wider applications of the urea-derived fuel. An appraisal of the methods available to manufacture urea was made, both historically, and with present processing systems. This encompassed an assessment of energy requirements for urea production and the environmental fate of both urea products and urea manufacturing by-products. Finally, this section had an objective to identify the present and long-term resource availability of urea, with emphasis made to sustainable and future supply routes. The state of knowledge and the availability of technology necessary to extract urea from these novel sustainable resources was investigated.

### 2.2 Hydrogen

Hydrogen forms just water when used to generate electrical power in fuel cells resulting in no greenhouse gas emissions, silent operation, and high efficiency. It has the highest energy to weight ratio of any fuel with an energy content of 141.78 MJ per kg (higher heating value), equating to the standard heat of formation of water [5]:



Hydrogen is considered to be the most abundant element in the universe. However, it does not occur in elemental form to a significant level in nature; being mainly combined with oxygen as water, or with carbon as hydrocarbons. The ideal engineering solution for hydrogen extraction would be to split water, because of its abundance; but water's thermodynamic stability makes dissociation difficult to achieve in practice.

Storing hydrogen in its pure form is a major challenge for adopting hydrogen as an energy carrier: high pressure and/or large vessels for gaseous phase storage, or cryogenic (-253 °C) enclosures for liquid phase [6], make storage costly and bulky. Even with these extreme measures, due to its small molecular size, evaporation losses of 2-3 % per day can still occur [5]. Consequently, either an advanced distribution and storage infrastructure would be required, or the utilisation of some stable hydrogen carrier substance creating the need for small-scale discharging technology, either on board vehicles/at point of use or at a local re-fuelling/supply station.

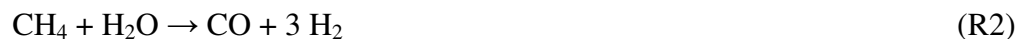
Ideal hydrogen carrier substances would have high hydrogen to weight and volume ratios. They would also possess simple, rapid and inexpensive dissociation mechanisms, have the ability to be either recharged (“two-way carriers” that have reversible reaction chemistry so that the carrier elements can be retained for re-hydrogenation) or release only environmentally benign by-products (“one-way carriers”).

One proposed target for the viable utilisation of hydrogen storage in transportation applications is having a hydrogen density of at least 6 wt% (gravimetric) and 0.045 kg/L (volumetric) H<sub>2</sub>, increasing to 9 wt% and 0.081 kg per Litre H<sub>2</sub> by 2015 [7, 8]. This refers to useable hydrogen in not just the storage medium, but the total onboard storage system.

### 2.3 Steam Reforming

Steam reforming is a mature technology for the production of hydrogen from hydrocarbons. Because natural gas is widely available, relatively easy to handle, *has* been relatively cheap, and has a high hydrogen to carbon ratio, this is usually the preferred choice, although other hydrocarbons, both fossil fuel and biomass are feasible alternatives [9]. Natural gas has a high component of methane, and therefore this process is sometimes referred to as methane steam reforming (MSR).

Steam reforming to produce hydrogen (following hydrogenation to remove any sulphur that might be present in the feedstock) is highly endothermic and brought to equilibrium at high temperatures (ca. 900 °C) and pressures of several MPa over nickel-based catalysts [10]:



The product of steam reforming is termed “synthesis gas” or “syngas”. Present reformers are suited to sustained steady operation, delivering relatively high concentrations of hydrogen (> 70 % in dry syngas) [10]. This is further processed by mildly exothermic “water gas shift” reactions that occur in two sub-stages at high (~ 400 °C) and then low (~ 200 °C) temperature:



Temperature, pressure and chemistry must be carefully controlled in order to suppress carbon build up (coking) which can deactivate the catalyst and block the reactor [10]. Steam to carbon feeds of 2 to 3 are usual [5].

The final process stage to produce hydrogen of fuel cell purity is “pressure swing adsorption”. This results in a hydrogen yield of > 99.9 % from the original feedstock [9] and separates H<sub>2</sub> from CO<sub>2</sub> and any other impurities that might be present at high pressure (up to 4 MPa) on an adsorbing medium.

The disadvantages of steam reforming to produce hydrogen are that it is highly energy intensive and the energy content of the natural gas is greater than the energy content of the H<sub>2</sub> produced per unit volume. Also, large quantities of CO<sub>2</sub> are created adding to atmospheric pollution. This is mitigated if a biomass feedstock is used. To try and improve the efficiency of steam reforming, a number of concepts have been proposed.

### 2.3.1 Partial Oxidation

This type of reformation uses sub-stoichiometric oxygen in the fuel/oxygen mixture instead of steam, causing some of the fuel to oxidise exothermically:



Because the entire hydrogen product comes from the hydrocarbon, this process creates a smaller hydrogen yield per volume of fuel. Also, if for cost reduction, air is used instead of pure O<sub>2</sub>, the syngas is further diluted. However, the subsequent internal heat generation of this reaction, raises the temperature in the reactor to over 1000 °C, enabling easier steam reforming of any fuel remaining [11].

### 2.3.2 Autothermal Steam Reforming

This uses the partial oxidisation concept at high temperature (or lower temperature in the presence of a catalyst) producing CO and H<sub>2</sub> exothermically. The objective is to attain ideal conditions so that no external heat input is required so that the endothermic steam reforming reaction and the exothermic partial oxidation run together at the same time as creating a H<sub>2</sub> yield that is higher than partial oxidation on its own [9].

### 2.3.3 Sorbtion Enhanced Steam Reforming

This process mixes a CO<sub>2</sub> *adsorbent* with the reforming catalyst. It allows temperatures to be reduced to 400-500 °C, and operates with the steam reforming and shift reaction stages combined [12].

### 2.3.4 Unmixed Steam Reforming

With the aim of achieving autothermal production, Unmixed Steam Reforming keeps the fuel-steam feed and the air feed un-mixed. An oxygen transfer material (OTM) stores the oxygen exothermically [13]. Nickel has been successfully used as the OTM, accepting oxygen to form NiO and releasing heat to the reactor bed [14]. The NiO then regenerates to Ni by reduction when it meets the fuel-steam feed. CO<sub>2</sub> capture can also occur if a suitable adsorbant is included in the design.

## 2.4 Fuel Cells

Fuel cells convert the chemical energy of a fuel directly into electric and thermal energy by reaction with an oxidizing agent. This is more efficient than combustion for it does not include the intermediate stages of conversion into thermal energy then mechanical energy. Additionally, fuel cells have no moving parts which means that friction is negated, they are virtually silent in operation, and they have no direct pollutant emissions. They can give rapid response times, and they have a good power to weight ratio [5]. Fuels cells can also operate continuously as long as a continuous supply of reactants are available for they do not store energy in the same way as batteries. This means that fuel reservoirs are required to achieve continuous operation.

There are many types of fuel cell, differing and categorised by their choice of electrolyte medium, feedstock, and operating temperature range. Each is composed of a central electrolyte bounded on either side by electrodes. The electrodes are invariably coated with a catalyst to accelerate the reaction and reduce reaction temperatures. On the outer side of these electrodes are “bipolar plates”. Functioning only at low voltages (typically 0.6 to 0.8 V), fuel cells are usually combined in stacks to increase the voltage with the bipolar plates separating individual cells within a stack and allowing gas flow into, and water flow out of, the cell.

In addition to being stable under both strongly reducing and oxidising conditions, the electrolyte must be an electron insulator, an ion conductor, and must not allow any gas crossover. To reduce resistance losses in the electrolyte, it is made as thin as possible without compromising its functionality.

Hydrogen is the cleanest fuel for fuel cells although they can be powered by other substances such as ammonia or hydrocarbons. Where other substances are used as a feedstock, these can either be supplied directly to the anode or “reformed” into fuel and by-products prior to use with the hydrogen (or other direct fuel) then being fed to the cell. Air is often used as the oxidiser for convenience and cost reduction at the opposite electrode.



Proton-exchange Membrane Fuel Cells [PEMFC] have acquired much of the recent focus for application to transportation. These are also called “polymer electrolyte membrane fuel cells” and “solid polymer electrolyte fuel cells (SPEFC)”. They operate at low temperature (80 – 90 °C) and pressure ranges thereby enabling rapid start up from cold. They are lightweight, compact, and have a high power density [15]. Although all modern fuel cells operate on the same physical principle and have the same components to optimise output, they can have differing electrolyte chemistry involving either anion or cation throughflow dependent upon their specific fuel type.

Where reference to the suitability of urea as a hydrogen fuel cell feedstock is made, most consideration is given to PEMFCs. This is because, at the time of writing, these were deemed to be the most attractive for vehicular application. Other types of fuel cell have attributes more favourable than PEMFCs in specific operating conditions and environments. A list of the major fuel-cell types is obtainable in many standard texts (see [5]).

PEMFCs use platinum catalysts which are susceptible to poisoning from impurities, particularly CO, which has to be kept below a few ppm to preserve the negative electrode [16]. This requirement for high purity hydrogen and the problems of its on board storage are the main obstacles for vehicular PEMFC implementation using hydrocarbon carriers. Furthermore, if there is a reforming step, polymeric carbon deposits can accrue during reforming, reducing system performance by aggregating and de-activating catalysts.

## 2.5 Current Hydrogen Carriers

A number of substances and materials have been considered as hydrogen carriers for fuel cells. These include reversible storage alloys (conventional metal hydrides), high surface area sorbents (such as carbon nanostructured materials and other porous media), ionic complex chemical hydrides, and simple hydrogen bearing chemicals.

A typical metal hydride storage system would comprise a tank containing granular metal which adsorbs hydrogen, and has the capacity to release it upon heating. This is a relatively established technology and although some can have a good volumetric energy density of hydrogen, their weight percentage is poor and they have exhibited problems with controlled hydrogen release [17].

Nanostructured storage materials are not yet at a stage where uniform and economic synthesis is determinable, plus there has been a lack of reproducibility on experiments into their functionality [5, 18]. Other porous media include zeolites and metal organic frameworks. The former have relatively low storage capacity [19], while

the latter are considered to have limited potential for hydrogen storage at present due to the extremely low temperatures (77 K) required for operation [20].

### 2.5.1 Simple Hydrogen-bearing Chemicals

Cheap industrial chemicals are attractive as hydrogen carriers because they have the benefit of some form of established technological infrastructure for manufacture, storage and distribution. They have covalent bonding with hydrogen, generally with high atomic concentrations and can be likened to crude oil sourced fuels since they are chemical energy carriers, supplying energy at the point of use. Instead of combustion however, hydrogen can be released from these compounds by a number of other well developed chemical techniques, usually requiring the control of pH and catalysts.

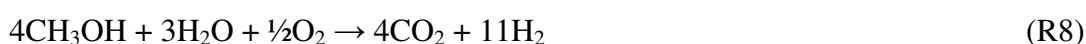
Thermolysis reactions are the route of dehydrogenation from all hydrocarbon hydrogen carriers. Although these major reforming techniques are relatively efficient, unfavourable operating conditions during reforming can create similarly unfavourable by-products, such as methane, carbon monoxide, and coke.

There follows a description of some of the major hydrogen-bearing chemical carriers that have been considered. This is not an exhaustive list and some categories such as alcohols and cycloalkanes encompass numerous compound options. Weight percentage hydrogen is given, and where known the extractable hydrogen weight percentage also. This latter value is of most relevance and as can be seen, often appears to be well below the carrier compound hydrogen content. **Table 2-2** shows a comparison of these chemical contenders against the properties of urea.

#### 2.5.1.1 Methanol (CH<sub>3</sub>OH)

Methanol (methyl alcohol) is the first member of the homologous series of alcohols and has the lowest molecular weight. Although produced naturally by anaerobic bacteria [21], it is presently obtained commercially from hydrocarbon fossil fuels utilising copper-based catalysts. Biomass however is identified as a viable alternative route [22].

Methanol thermolysis is undertaken at moderate temperatures (200-400 °C) with noble metal catalysts via four main reaction routes, steam reforming (R5), partial oxidation (R6), decomposition (R7) and oxidative steam reforming (R8) [22]:



It is reported that (R8) can be autothermal at 325 °C, while (R5) is known to give maximum hydrogen yields with 75 % in the product gas [23]. As can be seen from (R7) however, carbon monoxide is a by-product of dehydrogenation. Any PEMFC application requiring hydrogen conversion would therefore need to incorporate technology for oxidising this CO to CO<sub>2</sub>, posing major difficulties and also creating greenhouse gas emissions.

This need for reformation and gas purification is a major obstacle for methanol's use as a hydrogen feed in PEMFCs, with the present status of high temperature steam reforming technology that could alleviate these problems presently considered impractical for transport applications. Furthermore, there is also no apparent benefit to be gained from subjecting methanol to further energy and cost intensive processing as a hydrogen carrier due to the greenhouse gases it releases for it can, without alteration, be used directly in internal combustion engines. It is in this form of application where alcohols of biological origin are probably most suitable as they are proven alternatives to fossil fuels.

Methanol can be supplied directly without modification to certain fuel cells. This has been shown with high temperature Solid Oxide (SOFC) and Direct Methanol (DMFC) fuel cells, with the added bonus that the waste heat can aid the decomposition of methanol while also assisting with the cooling of the cell [5].

### **2.5.1.2 Ethanol (C<sub>2</sub>H<sub>5</sub>OH)**

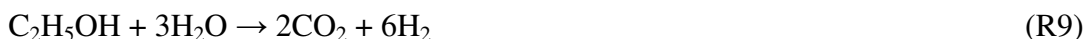
Ethanol (ethyl alcohol) has an advantage over methanol for it can be produced far more easily and therefore economically from a wide range of biomass feedstocks. This makes it a carbon neutral hydrogen source as long as no extra fossil-fuel energy input was used in the synthesis from biomass to ethanol or in associated distribution costs. It also has a high hydrogen content of 13.1 wt%.

Ethanol is mainly synthesised from ethylene in the petrochemicals industry. Bio-ethanol however is produced by the fermentation of sugars in vegetative matter, but can also be made by hydrolysis. Many countries also have energy policies that include increasing bio-ethanol production as a replacement for fuel in internal combustion engines. Consequently ethanol is a readily available potential hydrogen carrier, with flexible and stable future supply prospects.

There are concerns about the ethics of using biomass for energy. This relates to the deforestation and replacement of arable land to grow bio-fuel crops [24], with the implications of loss of carbon sinks (forests) offsetting the benefits of using bio-fuel, land use for fuel in regions where human food poverty is prevalent, and also the application of environmental pollutants for fertilisation and pest control of biomass

crops. It is probable that urea would be the most commonly used fertiliser in these situations, with the potential irony that it could be the better fuel alternative.

Ethanol is an irreversible hydrogen carrier and since it is a hydrocarbon, this creates the same disadvantages as methanol: greenhouse gas emissions and high purity reformation technology required to eliminate impurities from the inlet gas, all of which give it associated unfavourability. It is reformed to hydrogen at temperatures in excess of 800 °C, using noble metals as catalysts [25]. The steam reforming reaction for optimum hydrogen production is strongly endothermic [26]:



### 2.5.1.3 Cycloalkanes

A number of cyclic hydrocarbons have been considered as potential hydrogen carriers, with the two receiving most interest being cyclohexane ( $\text{C}_6\text{H}_{12}$ ) and methylcyclohexane ( $\text{C}_7\text{H}_{14}$ ). These are proposed as reversible hydrogen carriers that require independent hydrogen production prior to their formation, but their reaction chemistry is relatively well established and they have high boiling points meaning storage and transportation could be feasible with present infrastructure technology [27].

Hydrogenation/dehydrogenation reactions involve gas phase thermolysis over a catalyst, with noble metals presently achieving optimum temperature ranges of between 210 - 350 °C [27]:



### 2.5.1.4 Hydrazine ( $\text{N}_2\text{H}_4$ )

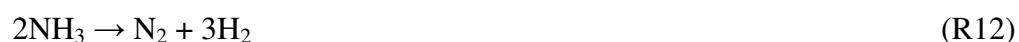
Hydrazine is relatively easy to dehydrogenate [5] though it has not been the focus of much research as a hydrogen carrier due to its high toxicity and explosivity (see **Table 2-2**). However, fuel cells powered by hydrazine have reportedly achieved comparable power outputs to hydrogen fed fuel cells without creating  $\text{CO}_2$  emissions, and significantly using much cheaper cobalt or nickel catalysts instead of platinum [28]. Whether this substance will “open the fuel cell age for vehicles” as its inventors suggest may depend on whether a method of detoxification can be found. A record in the primary literature source of attempts to address this by incorporating hydrazine into a less toxic carrier polymer are given, but no extended toxicity tests were reported [28]. Much further evidence is therefore required in order to prove the viability of this substance as a safe energy vector.

### 2.5.1.5 Ammonia (NH<sub>3</sub>)

Ammonia has many favourable attributes as a hydrogen carrier. It is not a greenhouse gas, is available in large quantities, and there presently exists a worldwide infrastructure for its manufacture, storage and distribution [29]. Ammonia has a high hydrogen content and is much safer than hydrocarbons when assessed on the criterion of being a fire and explosion hazard (see **Table 2-2**). Ammonia also has a density which is lighter than air meaning that any emissions dissipate rapidly and beneficially for safety reasons. It can be liquefied under mild conditions meaning that relatively simple and inexpensive storage solutions could be applied to give a volumetric hydrogen density that is 45 % greater than liquid hydrogen [30]. Evidence in support of this is that in industrial applications, ammonia is presently stored safely under similar conditions to propane: at 8 bar vapour pressure and room temperature [31].

The major obstacle however to ammonia's favourable consideration as a hydrogen carrier and fuel cell feed is that in pure form it is highly toxic to both humans and the environment (**Table 2-2**). Although this can be slightly mitigated by the fact that ammonia has a strongly pungent odour, thereby revealing itself for early detection of leaks, it is so hazardous that any large spillages are likely to result in local and lethal concentrations [32].

Dissociation of ammonia, known as "cracking" or "splitting", is the reverse of synthesis [30]:



This has advantages over hydrocarbon reformation because the dynamics are fast and the reaction occurs in one single step without the need for oxygen or steam, making the process requirements simpler and relatively cheap. In industry this process is catalysed with nickel supported on alumina at high temperatures. The literature quoted temperatures for this reaction are 900-1050 °C though this is for optimum conversion and at cooler conditions it is reported that ammonia dissociation will still occur. Using equilibrium modelling data, at atmospheric pressure it is reported that at 600 °C, 90 % of ammonia will be decomposed to N<sub>2</sub> and H<sub>2</sub> (see **Table 2-1**).

**Table 2-1.** Equilibrium ammonia cracking as a function of temperature and pressures of 1 and 10 bar [30].

Temperature (°C)	Unconverted NH <sub>3</sub> (1 bar)	Unconverted NH <sub>3</sub> (10 bar)
400	0.88%	7.91%
500	0.26%	2.55%
600	0.10%	1.00%
700	0.047%	0.47%
800	0.025%	0.25%
900	0.015%	0.15%

There always appears to be some trace of ammonia in the cracking process product. Even at the high temperatures that yield a 99.9 % conversion using pre-heated fuel feeds, residues of ammonia in the outlet gas of ca. 50 ppm occur [32]. Recent advances in the optimisation of ammonia decomposition technology have utilised ruthenium, caesium and barium catalysts to conditions at atmospheric pressure and reaction temperatures of 300 °C [33]. However, this research has not presently bypassed the problem of incomplete conversion.

Some fuel cells such as those using solid oxide and alkaline electrolyte are tolerant of ammonia [34, 35]. Poisoning of PEMFCs by ammonia is a deep process that creates resistance in the membrane and reduced conductivity elsewhere in the cell components that takes hours if not days to reach a steady state for both poisoning and recovery [36]. The exact mechanisms involved are not fully understood, but the holistic nature of the poisoning has been shown to include effects on both electrodes due to the rapid diffusion of ammonium ions (NH<sub>4</sub><sup>+</sup>) [36, 37]. Performance loss is significant, and although in most cases this can be reversed, long term operation has been shown to require ammonia concentrations of less than 1 ppm [36].

To overcome the human toxicity of ammonia it has been proposed to store hydrogen in an inert form as a compact metal ammine chloride [29, 38]. These reversible hydrogen/ammonia storage materials: Mg(NH<sub>3</sub>)<sub>6</sub>Cl<sub>2</sub>, Ca(NH<sub>3</sub>)<sub>8</sub>Cl<sub>2</sub>, Mn(NH<sub>3</sub>)<sub>6</sub>Cl<sub>2</sub>, and Ni(NH<sub>3</sub>)<sub>6</sub>Cl<sub>2</sub> reportedly require little energy in construction: Mg(NH<sub>3</sub>)<sub>6</sub>Cl<sub>2</sub> are formed at room temperature by passing ammonia over anhydrous magnesium chloride [29], have extremely fast reaction kinetics and can release hydrogen corresponding to 9.78 wt% [38]. They are made more attractive by being shaped into dense, stable tablets or powdered form with hydrogen content of 110 kg m<sup>-3</sup> [29, 38]. This is higher than liquid ammonia and many other proposed hydrogen storage mechanisms.

Some of the authors responsible for the metal ammine discovery concede that ammonia production is presently undertaken with natural gas as a feedstock and acknowledge that this cannot remain a long-term source of ammonia due to finite reserves [33]. In the context of long term supply and also dubiously as an environmentally favourable option, they then state that ammonia could equally be manufactured from coal utilising 200 years worth of reserves, and citing simultaneous sequestration as a means to carbon-zero ammonia production [33]. This statement is a weak argument for sustainability at best.

The combination of hydrogen with nitrogen to form ammonia is a relatively energy efficient process. It is the production of hydrogen that is responsible for the energy intensive component in present ammonia synthesis [32]. Taking a further step to produce urea might slightly improve on the environmental impact as some of the CO<sub>2</sub> would be used to form urea rather than emitted as process waste. However, this would just delay the release of the carbon until urea decomposition occurred.

It seems at present that until a cost-effective renewable source of hydrogen or ammonia synthesis can be developed it is unlikely that ammonia could be called an environmentally attractive long term energy carrier contender. To obtain ammonia sustainably, research is ongoing in the biological sciences to replicate the processes of leguminous plants that are able to fix atmospheric N<sub>2</sub> utilising microbial enzymes [39].

One such sustainable source of ammonia is urea, from which it decomposes enzymatically at room temperature or with heat. As can be seen in **Table 2-2**, urea has no associated toxicity and is a stable solid. Therefore it can be considered as a natural competitor to the metal ammine storage tablets as an ammonia carrier, and also as a potential hydrogen carrier – the object of this study.

**Table 2-2.** Comparison of physical properties, hydrogen content, toxicity and safety aspects of hydrogen carriers [40]

Substance	H <sub>2</sub> (wt%)	Safety Classifications	Toxicity TLV	Flammability in air	Melting Point	Boiling Point
Ammonia (NH <sub>3</sub> )	17.6	T,N,C	25ppm as TWA 35ppm as STEL	Auto-ignition temp 651°C. Explosive limits 15-28% vol%	-78°C	-33°C
Cyclohexane (C <sub>6</sub> H <sub>12</sub> )	7.2	F, N, Xn	100ppm as TWA	Auto-ignition temp 260°C Explosive Limits 1.3-8.4 vol%	7°C	81°C
Ethanol (C <sub>2</sub> H <sub>5</sub> OH)	13.1	F	1000ppm as TWA	Auto-ignition temp 363°C Explosive limits 3.3-19 vol%	-117°C	79°C
Hydrazine (N <sub>2</sub> H <sub>4</sub> )	11.2	T,N,E,Carc,C	0.01ppm	Auto-ignition temp 24-100°C Explosive limits 1.8-100 vol%	2°C	114°C
Hydrogen (H <sub>2</sub> )	N/A	F+	simple asphyxiant	Auto-ignition temp 500-571°C Explosive limits 4-76 vol%	N/A	-253°C
Methanol (CH <sub>3</sub> OH)	12.6	F,T	200ppm as TWA 250ppm as STEL	Auto-ignition temp 464°C Explosive limits 5.5-44 vol%	-98°C	65°C
Methylcyclohexane (C <sub>7</sub> H <sub>14</sub> )	6.2	F	400ppm	Auto-ignition temp 258°C Explosive limits 1.2-6.7 vol%	-126.7°C	101°C
Urea (NH <sub>2</sub> ) <sub>2</sub> CO	6.7 <sup>b</sup>	None	None established	Non-flammable	Crystalline solid. Decomposes at 133°C	

T = toxic, F = flammable, F+ = extremely flammable, N = dangerous for the environment, Xn = harmful, E = explosive; C = corrosive, Carc = carcinogen; TLV = threshold limit value, TWA = time weighted average (8h/day 40h/week), STEL = short term exposure limit (15 minutes); <sup>b</sup> 7.95wt % in aqueous solution.



## 2.6 Urea ((NH<sub>2</sub>)<sub>2</sub>CO)

### 2.6.1 History and Properties

Urea is a non-flammable, relatively non-toxic, colourless, anisotropic and birefringent crystalline substance that is perhaps best known for its presence in urine. It was first isolated some time before 1727 by Herman Boerhaave though many texts mistakenly attribute the discovery to H.M.Rouelle in 1773 [41]. In 1798-1799 urea was first obtained in crystalline form by Fourcroy and Vauquelin and ultimately synthesised from inorganic reagents in 1828 by F. Wöhler while heating what is now known to be its isomer: ammonium cyanate (NH<sub>4</sub><sup>+</sup> CNO<sup>-</sup>). This had historical significance for it began the eventual demise of the theory of vitalism among scientists, showing that ‘life process’ chemicals were not distinct from other substances, as had previously been thought. Many textbooks define this discovery as marking the foundation of modern organic chemistry. Accessible accounts of Wöhler’s work and its implications in a historical context are provided by Werner [42] and more recently, Cohen and Cohen [43].

The reaction mechanics of Wöhler’s synthesis, namely how the salt ammonium cyanate transforms into urea, are still not fully understood despite efforts being made by numerous researchers over the last century. This search described thirty years ago as ‘a saga in reaction mechanisms’ [44] continues to be appropriate today, as recent studies focused on ammonium cyanate had to be corrected by the same research group five years later [45, 46]. Work is apparently still in progress, with the theory now that solid state transfer to urea occurs by a proton (H<sup>+</sup>) jump from ammonium (NH<sub>4</sub><sup>+</sup>) to cyanate (NCO<sup>-</sup>) along one of the salt’s hydrogen bonds, followed by ammonia’s nucleophilic attack on the carbon atom of hydrogen cyanate [46].

Aside from this present uncertainty, methods of urea synthesis have been identified and applied both in the laboratory and in industry such that urea is now a widely used commodity. Because of this, its physical properties are known and available in standard literature (**Table 2-2 – Table 2-5**).

**Table 2-3.** Physical Data of Urea [47] except where stated.

Property	Value
Molecular formula	(NH <sub>2</sub> ) <sub>2</sub> CO
Synonyms	Carbamide, carbonyldiamide, isourea, B-I-K
Relative Molecular Mass (M <sub>r</sub> )	60.06g/mol
Freezing/melting point	133 °C [48]
Boiling point	N/A (decomposes)
Density	1.32g/cm <sup>3</sup>
Flash point	Non-flammable

Urea is stable at room temperature and atmospheric pressure. In pure form it is crystalline in habit, though is easily shaped into granules and prills [47]. This fact, combined with its stability, non-flammability and low density give urea favourability as a hydrogen carrier substance offering the potential for it to be easily transported and stored. Urea is however, hydrophilic and hygroscopic, being also soluble in alcohol, glycerol, and ammonia (see **Table 2.4** and **2.5**). This would necessitate dry containment for hydrogen supply applications.

**Table 2-4.** Properties of Saturated Aqueous Urea Solutions. Columns 1-5 from reference [47]. Column 6 calculated from column 2 by division through relative molecular masses of urea (60.06) and water (18).

Temperature (°C)	Solubility in water (wt%)	Density (g/cm <sup>3</sup> )	Viscosity (mPa/s)	Water vapour pressure (kPa)	Molar water: urea ratio (S:C)
0	41.0	1.120	2.63	0.53	4.80
20	51.6	1.147	1.96	1.73	3.13
40	62.2	1.167	1.72	5.33	2.03
60	72.2	1.184	1.72	12.00	1.28
80	80.6	1.198	1.93	21.33	0.80
100	88.3	1.210	2.35	29.33	0.44
120	95.5	1.221	2.93	18.00	0.16
130	99.2	1.226	3.25	0.93	0.03

**Table 2-5.** Solubility of Urea in Alcohol Solvents (wt% of urea) [49].

Solvent	Temperature (°C)			
	0	20	40	60
Methanol	13.0	18.0	26.1	38.6
Ethanol	2.5	5.1	8.5	13.1

## 2.6.2 Occurrence

Urea is produced synthetically on a commercial scale and is also naturally abundant as an *in-vivo* product of protein catabolism, where due to its high solubility it is present in bodily fluids and excreted in urine by mammals and all other animals except birds and saurian reptiles [50, 51, 52, 53]. In mammals, urea is concentrated in the kidney prior to excretion as a means of water conservation; while those animals that do not have a kidney that can concentrate urine in this way excrete waste forms such as uric acid and allantoin. These nitrogenous wastes and other nucleic acids such as purines [54] when acted on by micro-organisms and enzymes inside the body of higher animals degrade to urea thereby providing a further route to synthesis.

Plants are also found to contain urea, although the mechanisms of accumulation and transport are not fully understood. It is believed to be used as a nitrogen store, present through a combination of acquisition from the environment and by way of internal synthesis [55].

## 2.7 Urea Decomposition and Dehydrogenation

### 2.7.1 Enzymatic Decomposition

Because it is a naturally occurring part of the nitrogen cycle, organisms that are able to decompose urea enzymatically are widespread. This enzymatic decomposition is believed to be hydrolysis rather than ammonia elimination, given here as occurring via the intermediate compound ammonium carbamate [56]:

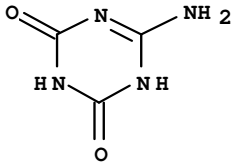
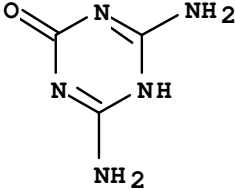
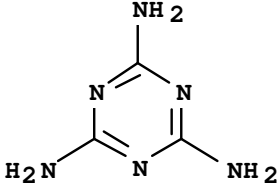
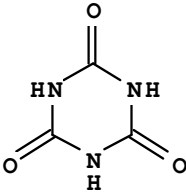


### 2.7.2 Thermal Decomposition

Articles reporting work that has attempted to clarify the mechanisms of thermal urea decomposition still appear in current scientific journals, evidencing the uncertainty that exists in this area. It has long been proved that when heat is applied to urea it primarily decomposes by eliminating the gases ammonia and isocyanic acid [42]:



The product HNCO (Isocyanic acid) is occasionally referred to in modern publications as its tautomer cyanic acid (HOCN) [48, 57] and the terms seem to be used interchangeably which is confusing. It has been shown, (though not with respect to urea decomposition) that in the vapour phase HNCO predominates, and that cyanic acid is an unstable species [58, 59]. Molecular formulae of the compounds named in this thesis are provided in **Figure 2-1**.

$\text{H}_2\text{N}-\overset{\text{O}}{\parallel}{\text{C}}-\text{NH}_2$ <p style="text-align: center;">Urea</p>	$\text{H}_2\text{N}-\overset{\text{O}}{\parallel}{\text{C}}-\text{NH}-\overset{\text{O}}{\parallel}{\text{C}}-\text{NH}_2$ <p style="text-align: center;">Biuret</p>	$\text{H}_2\text{N}-\overset{\text{O}}{\parallel}{\text{C}}-\text{NH}-\overset{\text{O}}{\parallel}{\text{C}}-\text{NH}-\overset{\text{O}}{\parallel}{\text{C}}-\text{NH}_2$ <p style="text-align: center;">Triuret</p>
 <p style="text-align: center;">Ammelide</p>	 <p style="text-align: center;">Ammeline</p>	 <p style="text-align: center;">Melamine</p>
$\text{HN}=\text{C}=\text{O}$ <p style="text-align: center;">Isocyanic acid</p>	$\text{HO}-\text{C}\equiv\text{N}$ <p style="text-align: center;">Cyanic acid</p>	 <p style="text-align: center;">Cyanuric acid</p>
$\text{HO}-\overset{\text{O}}{\parallel}{\text{C}}-\text{NH}_2$ <p style="text-align: center;">• NH<sub>3</sub></p> <p style="text-align: center;">Ammonium carbamate</p>	$\text{HO}-\text{C}\equiv\text{N}$ <p style="text-align: center;">• NH<sub>3</sub></p> <p style="text-align: center;">Ammonium cyanate</p>	

**Figure 2-1.** Molecular structure of some urea-derived compounds named in this document [60]. Note that isocyanic acid and cyanic acid are tautomers. Reference books sometimes refer erroneously to cyanic acid as a synonym for isocyanic acid.

By far the most thorough report of urea thermal decomposition is provided by Schaber *et al.* [48]. This study is of a batch process involving open reaction vessel heating of dry (non-aqueous) urea. Both evolved gases and residue were analysed using the following techniques: thermogravimetric analysis (TGA), high performance liquid chromatography (HPLC), fourier transform infra-red (FTIR) and ammonium ion-selective electrode. Other studies have applied additional analytical techniques of differential scanning calorimetry (DSC) [61] and mass spectrometry (MS) [57]. To summarise, it is generally accepted that urea thermal decomposition commences at ca. 133 °C [48, 57, 61], and though melting is commonly reported to occur first, the exact nature of the physical state of urea at this point is unclear [62]. In the absence of water, with continued increasing temperature, residual species (mainly HNCNCO and urea)

interact within this melt to form polymers, the first of those being biuret which is seen to occur in the temperature range between 135 °C to 220 °C [42, 48, 61]. With further temperature increases triuret, cyanuric acid (at low temperature), and ammeline, ammeline, and melamine (at higher temperature) appear [48]. Ammonium cyanate is also seen to form as a sublimate from the melt [42, 48]. A number of repeatable decomposition stages have been identified corresponding to enthalpy changes with increasing temperature up to complete urea decomposition prior to 500 °C [48].

Thargard *et al.* [63] relied on the work of Schaber *et al.* [48] and Stradella and Argentero [61] as citations for thermal decomposition products and stages. Their work involved thermal decomposition of urea between 150 °C to 200 °C using dielectric barrier discharge (DBD) under both dry and humid air flow. Analysis was by an NH<sub>3</sub>-NO<sub>x</sub> sensor and FTIR for gas species, and Nessler's reagent for ammonium in water. The major gaseous products were identified as NH<sub>3</sub>, HNCO, and NO<sub>2</sub>. Since no CO<sub>2</sub> was detected in their product gas analyses, they confirmed that the reaction for first stage urea thermolysis was (R14). They also deduced that the NO<sub>2</sub> product was a consequence of using an air flow (i.e. oxidation of ammonia and HNCO) since this was the only major by-product when the DBD was run using only air.

A soluble white powder was observed to form on the inside reactor walls and post-reactor tubing, light in structure and having a flaky-type appearance. Their tests on this substance involved a colorimetric test which indicated ammonia and they concluded that it was ammonium cyanate (NH<sub>4</sub><sup>+</sup>NCO<sup>-</sup>). A second type of solid was also observed as being insoluble in both cold and 70 °C water, though later they describe it *as* being soluble in hot water (without giving a temperature). Their FTIR analysis on this substance suggested that it could be cyanuric acid (C<sub>3</sub>H<sub>3</sub>N<sub>3</sub>O<sub>3</sub>).

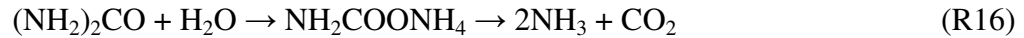
The decomposition of urea in both air and inert (argon) gas up to 1200 °C was reported by Carp [57]. Simultaneous TGA, MS, and differential thermal analysis (DTA), were used. The presence of ammonium cyanate (NH<sub>4</sub><sup>+</sup>NCO<sup>-</sup>) was observed leading the author to conclude that reaction (R14) had occurred with ammonium cyanate as an intermediate by the detection of an ionic mass of 18 (NH<sub>4</sub><sup>+</sup>) post decomposition and immediately prior to a detection peak of mass 17 (NH<sub>3</sub>):



The presence of biuret and triuret was inferred and the onset of their decomposition was above 260 °C.

Elkanzi [64] gives a review of side reactions common in urea synthesis with elevated temperature (160-200 °C) and pressure (10-25 MPa). In this the following side reactions are considered:

1. Hydrolysis of Urea (R16), which is the reverse synthesis reaction, and as previously quoted for urease-catalysed decomposition. This is promoted by high temperatures and long residence times:



2. Biuret formation from urea (R17) occurs where urea concentration in the solution is high. This can be minimised with increased  $\text{NH}_3$  concentrations, but also by avoiding high temperature and long residence times.



Kinetic parameters of (R16) were assessed by Zanoelo [65], who found greatest accuracy in a method that resulted in a value of  $E_a = 61.36 \text{ kJ mol}^{-1}$  though with a large error range of  $\pm 20.86 \text{ kJ mol}^{-1}$ . Mahilik *et al.* [66], then reported the thermohydrolysis of non-catalytic semi-batch reactor experimentation of urea solutions from  $7 \leq \text{wt}\% \leq 40$ , up to  $160 \text{ }^\circ\text{C}$ , and calculated Arrhenius kinetic variables for (R16) of frequency factor ( $A$ ) =  $3.9 \times 10^6 \text{ min}^{-1}$ , and activation energy ( $E_a$ ) of  $59.85 \text{ kJ mol}^{-1}$ . These findings were based on refractive index analysis of urea conversion. They did not therefore involve product or residual composition analyses, which introduce error since the assumption is made that no reaction other than (R16) occurred.

Limited experimental range with respect to product analysis is common among current publications which have the objective of determining the extent of  $\text{NH}_3$  production for combustion-derived  $\text{NO}_x$  reduction systems. Therefore most of the recent work on urea thermolysis is limited in scope for elucidating the mechanisms involved in hydrogen production. Of relevance to urea steam reforming are some of the studies on aqueous urea thermolysis.

Lundström *et al.* [67] analysed the thermal decomposition of aqueous urea solution using DSC and FTIR. Only one type of urea aqueous solution was used; that being a 32.5 wt% urea in de-ionised water - a mixture sold commercially as Adblue for selective catalytic reduction of combustion emissions (see **Table 2-7**) - and only the gaseous products  $\text{NH}_3$  and  $\text{HNCO}$  were measured. In these experiments the solution was loaded into a reactor and a sweep gas of  $100 \text{ ml min}^{-1}$  was applied. Temperature range was between  $25 \text{ }^\circ\text{C}$  and  $700 \text{ }^\circ\text{C}$ . Maxima of ca. 650 ppm for  $\text{NH}_3$  and ca. 800 ppm for  $\text{HNCO}$  were reported. Calculations for their mass balances are not given, and it is not suggested whether any  $\text{N}_2$  was produced.

According to Koebel and Strutz [68], aqueous urea solution thermolysis progresses firstly via water evaporation:



then via urea decomposition (R19) giving equimolar products of  $\text{NH}_3$  and  $\text{HNCO}$ :



In water-rich solutions, further reactions then involve the creation of a second mole of  $\text{NH}_3$  via reaction (R20) as the isocyanic acid interacts with steam that has not yet evolved and/or it encounters coming through the feed flow:



It has been shown that (R20) proceeds quickly with temperatures above 400 °C [69], and rapidly in the presence of metal oxides with alumina identified as one of the most favourable [70]. Kleemann *et al.*, experimenting in a temperature range up to 500 °C, calculated an apparent  $E_a$  value for (R20) of  $\sim 13 \text{ kJ mol}^{-1}$  suggesting that it was limited by mass transfer control [70]. Yang *et al.*, also found very low activation energies ( $18.4 \text{ kJ mol}^{-1} \leq E_a \leq 26.1 \text{ kJ mol}^{-1}$  for (R20) at  $T > 250 \text{ °C}$  in the presence of zeolites [71].

Aqueous urea thermolysis flow reactor experiments have been studied using a weak urea aqueous solution (1.0 M) in a 93%  $\text{N}_2$  flow at atmospheric pressure up to 450 °C [69]. This study reported complete decomposition of urea into  $\text{NH}_3$  and  $\text{HNCO}$  above 350 °C for residence times longer than 0.1 seconds. It also confirmed that higher urea-derived product molecules were negligible, corroborating previous work reported by Krocher and Elsener [72].

The higher molecular compounds that form in pure urea thermolysis due to the retention of  $\text{HNCO}$  can also form in aqueous urea solutions. As water evolves first at 100 °C, urea-rich conditions have a propensity to occur. These polymers are easily suppressed however by designing for rapid sample heating and short residence times [72], as would occur in a flow reactor.

It is generally believed that urea does not enter a vapour phase, and that the vapours emitted on thermolysis are its product species. Where reference was found of urea being mentioned as having a vapour phase following thermal decomposition, this was either with theoretical modelling [73], or when the cited reference was pursued it was found that the citation had been quoted erroneously [69] citing [74]. This uncertainty is touched upon by Birkhold *et al.* who used computational fluid dynamics in order to elucidate the matter [62]. They concluded that water evaporates at a faster rate than urea resulting in increased urea concentrations and potentially incomplete decomposition particularly at temperatures below 300 °C.

### 2.7.3 Spontaneous Decomposition

Non-enzymatical decomposition pathways for urea have been identified and with these the presence of water is essential. For spontaneous decomposition the half-life times are estimated to be from 40 years at 25 °C for elimination, to  $\sim 10^{19}$  years for non-enzymatic hydrolysis [75]. This knowledge gives a measure of the proficiency of the



urease catalyst, and also indicates that a dry air environment should be maintained to preserve urea, necessitating storage systems that prevent moisture ingress.

Kinetic analyses have identified that the reason a solvent is required for standard temperature spontaneous elimination is that water lowers the activation energy and stabilises the products of urea decomposition [76]. This type of interaction between water and urea is not unique to just decomposition mechanics. Many of urea's properties that are utilised commercially are attributed to its presence in aqueous solution (see section 2.8.2). Computer modelling has shown that the hydrogen bonds in urea are weaker than the hydrogen bonds between water molecules thereby creating a tendency for urea to aggregate in solution and to influence the stability of water structure [77].

#### **2.7.4 Previous Reports of Urea Steam Reforming**

No prior reports of urea steam reforming for hydrogen production were found. The only previous account of steam thermolysis as a means of urea decomposition was with three test runs on an experimental set up with combined gasifier and reformer in the context of waste conversion with application to spacecraft occupancy [78]. This formed a minor part of waste thermolysis along with other substances, and did not measure hydrogen produced. The study did not give detailed values for energy requirements or reaction kinetics, though substantial uncatalysed decomposition of urea was qualitatively reported at low temperatures, with the main product being ammonia. Evidence of urea's low melting point was confirmed with the recording of volatisation post-gasification and prior to the reformer stage.

#### **2.7.5 Previous Reports of using Urea for Hydrogen and Energy.**

In 2009 a study reported that hydrogen can be produced from urea by electrolysis, using aqueous urea solutions replicating those found in urine [79]. In 2010, a direct urea fuel cell was reported [80] with the assertion that PEMFCs cannot be operated using urea fuels due to potential ammonia content. This statement fails to consider ammonia scrubbing methods. A novel approach to produce hydrogen from the wastewater of a urea production plant was reported in 2010. This modelled the feasibility of system design, using a nickel-alumina catalyst bed [81].

## **2.8 Production of Urea**

### **2.8.1 Present Industrial Synthesis**

Urea is a widely available market commodity with present commercial production plants operating on well-established technological methods. The chemistry of current manufacture is well documented and involves the combination of the reagents ammonia and carbon dioxide (CO<sub>2</sub>). This synthesis is called the Bosch-Meiser process and

proceeds according to the Basaroff reactions at heightened pressures of 13-25 MPa and temperatures of 170 – 200 °C [49]:



The reagents for R21 and R22 are obtained by the steam reforming of fossil fuels (usually natural gas; although naphtha, fuel oil and coal are alternative feedstocks) to yield hydrogen and then ammonia using  $\text{N}_2$  from air over iron catalysts. The process of ammonia production (Haber-Bosch), at high temperatures and pressures, also creates  $\text{CO}_2$  and consequently commercial urea production is undertaken adjacent to ammonia production plants.

At operating conditions, (R21) using liquid-phase  $\text{NH}_3$  and  $\text{CO}_2$  to form ammonium carbamate is fast and complete. Both reactants are in their supercritical states and no catalysts are involved due to the high corrosivity of the ammonium carbamate containing mixture. Reaction (R22), carbamate dehydration, occurs at lower pressure, is slow, and never results in complete conversion of reactants.

Processing of the effluent from (R22) is where present production methods differ, with either the un-changed products being utilised in downstream processing to create by-product commodities of nitric acid and ammonium salts (“once-through systems”), or re-cycled to increase percentage urea conversion (“total-recycle systems”). With total recycle, a 99 % conversion to urea can be achieved [82] either separating the reactants by scrubbing with a solvent or passing the solution through a stripper which reduces the concentrations of either  $\text{NH}_3$  (Snamprogetti process) or  $\text{CO}_2$  (Stamicarbon process, or Toyo-ACES process). Total recycle processing therefore requires additional energy, of which all have similar requirements but produce a higher urea yield [83].

In its product form, urea is supplied as required according to grade in either liquid, crystalline, or as solid agglomerate (prills or granules). Prills and granules are produced for fertiliser applications as this form allows for efficient and flexible utilisation. Reagent grade urea can be over 99 % pure according to manufacturing specifications. Trace elements are ubiquitously present through contamination with process piping or from the original feedstocks [84] which may necessitate further processing prior to steam reforming for fuel cell applications in order to protect catalyst and fuel cell component integrity. The chemical composition of the reagent grade urea used in this project is given in **Table 2-6**.

**Table 2-6.** Urea reagent composition using in experimentation. Purchased from Fisher Scientific (U/P610/50).

Product Specification	Composition (wt%)
Urea	> 99.5 %
Insoluble (5M aq. sol)	< 0.005 %
Cadmium	< 0.5 ppm
Cobalt	< 0.5 ppm
Copper	< 0.2 ppm
Iron	< 0.2 ppm
Lead	< 0.5 ppm
Magnesium	< 0.2 ppm
Potassium	< 5 ppm
Total chloride	< 5 ppm

### 2.8.2 Production Status and Trends

Demand for urea is high with an increase of 3.8 % per annum anticipated, giving an annual total demand of 174.6 Mt by 2014 [85]. Production plant capacity is expected to grow by 51.3 Mt or 30 % from 2009 levels to an estimated global production of 222 Mt by 2014 [85]. 55 new production plants are expected to open, with the major regions of production being Asia, Latin America and Africa. There are no longer any production plants in the UK and all commercially manufactured urea is imported [86]. Due to the expansion in global production the supply/demand balance shows an anticipated rise in surplus from 3 Mt per year in 2010 to 10 Mt per year in 2014 [85].

Urea's main commercial application is as a slow release fertiliser. In the 1960s, it represented 5 % of global fertiliser consumption which had increased to ca. 40% by the early 1990s [87] and is now estimated at >50 % [88]. Urea is now also the primary means of NO<sub>x</sub> abatement in > 2.0 litre diesel engines where it is employed as a selective catalytic reductant [89]. Usually this involves an aqueous solution of the eutectic mixture at 11 °C and 32.5 wt% [84]. The values quoted for urea product growth are inclusive of non-fertiliser product applications. Non-fertiliser demand is anticipated to account for 13 % of the total usage by 2014. New uses for urea are increasing and some present applications are shown in **Table 2-7**. These new markets, plus the potential for urea as a hydrogen carrier could provide the lever for future sustainable urea production which will be discussed in section **2.10**.

**Table 2-7.** Present applications of urea.

Use	Description
Slow-release fertiliser	Main commercial outlet. 85-90% of commercial application [88]. Agricultural grade flakes or prills.
Explosives additive	A propellant stabiliser in nitro-cellulose explosives [90].
Reagent in catalytic reactions to reduce oxides of nitrogen.	Urea reacts with NO <sub>x</sub> and is utilised for the catalytic and non-catalytic reduction of combustion gasses to mitigate pollutant emissions [84].
Pharmaceuticals/Medicine	Used to make emollient creams for treatment of dry skin due to its water-binding capacity and softening effects on the epidermis [77, 91]. It is also used to detect the presence of pathogenic bacteria in the stomach [92].
Animal feed additive	As an inclusion in cattle feed to aid the assimilation of proteins [93].
Material in glue manufacture	Urea-formaldehyde and urea-melamine-formaldehyde (waterproof glue for marine plywood) [94].
De-icer	Urea is a non-corrosive alternative to sodium chloride as a de-icer [95].
Cosmetics ingredient	In antiperspirants, a preservative in water-based soaps, and in moisturisers and skin creams [96].
Cloud seeding agent	Due to its hygroscopic, non-toxic and non-corrosive properties [97].
Petroleum processing	Urea has the ability to form clathrates and occlude hydrocarbons; used in petroleum refining to produce jet aviation fuel and for de-waxing of lubricant oils [47].
A flame-proofing agent in dry fire extinguishers	Urea-K bicarbonate is a dry powder extinguisher for flammable liquids, ordinary combustibles, and electrical fires [98].
Ingredient in dental products	Carbamide peroxide for bleaching [99]. Urea also has pH-elevation properties that make it effective at neutralising acidic plaque [100].
Food additive	Formulation of alcoholic beverages, and gelatine [101].
Dispersion and degradation of hydrocarbon oil spills	Stimulates the growth of bacteria which break-up the oil [102, 103, 104].

### **2.8.3 Economics of Present Production**

Present commercial urea production is energy intensive and its economic cost is linked to the price of its feedstock Natural Gas. Any consideration of environmental and economic factors must also include creation of the raw materials ammonia and carbon dioxide. Ammonia production is estimated to contribute ca. 80 % of the total manufacture cost for present urea production [84]. Transport costs are taken as nil since ammonia plants are sited adjacent to urea production. Current values of technical grade urea in the quarter up to April 2010 were €160 - €214 per tonne [105].

## **2.9 Environmental Impact of Urea**

### **2.9.1 Environmental fate of Urea**

Urea is biodegradable and classified as having “no indication of concern for human health or the environment” [106]. Long-term human exposure studies have also indicated that it is non-allergenic and virtually free of side effects [106]. Biodegradation is rapid upon contact with soil and water due to the presence of the enzyme urease (urea amidohydrolase), and urea is reported as being unlikely to undergo bio-accumulation [106]. Toxicity studies have indicated that only with levels above several thousand mg/litre may it become toxic to mammals and birds, with low levels of ingestion permissible without ill effect [84, 106].

Urea is excreted by fish, amphibians, zooplankton and bacteria [50, 51, 52, 53, 107] and it is therefore naturally present in balanced water ecosystems, both in the water column and also in sediments. Its presence, transport and dynamics are not well understood, and along with other reduced nitrogenous compounds, these substances comprise the least known parts of the nitrogen cycle [108].

There has been recent work attempting to assess the environmental role of urea with some authors having concerns that with the present global scale of urea production and applications, its usage could have adverse ecosystem effects [109]. The basis for this conjecture is due to scientific evidence reported on other artificial fertiliser applications being responsible for a large influx of nitrogen (along with other elements such as phosphorous and sulphur) that consequently disturb naturally balanced ecology. Nutrients containing these elements have been shown to cause the onset of eutrophication in water bodies where excessive compound leachate from soil has led to an increase in primary production, oxygen depletion and aquatic mortality [110, 111]. It is this that has been proposed as a potential cause for concern about the escalating use of urea and agricultural urease inhibitors that slow down its hydrolysis [109]. The proponents of these hypotheses concede that causal links with anthropogenic sourced urea driving any ecosystem change have yet to be established and that there are many

other factors that affect algal bloom dynamics [109]. Furthermore, where in-situ studies of urea influx on coastal waters and shorelines have been performed, results refute suggestions of harmful environmental disturbance. Evidence of this comes from two sources; firstly with bioremediation applied to the Exxon Valdez oil spill in 1989, a summary of which can be found in publications by Bragg *et al.* [102], and Pritchard and Costa [103]. This application of urea to the Alaskan shoreline was independently monitored for eutrophication by sampling ammonia concentration, chlorophyll bacteria and primary production, along with potential toxicity caused by degradation products and no such adverse ecological effects were observed [103]. A PhD thesis from 1980 looked at the distribution of urea in coastal waters and found no evidence to indicate that land-derived urea was an important contributor to oceanic urea concentration, with the major source likely to be from in-situ production [112].

The increase in urea production seems therefore to be at the expense of more environmentally damaging substances which would undoubtedly be used in the absence of urea for anthropogenic crop fertilisation. Naturally occurring nitrogen is only considered capable of supplying half the present global agricultural need, and this does not take into account predicted future population growth or changing food preferences that might require higher fertilisation rates [87]. Taken in comparison with other nitrogenous fertilisers and indeed many of its other commercial applications, urea is chosen because it is a stable and less toxic alternative. With fertiliser use, although soluble in water, urea hydrolyses relatively quickly and is taken up by plants rapidly thus minimising nitrogenous leachate to water and ammonia volatilisation [55].

### **2.9.2 Environmental Aspects of Present Production**

Due to stringent safety emissions legislation and the high commodity cost, direct losses of urea and ammonia to the environment from industrial production is relatively small [108]. The synthesis section of a modern urea plant will create wastewater in a ratio of 0.3:1 for every unit of urea produced [88]. On the level of present production plants creating 2000 tonnes of urea per day, these large amounts of water must be treated to comply with local legislation and to moderate adverse environmental impact. Urea process water treatment systems therefore are able to reduce the effluent by desorption, distillation and stripping to create effluent  $\text{NH}_3$  and urea concentrations of 5 mg/litre and 1 mg/litre respectively [88].

Gaseous emissions have been estimated for a urea processing plant and are given in **Table 2-8**. These include total production costs for natural gas processing and electricity consumption.

**Table 2-8.** Life Cycle Greenhouse Gas Emissions from Urea Production Plant [84].

Emissions (grams per tonne of urea)		
CH <sub>4</sub>	N <sub>2</sub> O	CO <sub>2</sub>
6,428	10	746,797

Airborne particulate emissions from urea production plants are potentially high because prilling generates very fine dust which is technically difficult and expensive to mitigate. Granulation dust emission is considerably higher at 5-40 kg per tonne of urea produced [88], but its larger particle size decreases its health risk and increases its ease of abatement. Wet scrubbing is identified as the optimum particulate abatement method and efficiencies of 98 % can be achieved [88]. Emissions of this kind (though effectively abated) are related to process shaping requirements for agricultural fertiliser products and so should not be relevant in the context of reagent purity grade used for application to a potential hydrogen economy. Where airborne urea particles are released, a half-life of less than a day is expected due to photochemical reaction with hydroxyl radicals resulting in ammonia and carbon dioxide [84].

## 2.10 Alternative/Sustainable Routes of Urea Production

It has been described that urea is manufactured, at present, cheaply using fossil fuels, so attractively enabling rapid implementation for hydrogen supply infrastructure. As this does not offer long-term supply security and is environmentally damaging, this section identifies and assesses potentially sustainable production routes. These would also detach production from the need for adjacency to hydrocarbon reserves allowing global energy independence. Furthermore it would reduce overall processing as presently hydrogen has to be created and then re-formed into urea to be re-formed back to hydrogen again. An illustration of the potentially available urea resource is given in **Figure 2-2**.

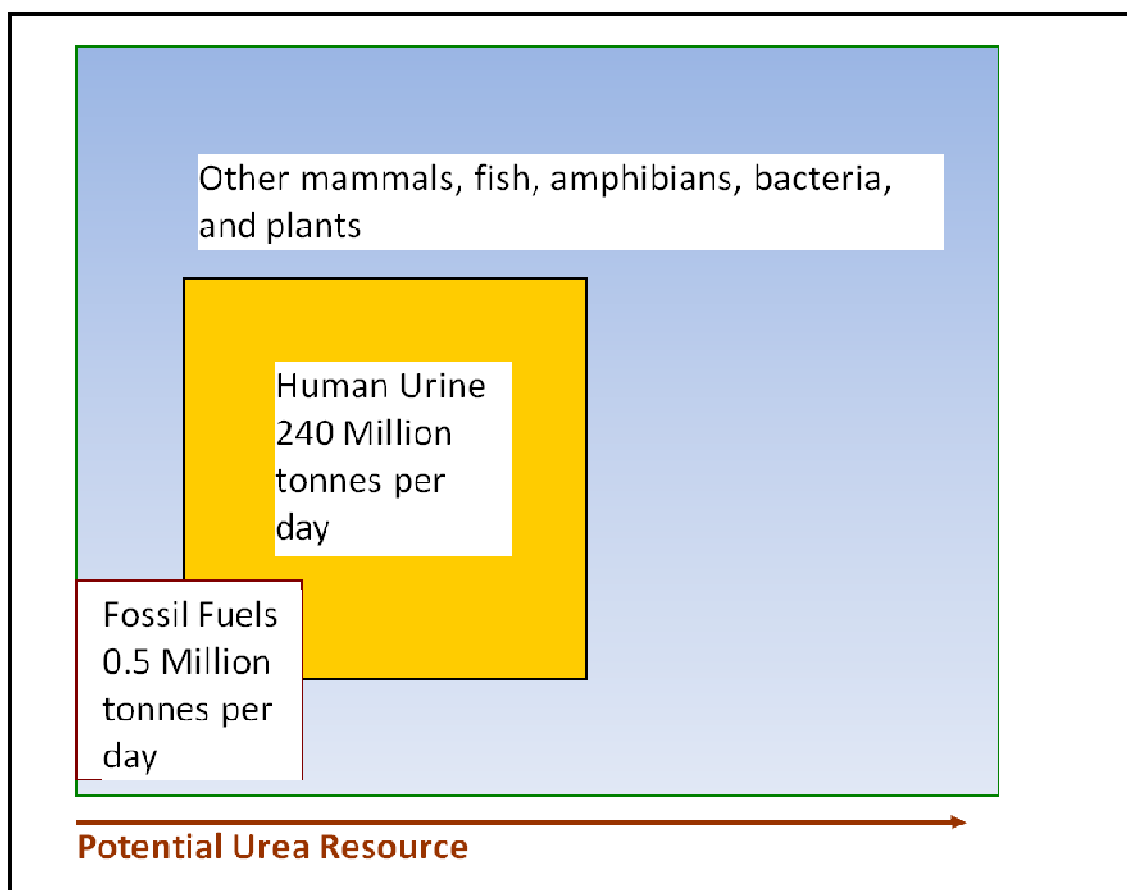


**Figure 2-2.** Potential global urea resource. Human urine resource estimated from average daily production of 35 g [113] multiplied by world population of 6.8 billion.

### 2.10.1 Urea from Urine

Large quantities of urea are produced to fertilise land for food production, yet at the same time, the natural quantities of urea produced by catabolism in urban areas, are flushed away through wastewater sewage systems; a process which then involves the additional expense of energy intensive methods of removing nitrates that would otherwise have completed a closed nitrogen cycle by being utilised in plant metabolism. The mammalian catabolic route of urea synthesis is both abundant and well understood yet there is little written about the scope for exploiting this natural route and obtaining urea from urine.

Medical texts quote that urea is excreted (quantified and termed as urea “clearance”) in urine at a rate of approximately 33-35 g day<sup>-1</sup> in a healthy adult, dependent on diet - with concentration increasing with increasing dietary protein intake [113]. For an estimated average adult, the urine excretion rate is 1.5 litres day<sup>-1</sup> [114] giving an approximate concentration of urea as 22-23 g litre<sup>-1</sup>. It can be assumed however that these values based on medical estimates will differ outside of the clinical



environment due to dilution and contamination with other elements when mixed with flushing water in a modern sanitary system [115]. Of more importance is the fact that urea decomposes quickly outside of the non-sterile environment due to the ubiquitous presence of enzymatic micro-organisms. A study in 2003 identified that urine in a collection tank would be completely hydrolysed within little more than a day, and for a supply pipe completely filled with urine, ureolysis would be completed in about two minutes [116].

Before attempts can be made to stabilise urine and extract urea, the urine must first be separated from faeces and any other components presently disposed of in wastewater. Separation will be easier if urine is not well mixed with other contaminants, and due to the extended residence times in wastewater, providing adequate mixing with urease containing bacteria, end of pipe treatments for urea collection would appear to be too challenging. Similarly, the collection, and preservation of urea from animal wastes would pose identical difficulties through mixing with other contaminants. A patent from 2005 however cites as one aspect of its invention the proposal of separating urine from livestock waste into a urea-rich fraction having the potential to be a saleable commodity [117]. The methodology of this patent is not detailed but involves the use of urease inhibitors to stop ureolysis and subsequent decomposition.

Urease inhibitors are not a new discovery. Several microbial urease inhibitors are known along with a number of chemical elements and compounds [118]. These microbes are widespread, and the high concentration of carbon in urine also accentuates their growth [114].

Biological catalytic decomposition of a urea solution occurs at an optimum neutral pH but causes it to rise to 9.5 at which point ammonia evaporates from the mixture [114]. It is known that below pH 5 microbial urease is denatured [116]. The acidification of urine is therefore the major research method of urease inhibition. In tests, the addition of sulphuric or acetic acid could inhibit urea decomposition for over 100 days [119].

Studies into the separation and stabilisation of urine come mainly from the perspective of wastewater treatment. Most of this is driven by environmental concerns with the focus on sustainability, reducing waste, and mitigating nitrate build up in watercourses. There is also a focus on the possibility of utilising nutrient components of separated urine for fertiliser applications, but not specifically urea. The preservation of pure urea is occasionally mentioned, but then only as a minor aspect and consequence of the main study.

Modern attempts at urine separation and stabilisation have yet to go beyond the research and development stage. Source separation “no-mix” toilets have been created and tested. In one project application the results were disappointing, with dilution and

contamination of the urine occurring. This was attributed to a combination of inadequate system design and construction, plus inappropriate usage [120].

In space station environments, urine can be acidified to inhibit urease activity then subjected to distillation and filtration [121]. Again this research was with the objective of volume reduction and hygienation rather than the isolation and extraction of urea. One recent publication revealed that as a consequence of attempting to separate pharmaceutical pollutants from urine by the use of a nanomembrane, urea was found to permeate on the membrane in relatively high yields [122]. Once more this result was reported as a side issue and not the main focus of the research.

The potential to extract urea in sufficient quantity from mammalian waste to offset some of the present commercial stock therefore seems a long way from reality. The resource is available, and the chemistry is in the most part understood, but it seems that not enough work is being done at present to adapt technology that is fit for purpose, and the required paradigm shift in modern waste removal seems to be too dramatic a step. A summary of these findings are illustrated in **Figure 2-3**. Drivers for change such as increasing prices of fossil fuels, depletion of resources, and uncertainty of supply, coupled with concerns about environmental damage caused by additions to the nitrogen budget, are however becoming increasingly prominent. If urea was shown to be a promising hydrogen carrier then this would undoubtedly generate interest in combining this knowledge to tap the huge waste resource.

Process Stage	1.Source Separation	→	2.Urease Inhibition	→	3.Urea Concentration
Solution	No-mix toilets for humans	→	Chemical, Microbial and Temperature	→	Solar, wind and battery/grid electrical
Status	Simple Technology Product Designed Product Implemented	→	Simple technology Currently applied in laboratories	→	Electrical heaters are a mature technology. Solar concentrators not known as being applied in this situation
Obstacles	Paradigm shift in waste disposal required.	→	Would need incorporating into no-mix toilet design due to rapid enzymatic decomposition of urea	→	Prolongs process stages.
Further Observations	Considerably greater resource from animals and plants. Animal sourced urea more challenging to separate. Absence of adequate knowledge on urea content in plants.	→	May require further sterilisation for safe handling to remove potential pathogens.	→	Solar concentrators, combined with urea's ease of transportation and storage make this combination highly attractive for remote applications

**Figure 2-3.** Status of technology and process stages necessary for utilising the urea produced by animals and plants in preparation for steam reforming.

### 2.10.2 Urea from Bacteria

Arginine is a ubiquitous amino acid, found in most organisms, throughout all biological kingdoms [123]. Those that also contain the arginase enzyme are able to synthesise urea.

In ureotelic organisms (mainly mammals and marine fish) urea is created *in vivo* by the catalytic hydrolysis of the amino acid arginine in the presence of the enzyme arginase. This mechanism is part of the ornithine-urea cycle (or Krebs-Henseleit Cycle) which involves four other enzymes along with the intermediate amino acids citrulline and aspartate [124]. Arginase is the key enzyme in the stage of the cycle that creates urea [123]. Bacteria are able to catabolise arginine [125] and it has been shown that urea can also be created *in-vitro* using the arginase enzyme [126]. It therefore follows that if a cost effective and abundant source of arginine could be found then an alternative route of urea production is theoretically achievable (see **Figure 2-4**).

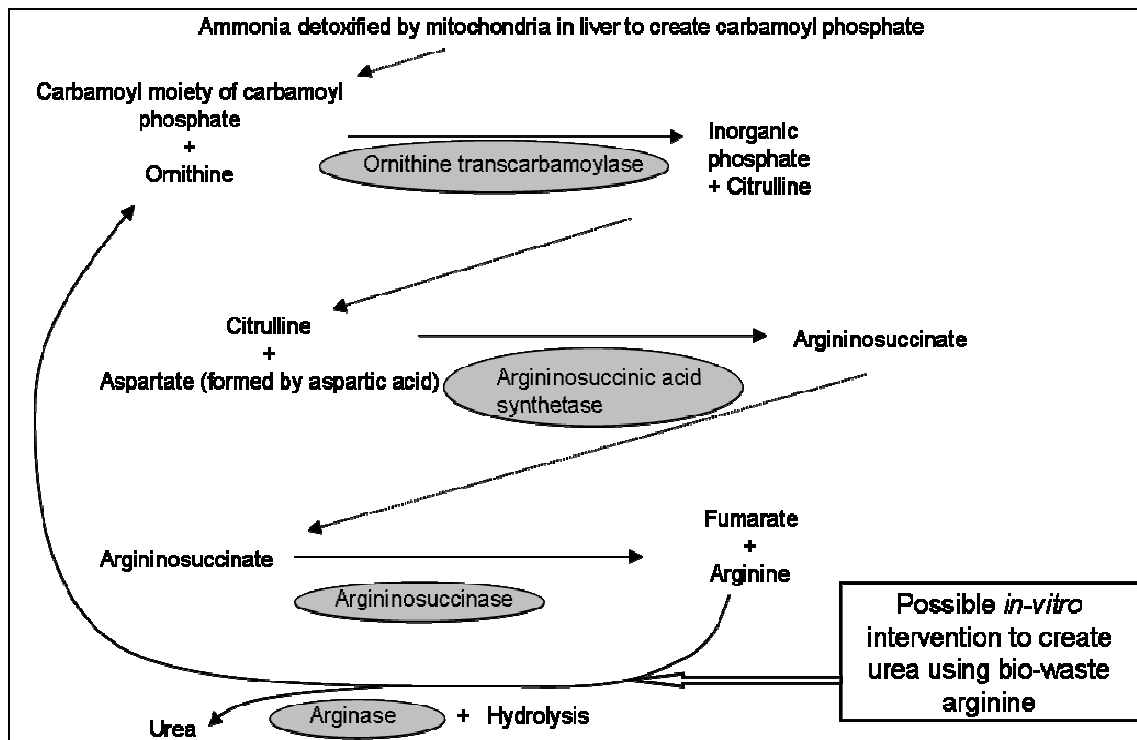


**Figure 2-4.** Ornithine-urea cycle in ureotelic organisms showing possible *in-vitro* mechanism for urea production.

One naturally-occurring source of arginine is in cyanophycin (Cyanophycin Granule Polypeptide: CGP). Cyanophycin is an organic granule that is synthesised in and used as an energy store by cyanobacteria [127, 128] and some heterotrophic bacteria [129] at relatively low temperature and light intensity. The cyanophycin synthelase enzyme has also been isolated and inserted into genetically modified recombinant

bacteria. These have subsequently been tested on different ferment media [130]. A patent was submitted by Elbahloul *et al.* in 2006 [131] to make use of this microbial synthesis using bio-refinery waste streams as a substrate for fermentation.

Biomass has ecological advantages since the CO<sub>2</sub> released by combustion is only that which the plant has captured during its lifetime. Theoretically therefore biomass is “carbon-neutral”, and does not add to the atmosphere in the same way as fossil fuels. Moreover, there is presently a large volume of protein-rich waste streams that are generated with biofuel production and in established bio-refineries such as starch fractionation from wheat, sugar and potatoes and oil, proteins and nutraceuticals from soyabeans [132, 133]. These amino-acid wastes have financial advantages since their calorific values are reportedly comparable with presently used petrochemical feedstocks, and furthermore they have in-built chemical functionality that could allow the circumvention of some or all of the process stages [133]. Using biomass in this way could be a more efficient use of inherent chemistry than for the production of power which is biomass’ present commodity outlet. Biological fermentation is one possible route of isolating these functional compounds for utilisation.

In Elbahloul’s study, a 28 wt% yield of cyanophycin was produced per dry cell matter within 24 hours using a potato starch waste stream of which an estimated 22,000 tonnes of amino acid are created every year. Present knowledge gaps occur on how to extract urea in useable form from bio-fuel ferment CGP, and also with the optimisation of substrate media and conditions. One interesting result from the study by Elbahloul *et al.* was that the ferment apparently synthesised CGP from amino acids other than arginine. This, and the opportunity to isolate other synthetase enzymes for insertion into genetically modified bacteria, is an area that requires further examination.

A study in 1984 also found that urea could be synthesised from arginine using inorganic montmorillonite clay particles as a shape selective catalyst [134]. This result does not appear to have been pursued since then.

## 2.11 Conclusions

Urea possesses many favourable attributes as a fuel cell energy vector to justify further study on its use for hydrogen supply and to fill the need of future global energy requirements. Compared with present hydrogen carrier chemicals, urea is stable, non-toxic and in most circumstances can be described as environmentally benign. The only controls required for adequate storage would be dry containment due to its hygroscopic nature and ease of decomposition in the presence of water, unless urease inhibitors were incorporated. Like the other simple chemical hydrogen vectors, urea is a well known and understood compound. A benefit of having half a century of commercial urea

production means that there is a good understanding of knowledge to draw upon for working with urea as a process chemical. The transferability of this knowledge is definitely a boon.

Urea decomposes relatively easily with heat and at room temperature with enzymes. This review has identified that there are possibilities that urea might initially be suitable for supplying  $\text{NH}_3$  either directly into fuel cells or as an intermediate for hydrogen evolution. Many of the advantageous aspects of the recently developed metal ammine storage tablets could also be said of urea. These comparisons and therefore the potential for urea as a similar stable and dense ammonia/hydrogen carrier do not appear to have so far been made. In comparison, pure urea has a lower hydrogen weight percentage (6.7 wt%) but this value increases to 7.7 wt% when steam reforming is considered.

Urea is a cheap and readily available substance. The resource of urea is high, with production increasing and an annual surplus expected for the near future based on fossil fuel synthesis. Present manufacture of urea releases quite high greenhouse gas emissions which is not sustainable. Also, with this manufacturing process, as with many other hydrogen carrier options, hydrogen is a reagent in the synthesis reaction meaning it is extracted from other substances to be made into urea to be released again. To overcome this problem, urea does have many varied natural production routes that have been combined and discussed in this review for the first time in the context of using them as an alternative source of urea for energy. Based on this assessment, it is considered realistic that these routes could be exploited if they are given sufficient focus of research attention.

## 3 Thermochemical Equilibrium Modelling

### 3.1 Objectives

Equilibrium modelling was used to ascertain the feasibility of urea steam reforming and then to help identify potentially optimum operating conditions. Modelling was also used to explore reactor design by observing changes in syngas equilibrium products with varying diluent flow rates and fuel feed rates. Throughout the reactor experimental work, modelling was used to assess process performance by applying the same variables used for experimentation to modelling and comparing the results. Consequently, in addition to the presentation of modelling results in this chapter, they are also presented in comparison with experimental results in Chapter 5 and Chapter 6. To assess the economics of urea steam reforming, calculations were made to determine total energy requirements per mol of hydrogen ( $H_2$ ) produced at a range of temperatures and reactant fraction variables.

### 3.2 Method

#### 3.2.1 Conditions of Simulation

Equilibrium calculations were performed using EQUIL in CHEMKIN software [135]. This allows the user to input a range of reactants, temperatures and pressures then, once running, accesses thermochemical data libraries to calculate and generate equilibrium outputs. The model considers the distribution of the number of moles of each species which in total minimises the system Gibbs free energy at the set state parameters of temperature and pressure using STANJAN routines [136]. The results provide values of gas phase concentrations at equilibrium in addition to reaction enthalpy for a range of temperatures.

EQUIL in CHEMKIN was programmed to run with the following chemical species:  $CH_4$ ,  $CO$ ,  $CO_2$ ,  $O_2$ ,  $H_2O$ ,  $H_2$ ,  $N_2$ ,  $NH_2$ ,  $NH_3$ ,  $CH_4N_2O$  (urea),  $Ar$ ,  $HNCO$  and  $HCN$ . The model was also tested with:  $HCO$ ,  $HOCN$ ,  $H_2CN$ ,  $HCN$ ,  $HNO$ ,  $N_2H_2$ ,  $N_2O$ ,  $HCNO$ ,  $H_2NO$ ,  $NO$ ,  $NO_2$ , but these were ultimately eliminated from the program input files as their product fractions were deemed negligible. Negligibility was defined as product concentrations  $< 10^{-9}$  mol fraction in the wet syngas at equilibrium. Reaction temperatures were set to a range between and including 300 K to 1280 K (27 °C to 1007

°C) for all analyses with output values obtained for every 10 K interval within this range.

### 3.2.2 Products at Equilibrium

Reactant water to urea molar ratio (S:C) was input in the range  $0.1:1 \leq S:C \leq 8:1$  at atmospheric pressure with a range of diluent concentrations from zero to 84 %. Diluents of N<sub>2</sub> and argon (Ar) were used to simulate the presence of process carrier gas. Thermodynamic equilibrium was also modelled at increased pressure up to a maximum of 20 atmospheres, this being identified as the maximum quoted in literature for methane steam reforming [10].

Following each programmed EQUIL in CHEMKIN run, results were used to generate further data using the following terms, where  $i$  = chemical species,  $N_{out}$  = total number of moles out,  $N_{in}$  = total number of moles in (this is always = 1), and  $x$  = mole fraction:

$$\text{Steam conversion} = \frac{(x_{H_2O,in})(N_{in}) - (x_{H_2O,out})(N_{out})}{(x_{H_2O,in})(N_{in})} \quad (\text{Eq. 1})$$

$$\text{Urea conversion} = \frac{(x_{urea,in})(N_{in}) - (x_{urea,out})(N_{out})}{x_{urea,in}} \quad (\text{Eq. 2})$$

$$\text{Hydrogen yield} = \frac{(x_{H_2,out})(N_{out})}{(x_{H_2O,in})(N_{in}) + 2(x_{urea,in})(N_{in})} \quad (\text{Eq. 3})$$

$$\text{Hydrogen yield per reactant urea} = \frac{(x_{H_2,out})(N_{out})}{(x_{urea,in})(N_{in})} \quad (\text{Eq. 4})$$

Carbon selectivity for species CO, CO<sub>2</sub>, and CH<sub>4</sub>

$$\text{Sel}_{\text{Ceq}} = \frac{x_{i,out}}{x_{CO,out} + x_{CO_2,out} + x_{CH_4,out}} \quad (\text{Eq. 5})$$

Hydrogen selectivity for species H<sub>2</sub>, CH<sub>4</sub>, NH<sub>3</sub> and NH<sub>2</sub> (plus if steam conversion is negative then H<sub>2</sub>O is also a product)

$$\text{Sel}_{\text{Heq}} = \frac{x_{i,out}}{x_{H_2,out} + x_{CH_4,out} + x_{NH_3,out} + x_{NH_2,out} + x_{H_2O,out}} \quad (\text{Eq. 6})$$

Dry corrected syngas (the syngas product mole fraction excluding water and diluent) for species  $i$

$$= \frac{(x_{i,out})(N_{out})}{(N_{out})(1 - x_{H_2O,out}) - (x_{diluent,out})(N_{out})} \quad (\text{Eq. 7})$$

All references to syngas in the Products at Equilibrium section relate to a dry corrected syngas. Wet syngas H<sub>2</sub> is discussed in section 3.3.2.2.



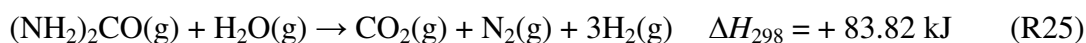
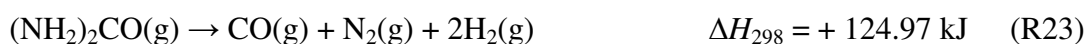
### 3.2.3 Thermochemistry

Calculations were devised to determine the energy needed to produce one mol of hydrogen gas by reforming of urea with steam for various reactant mixtures. An assessment of the energy required for each component in the overall process was also determined, including the energy for different types of carrier gas. Change in energy was calculated in terms of the state function Enthalpy ( $H$ ) = energy at constant system pressure.

#### 3.2.3.1 Stoichiometric Calculations

##### Step1) Reaction Enthalpy

Product concentrations at optimum temperatures from both EQUIL in CHEMKIN modelling (see section 3.3.1) and experimentation (Chapter 6 and Chapter 7), gave corroborative results for a global urea steam reforming reaction (R25). This was seen as potentially yielding two moles of  $H_2$  via decomposition, as illustrated in reaction (R23), then with the involvement of steam, a further mole of  $H_2$ , as in reaction (R24) was provided, showing that the stoichiometric steam to carbon ratio is 1:1 (R25):



The above reaction enthalpy ( $\Delta H_r$ ) values were obtained by summation of the constituent's molecular enthalpy of formation ( $\Delta H_f^\circ$ ). These values for  $\Delta H_f^\circ$  are shown in **Table 3-1**.

**Table 3-1.** Values for molecular enthalpy of formation [137].

Molecule	$\Delta H_f^\circ$ kJ mol <sup>-1</sup>
NH <sub>3</sub>	-46.1
CO <sub>2</sub>	-393.5
H <sub>2</sub> O (g)	-241.82
H <sub>2</sub> O (l)	-285.83
CH <sub>4</sub>	-74.6
CO	-110.53
HNCO	-101.67
Urea (s)	-333.1 (±0.69)
Urea (g)	-235.5 (±1.2)

The value of reaction enthalpy for (R25) at heightened temperature was obtained using a variation of Kirchhoff's Law [138]. This is shown as (F1), where  $T_2$  = final temperature,  $T_1$  = initial temperature (25.15 °C),  $\nu$  = species stoichiometric co-efficient. The values of  $\Delta H_{\text{sens}}$  in (F1) were calculated from Step 2.

$$\Delta H_{T_2} = \Delta H_{T_1} + \sum_{\text{PRODUCTS}} \nu(\Delta H_{\text{sens}})_{T_2} - \sum_{\text{REACTANTS}} \nu(\Delta H_{\text{sens}})_{T_2} \quad (\text{F1})$$

For the purposes of rigour, (F1) was tested by comparison with Kirchhoff's law using (F2), where  $C_p$  = species constant pressure heat capacity was calculated using formula (F3), and values contained in **Table 3-3**:

$$\Delta H_{T_2} = \Delta H_{T_1} + \left( \sum_{\text{PRODUCTS}} \nu(C_p)_{T_2} - \sum_{\text{REACTANTS}} \nu(C_p)_{T_2} \right) (T_2 - T_1) \quad (\text{F2})$$

$$C_p = A + Bt + Ct^2 + Dt^3 + E/t^2 \quad \text{where } t = T/1000 \quad (\text{F3})$$

### Step 2) Sensible Enthalpy

Urea sensible enthalpy ( $\Delta H_{\text{sens}}$ ) was calculated independently by the integration of  $C_p$  using a polynomial formula provided by the EQUIL program (F4). The variables used for calculating ( $\Delta H_{\text{sens}}$ ) via (F4) are shown in **Table 3-2**.

$$\Delta H_{\text{sens}} \text{ for urea} = \int_{H_{T_1}}^{H_{T_2}} C_p dT \quad (\text{F4})$$

Where  $C_p = (R)(A) + (R)(B)(T) + (R)(C)(T^2) + (R)(D)(T^3) + (R)(E)(T^4)$ ;  $H_{T_1}$  and  $H_{T_2}$  are as stated for (F1); and  $R$  = universal molar gas constant (8.314 J K<sup>-1</sup> mol<sup>-1</sup>).

**Table 3-2.** Values used to calculate urea sensible enthalpy [139].

Temp	-73 to 727 °C	727°C to 5727 °C
A	-0.210707501	1.03E+01
B	0.043694861	8.95E-03
C	-4.60608E-05	-3.10E-06
D	2.36548E-08	4.90E-10
E	-4.42051E-12	-2.89E-14
F	-29419.8537	-3.20E+04
G	26.0661959	-2.70E+01

Sensible enthalpy values for H<sub>2</sub>O, N<sub>2</sub>, H<sub>2</sub>, Ar and CO<sub>2</sub> were calculated using formulae provided by NIST [137]. Polynomial functions provided data on sensible enthalpy using formula (F5) and variables contained in **Table 3-3**.

$$\Delta H_{\text{sens}} = At + Bt^2/2 + Ct^3/3 + Dt^4/4 - E/t + F - H \quad \text{where } t = T/1000 \quad (\text{F5})$$

**Table 3-3.** Values used to calculate reactant and product species  $\Delta H_{\text{sens}}$  and Cp [137].

	CO <sub>2</sub>	Ar	H <sub>2</sub> O	H <sub>2</sub>		N <sub>2</sub>	
	≤5727°C	≤5727°C	≥227 °C	25-727°C	≥ 727°C	25-227°C	≥227 °C
A	24.9974	20.7860	30.0920	33.0662	18.5631	28.9864	19.5058
B	55.1870	0.00000	6.83251	-11.3634	12.2574	1.85398	19.8871
C	-33.6914	0.00000	6.79344	11.4328	-2.85979	-9.64746	-8.59854
D	7.94839	0.00000	-2.53448	-2.77287	0.26824	16.6354	1.36978
E	-0.13664	0.00000	0.08214	-0.15856	1.97799	0.00012	0.52760
F	-403.608	-6.19735	-250.881	-9.98080	-1.14744	-8.67191	-4.93520
G	228.243	179.999	223.397	172.708	156.288	226.417	212.390
H	-393.522	0.00000	-241.826	0.00000	0.00000	0.00000	0.00000

### Step 3) Reactant Latent Heat

Latent heat of urea sublimation was taken as  $\Delta H_{\text{sub, UREA}} = 97.6 \text{ kJ mol}^{-1}$  at 133 °C [137]. This value was applied to all S:C mixtures modelled at temperatures  $T \geq 133 \text{ °C}$ . Latent heat of vaporisation of water was taken from literature as  $\Delta H_{\text{vap, H}_2\text{O}} = 40.6 \text{ kJ mol}^{-1}$  at 100 °C [137]. This value was applied to all S:C mixtures modelled at temperatures  $T \geq 100 \text{ °C}$ .

### Step 4) Excess water from S:C Ratios

Since water and urea mixtures of  $1:1 \leq \text{S:C} \leq 7:1$  were considered, an extra calculation to account for the energy input for water above the stoichiometric amount (R25) was required. This was obtained by multiplication of the combined energy for the water component obtained in Steps 2 and Step 3 ( $\Delta H_{\text{vap, H}_2\text{O}} + \Delta H_{\text{sens H}_2\text{O}}$ ) with the S:C of the reactant mixture to give a total energy component for the vaporisation of water and heating to the desired reaction temperature:

$$\Delta H_{\text{total, H}_2\text{O}} = (\Delta H_{\text{vap, H}_2\text{O}} + \Delta H_{\text{sens H}_2\text{O}})(\text{S:C}) \quad (\text{F6})$$

### Step 5) Total Energy

Combining the formulae in Step 1 through to Step 4, gave a formula for the total energy required for urea steam reforming at constant pressure and volume:

$$\Delta H_{\text{total}} = \Delta H_{\text{r}} + ((\Delta H_{\text{sens, H}_2\text{O}} + \Delta H_{\text{lat, H}_2\text{O}})(\text{S:C})) + \Delta H_{\text{sub, UREA}} \quad (\text{F7})$$

### Step 6) Standardisation for 1 mol of Product H<sub>2</sub>

Calculations were standardised to give total enthalpy based on 1 mol of reactant mixture. According to (R25) three mols of H<sub>2</sub> are created for 1 mol of urea and 1 mol of water, the final values for total energy were based on three mols of urea and so were divided by 3 to give final energy per one mol of H<sub>2</sub> gas.

#### **3.2.3.2 Equilibrium Mol Fraction Calculations**

In order to relate thermodynamic equilibrium modelling to the experimental work presented in later chapters of this thesis, the stoichiometric method was adapted to include data predicted by EQUIL in CHEMKIN software. This permitted greater accuracy and a directly comparable set of results for the energy needed to produce H<sub>2</sub> to the process parameters reported in the Chapter 6 experimental work where steam reforming of urea was optimised. To achieve this, the programmed input mol fractions and the output mol fractions at equilibrium predicted by EQUIL in CHEMKIN were used instead of the stoichiometric co-efficients of (R25).

During experimentation, carrier gas dilution was necessary for mass balance analysis and for the operation of experimental gas analysers (see sections 5.2 and 6.2). Two molar flow rates of urea solution were used for the two experimental parametric studies (4 ml hr<sup>-1</sup> and 10 ml hr<sup>-1</sup>) which together with the fixed carrier gas flow rate of 300 cm<sup>3</sup> min<sup>-1</sup> resulted in the carrier gas dilution constituting 0.84 and 0.63 respectively of the total molar flow into the reactor. 63 % dilution was applied to the optimised process parametric study so has been used here.

EQUIL in CHEMKIN calculates  $\Delta H_r$  as the difference between mean molar enthalpy values for product and reactant gas mixtures. Enthalpy for the initial gas mixture and for the gas mixture at predicted equilibrium state for the temperature specified is calculated from:

$$\bar{H} = \sum_i^{i_{TOTAL}} H_i x_i \quad (F8)$$

The mol fractions ( $x_i$ ) in the output gas composition were determined by the EQUIL in CHEMKIN Gibbs free energy minimalisation method as previously described in section 3.2.1. Input gas composition was chosen as shown in Table 3-4. Using these values for gas composition mol fraction, EQUIL in CHEMKIN calculates the species molar enthalpy ( $H_i$ ) necessary for (F8) using thermodynamic data of molar heat capacity contained in its database. This database draws from literature sources such as Burcat [139] and NIST [137] as also used for the calculations in section 3.2.3.1. Also, following the method in section 3.2.3.1,  $\Delta H$  was calculated from a baseline standard state of 25.15 °C, and pressure maintained at 1 atmosphere.

Four reactants were used at varying mol fractions: urea, H<sub>2</sub>O, and diluents nitrogen and argon. The range of steam to carbon ratios input was varied from  $2 \leq \text{S:C} \leq 7$  for a dilution fraction of 0.63 (**Table 3-4**). S:C = 2 is added to the range reported in Chapters 5 and 7 ( $3 \leq \text{S:C} \leq 7$ , representing the mixtures used in the reactor experiments), to show the trend for moving outside the range as this may be possible in future work with a pre-heat system (see Chapters 5 and 7).

**Table 3-4.** EQUIL modelled reactant mole fraction values for 63% dilution. Diluent = Ar or N<sub>2</sub>

$X_{\text{reactant}}$	S:C					
	2	3	4	5	6	7
Urea	0.123	0.092	0.074	0.061	0.053	0.046
H <sub>2</sub> O	0.245	0.276	0.294	0.307	0.315	0.322
Diluent	0.632	0.632	0.632	0.632	0.632	0.632

The values of  $\Delta H_r$  calculated by EQUIL in CHEMKIN are inclusive of  $\Delta H_{\text{sens}}$  for each species but since this is a gas phase model they are exclusive of  $\Delta H_{\text{vap, H}_2\text{O}}$  and  $\Delta H_{\text{sub, UREA}}$ . Two additional terms were therefore included in the calculations to account for the energy needed to vaporise water and sublime urea. The urea sublimation enthalpy term was obtained by multiplication of the reactant urea mol fraction ( $x_{\text{urea, in}}$ ) by  $\Delta H_{\text{sub, UREA}}$  (97.6 kJ. mol<sup>-1</sup> [137]) at  $T \geq 133$  °C, and the water vaporisation term by multiplication of the steam mol fraction ( $x_{\text{H}_2\text{O, in}}$ ) by  $\Delta H_{\text{vap, H}_2\text{O}}$  (40.6 kJ [137]) at  $T \geq 100$  °C.

Values for the hydrogen product mol fraction at equilibrium were obtained from the EQUIL in CHEMKIN software for each run. To standardise for the difference in total number of input and output moles, uncorrected (wet and dilute) syngas H<sub>2</sub> mol fraction was used as denominator to leave the kJ/mol H<sub>2</sub> product with the same term of 1 mol of reactant mixture. H<sub>2</sub> product was therefore obtained by multiplying total product moles (obtained from EQUIL in CHEMKIN) by the wet and undiluted H<sub>2</sub> mol fraction. The total enthalpy was divided by this sum to leave kJ of energy per mol of H<sub>2</sub> product.

### 3.3 Results/Discussion

Results shown and discussed in this section all report predicted modelling outputs at 1 atmosphere pressure. The effects of varying pressure are discussed in section 3.3.1.6 only.

### 3.3.1 Products at Equilibrium

#### 3.3.1.1 Syngas Composition

**Figure 3-1** illustrates how at the attainment of steam reforming temperatures hydrogen production occurs, then increases to a maximum of ca. 50 % at temperatures  $\geq 500$  °C. Hydrogen thereafter remains the major product. This H<sub>2</sub>-rich syngas is made more favourable for direct supply to fuel cells by the ubiquitous by-product diluent N<sub>2</sub>, shown to improve PEMFC performance [140]. Methane occurs as a major product pre-steam reforming, but declines to negligible concentrations thereafter, resulting in carbon selectivity favouring CO<sub>2</sub> and CO, with CO increasing and CO<sub>2</sub> decreasing with greater temperatures as would be expected by the endothermic reverse water gas shift reaction (R24) becoming increasingly dominant. Urea steam reforming at optimum temperature is therefore predicted to create a relatively simple syngas with no hydrocarbons higher than CH<sub>4</sub>. This is highly advantageous in terms of hydrogen purity (with minimal post-reforming processing required). The methane component being relatively low is also favourable in terms of the overall synthesis product greenhouse gas potency. Results of calculated dry corrected syngas products (excluding hydrogen which is described by its yield) with temperature for varying steam to urea ratios are shown in **Figure 3-4** to **Figure 3-7**. NH<sub>3</sub> values are not shown on **Figure 3-1** due to their low concentrations but are discussed in section 3.3.1.5. H<sub>2</sub>CO, and all other product species evaluated did not occur in concentrations above 10<sup>-8</sup> mol fraction in the dry corrected syngas across all the temperatures modelled. This was four orders of magnitude less than the next concentrated species (NH<sub>3</sub>).

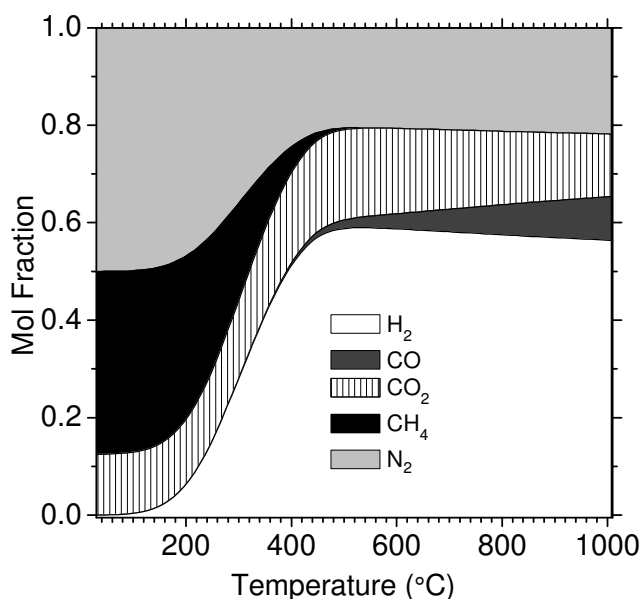


**Figure 3-1.** Dry corrected syngas (excluding water and diluent) with argon diluent to show product nitrogen from reactant mixture of S:C = 7. All significant species are shown.

### 3.3.1.2 Reactant Conversions

Urea conversion was 100% for all conditions and temperatures.

Steam conversion (**Figure 3-2**) is important as it provides evidence of the extent of steam reforming. By optimising steam conversion, hydrogen from a relatively cheap and abundant reagent is produced. Modelling showed that below 300 °C no steam reforming occurred for all programmed operating conditions. The onset of steam reforming was pushed to higher temperatures by increasing the fraction of urea in the reaction mixture.

Plots of steam conversion with varying temperature for varying S:C of the reactant mixture exhibited curves with maxima at mid-range ( $450\text{ °C} \leq T \leq 750\text{ °C}$ ) temperatures (**Figure 3-2**). With increasing temperature, pre-maxima values increased steeply for all S:C mixtures. The post-maxima declination trend with increasing temperature was greatest for urea-rich mixtures. Negative values at low temperatures occurred, indicating that water production becomes thermodynamically favoured. These variations can be explained by the endothermic global steam reforming reaction (R25) predominating at lower temperatures and the endothermic reverse water gas shift reaction becoming more favourable at higher temperatures thus limiting overall conversion. That the maximum steam conversion is seen around equimolar reactant mixtures can be attributed to the requirements of the stoichiometric urea steam reforming reaction with excess water resulting in availability of urea limiting overall water conversion, thus a reduction in steam conversion above S:C = 1. Similarly, water will be limiting at highest urea concentrations.

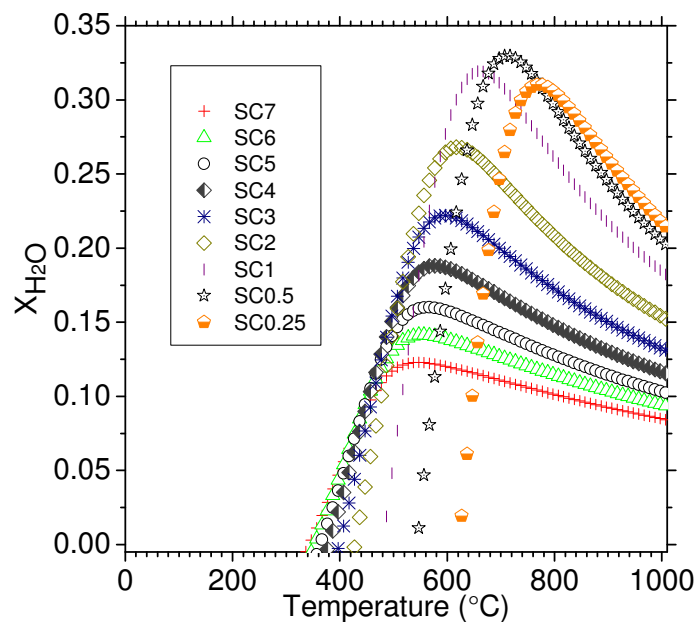


**Figure 3-2.** Steam conversion for urea steam reforming.

Beneficially, for the mixtures that are practically achievable at laboratory temperatures, due to the solubility of urea in water ( $S:C \geq 3$ ), optimum temperatures for steam conversion were in a range of moderate  $400\text{ }^{\circ}\text{C} \leq T \leq 600\text{ }^{\circ}\text{C}$ . This is a temperature range where the water gas shift reaction still dominates over its reverse. Consequently, and unlike methane steam reforming, there would in practice be no need for separate high temperature and low temperature WGS reactors, as the unreacted CO at these temperatures would be less than a few percent for  $S:C = 3$  as shown in **Figure 3-4**.

### 3.3.1.3 Hydrogen Yield

**Figure 3-3** shows hydrogen yield per mol of reactant urea as a function of temperature for a range of S:C mixtures.  $\text{H}_2$  yield with increasing temperature, as predicted by the urea steam reforming reaction (R25) was seen to exhibit a peak that approached the ideal value of 3 (corresponding to the complete conversion of urea and steam to  $\text{H}_2$ ,  $\text{CO}_2$ , and  $\text{N}_2$ ). A steep rise with increasing temperature in pre-maxima yield for all S:C mixtures was observed. This can be explained by the medium endothermicity of urea steam reforming (R25) and of its thermal decomposition products (R23). The gradual post-maxima decrease in  $\text{H}_2$  yield is likely attributable to the mild exothermicity of (R24) and thus by the reverse water gas shift becoming more favourable.

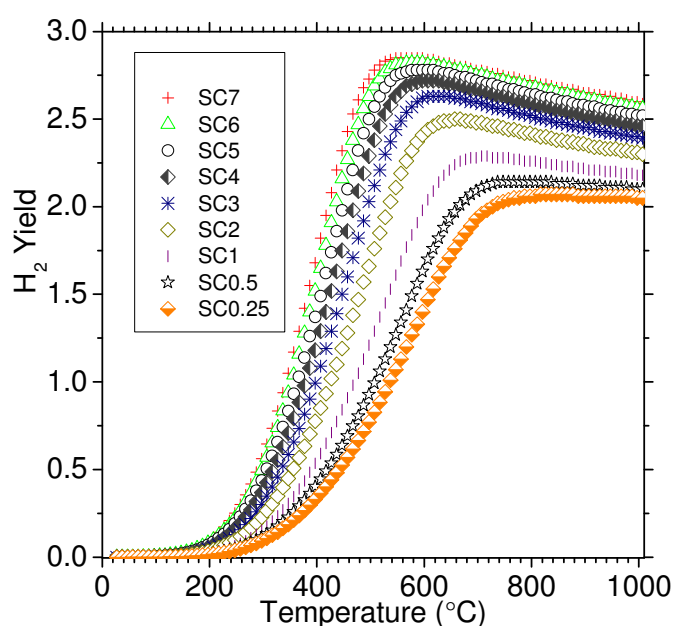


**Figure 3-3.**  $\text{H}_2$  Yield per mol of reactant urea with 63 %  $\text{N}_2$  dilution

### 3.3.1.4 Carbon Selectivity

Carbon-species syngas mol fraction was independent of diluent type and diluent concentration. The fraction of carbon monoxide in the calculated equilibrium dry



corrected syngas (**Figure 3-1**) was seen to increase with increasing urea concentration in the reactant mixture though this was observed to be a relatively minor dependence compared to temperature. Values of CO below a few ppm level were only recorded at temperatures well below the onset of steam conversion: ca. 300 °C for all reactant compositions. Carbon monoxide only occurred below the ppm value at temperatures below 177 °C where steam reforming had yet to begin. This could necessitate post-reactor processing for direct supply to PEMFCs which are intolerant of CO above ppm levels [16]. At steam conversion temperatures, CO constituted between 5 to 23 % of the dry corrected syngas, dependent on reactant S:C (see **Figure 3-4**).

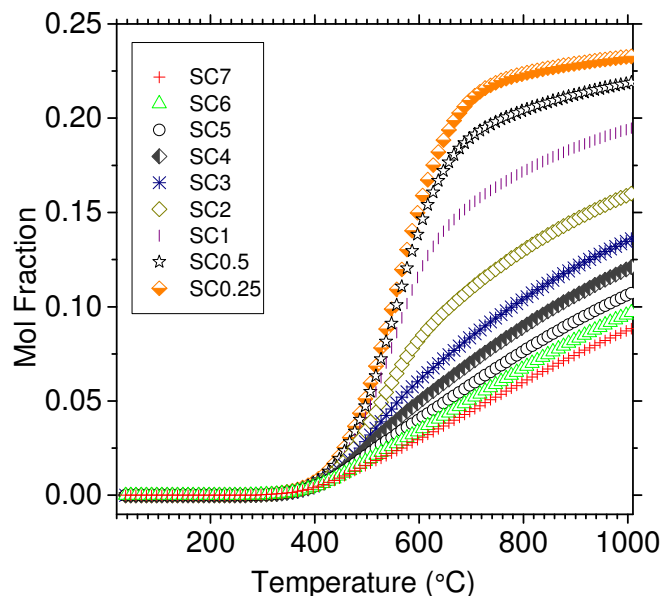


**Figure 3-4.** CO in the dry corrected syngas.

CO<sub>2</sub> was seen to increase with increasing temperature to a maximum output fraction in the dry corrected syngas that occurred for all S:C ratios at ca. 500 °C (**Figure 3-5**). Reactant mixture S:C variation dictated both the rate of increase in dry corrected syngas CO<sub>2</sub> before reaching its maxima and also its post-maximum decrease with increasing temperature. This post-maxima function changed from a linear trend at low urea-lean reactant concentrations to exponential decay for stoichiometric and super-stoichiometric urea-rich mixtures as reaction temperature increased as shown in **Figure 3-5**.

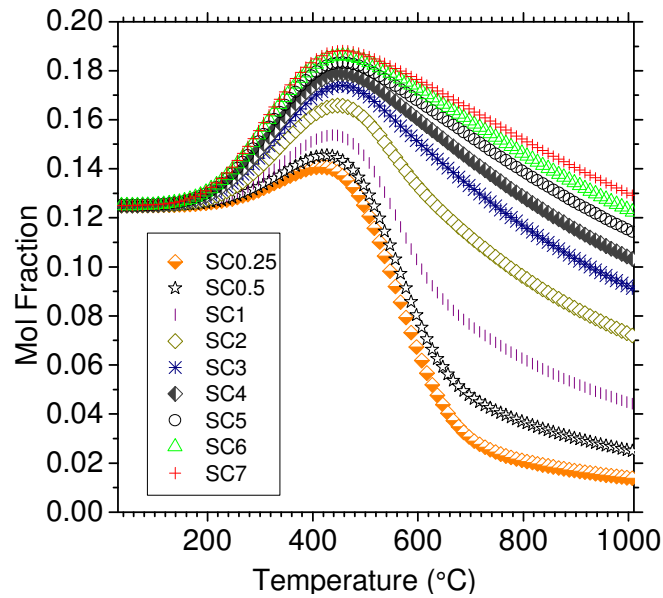


**Figure 3-5.** CO<sub>2</sub> in the dry corrected syngas.

Methane mol fraction in the dry corrected syngas decreased linearly with increasing temperature, with the onset of steam reforming, then decreased asymptotically with increasing temperature to negligible values of  $\times 10^{-4}$  to  $\times 10^{-7}$  dependent on S:C. Decrease in dry syngas CH<sub>4</sub> with increasing temperature was steepest with water-rich reactant concentrations. These results are shown in **Figure 3-6**.

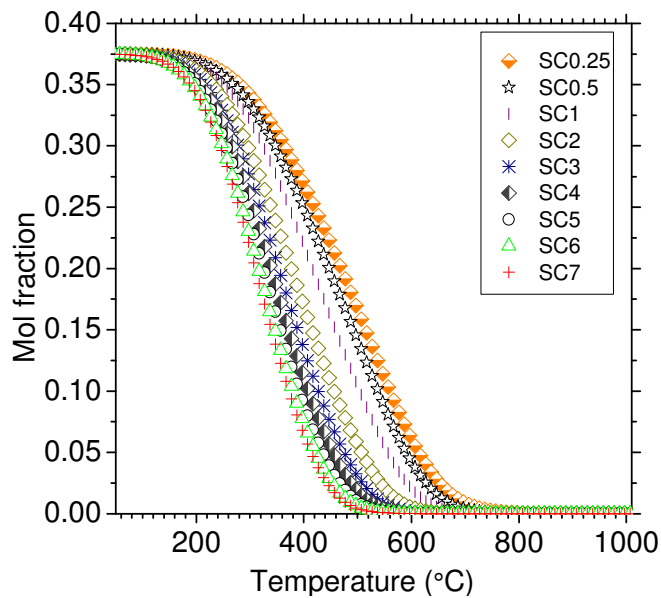


**Figure 3-6.** CH<sub>4</sub> in the dry corrected syngas.

### 3.3.1.5 Ammonia (NH<sub>3</sub>) in Dry Corrected Syngas.

Equilibrium maxima of predicted product mol fraction NH<sub>3</sub> in the dry corrected syngas occurred advantageously prior to the onset of steam conversion. Of further benefit was the identification that during steam reforming, NH<sub>3</sub> concentrations in the dry syngas had a decreasing trend with increasing temperature. This decrease approximated to an exponential decay at ca. 700 °C. Results of NH<sub>3</sub> content in the dry corrected syngas with temperature and variables of S:C and dilution representative of the range of conditions modelled are displayed in **Figure 3-7**. Concentrations of 10 to 100 ppm NH<sub>3</sub> were predicted at moderate steam reforming temperatures of 550 °C to 600 °C. Also, at temperatures where steam conversion occurred, NH<sub>3</sub> values decreased with increasing reactant mixture water content.

Throughout all calculation parameters, NH<sub>3</sub> in the dry corrected syngas never occurred below the ppm level. This level of concentration is identified as the minimum necessary to avoid poisoning of PEMFCs [36]. Dependent on S:C and level of dilution, this means that very high reforming temperatures would be needed to achieve a dry syngas NH<sub>3</sub> fraction of >10 ppm as required by the present technology for this type of fuel cell. For supply to solid oxide and alkaline fuel cells, trace ammonia in the syngas would not be a problem [34, 35]. The 10-100 ppm NH<sub>3</sub> predicted at 500 °C ≤ T ≤ 600 °C is advantageous as it coincides with the temperature region where steam conversion and H<sub>2</sub> yield were highest. In practice, gaseous NH<sub>3</sub> will likely dissolve in the unconverted water exiting the reactor due to its high solubility. This can then simply be removed by the inclusion of a post-reactor condensate trap, and so should not be considered a problem of the process.

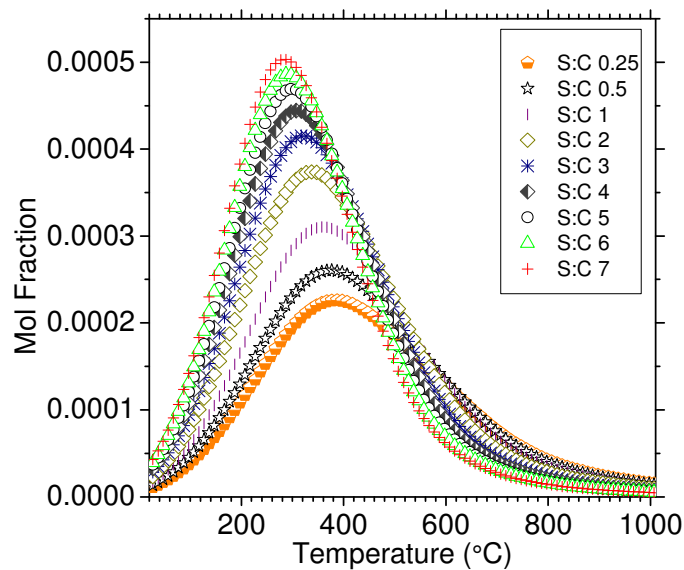


**Figure 3-7.** NH<sub>3</sub> in dry corrected Syngas.

The absence of an NH<sub>3</sub>-rich syngas, particularly at low temperature differs from what might be expected based on some previous reports of simple urea solution thermolysis where the pathway was considered to be firstly via water evolution, then urea decomposition with the initial products of NH<sub>3</sub> and HNCO, with further decomposition to NH<sub>3</sub> in the presence of water as temperature increased (section 2.6). This apparent discrepancy is not surprising considering that previous published work has neglected any consideration of H<sub>2</sub> production or the involvement of high temperature steam. Since this is a first attempt at urea steam reforming interpretation, the model does not allow any further elucidation of reaction mechanisms other than by product fractions at equilibrium. Evidence that NH<sub>3</sub> cracking occurs could however be inferred from these results as the exponential decay of NH<sub>3</sub> concentration at higher temperatures is comparable with previous analysis [32]. The reactions that determine the presence of high quantities of CH<sub>4</sub> and to a lesser extent N<sub>2</sub> predicted by these calculations at pre-steam reforming temperatures are also less certain.

In terms of life cycle analysis of the other products, CO could be reformed to more hydrogen in downstream water gas shift reactors, and CO<sub>2</sub> captured on materials such as ethanolamine which work best at room temperatures or with pressure swing adsorbers. Product N<sub>2</sub> is inert and could be released or used as a commodity. NH<sub>3</sub> captured in the unconverted water condensate could theoretically be re-cycled back into the reactor – an area for future study.

### 3.3.1.6 Pressure

Increasing pressure for all S:C mixtures had an adverse effect on steam conversion, reducing its total value and requiring higher temperatures to achieve the same fraction of steam conversion as at lower pressure. Hydrogen yield and syngas hydrogen mol fraction also decreased with increasing pressure at any given temperature. The influence of varying system pressure on urea steam reforming dry synthesis gas equilibrium content of NH<sub>3</sub>, H<sub>2</sub>, and CH<sub>4</sub>, and H<sub>2</sub>O conversion, is shown in **Figure 3-8** to **Figure 3-11**.

The equilibrium hydrogen mol fraction in the dry syngas decreased by 38 % at 600 °C with increasing pressure from 1 to 20 atmospheres (**Figure 3-9**). Overall maxima of syngas hydrogen mol fraction also decreased, with the temperature required to achieve maximum mol fraction increasing by 250 °C for pressure up to 20 atmospheres. H<sub>2</sub>O conversion was predicted to be suppressed by increasing pressure. From 1 to 20 atmospheres at 600 °C there was a 100 % predicted reduction in steam conversion with the temperature required for maximum conversion being increased with increasing pressure (**Figure 3-10**). To achieve maximum steam conversion at 20 atmospheres required an increase in temperature of 230 °C compared to that achievable at 1 atmosphere. A large increase in NH<sub>3</sub> with increasing pressure across all temperatures

was observed at equilibrium (**Figure 3-8**). At 600 °C this increase was 808 % by raising the pressure from 1 to 20 atmospheres. Carbon selectivity with increasing pressure (not shown) showed an increase in methane and decrease in carbon monoxide at steam reforming temperatures. Methane mol fractions in the dry syngas followed a similar relation as with increasing urea content such that for any temperature in the region of steam reforming, methane content was higher in the dry syngas with increased pressure. Carbon dioxide mol fractions fell with increasing pressure, for any fixed reaction temperature up to an inflexion point at ca. 600 °C. Therefore, in terms of syngas products, it would not appear advantageous to steam reform urea at increased pressure, with the greatest adverse consequence of increased pressure being the reduction in steam conversion, subsequent hydrogen yield and an increase in ammonia product concentration.

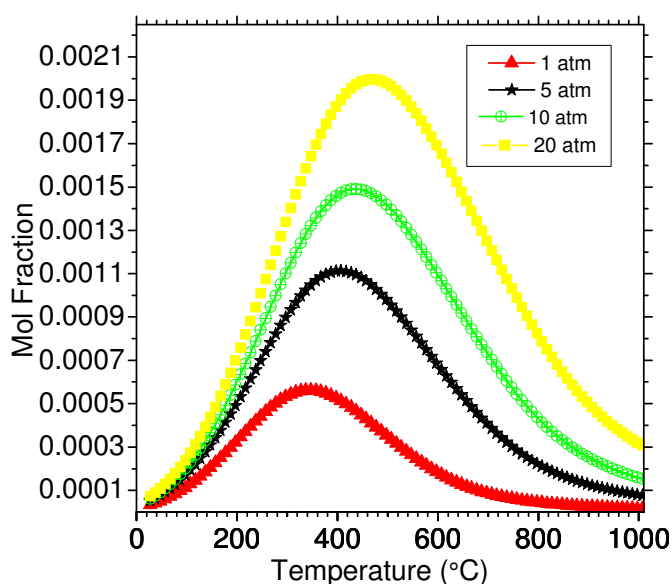


**Figure 3-8.**  $\text{NH}_3$  in dry corrected syngas as a function of temperature, with varying pressure.

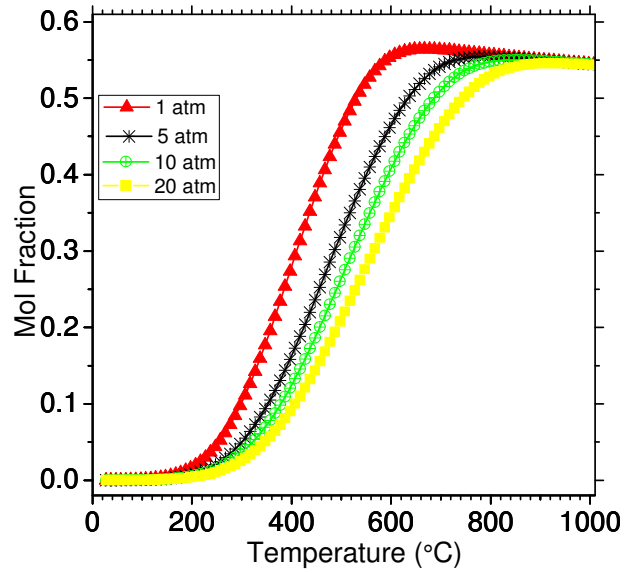


**Figure 3-9.** H<sub>2</sub> in dry corrected syngas as a function of temperature, with varying pressure.

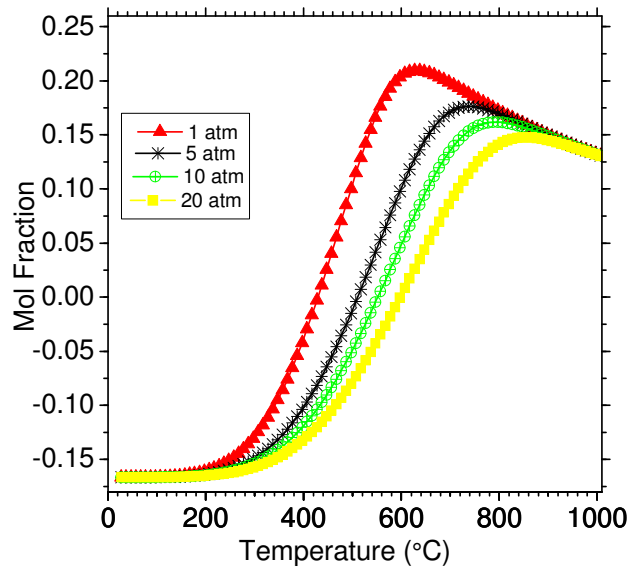


**Figure 3-10.** Conversion of H<sub>2</sub>O as a function of temperature, with varying pressure.

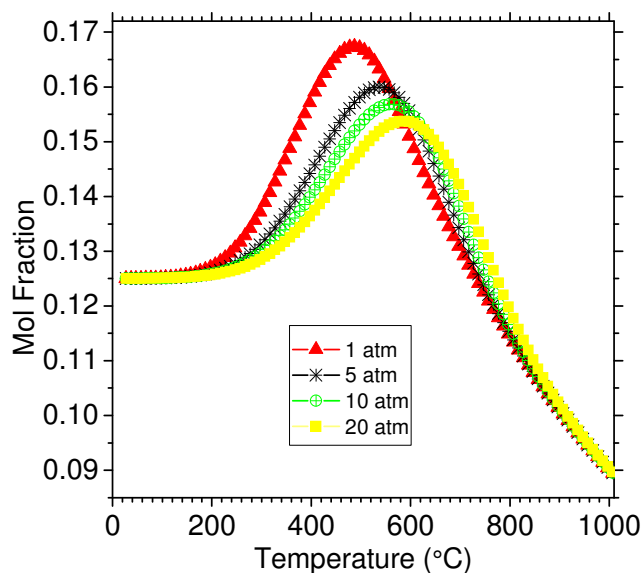


**Figure 3-11.** CO<sub>2</sub> in dry corrected syngas as a function of temperature, with varying pressure.

### 3.3.2 Thermochemistry

#### 3.3.2.1 Stoichiometric Calculations

The results of this method provided an idealised maximum model only, accounting for no carrier gas and assuming a complete forward reaction of (R25) for total product creation. Therefore this is the most simplistic of the two approaches studied to determine total process enthalpy per mol of H<sub>2</sub> produced. This is not necessarily a weakness of the method as it does permit an easy “field” judgement of the process determining factors plus permitting the incorporation of additional impositions on the energy budget, through for example process inefficiencies or post-processing stages. Furthermore, as will be seen in Chapter 5 and Chapter 6, the validity of this method, based on (R25) is in fact supported by the, as predicted, composition ratio of experimental products during steady state operation.

**Figure 3-12** shows the results of these calculations on the total energy needed to produce one mol of H<sub>2</sub> from urea by steam reforming at equilibrium at optimum temperatures ( $500\text{ °C} \leq T \leq 700\text{ °C}$ ). This temperature range is chosen due to the modelling predictions for greatest proximity to high H<sub>2</sub> yield and maximum steam conversion, and for which the stoichiometric reaction mechanism (R25) is seen to be most valid.

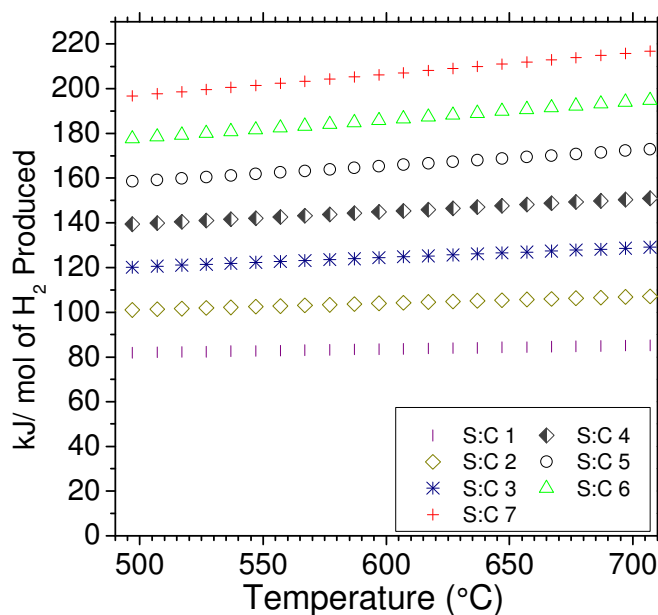


**Figure 3-12.** Total kJ per mol of H<sub>2</sub> produced at equilibrium.

Both water vapourisation and urea sublimation need to be overcome prior to steam reforming with relatively high energy demands at 100 °C and 133 °C respectively. It is apparent from **Figure 3-12** that increasing water content for higher S:C mixtures resulted in greater energy demand due to the need to raise the temperature of excess steam. For future applications, enzymatic urea decomposition (R13) could be utilised. This would also overcome the  $\Delta H_{\text{sub UREA}}$  energy (96 kJ mol<sup>-1</sup>) that was a feature of the urea enthalpy intermediate stage and potentially lead to a substantial reduction in total energy required for the process. The gradual increase in enthalpy per mol of H<sub>2</sub> with temperature for all S:C variables is indicative of the  $\Delta H_{\text{sens}}$  involved.

**Table 3-5** shows comparisons between these results and the energy content of H<sub>2</sub>. The total mean energy to produce one mol of H<sub>2</sub> in the range 500 °C ≤ T ≤ 700 °C is shown, compared to the higher heating value of hydrogen (-285.83 kJ mol<sup>-1</sup>). This was considered most appropriate as the lower heating value excludes the latent heat of condensation of steam, and fuel cells release water in liquid phase [5]. The column headed “kJ surplus” in **Table 3-5** shows the energy of the process for one mol of H<sub>2</sub> produced subtracted from the higher heating value of hydrogen. Values are also given in terms of power available per unit time (in Watt hours) which is derived from the kJ surplus column.



**Table 3-5.** Values of minimum energy needed to produce 1 mol of H<sub>2</sub> from urea and steam. kJ surplus and power available has been calculated by deducting from the energy content of H<sub>2</sub> (285.83 kJ mol<sup>-1</sup>).

S:C	kJ per mol H <sub>2</sub>	kJ surplus per mol of H <sub>2</sub>	Power available (Wh)
1	76.05	209.78	58.27
2	94.45	191.38	53.16
3	112.84	172.99	48.05
4	131.24	154.59	42.94
5	149.64	136.19	37.83
6	168.04	117.79	32.72
7	186.44	99.39	27.61

It can be seen in **Table 3-5** that based on these calculations, surplus power is available with all S:C mixtures. Note that these values of power availability are not only theoretical maxima for each reagent mixture, since they assume the optimum forward reaction for urea steam reforming (R25) as has been described, but they take no account of process inefficiencies, the inclusion of which is easily applicable but which would reduce the overall surplus of power available. Additionally, these results also exclude final power conversion inefficiency. Factorisation for this is non-generic and outside the scope of this study, but to use the H<sub>2</sub> produced by urea steam reforming in the most efficient power generation device (a fuel cell) would need to incorporate a value for its operating efficiency which can be estimated to create an additional reduction of between 47 % - 40 % [5].

If urea is supplied to the steam reforming process combined with water in aqueous solution, then an additional energy demand is incurred for solvation, which will decrease further the power available as shown in **Table 3-5**. Solvation of urea in water is mildly exothermic with the enthalpy change for this reaction at 25 °C quantified by Koebel and Strutz [68]:

$$\Delta H_{\text{solv}} = [(3656.308 - 89.9082(M) + 5.54228(M^2) - 0.24071(M^3) + 0.00449022(M^4)] \times 4.186 \text{ J mol}^{-1} \quad (\text{F9})$$

where, M = molality. (F9) is reportedly valid within the molar range  $0.319 < M < 20.18$ . [See **Table 4.1** for a comparison of molar and S:C urea solutions.] For the range of experimental mixtures  $3 \leq \text{S:C} \leq 7$ , the mean average energy required is found to be  $13.115 \pm 0.411 \text{ kJ mol}^{-1}$ . This energy demand has been excluded from the calculations in this section as for  $4 \leq \text{S:C} \leq 7$ , solvation will occur with heat flow from its room temperature surroundings (see **Chapter 4**).

Though the incorporation of carrier gas is not a pre-requisite for steam reforming, it was used in this study's reactor experimentation. Diluting the reactant mixture incurs extra energy costs and reduces the concentration of H<sub>2</sub> in the syngas. Argon was found to be the least energy intensive carrier gas as can be seen in the comparisons of diluents  $\Delta H_{\text{sens}}$  in **Table 3-6** due to its lower heat capacity. However, due to the relative higher cost of using argon, it is likely to be more favourable to operate with N<sub>2</sub> as a carrier gas although it is predicted to have higher enthalpy requirements. Furthermore, for a PEMFC, the dilution affects of N<sub>2</sub> with the H<sub>2</sub> feed have a beneficial effect in stabilising power outputs when demand fluctuates [140]. Though this citation specifies the effects of N<sub>2</sub> only, its benefit is related to dilution, therefore Ar (or any inert gas) should have the same positive effects. It is feasible, and advantageous as perhaps a means of mitigating its release to the atmosphere, that CO<sub>2</sub> may be used as a carrier gas, and then be removed by a CO<sub>2</sub>-sorbent either in the reformer or downstream, prior to feeding a fuel cell. Though an assessment of the feasibility of urea steam reforming with a CO<sub>2</sub> diluent was not attempted, the  $\Delta H_{\text{sens}}$  of this diluent was found to be more energy intensive than both Ar and N<sub>2</sub>.

**Table 3-6.** Calculated enthalpy of different carrier gases at the range of optimum urea steam reforming temperatures.

Temperature (°C)	N <sub>2</sub> $\Delta H_{\text{sens}}$ (kJ)	Ar $\Delta H_{\text{sens}}$ (kJ)	CO <sub>2</sub> $\Delta H_{\text{sens}}$ (kJ)
500	14.1064	9.8078	21.2719
550	15.6767	10.8472	23.8395
600	17.2635	11.8865	26.4483
650	18.8663	12.9258	29.0946
700	20.4846	13.9651	31.7753

### 3.3.2.2 Equilibrium Mol Fraction Calculations

The parameters of this model are identical to the parameters of results reported in Chapter 6, and are therefore directly comparable. Therefore they provide an economic assessment of this optimised process. **Figure 3-13** shows the results of calculations on the total energy needed to produce one mol of H<sub>2</sub> from urea by steam reforming with 63% carrier gas dilution plotted as curves as a function of temperature. For the S:C mixtures attainable at room temperature and used in experimentation  $3:1 \leq S:C \leq 7:1$ , these curves are seen to have minima that occur at relatively low mid-range temperatures:  $500 \text{ °C} \leq T \leq 700 \text{ °C}$  which is advantageous in energy input terms. This temperature range is also advantageous as it coincides with the range for optimum

functioning of industrial nickel steam reforming catalysts [12, 141], and see Chapter 7. Furthermore, it is a temperature range which has been shown as attractive based on lower CO product, and rapidly declining  $\text{NH}_3$  concentration (see section 3.3.1).

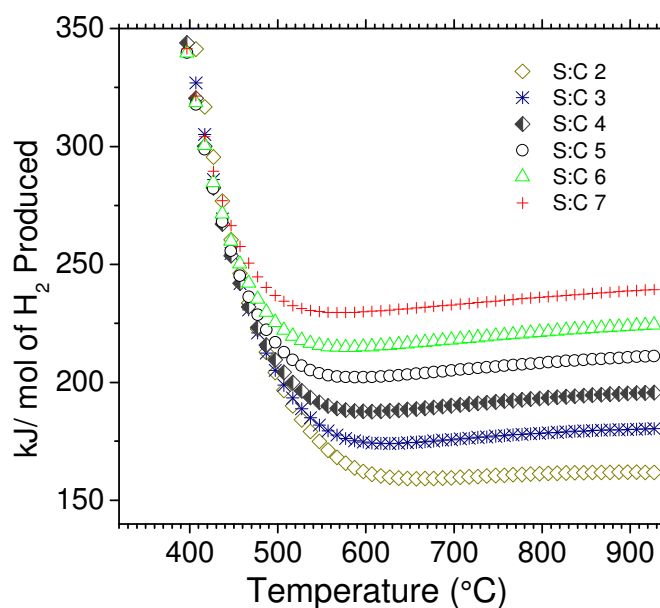


**Figure 3-13.** Total kJ per mol of  $\text{H}_2$  for 63% diluent urea steam reforming.

The calculations predicted that an energy requirement of  $\geq 250$  kJ per mol of  $\text{H}_2$  would be necessary to produce  $\text{H}_2$  at low pre-steam reforming temperatures; a factor that is independent of reactant S:C or dilution concentration, making these conditions unfavourable despite the lower heating demand. Post-minima kJ per  $\text{H}_2$  values for all reactant mixtures were predicted to remain relatively low and begin to increase gradually with increasing temperature. To understand the cause of this dependency, intermediate stages in the enthalpy calculation were assessed.  $\Delta H_{\text{total}}$  was found to increase up to  $T = 900 \text{ °C} \pm 10 \text{ °C}$  and then to decrease relatively gradually as a function of temperature at these highest temperatures for all mixtures. The high energy required to heat urea resulted in an increase in  $\Delta H_{\text{total}}$  directly proportional to the urea content of the reactant mixture for all temperatures. Thus despite the extra heat necessary to generate and heat up steam, urea was the most energy intensive reagent.

Though it would seem attractive to operate urea steam reforming at  $T \geq 800 \text{ °C}$ , the disadvantages are that an increased CO content will result, caused by an increase in the reverse water gas shift reaction, and a reduced  $\text{H}_2$  yield per mol of urea input and reduced steam conversion due to the shift away from the forward reaction of (R25). Higher temperatures of operation would incur extra process running costs to maintain temperature and avoid heat losses. These inefficiency factors are idiosyncratic and so were not quantifiable in the model.

Increasing the urea concentration in the fuel S:C mixture was predicted to decrease the energy required to produce one mol of  $H_2$ . The cause of this lower energy demand with increasing urea enrichment was found to be due to the increased  $H_2$  mol fraction in the corrected wet syngas since these mixtures also had the highest reaction enthalpy. This is shown in the graph of the hydrogen product mol fraction as a function of temperature for 63 % carrier gas dilution (**Figure 3-14**). In contrast to **Figure 3-3** showing hydrogen yield based on mol of urea reactant, **Figure 3-14** is calculated per mol of reactant mixture and consequently shows decreased hydrogen output with decreasing urea content. This is due to the greater amount of unconverted water present, a result of water content in excess of the stoichiometric amount. A larger number of  $N_{out}$  with increasing urea content in the reactant mixture also accentuates the differences in  $H_2$  product across the range when compared in this way.

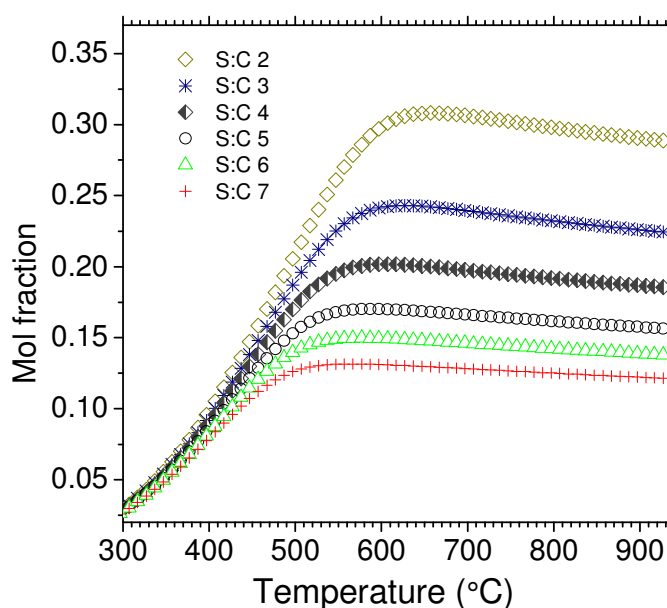


**Figure 3-14.** Hydrogen product mol fraction in the wet syngas for urea steam reforming with 63% carrier gas dilution.

With increasing dilution of the reactant mixture, the  $H_2$  output mol fraction varied from 0.35 (at zero dilution) to 0.05 (at 84 % dilution) in the wet syngas at 600 °C. Reaction enthalpy increased with decreasing dilution, due to the higher sensible and latent heat demands of urea and water.

It is interesting to compare these results with the energy demands to produce  $H_2$  by conventional methane steam reforming. Methane steam reforming was modelled with EQUIL in CHEMKIN at S:C = 3 which is mid-range in the optimum ratio for industrial applications [142]. The same method as for urea modelling was followed. In the regions of temperature where steam reforming was optimum, results showed that an increase in energy of 58 % was necessary to produce one mol of  $H_2$  from urea compared to the

energy necessary from MSR at  $T = 500\text{ }^{\circ}\text{C}$ . This is shown in **Figure 3-15**. The difference in energy fell slightly to 54 % at  $T = 700\text{ }^{\circ}\text{C}$  and remained consistent (correct to 1% difference) with increasing temperature thereafter. The cause of this increase in energy demand was due to the slightly higher concentration of  $\text{H}_2$  in the methane derived syngas, since  $\Delta H_r$  was comparable between both processes from  $550\text{ }^{\circ}\text{C} \leq T \leq 600\text{ }^{\circ}\text{C}$ , and became less for urea reforming than MSR at temperatures greater than  $600\text{ }^{\circ}\text{C}$  (not shown). Though disadvantageous in energy terms, choosing the urea steam reforming process over MSR is mitigated by the potential sustainability and future supply security of urea, plus the advantage of slightly lower temperature creating a process environment that may negate the need for post-reactor stages to reduce CO content.

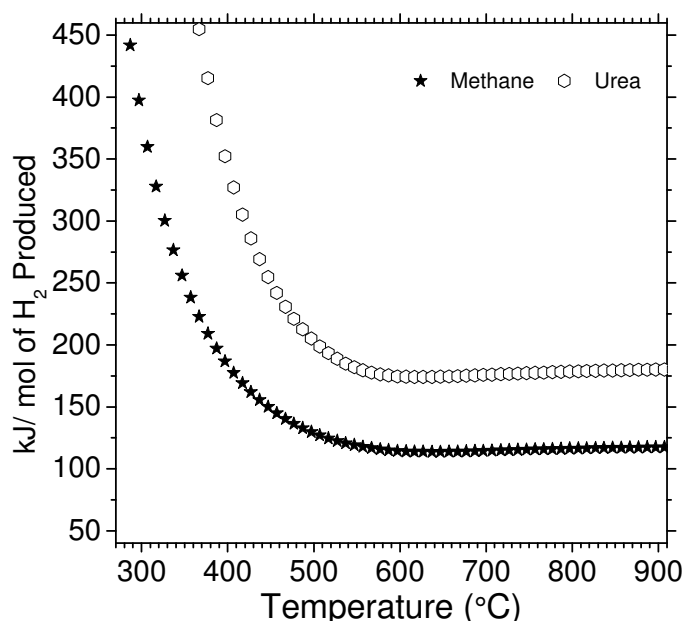


**Figure 3-15.** Comparison between the energy needed to produce one mol of  $\text{H}_2$  by steam reforming urea and methane. Both results shown are for reactant mixtures of S:C = 3, and with a 63% dilution of carrier gas.

### 3.3.3 Model Limitations

The reference source that provided the polynomial data [139] for urea gives heat capacity values attributable to a gas phase only. These urea  $C_p$  and  $\Delta H_{\text{sens}}$  values were used throughout yet, as has been described in section 2.6.2, there is uncertainty about whether urea has a gas phase or whether it dissociates upon heating. To test the method, modelling was done with HNCN and  $\text{NH}_3$  (the predicted urea sublimation products) as alternatives to urea and found to give outputs correct to  $\geq 90\%$ , with  $C_p$  values varying by  $14 \pm 0.2\text{ J mol}^{-1}\text{ K}$ .

For energy demand modelling, it was also chosen to use urea instead of combined values of sensible enthalpy for  $\text{NH}_3$  and  $\text{HNCO}$  following urea sublimation at  $133\text{ }^\circ\text{C}$ . The influence of this on urea total enthalpy was checked by comparison and the values were found to be correct to  $< \pm 0.005\text{ kJ}$ . This low variation and the closeness of these predictions to experimental outputs at steady state, calculated to give adequate residence time for equilibration (Chapters 4, 5, and 6), support the validity of this chosen model.

Enthalpy of water vaporisation was placed at  $100\text{ }^\circ\text{C}$  when calculating  $\Delta H_{\text{vap, H}_2\text{O}}$ . However the reference source [137] gives  $227\text{ }^\circ\text{C}$  as the transition point between phase change polynomials co-efficients, despite this temperature being  $127\text{ }^\circ\text{C}$  above water boiling point. Since these values are below steam reforming temperatures, though uncertainties remain, they are prior to optimum operating temperatures and so will not have influenced the total energy per mol of  $\text{H}_2$  values. Burcat [139] gives two sets of polynomial values for the different phases of water with the partition being  $227\text{ }^\circ\text{C}$ . For consistency, the steam polynomial values were extrapolated to  $100\text{ }^\circ\text{C}$ .

In the Equilibrium Mol Fraction Calculation Method it was stated that direct comparability was achieved between the model and the experimental reactor results in Chapter 6 excluding unknown system operating inefficiencies. In the experimental process system, unconverted water was condensed upon leaving the reactor. Therefore the values for  $\Delta H_{\text{vap H}_2\text{O}}$  could, in theory, be added back on to the calculation, thereby reducing the overall energy demand. This was not done based on the rationale that the condenser is outside of the reactor bed and therefore any heat gain would be to the surroundings rather than the reactor system model.

### 3.4 Conclusions

Resolution of the chemical reactions involved in urea steam reforming cannot be achieved by equilibrium modelling, but factors influencing conversion (temperature, pressure, S:C, diluent) can be assessed. Syngas composition, reaction enthalpy, steam conversion and  $\text{H}_2$  yield were predicted with software that calculates outputs using Gibbs minimisation algorithms. Total energy needed to produce  $\text{H}_2$  was then calculated from these results. The results were used to set system parameters for the experimentation described in Chapter 5 and Chapter 6. They also have importance for the utilisation of urea as a hydrogen carrier, as they give information to help assess the need for any post-reforming process stages to further purify the syngas, and, particularly if remote/renewable technologies were required, to assess the energetic and economic viability of the process for dehydrogenation.

Hydrogen was seen to be the major product from urea steam reforming, with a predicted volume fraction of ca. 50% excluding carrier gas and unconverted steam.

Minor by-products of CO<sub>2</sub>, little CO, and negligible CH<sub>4</sub> were present in the equilibrium syngas with no other higher hydrocarbons predicted. This simple syngas composition is favourable due to its low greenhouse gas potential and the ease with which further purification could be achieved in a practical setting. Ammonia values were low at the tens of ppm level, but these may still be too high for direct application of reformed urea syngas into certain fuel cell types. All other species (including HNCO) were absent at mol fractions of  $\geq 10^{-8}$  in the dry corrected syngas.

Increasing pressure was seen to have an adverse effect on equilibrium in terms of desirable products and outputs. It was predicted to decrease steam conversion and hydrogen yield for any given temperature, and also to increase ammonia production.

Two methods were employed for the estimation of determining energy required to produce one mole of hydrogen. EQUIL in CHEMKIN output results, combined with similar concentrations of chemical species found during experimental steady state operation support the stoichiometric model based on a global urea steam reforming reaction. This provides an easy calculation of total energy requirements with values of 80 to 220 kJ minimum for reactant mixtures in the range  $1:1 \leq S:C \leq 7:1$ . This equates, based on the energy content of H<sub>2</sub> to an energy gain of between 99 to 210 kJ per mol of H<sub>2</sub>, or a power capacity of between 28 to 58 Wh. The stoichiometric model predicts a theoretical maximum energy and power gain as it fails to account for thermodynamic limitations and possible competing reaction mechanisms. To incorporate extra detail, to apply factors to account for carrier gas dilution and to model energy demand comparable to successfully reported urea steam reforming operating parameters, values of enthalpy and equilibrium mol fraction predictions based on Gibbs free energy minimalisation were obtained from EQUIL in CHEMKIN. Not surprisingly it was found that mixtures closer to the stoichiometric amount were predicted to create H<sub>2</sub> for the lowest energy demand. Advantageously, these minima were in the mid-range ( $500\text{ °C} \leq T \leq 650\text{ °C}$ ) temperature region. In a practical setting however, this will need to be balanced against the difficulty posed by the solubility of urea in water at concentrations higher than S:C = 3. This will be explored in the next chapter.

Energy needed to make one mol of H<sub>2</sub> from urea steam reforming was found to be 58 % - 54 % greater than if using CH<sub>4</sub> as a fuel in the temperature range  $T \geq 500\text{ °C}$ .

## 4 Fuel Characterisation

### 4.1 Introduction

#### 4.1.1 Solubility

Urea is soluble in water for a range of water-rich S:C mixtures. As a function of temperature, the concentrations practically attainable at standard conditions (25 °C and 1 atm) are S:C  $\geq$  3:1 (see **Table 2-4**). The molality of these concentrations is shown in **Table 4-1**.

**Table 4-1.** Concentrations of urea in de-ionised water solution in Molar and S:C terms.

\* represents the concentration of urea in human urine.

Molar concentration (mol litre <sup>-1</sup> )	S:C
0.33 M*	S:C = 150:1
7.9 M	S:C = 7
9.26 M	S:C = 6
11.1 M	S:C = 5
13.9 M	S:C = 4
18.5 M	S:C = 3

It simplifies the process of steam reforming to have one fuel feed line consisting of urea in solution, rather than a separate water feed and urea feed. Consequently, an assessment of the urea reagent's solubility in de-ionised water was required to understand the nature of urea solvation. This aided the design and optimisation of urea steam reforming experimentation, and gave a greater understanding of the state and composition of the fuel as it enters the reactor.

In aqueous solution, the isomerisation of urea to ammonium cyanate can occur (R26):



Shorter [44] quotes an equilibrium constant value of ca.  $1 \times 10^4$  mol L<sup>-1</sup> in favour of the reverse reaction to urea, but does not give details of the range of aqueous urea mixtures to which this value relates, merely stating that it is applicable to solutions used



“in most of the kinetic work”. As will be discussed below, previous reports have not extended investigations to the urea-rich ratios used in this study’s experimentation.

The forward reaction of (R26) increases with temperature. For 8 M urea in de-ionised water solutions only, equilibrium constant values of  $2.48 \times 10^{-5}$  at 18 °C,  $3.65 \times 10^{-5}$  at 25 °C, and  $19.0 \times 10^{-5}$  at 60 °C have been reported [143]. The same authors report that acidification inhibits cyanate formation. Again with investigations on an 8 M solution, with pH at 6, 7, and 8, the concentrations of cyanate were detected at a maximum of  $\times 10^{-5}$  M up to 5 hours after solvation [143]. In gravimetric terms, based on the molecular weight ( $M_r$ ) of  $\text{CNO}^- = 42 \text{ g mol}^{-1}$ , this concentration is 0.42 ppm.

Lin *et al.* [144] quantified (R26) with greater precision using ion chromatography, though still limited to an assessment of only 8 M urea solutions. Their results showed significantly low levels of urea isomerisation, with one week residence time at high alkalinity (pH = 10) necessary to detect cyanate above  $\mu\text{M}$  levels.

Welles *et al.* [145] studied isomerisation of urea in aqueous solution at 2, 4, 6, and 8 M at 25 °C. They confirmed that cyanate production was negligible and that the rate of production was independent of concentration. Their values for the rate constants of (R26) were:

$$\text{Forward reaction} = 0.2 \text{ mole}^{-1} \text{ hr}^{-1}$$

$$\text{Reverse reaction} = 0.3 \times 10^5 \text{ hr}^{-1}$$

Based on the values quoted by Hagel *et al.* [143], an 8 M aqueous urea solution (S:C  $\approx$  7), up to five hours after solvation would contain:

$$8 - 0.00001 = 7.9999 \text{ M urea, or } 99.9988 \% \text{ urea.}$$

Though the work of Welles *et al.* [145] stated that the reaction rate constants were independent of concentration, this can only be assumed relevant in the context of the mixtures used in their study. Their study did not extend to the relatively high urea concentrations ( $3 \leq \text{S:C} \leq 6$ ) used in these urea steam reforming experiments. A short investigation by ion chromatography of urea solutions for  $3 \leq \text{S:C} \leq 6$  was therefore required to assess the extent of urea isomerisation prior to its contact with the reactor catalyst bed.

#### 4.1.2 Thermolysis

The aim of urea thermolysis experimentation was to provide a greater understanding of the nature of the gaseous fuel as it entered the temperature gradient inside the reactor and at the catalyst bed. It also permitted further examination of how initial heat exposure could affect the extent of urea isomerisation as previously considered in section 4.1.1. Analysis of controlled thermal decomposition and

associated mass loss can also be used to quantify the kinetic parameters of underlying reaction mechanisms. The acquisition of all this information was considered pertinent for optimising reactor design, for setting steam reforming operational/experimental parameters, and as a means of verifying whether all significant species were considered in the material balances used to quantify steam reforming reactor product analysis.

Though urea thermolysis is one area where scientific literature is relatively abundant (a discussion of which has already been critiqued in section 2.6.2) compared to other aspects of this project's theme, the existing literature is found to be limited by its focus on NH<sub>3</sub>-producing reaction mechanisms for NO<sub>x</sub> reduction, a narrow range of gaseous product analyses, and an absence of experimentation involving nickel catalyst. The need for greater analysis is best described by a quote from one of the recent authors [48]:

*“the intricate and undoubtedly complex kinetics associated with [urea thermolysis] largely remain a mystery and a challenge to investigators”*

Previous studies using Simultaneous Thermal Analysis (STA) have monitored evolved gases by FTIR [48, 61, 63] and MS [57] to elucidate thermolysis, but for anhydrous (pure) urea only. Extended analysis was therefore required to include thermolysis of aqueous urea mixtures, with also a greater range of ions monitored by MS. Additionally, nickel catalyst (as used in urea steam reforming experimentation – see Table 5-1) was incorporated into thermolysis samples to try and reveal its influence on steam reforming. The rationale for these fuel characterisation experiments was given extra weight by the need to investigate possible early (very low temperature) H<sub>2</sub> evolution as observed in some experimental results where aqueous urea mixtures close to the eutectic range (S:C = 7) were used (see section 5.4.1).

## 4.2 Method

### 4.2.1 Urea in Water Solubility

The composition of the urea reagent is given in Table 2-6. Room temperature de-ionised water (obtained using an Elgastat water purification system) was used as the solvent. The desired ratio of urea in water on a molar S:C basis was determined from the following formula:

$$S:C = \left( \frac{M_{r(urea)}}{M_{r(water)}} \right) \times \left( \frac{measured\_mass_{(water)}}{measured\_mass_{(urea)}} \right) \quad (F10)$$

Volumes of water used were < 50 ml, and typically between 20 – 40 ml. Relative molecular masses of the reagents were taken as  $M_{r(\text{urea})} = 60.06 \text{ g/mol}$ , and  $M_{r(\text{water})} = 18 \text{ g/mol}$ .

A quantity of de-ionised water was first poured into a 50 ml graduated flask and its mass was determined using an electronic balance that had been calibrated to discount the weight of the flask. Mass measurements were obtained to an accuracy of  $\pm 0.0005 \text{ g}$ . A relative density of 1.000 was assumed for water. By transposing (F10), the mass of urea was determined by inserting the desired value of the S:C mixture:

$$\text{measured mass}_{(\text{urea})} = \left( \frac{\text{measured\_mass}_{(\text{water})}}{S:C} \right) \times \left( \frac{M_{r(\text{urea})}}{M_{r(\text{water})}} \right) \quad (\text{F11})$$

A mass of urea – value obtained from (F11) – was then measured out using the calibrated electronic balance. This was then combined with the water and its solubility observed. Complete solvation was determined by visible observation. This procedure was conducted at a laboratory temperature of 20 °C.

#### 4.2.2 Ion Chromatography

Based on the method by Lin *et al.* [144], a Dionex DX-100 Ion Chromatograph with an AS14A column (4 mm × 250 mm), was used to determine the concentration of cyanate ions in urea solution and therefore by inference the extent of the urea isomerisation for solutions S:C = 3, 4, 5, 6, and 7. An eluent of 3.5 mM/1.0 mM  $\text{Na}_2\text{CO}_3/\text{NaHCO}_3$  was prepared by dissolving 3.710 g (350 mM)  $\text{Na}_2\text{CO}_3$  and 0.840 g (100 mM)  $\text{NaHCO}_3$  in 1 litre of distilled water and diluting this ten times. A de-ionised water sample was run through the column prior to analysis of cyanate to calibrate a baseline.

Prior to analysis of the urea solutions, a 100.60 ppm sodium cyanate ( $\text{NaCNO}$ ) stock solution was prepared by dissolving 160.51 mg of 97% sodium cyanate (Alfa Aesar) in 1 litre of distilled water. Serial dilutions of this stock solution were then made at 1.006, 5.031, 10.060, 20.124, and 40.248 ppm. These standards were eluted through the chromatograph to create a calibration plot. The five calibration points and resultant peak detection values were also plotted using Microsoft Excel. By linear regression a trendline was added to quantify the linearity using the statistical co-efficient of determination ( $R^2$ ) method. The analytical limit of detection was determined from this plot by the trendline's axial intersection.

Urea solutions were prepared as described in section 4.2.1. All sample preparation was performed immediately prior to analysis. At most, three samples were loaded into the Dionex “rack”. The eluent flow rate during analysis was  $1 \text{ ml min}^{-1}$  with a run time

of 15 minutes, making a maximum residence time of the samples prior to analysis of < 1 hour after preparation.

The urea solution samples were also tested for pH using a Corning 135 pH/ion meter. This test was done by insertion of the ion probe into the volumetric flask containing the remainder of the sample. The remaining portion of sample was that which had been left over after a quantity had first been loaded into the ion-chromatograph. This was to avoid contamination of the sample prior to ion chromatography. The pH/ion meter was calibrated by pH buffers prior to analysis.

### 4.2.3 Thermal Analysis

Urea was in its as-supplied dry crystalline powder form (see Table 2.6 for composition). Urea solutions were prepared as described in section 4.2.1. Where catalyst was included in the sample, this was nickel catalyst as used in all urea steam reforming reactions. The catalyst had been subject to a chemical reduction experiment prior to analysis and had then been crushed to a fine powder. This is described fully, along with the sample's provenance, preparation and mode of storage in section 7.1. Samples were weighed on an electronic top pan balance accurate to  $\pm 0.005$  mg.

Previous studies had identified initial urea decomposition as a first order reaction [69]. Therefore the reaction rate constant method was used to derive the kinetic parameters of urea thermolysis as it has been found to give excellent results, comparable with more complicated methods [146]. It assumes that the reactions obey the Arrhenius equation:

$$k = A \exp\left(-\frac{E_a}{RT}\right) \quad (\text{F12})$$

where:

$k$  = experimental reaction rate constant

$E_a$  = activation energy, in  $\text{J mol}^{-1}$

$A$  = frequency factor, in units of collisions  $\text{sec}^{-1}$

$R$  = universal gas constant, in  $\text{J K}^{-1} \text{mol}^{-1}$

$T$  = temperature, in Kelvin

The apparent first order rate constant ( $k$ ) for each stage of mass loss per unit time was calculated over numerous small (seven second) iterations from:

$$k = -\frac{1}{(w_i - w_\infty)} \times \frac{dw}{dt} \quad (\text{F13})$$

where:

$w_i$  = initial mass

$w_\infty$  = terminal mass

$dw$  = small change in weight

$dt$  = small change in time

From these calculations of  $k$ , a plot of  $\ln(k)$  versus  $1/T$  (where  $T$  is the mid-range temperature of each iteration) was created. The slope of the trendline was used to determine  $E_a$  and  $A$ , with  $A$  being the  $\ln(k)$  axis intercept and  $E_a$  being calculated by the slope value multiplied by  $R$  according to (F12).

These Arrhenius parameters were then used to provide values of  $k$  at a range of temperatures. Residence time ( $t$ ) was then determined for urea conversion using:

$$\frac{d[\text{urea}]}{dt} = -k[\text{urea}] \quad (\text{F14})$$

and

$$\text{Residence time (t)} = \frac{-\ln \frac{[\text{urea}_t]}{[\text{urea}_0]}}{k} \quad (\text{F15})$$

where:

$[\text{urea}]$  = concentration of fuel,

$t$  = terminal,

$0$  = initial

Two analytical systems were used for these experiments:

#### 4.2.3.1 Thermogravimetric Analysis

A mass of 19.35 mg urea was weighed and inserted into a Stanton Redcroft TGH100 Thermogravimetric Analyser, Starting at 14 °C, the urea sample was subjected to increases in temperature at a rate of 3 °C min<sup>-1</sup>, under a 50 ml min<sup>-1</sup> N<sub>2</sub> gas flow. The N<sub>2</sub> gas was zero grade > 99.99 % purity from BOC cylinders. At 900 °C, the gas flow was changed to air (also from BOC cylinders) and the temperature was held for ten minutes, following which the experiment was stopped. Sample weight loss was obtained every second by the analyser and recorded onto a personal computer. Only a urea sample (**Table 2.6**) was analysed with this apparatus.

#### 4.2.3.2 Simultaneous Thermal Analysis

Four samples were analysed:

1. Urea
2. De-ionised water and urea (in a mixture ratio of S:C = 7)
3. Urea and catalyst
4. Catalyst, plus de-ionised water and urea (in mixture ratio of S:C = 7)

The samples contained a mass of urea in the range  $10.07 \leq \text{mg} \leq 33.49$ . The dry urea and nickel sample (sample 3) was prepared by mixing an identical weight of each reagent and then taking the final sample from this on the assumption that it represented a 50:50 mix. For the urea solution with nickel (sample 4), catalyst was added to the crucible and then drops of urea solution were administered using a pipette.

An alumina crucible that had been pre-heated to 1050 °C then allowed to cool was used to contain the samples. This was inserted into a Netzsch 449C Jupiter thermo-microbalance which was coupled (by a transfer line heated to 250 °C) to a Netzsch TA Quadruple Mass Spectrometer (QMS) 403C Aëolos for simultaneous detection and quantification of the evolved gases. The analyser was calibrated immediately prior to experimentation and a buoyancy baseline calibration also completed.

Once the crucible and sample were in-situ, the system, at 30 °C, was evacuated and de-pressurised from 1.0 atm to -1.0 atm three times, then purged with 80 ml min<sup>-1</sup> pure helium flow for at least 30 minutes. For samples containing water, the evacuation and de-pressurisation steps were omitted and the helium flow purge was maintained for 90 minutes to compensate.

The helium flow was maintained and the pressure set to 1.0 atm for the duration of the analyses. Helium was used instead of N<sub>2</sub> to identify any product N<sub>2</sub> evolved. The sample was then heated at a rate of 5 °C min<sup>-1</sup> from 30 °C to 700 °C and the results of mass loss logged on a personal computer. A range of m/z values, compiled from literature and including speculative species was programmed into the QMS for detection. This list, which is shown in **Table 4-2**, included all parent ions, plus fragment ions with an intensity  $\geq 2\%$  of the parent. Evolved gases were scanned approximately every 15 seconds and all (m/z) values were monitored simultaneously, with dwell times of 0.5 seconds for each. Recorded data was saved on a personal computer using Aëolos software.

The experiments were repeated for each sample under identical TGA operating conditions but this time with a gas splitter installed prior to the QMS and a transfer line connected to divert evolved gases into an FTIR analyser. The FTIR transfer line was heated to 150 °C. A laser controlled Nicolet AVATAR 370 DTGS FTIR was used, with

the results processed by OMNIC software. This analyser had a detection cell volume of 400 ml. Residence time of gases in the transfer line was considered to be negligible.

**Table 4-2.** Mass/charge values programmed for detection in QMS. Values obtained from [137] unless otherwise stated.

Parent Species	m/v	Fragment Ion	m/v	Abundance (Intensity relative to Parent Species)
H <sub>2</sub>	2	n/a	n/a	n/a
C	12	n/a	n/a	n/a
CH <sub>4</sub>	16			100 %
		CH <sub>3</sub> <sup>+</sup>	15	90 %
		CH <sub>2</sub> <sup>+</sup>	14	21 %
		CH	13	13 %
		C <sup>+</sup>	12	5 %
NH <sub>3</sub>	17			100 %
		NH <sup>+</sup>	16	80 %
		NH <sub>2</sub> <sup>+</sup>	15	8 %
		N <sub>2</sub> <sup>2+</sup> , N <sup>+</sup>	14	2 %
H <sub>2</sub> O	18			100 %
		OH <sup>+</sup>	17	20 %
N <sub>2</sub>	28			100 %
		N <sub>2</sub> <sup>2+</sup> , N <sup>+</sup>	14	17 %
CO	28			100 %
		C <sup>+</sup>	12	5 %
HNCO [59, 147]	43			100 %
		NCO <sup>+</sup>	42	22 %
		HCO <sup>+</sup>	29	14 %
		NH <sup>+</sup>	15	7 %
		CO <sup>+</sup>	28	7 %
		u/k	44	2 %
		NO <sup>+</sup>	30	2 %
		HCN <sup>+</sup>	27	2 %
		CN <sup>+</sup>	26	2 %
CO <sub>2</sub>	44			100 %
		CO <sup>+</sup>	28	10 %
		O <sup>+</sup>	16	10 %
		C <sup>+</sup>	12	9 %
CN <sub>2</sub>	52	n/k	n/a	n/k
Urea	60	n/k	n/a	n/k



## 4.3 Results/Discussion

### 4.3.1 Solubility

Urea dissolved within seconds for S:C = 7 and all increasingly water-rich mixtures. For S:C = 5 and 6, solvation took a few minutes and required the application of energy by holding the flask tightly in cupped hands with gentle agitation (refer to section 3.3.8 for energy of solvation). Urea dissolved by the same method with S:C = 4 but took between five to ten minutes. To obtain an S:C = 3 solution, it was necessary to apply heat from a Bunsen burner to the base of the flask. Solvation took 30 minutes. The solvation of the S:C = 2 mixture was attempted using heat from a Bunsen burner. After twenty minutes these attempts were aborted due to the observations of evaporate being emitted from the flask and also a precipitate forming around the flask's rim evidencing that the solution ratio was no longer accurate.

The values of solubility are consistent with those quoted in literature, as shown in **Table 2-4**. Accordingly, the maximum solubility attainable at 20 °C is 51.6 wt%, corresponding to S:C = 3.13. Higher temperatures would be expected to dissolve urea to S:C = 2 and greater. It is probable that with a less direct source of heat, evaporation could be avoided and therefore complete solubility of S:C = 2 mixtures achieved. This was not pursued further as it would have required that the reforming reactor be fitted with apparatus to maintain the feed line temperature at  $\geq 40$  °C. These requirements were considered impracticable due to the low temperature tolerance of the dispensing syringe, and the dispensing mechanism of the syringe pump prohibiting any form of insulating cover attachment (see Chapters 5 and 6).

Extending the time allowed for complete solvation was disfavoured due to the potential for enzymatic urea decomposition occurring in the non-sterile flask. All equipment was however clean and rinsed with de-ionised water prior to usage so it is considered that best practice was adopted to avoid sample degradation.

### 4.3.2 Ion Chromatography

Well defined cyanate peaks occurred with the calibration standards, eluting at 6.9 minutes ( $\pm 0.1$ ). An example for the 40 ppm stock dilution, and representative of all the calibration standards is given in **Figure 4-1**. An  $R^2$  value of 0.9999 was obtained for the calibration plot trendline. A limit of detection value of 0.5 ppm was obtained from this same trendline's intersection with the x-axis.

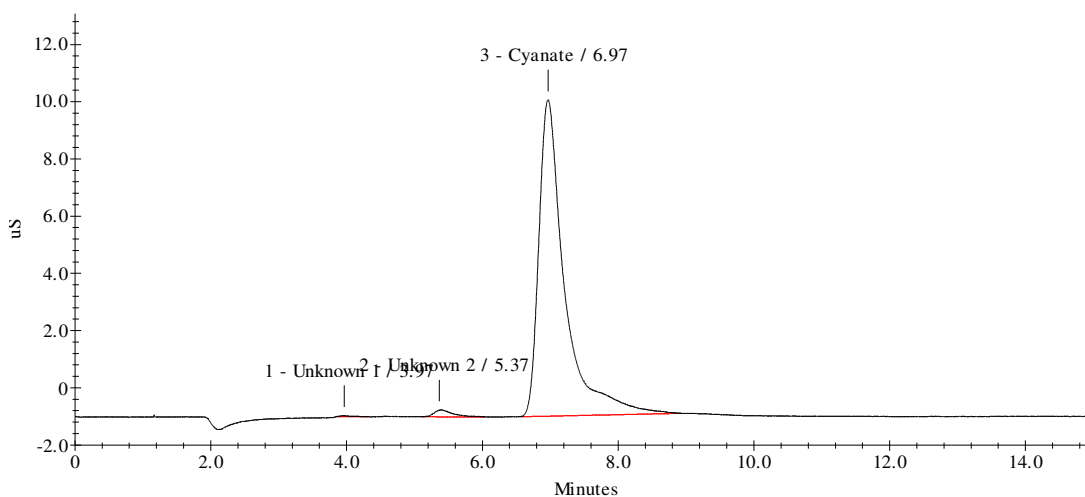


**Figure 4-1.** Ion chromatogram for 40 ppm cyanate stock dilution used in calibration.

No cyanate peaks were detected in any of the urea samples. An ion chromatogram showing the urea sample for S:C = 3, and representative of all the urea solutions analysed is given in **Figure 4-2**.

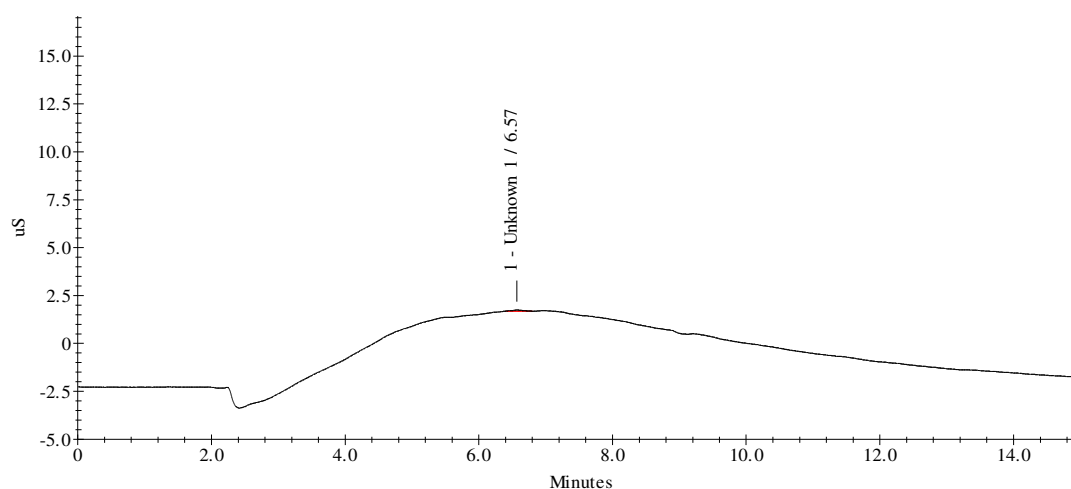


**Figure 4-2.** Ion chromatogram of S:C = 3 (18.5 M) urea in distilled water.

The raised baseline shown in **Figure 4-2** was evident in all samples analysed. This phenomenon was also observed by Lin *et al.* for samples containing high concentrations of urea [144]. No explanation was offered by the authors, but since a de-ionised water baseline test was run in this analysis prior to the samples and seen to show a level baseline at zero conductivity, the influence of the water can be discounted. It is likely therefore that the raised baseline is symptomatic of urea's interaction with the column matrix. As this experiment used much higher concentrations of urea in solution, the presence of a raised baseline, and its probable amplification, is corroborative of the

reports made by Lin *et al.* Despite the raised baseline, cyanate peaks were still present in Lin *et al.*'s report, evidencing the adequacy of this method if cyanate were present in sufficient concentration.

Due to the good resolution of cyanate detection with the calibration standard dilutions, the absence of a cyanate peak in these results is good evidence that cyanate was not present above the detection limit of 0.5 ppm in any of the urea samples analysed. The higher standing time for the solution prior to analysis in the work of Lin *et al.* [144] can explain why cyanate was detected only in their study.

Further validation for the rigour of the experimental method is provided by results of sample pH. These results revealed values of  $\text{pH} = 7.3 \pm 0.1$ . Thus, according to Hagel *et al.* [143], the presence of cyanate, if sample urea decomposition had occurred, should not have been inhibited.

For future work, this method may detect cyanate in urea solutions by repeating the calibration to a lower level of concentration. However, the limit of detection at 0.5 ppm is considered adequate for the aims of this study since it confirms the maximum limit detected by Hagel *et al.* up to 5 hours after urea solvation [143].

### 4.3.3 Thermal Analysis

#### 4.3.3.1 Stanton Redcroft TGH100

The mass loss curve from the thermolysis experiment in the Stanton Redcroft TGH100 is shown in **Figure 4-3**. An apparent increase in mass of  $\leq 0.5\%$  was observed from the commencement of the experiment and prior to the first decomposition stage. A corresponding value of mass gain was detected after the introduction of airflow at 900 °C. This is attributed to buoyancy effects on the sample within the analyser and therefore not a truly representative phenomenon of thermolysis. The switch to air flow at 900 °C was to detect whether any additional mass loss may occur due to oxidation.

Results were analysed as a function of time and temperature on a mass, and on a weight percent basis. A multi-step decomposition was observed up to complete sample thermolysis ( $< 0.5\%$  mass remaining  $\pm 0.1\%$ ) at 506 °C. The results of this analysis are shown graphically on a weight percent basis as a function of temperature in **Figure 4-3**. A thorough discussion on the shape of the urea decomposition curve is given later in section **4.3.3.2** combined with the results of EGA (Evolved Gas Analysis).

No additional mass loss was observed when the system was then switched to air flow at 900 °C. These results indicate that a reactor temperature of 700 °C maximum would be sufficient for 99.9 % urea conversion, with 99.5 % conversion above 500 °C.

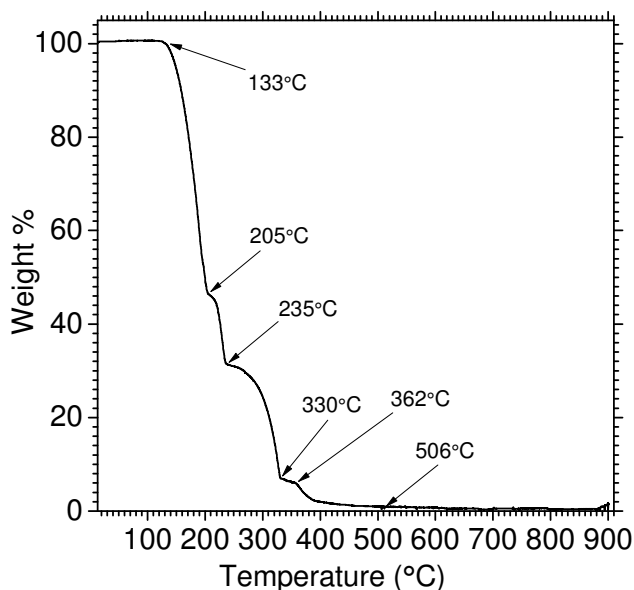


**Figure 4-3.** TGA curve of urea at a heating rate of  $3\text{ }^{\circ}\text{C min}^{-1}$ . Weight percent mass loss shown as a function of temperature under  $\text{N}_2$  flow of  $80\text{ cm}^3\text{ min}^{-1}$ .

#### 4.3.3.2 Simultaneous Thermal Analysis

The usual procedure in STA-MS is to evacuate the sample prior to analysis in order to lower the baseline signal. However, high mass losses were observed in the samples containing water during the preparatory evacuation step with the sample in-situ. This was investigated by testing evacuation on a pure water sample and on a pure urea sample. It was found to be due to water evolution accentuated by system depressurisation. Thereafter, the evacuation step was omitted for all analyses on samples containing urea solution. To compensate, the helium transfer line purge was increased to 90 minutes duration.

Even under atmospheric pressure, samples containing aqueous urea solution exhibited a small but constant mass loss. This was observed during transfer line purge to be at a rate of  $0.01\text{ mg sec}^{-1}$ . Consequently there is experimental error associated with the accuracy of the urea solution's final concentration during analysis. To correct for this phenomenon, the mass immediately prior to the onset of heating was recorded and taken as the initial mass, with the difference attributed to loss of water. For urea samples of S:C = 7, given the mass loss rate of  $0.01\text{ mg sec}^{-1}$  over a time of 90 minutes, this is negligible, with the water to urea ratio still remaining as S:C = 7.00 correct to two decimal places: a 0.03 % change.

**Figure 4-4** shows the TGA curve of mass loss for urea as a function of temperature. The apparent mass increase prior to 133 °C has been removed by the buoyancy calibration; otherwise the results show a mass loss curve similar in shape to

**Figure 4-3** though less well resolved in smaller features such as the small step change in mass loss at 205 °C and the gradient change in mass loss at 362 °C. These are probably a consequence of the lower heating rate applied to the Stanton method creating greater accuracy.

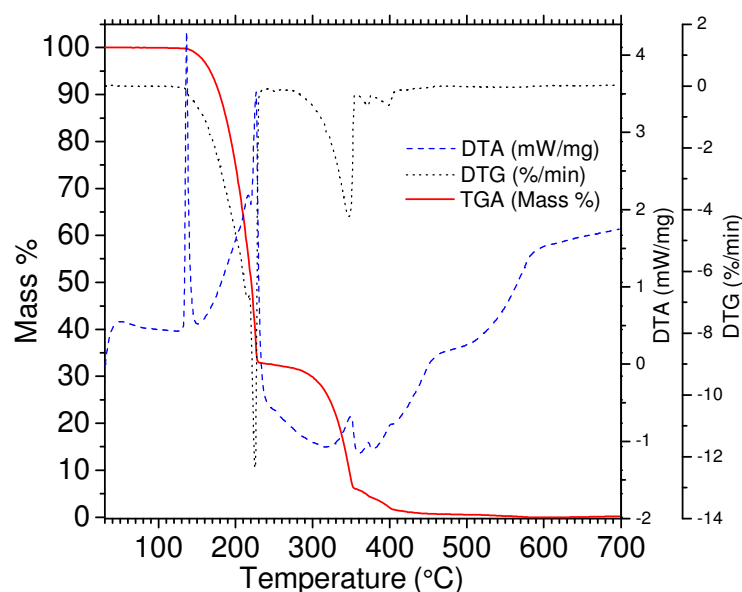


**Figure 4-4.** TGA, DTA, and DTG curves for urea as a function of temperature under a He flow of  $80 \text{ cm}^3 \text{ min}^{-1}$ . A heating rate of  $5 \text{ }^\circ\text{C min}^{-1}$  was applied.

Superimposed on the TGA curve in **Figure 4-4** are the results of DTA, which shows the difference in temperature between the sample and an inert reference, and Derivative Thermogravimetry (DTG) which shows the rate of mass change. Two heat absorption peaks during the first stage of mass loss are apparent from the DTA and evidence the endothermic events of first urea melting at 133 °C (evident as melting rather than decomposition from the DTG curve by the absence of any detected mass loss) and then the urea decomposition reaction (R19) up to 215 °C as previously reported (see section 2.6). The second episode of urea thermolysis, from  $\text{ca } 235 \text{ }^\circ\text{C} \leq T \leq 330 \text{ }^\circ\text{C}$ , is seen from the DTA curve to involve multiple reaction mechanisms when the decomposition of urea melt constituents (cyanuric acid, ammeline, and ammeline) occurs; an overall exothermic event as it reaches completion.

EGA detected an increase in ion intensity for all species measured except ions  $m/z = 52$  and  $60$ . These species were not detected throughout the full temperature programme in any of the samples tested therefore they have been omitted from all graphs that show Multiple Ion Detection (MID). Since there is no ambiguity in the detection of urea at  $m/z = 60$ , the analysis evidences that it did not evolve at all. In all MID graphs, the ion intensity curves have been corrected to a zero baseline. Note the difference in scale on the y-axis where stacked MID graphs are displayed (e.g. **Figure**

4-5). The bottom stacked graph shows a higher resolution of the detection range to reveal low ion intensity species variations. Concentration cannot be revealed from the individual ion intensities, but qualitative relations can be inferred based on comparisons between experimental samples. Similarly FTIR results were not calibrated to provide values of concentration; and though high accuracy in identification can be assumed by the transmissions, only comparisons between the spectra from different samples can be used to provide inferences on species abundance. FTIR did provide a rigorous means for resolving ambiguities in identification of species that have the same mass/charge number as shown in **Table 4-2**.

The dry urea sample thermolysis MID plot (**Figure 4-5**) shows ion intensity peak maxima coincident with the DTG minimum for stage one mass loss. Upon closer examination this region can be seen to result from two separate episodes of species evolution, a feature not seen in the previous urea MS study by Carp [57]. Carp's study did not analyse for the ions that permit this identification. The earlier ion intensity maxima region occurs at ca. 185 °C and coincides with the onset of endothermicity seen on the DTA curve (**Figure 4-4**). At this lower temperature,  $m/z = 16$  and 17 had major ion intensity peaks. These were identified as being from  $\text{NH}_3$  by FTIR [137, 148], with the MS  $m/z = 16$  intensity peak originating from the 80 % abundance fragment ion  $\text{NH}_2^+$  (see **Table 4-2**) and, therefore confirming the proposal of Carp [57]. The MID curves of dry urea thermolysis shown in **Figure 4-5** also reveal the three most abundant  $m/z$  numbers that originate from HNCN ( $m/z = 43, 42,$  and  $29$  – see **Table 4-2**) peaking at this earlier episode of stage one mass loss and following similar trends with respect to temperature; thus firmly evidencing the detection of HNCN. This initial thermal decomposition of urea via reaction mechanism (R19) is as suggested by some previous authors. HNCN was not however seen in the spectra from FTIR at all in the temperature range  $T \leq 180$  °C (see **Figure 4-6**), corroborating the results of the study by Schaber *et al.* [48]. HNCN has uniquely strong peaks in the 2250 – 2300  $\text{cm}^{-1}$  wavenumber and 3500 – 3530  $\text{cm}^{-1}$  wavenumber regions [147, 149], which, as can be seen in **Figure 4-7** at  $T = 170$  °C are clearly absent. Relatively smaller peaks, attributable to  $\text{CO}_2$  (doublets in the region 2350 – 2361  $\text{cm}^{-1}$ ) [137] were however detected by FTIR and are also shown by **Figure 4-7**. This may indicate a detection of background air contamination, or that some HNCN was produced, but rapidly hydrolysed according to (R20) as predicted by kinetic studies [69, 70, 71]. For this latter reaction to have occurred would necessitate the presence of water. This water could have originated as a by-product of ammeline production as previously suggested by Schaber *et al.* [48]. Evolved gas profiles for wavenumbers specific to HNCN do highlight a difference in HNCN detection between dry urea samples and those containing urea solution. The urea in solution samples show little or no HNCN released until ca.  $T \geq 330$  °C, whereas the dry urea samples show some HNCN released in the temperature region ca. 100 °C earlier

(**Figure 4-6**). This can be attributed to the occurrence of HNCO hydrolysis (R20), promoted by the presence of water in the urea solution samples.

The occurrence of partial and preliminary thermal decomposition to ammonium cyanate (R15) appears evident by the peak in intensity  $m/z = 42$  ( $\text{NCO}^+$ ), but is refuted by FTIR due to an absence of its unique spectral peak in the region  $2180\text{ cm}^{-1}$  [150] (see **Figure 4-7**). FTIR also confirmed the absence of CO and  $\text{CH}_4$ , resolving the ambiguity over assignment of numbers  $m/z = 28$  and  $m/z = 16$ .

With increasing temperature, the species observed by MS and attributed to HNCO then decline in intensity, with ion intensities related to ammonia,  $m/z = 17$  ( $\text{NH}_3^+$ ) and  $m/z = 16$  ( $\text{NH}_2^+$ ) continuing to increase, both reaching maxima at  $228\text{ }^\circ\text{C}$ . This tends to accord with the reaction mechanisms proposed by previous authors where, at  $T > 185\text{ }^\circ\text{C}$ , it is suggested that further evolution from secondary decomposition polymer products occur (section **2.6.2**). Note the small step change in ion intensity for species  $m/z = 15, 16, 17, 44,$  and  $12$  at ca.  $220\text{ }^\circ\text{C}$  representing the region of biuret stability prior to the onset of its decomposition and further species evolution thereafter. An increase in intensity for probable fragment ions from both nitrogen ( $m/z = 28$  and  $14$ ) and carbon ( $m/z = 12$ ) at these temperatures support this.

The plateau region seen in **Figure 4-3** between  $330\text{ }^\circ\text{C}$  and  $360\text{ }^\circ\text{C}$ , and less well resolved in the DTA curves at  $350\text{ }^\circ\text{C}$  in **Figure 4-4**, reveals the thermal stability of cyanuric acid. As temperature increases, decomposition of cyanuric acid, and the residual polymers ammelide and ammeline has been shown to occur [48]. This represents the final asymptotic mass loss from anhydrous urea. One interesting observation from this EGA experiment with pure urea was the relatively prominent peak for  $m/z = 15$  ( $\text{NH}^+$ ), having a maximum at  $220\text{ }^\circ\text{C}$ . In Carp's study, though it was one of the species monitored, it had negligible ion intensity variation from its baseline throughout [57]. A reason for this discrepancy cannot be explained other than it being due to differences in instrumentation and/or methodology.

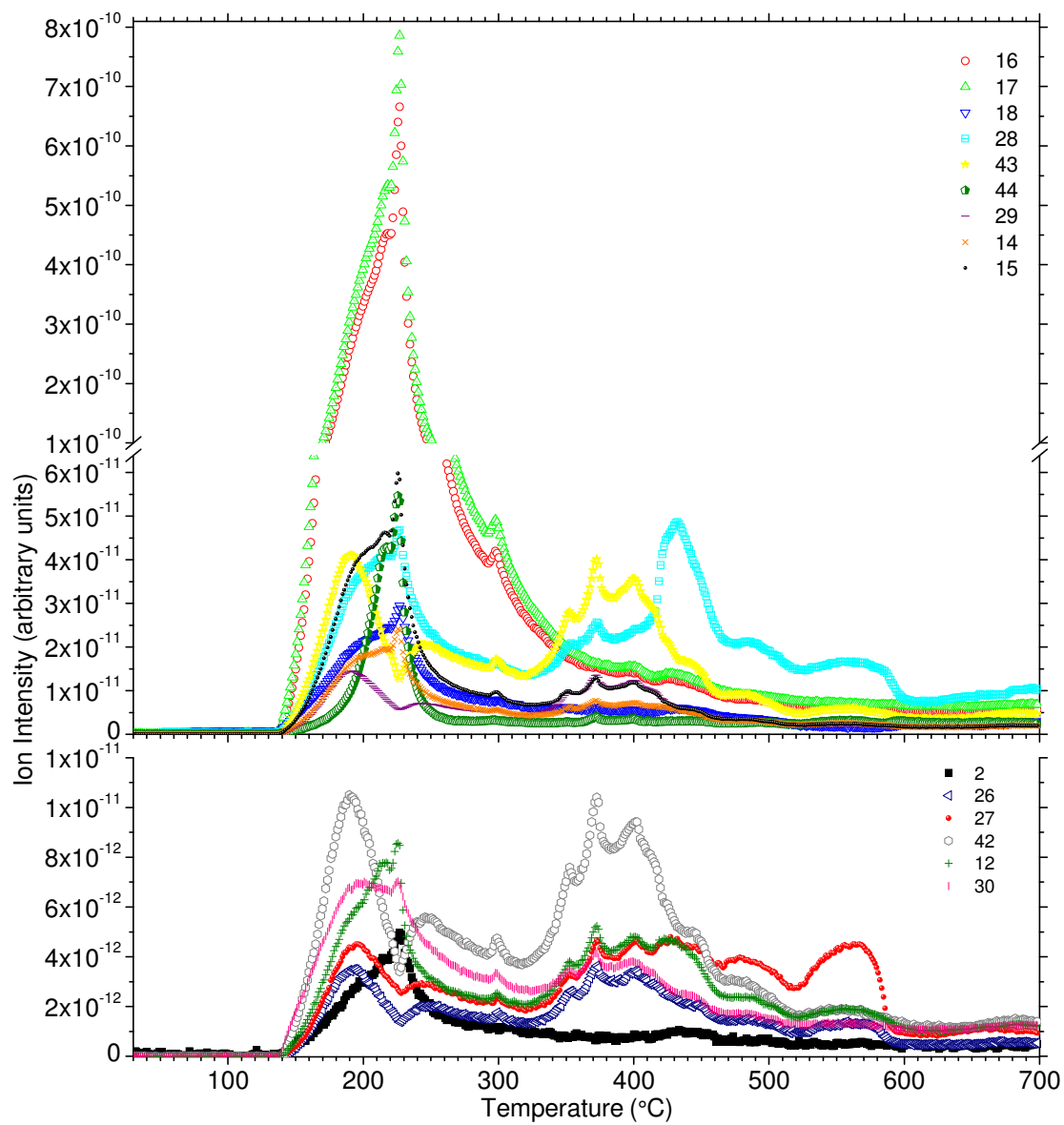


**Figure 4-5.** Selected MS multiple ion detection curves for pure urea thermolysis EGA.



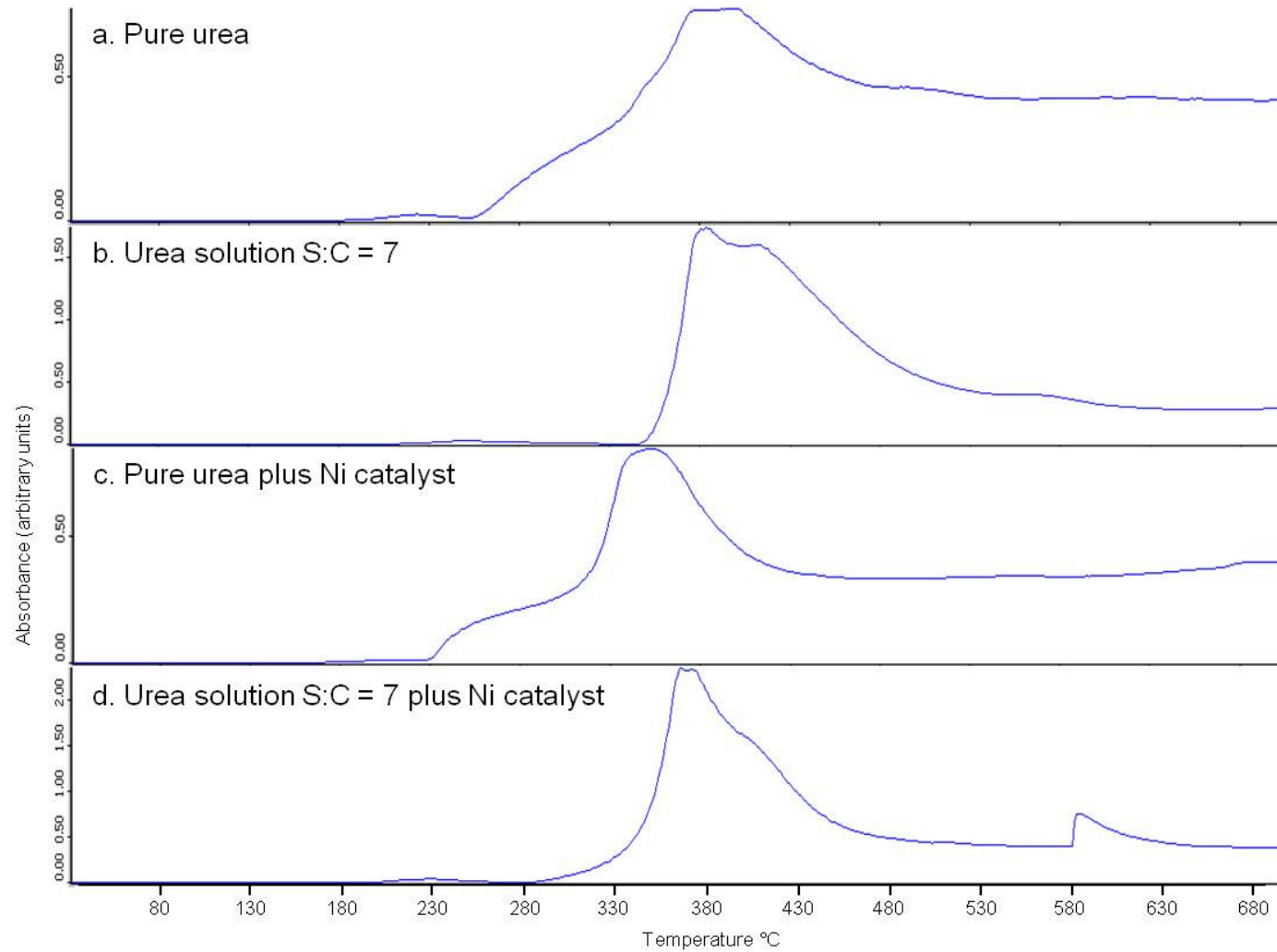


**Figure 4-6.** Evolved gas profiles for H<sub>2</sub>CO, detected via FTIR absorbance at wavenumber 2271 – 2285 cm<sup>-1</sup>.

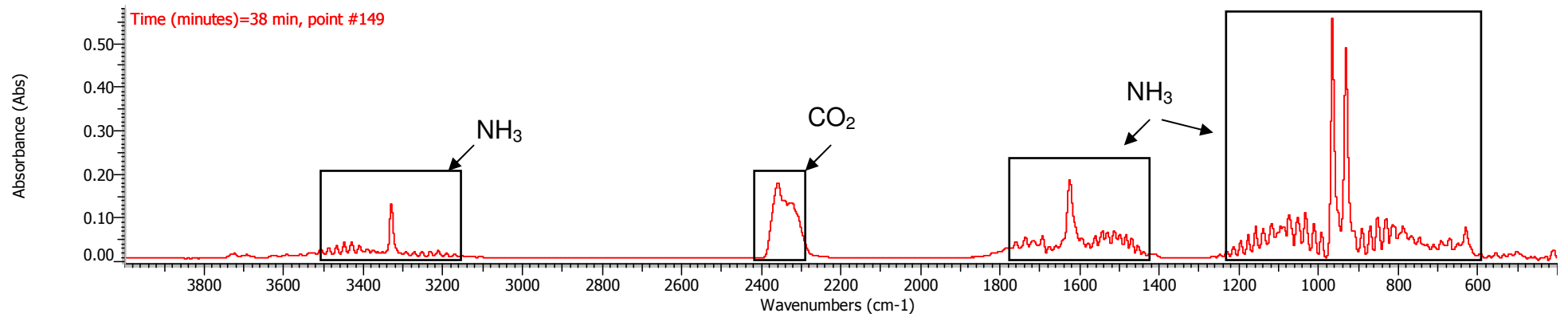


**Figure 4-7.** FTIR transmittance spectrum from STA of pure (anhydrous) urea sample at T = 170 °C. Spectral peaks identified from [137] and [148].

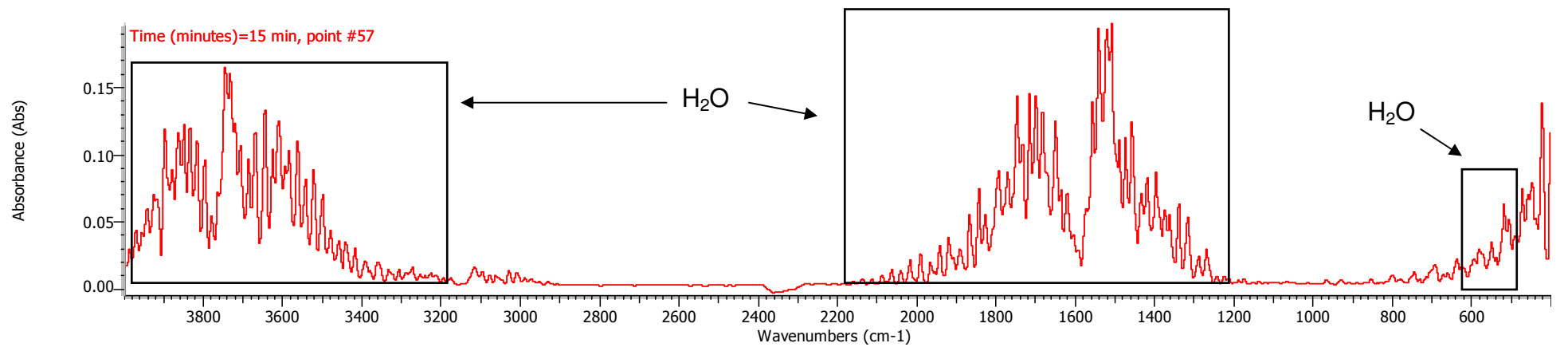


**Figure 4-8.** FTIR transmittance spectrum from STA of S:C = 7 aqueous urea sample at T = 105 °C. Spectral peaks identified from [137].

The relevance of anhydrous urea sample decomposition (particularly at  $T \geq 185$  °C) to the context of flow reactor urea steam reforming is considered to be limited for a number of reasons. The absence of water from this TGA experiment precludes the full realisation of the urea steam reforming reaction (R25) and also isocyanic acid hydrolysis (R20). Consequently in a urea flow reactor (and particularly one containing a metal oxide catalyst) any HNCO acid is anticipated to rapidly hydrolyse as reported previously by Yim *et al.* [69] and Kleeman *et al.* [70], rather than remain to form a melt, to which this second TGA mass loss stage is attributed. Therefore, further discussion of pure (anhydrous) urea thermolysis from these fuel characterisation experiments is avoided as it is considered to provide little to enhance previous literature reports. The remainder of this chapter will focus on the novel approach of analysing the observed effects of incorporating water and nickel catalyst into the thermolysis samples. Furthermore, and in general to all samples analysed in this series of characterisation experiments, the gradual heating rate of this methodology is not directly comparable with the temperature exposure that the reagents would encounter in a flow reactor. In a flow reactor, the process design would create instantaneous exposure of the urea solution to the high temperature at the catalyst bed, at which completely different reaction mechanisms may prevail.

Analysis of the TGA/DTA/DTG curves for urea solution thermolysis add little to permit elaboration on the relevancy of this method since they show a pronounced peak in mass loss and temperature differential due to endothermic water vaporisation prior to urea decomposition (**Figure 4-9**). With the water component evolved, all curves thereafter exhibit apparently identical features to those of pure urea thermal decomposition. EGA results however did indicate the occurrence of different reaction mechanisms when water was included.

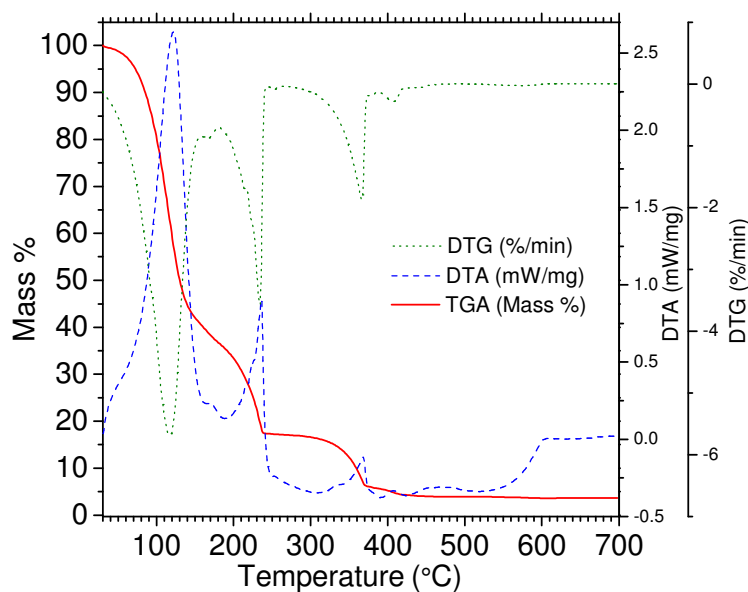


**Figure 4-9.** TGA, DTA, and DTG curves for S:C = 7 urea solution as a function of temperature under a He flow of  $80 \text{ cm}^3 \text{ min}^{-1}$ . A heating rate of  $5 \text{ }^\circ\text{C min}^{-1}$  was applied.

As expected, the MID curves for S:C = 7 urea in de-ionised water (**Figure 4-10** and **Figure 4-11**) revealed water evolution by a broad peak of  $m/z = 18$ , coincident with the DTA, and TGA curves ca.  $105 \text{ }^\circ\text{C}$ . The evolution of water was also detected by FTIR at this temperature region (see **Figure 4-8**). An increase in ion intensity for  $m/z = 17$  at this same temperature is likely due to the water fragment ion  $\text{OH}^+$ , previously shown to occur at 20% relative abundance to the parent species [137]. The increase in ion intensity for  $m/z = 16$  at this early temperature, could also be attributed to fragmentation from water vapour as previous MS studies have identified it as present though with very low relative abundance of ca. 1 % [137, 151]. There are complications to this simple model of pure water vapour evolution however, as the MS results suggested that other species were apparently released at the same temperature. This is in contrast to the pure urea sample thermolysis. **Figure 4-11** shows increases in ion intensity for  $m/z = 28$ ,  $m/z = 14$ , and  $m/z = 2$  as having occurred simultaneously with water vapour from ca.  $80 \text{ }^\circ\text{C}$  and peaking (again coincident with water vapour) at ca.  $105 \text{ }^\circ\text{C}$ . The  $m/z = 28$  and  $m/z = 14$  detections are obviously unrelated to the  $\text{H}_2\text{O}$  molecule; and no fragmentation of  $m/z = 2$  has been previously reported to occur from water vapour MS [151]. The presence of  $\text{H}_2$  (probable source of  $m/z = 2$ ) and  $\text{N}_2$  (probable source of  $m/z = 28$  and 14), cannot be revealed by the FTIR technique due to these species being diatomic molecules and not capable of infra-red induced interbond vibrations.

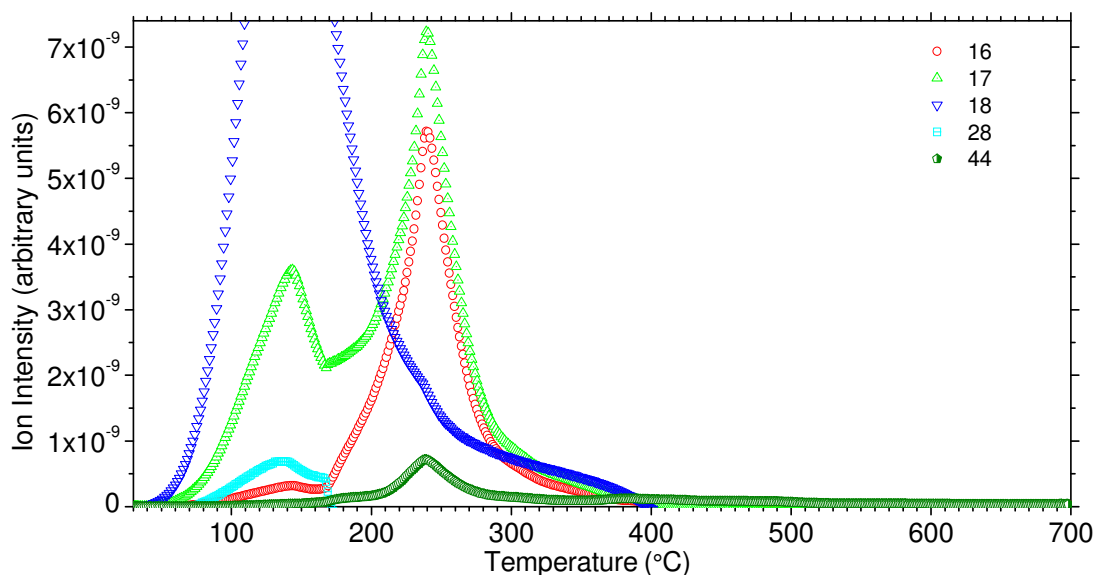


**Figure 4-10.** Urea in de-ionised water at S:C = 7 MS full ion intensity range curves.

The most likely explanation for the appearance of these unexpected mass/charge numbers is that some air was dissolved in the sample's water component (the source of the  $m/z = 28$  and  $m/z = 14$  ion detection being  $N_2$ ), however this would be unlikely to account for the increase in  $m/z = 2$  intensity. If this were not the cause, then the alternative would be that some  $NH_3$  or  $NH_4$  (producing  $m/z = 18$ ,  $17$  and  $16$ ) and  $H_2$  ( $m/z = 2$ ) was actually released with the water. To support this in theory, it has previously been reported that urea has a unique bonding interaction with water (see [77] and section 2.6.3) that could be responsible. It is also known that  $NH_4^+$  can be created via isomerisation of urea when heated (see section 4.1) and that  $NH_4^+$  is highly soluble in water. This alternative conjecture is weakened by the FTIR results which show an absence of absorbance peaks corresponding to the molecular vibrations from  $NH_3$  as seen by comparison of **Figure 4-7** and **Figure 4-8**. Common N-H stretching and deformation vibrations occur for ammonia in the wavenumber  $1600 - 1650\text{ cm}^{-1}$  and  $3200 - 3500\text{ cm}^{-1}$  regions respectively [148], and though these could be masked by the  $H_2O$  spectra also having transmittance in these regions (very broad peaks at  $3656$ ,  $3755$ , and  $1595\text{ cm}^{-1}$  [137]), the unique ammonia peaks in the fingerprint region between  $800 - 1100\text{ cm}^{-1}$  [137] are absent from **Figure 4-8**. Similarly, FTIR discounts the presence of  $CO^+$  as being the source of the  $m/z = 28$  detections, with  $CO^+$  having a strong peak doublet in the wavenumber  $2100\text{ cm}^{-1}$  and  $2200\text{ cm}^{-1}$  region, which again is clearly absent.

Of note here, to add to the discussion on possible release of  $H_2$  from urea-water solutions at low temperature, is that some  $H_2$  was detected as being released earlier than expected during urea flow reactor steam reforming experimentation (see Chapter 5).

Elucidation of this phenomenon is considered of relevance for future study as it may reveal a mechanism that can be utilised beneficially for low temperature H<sub>2</sub> production.

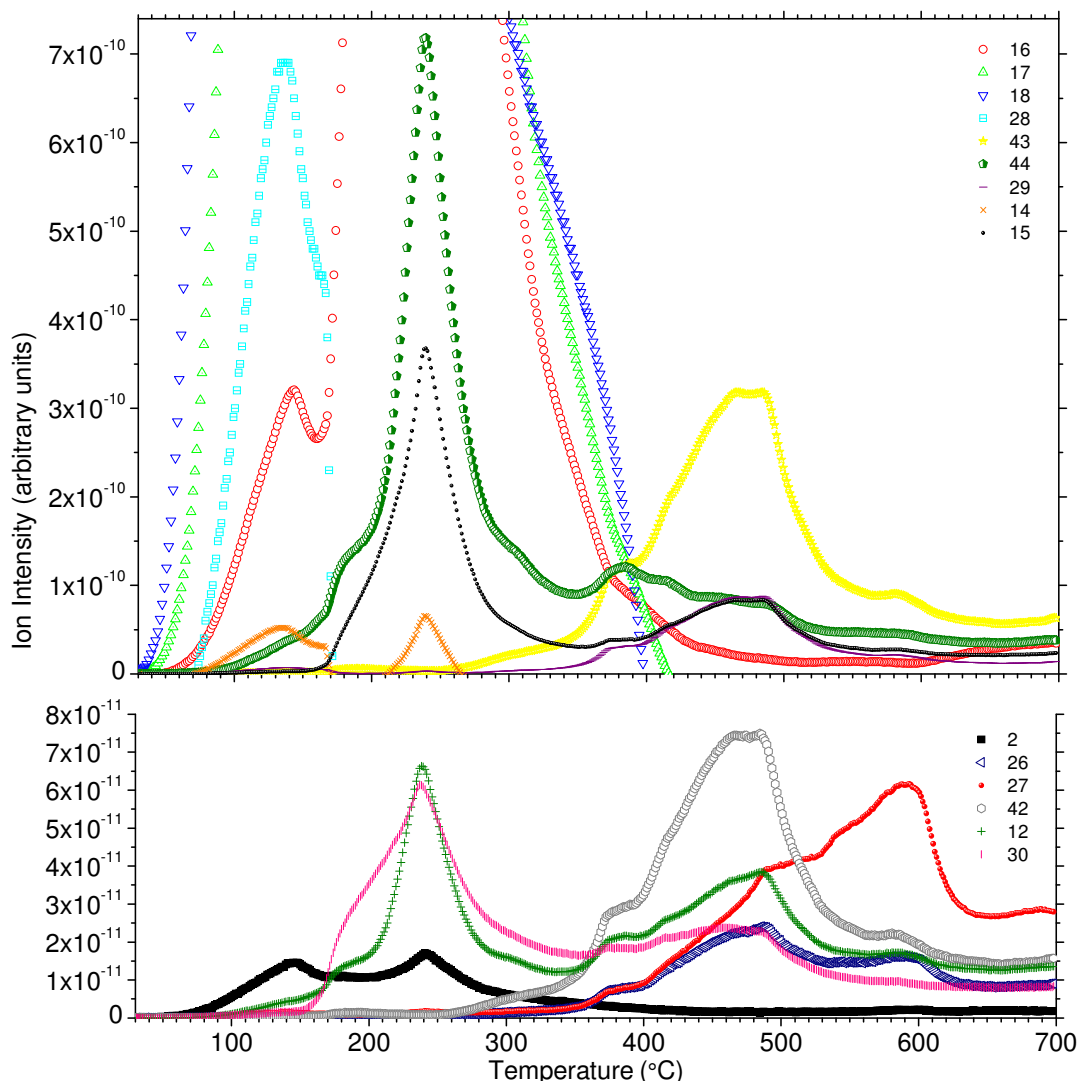


**Figure 4-11.** Urea in de-ionised water at S:C = 7 MS multiple ion detection curves (low and medium intensity detection).

As temperature increased further, and with water now mostly evolved, peaks for  $m/z = 17$  and  $m/z = 16$  were seen to occur in the ratio 1 : 0.8 as predicted for definite identification of NH<sub>3</sub>. Additionally,  $m/z = 44$  (CO<sub>2</sub>),  $m/z = 15$  (NH), and  $m/z = 14$  (N<sub>2</sub><sup>2+</sup> or N<sup>+</sup>) occurred with maxima at 238°C ( $\pm 1^\circ\text{C}$ ) corresponding to ions detected from gases evolved during thermolysis of the dry urea sample.

A significant difference with the HNCO ion intensities for dry urea and aqueous urea was detected. The HNCO ( $m/z = 43$ ) peak doublet previously seen with the dry urea sample (at 185 °C and then ca. 240 °C) was absent in the aqueous urea EGA results, with now only one low intensity maximum for  $m/z = 43$  coinciding with

maxima for  $m/z = 17$  ( $\text{NH}_3^+$ ),  $m/z = 16$ , and  $m/z = 44$  ( $\text{CO}_2^+$ ) at  $238\text{ }^\circ\text{C}$  ( $\pm 1\text{ }^\circ\text{C}$ ). To quantify this, in comparison with the dry urea EGA experiment, the peak height ratios of  $\text{NH}_3\text{:HNCO}$  were 57:1 for dry urea and 1567:1 for urea solution; and for  $\text{CO}_2\text{:HNCO}$  these were 14:1 for dry urea and 153:1 for urea solution for this first stage of urea decomposition. This significant difference can be explained by the prevalence of the HNCO hydrolysis reaction (R20) as predicted because water was present in the sample. Despite the limitations of drawing parallels between the slower batch heating of this TGA and the rapid heating, flow conditions of the steam reforming reactor, these results show how water can significantly reduce the concentration of any HNCO emitted from urea decomposition, a phenomenon likely to be assured of with a process containing excess flowing water.

Close observation of the dry urea and catalyst TGA curve shows an apparent affect on the mass loss compared to the non-catalyst containing sample by smoothing out the end of each decomposition stage (labelled point 'a' and point 'b' on **Figure 4-12**). This suggests that the catalyst could have reduced the thermal stability of residual products in the melt and/or brought forward the onset of next stage decomposition to a lower temperature by reduction of activation energy  $E_a$ , a beneficial effect as it is reducing the overall product stability. This phenomenon was not however seen for the S:C = 7 urea solution with catalyst sample (**Figure 4-13**) which tends to refute the hypothesis.

The TGA curve shown in **Figure 4-12** has been normalised to discount the mass remaining after analysis (assumed to be solid nickel). The initial mass, assumed according to the method of preparation to be a 50:50 mix of urea and nickel, was 20.13 mg. The residual mass following analysis was however 7.92 mg, rather than the 10.07 mg expected with total decomposition of the urea component. The method of preparation which involved first mixing the urea and nickel and then taking a portion of this as the sample rather than adding each constituent individually, though considered to be the best possible choice, did not allow precision in ensuring that the initial sample contained an equal mixture of urea and nickel. Uncertainly here was not considered relevant to valid analysis of the results. One influencing factor on the residual mass value may be that some of the nickel had been oxidised by urea decomposition products, but this would have increased rather than decreased the final mass. Catalyst oxidation is supported by the apparent exothermic heat difference detected after  $350\text{ }^\circ\text{C}$ , and shown by the DTA curve on **Figure 4-12**. However it is not supported by the multi ion detection plots for this sample as a relative dip in oxygen-containing species, which would be expected, did not occur. It is feasible also to consider that some moisture may have been present in the catalyst at the time that its weight was measured, resulting in a loss of mass during heating. However, the most likely cause is that the final mass of nickel reflects the unequal ratio of the sample mixture.

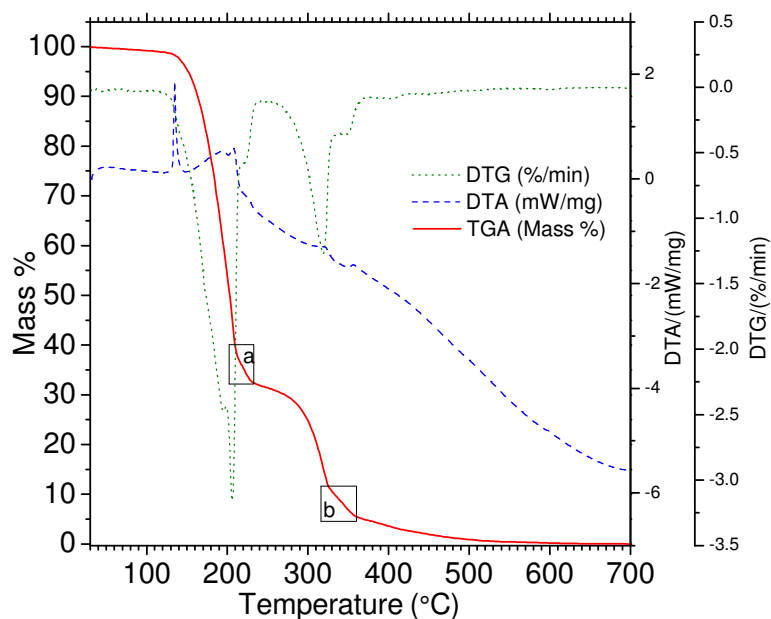


**Figure 4-12.** TGA, DTA, and DTG curves for urea and nickel catalyst as a function of temperature under a He flow of  $80 \text{ cm}^3 \text{ min}^{-1}$ . A heating rate of  $5 \text{ }^\circ\text{C min}^{-1}$  was applied. Marked regions are referred to in text.

The nickel catalyst and S:C = 7 urea solution sample TA (**Figure 4-13**) revealed, as expected, initial mass loss and endothermicity associated with water evolution as per **Figure 4-9**. With increasing temperature, TGA, DTA, and DTG curves were indistinguishable from **Figure 4-9** and similar to **Figure 4-12**.

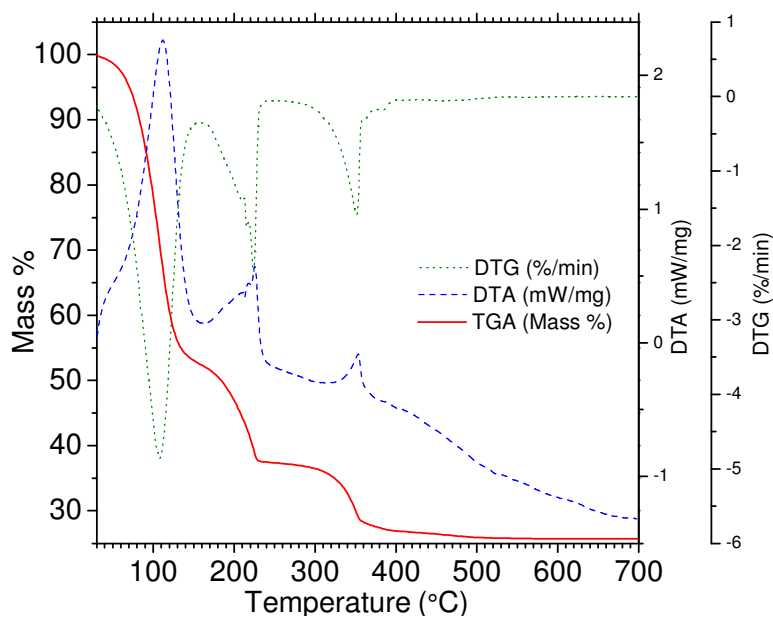


**Figure 4-13.** TGA, DTA, and DTG curves for S:C = 7 urea solution and nickel catalyst as a function of temperature under a He flow of  $80 \text{ cm}^3 \text{ min}^{-1}$ . A heating rate of  $5 \text{ }^\circ\text{C min}^{-1}$  was applied.



The MID  $m/z = 43$  ( $\text{HNCO}^+$ ) peak at ca. 185 °C appeared again in the absence of water when the experiment was repeated with dry urea mixed with nickel catalyst (**Figure 4-14**), but did not when urea was mixed with water (**Figure 4-15**). Similarly, the urea solution sample with catalyst was seen to exhibit the same phenomenon of evolving  $m/z = 16$  and 17 (water fragmentation or ammonia) plus  $m/z = 28$  ( $\text{N}_2^+$ ),  $m/z = 14$  ( $\text{N}_2^{2+}$ ,  $\text{N}^+$ ), and  $m/z = 2$  ( $\text{He}^+$  or  $\text{H}_2^+$ ) along with water at  $80\text{ °C} \leq T \leq 150\text{ °C}$ .

Both dry urea samples exhibited, via EGA, a release of  $\text{N}_2$  at 410 °C which was completely absent when water was included. This could be explained by the source of the  $\text{N}_2$  being  $\text{HNCO}$ , a species greatly reduced in quantity because of the hydrolysis reaction (R20) having occurred at lower temperatures.

There were few other observable differences between the EGA multi-ion detection plots for samples with and without catalyst at temperatures below 500 °C. This is not surprising considering that this catalyst has been shown to be relatively inactive at temperatures  $T \leq 500\text{ °C}$  ([12] - see also Chapter 5 and Chapter 6). At temperatures greater than this, in the region of proven catalyst activity, the difficulty however of drawing parallels between the conditions of this TGA and those of steam reforming are perhaps too great to be of any significance. Prior to 500 °C all water had evolved, and only a  $\leq 0.5\%$  residue (derived from urea decomposition products and therefore having a completely different chemical structure) remained. Steam reforming conditions do not pertain, and therefore the methodology here is considered limited in terms of assessing the influence of nickel catalyst on urea thermolysis in a flow reactor with excess steam. Consequently it is not possible to observe the influence of the predicted global urea steam reforming reaction (R25). Some interesting results at higher temperatures were observed however, and conjectures as to their origins in the context of applicability to urea steam reforming can be made.

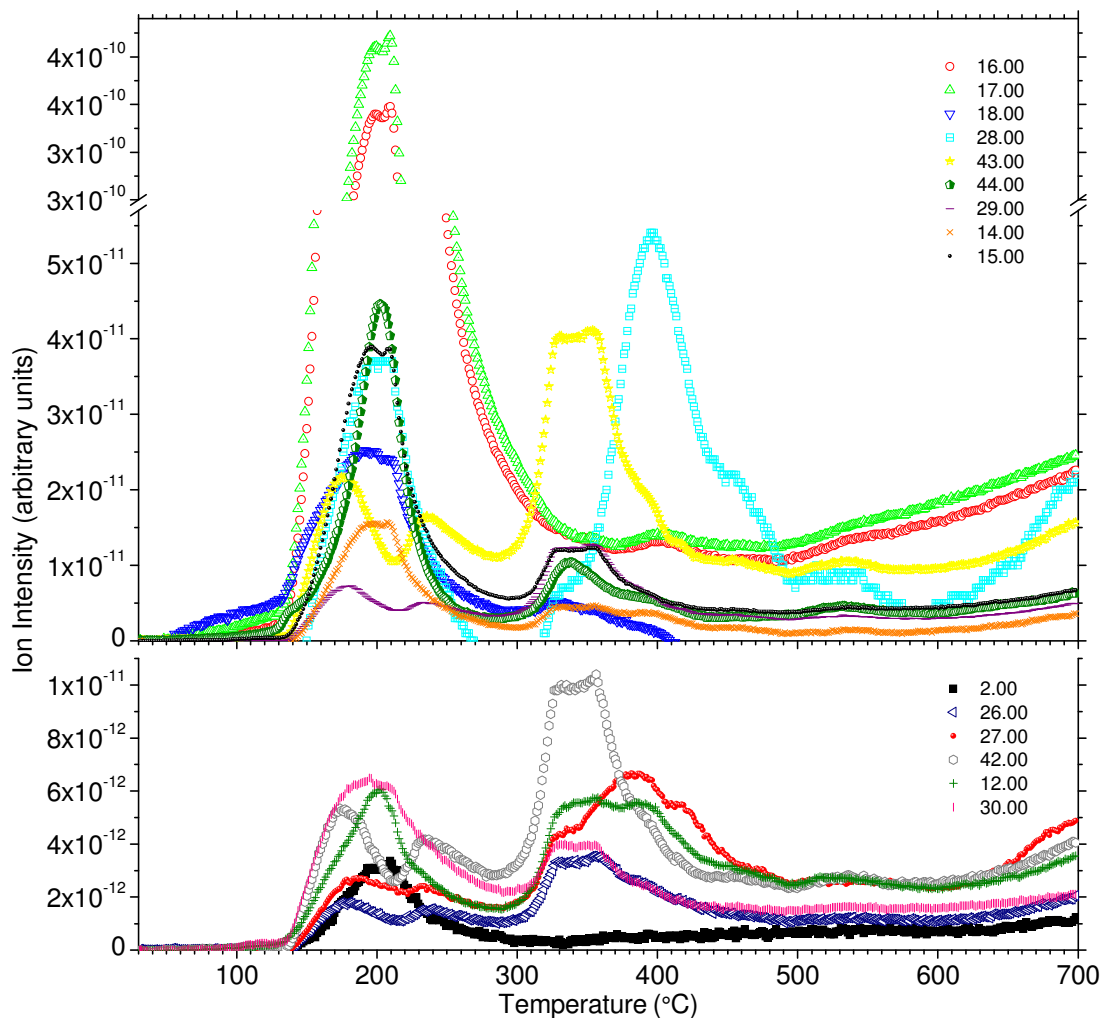


**Figure 4-14.** Urea and reduced nickel catalyst MS multiple ion detection curves.

Of interest is the  $m/z = 27$  ( $\text{HCN}^+$ ) ion intensity curve, which at higher temperature showed marked differences due to the inclusion of catalyst in the sample. Both with and without water in the sample,  $m/z = 27$  exhibited an ion intensity peak at higher ca. 600 °C temperatures without catalyst, but had no peak in this temperature region with catalyst in the sample. The precise cause of this is unknown other than it being evidential of catalytic activity enabling a reaction that releases its source molecule at a lower temperature. That this species contains hydrogen reveals indirectly evidence of catalyst activity on urea decomposition and hydrogen release.

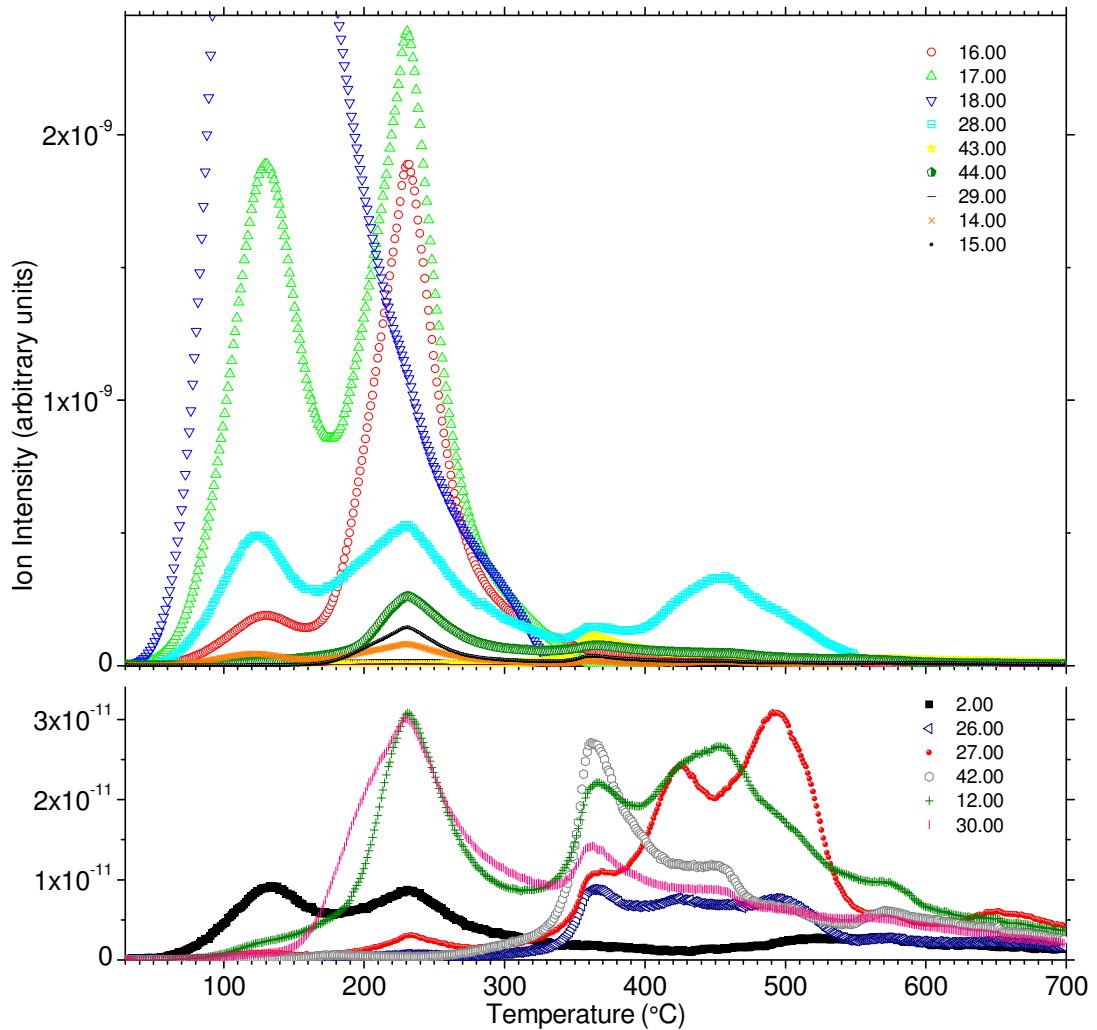


**Figure 4-15.** Urea in de-ionised water at S:C = 7 plus reduced nickel catalyst MS selected multiple ion detection curves.

Comparable with all sample MS results, the FTIR results revealed that above ca. 350 °C transmittance peaks attributed to  $\text{NH}_3$  diminished to the state of levelling slightly above baseline levels thereafter (not shown). This was not identified as being a symptom of the catalyst's ability to "crack"  $\text{NH}_3$  due to comparable results found with the non-catalyst samples and the likelihood of there being little  $\text{NH}_3$  available due to its prior evolution. It is considered that the method does not permit an adequate assessment of the catalyst's ability to produce hydrogen from  $\text{NH}_3$ , though an indication that this reaction (R12) did occur can be inferred by the small increase in  $m/z = 2$  ( $\text{H}_2^+$ ) evident at  $T \geq 500$  °C in **Figure 4-15**.

### 4.3.3.3 Reaction Kinetics

Reaction kinetics for mass loss observed with urea, and urea with nickel samples were found to have linear plots of  $\ln(k)$  versus  $1/T$  only within the range of  $140 \leq T \leq 185$  °C (coinciding with the early stages of step one in the multi-step TGA curves). Outside of this region, the non-linear relation proved that the reaction mechanisms were complex as inferred by the variation in DTA curves and that the parameters  $A$  and  $E_a$  varied with temperature. This was not surprising considering that the multiple and non-simultaneous decomposition of melt polymers is known to occur above this temperature with non-aqueous urea thermolysis (see section 2.6.2). Kinetic values obtained from the trendline fitted by linear regression on these plot's apparent first order reaction kinetics are shown for the three comparable TGA experiments in **Table 4-1**, along with their statistical co-efficient of determination ( $R^2$ ) values.

**Table 4-3.** Kinetic parameters, and statistical co-efficient of determination calculated from results of urea thermolysis over temperature range  $140$  °C  $\leq T \leq 185$  °C. Name of analyser used given in brackets.

	$E_a$ (kJ mol <sup>-1</sup> )	Ln (A) (sec <sup>-1</sup> )	$R^2$
Urea (Stanton)	81.45	15.47	0.984
Urea (Netzch)	93.12	18.69	0.998
Urea and reduced nickel catalyst (Netzch)	89.95	18.03	0.999

The  $R^2$  values report a good statistical fit, revealing high accuracy to the Arrhenius model, particularly with the Netzch (STA) analyser. The Netzch results are slightly outside the range of  $E_a$  values ( $E_a = 61.36$  kJ mol<sup>-1</sup>  $\pm$  20.86 kJ mol<sup>-1</sup>) previously considered most accurate for (R19) in literature [65].

Comparison of the Netzch results show a slight reduction in  $E_a$  in the presence of catalyst as would be expected. However, considering the small difference in values between the two Netzch analyses, plus the Stanton results that show a lower  $E_a$  value than that obtained from the Netzch analyser with catalyst, and the temperature of this thermolysis reaction being well below the range of identified activity for this catalyst (see section 6.5.1), it is not considered strong enough evidence of catalytic influence.

Estimates of residence time for urea conversion from 90 % to 99.9 % based on the kinetic results shown in **Table 4-3** are provided in **Table 4-4**. Based on the assumption that these kinetics apply throughout the whole of urea decomposition, then  $\geq 99$  % conversion will be achieved within 2 seconds at  $T \geq 400$  °C. For a reactor with rapid entry of fuel, and temperatures close to the considered optimum for steam reforming based on modelling (Chapter 3) and on the known activity range of this catalyst ( $T \geq$

500 °C), a 99.9 % conversion is predicted within half a second. With the anticipated reactor settings of  $T \geq 550$  °C, any urea remaining would be instantly decomposed upon contact with the catalyst bed.

**Table 4-4.** Residence time (in seconds) for values of urea conversion as a function of temperature based on derived thermal decomposition parameters in the range  $140$  °C  $\leq T \leq 185$  °C.

Analyser	Conversion Urea %	Temperature (°C)					
		700	600	500	400	300	200
Stanton (urea)	99.9	0.031	0.098	0.420	2.766	35.09	1303
	99.0	0.020	0.065	0.280	1.844	23.39	868.6
	90	0.010	0.033	0.140	0.922	11.70	434.3
Netzch (urea)	99.9	0.005	0.020	0.103	0.888	16.22	1011
	99.0	0.004	0.013	0.069	0.592	10.81	674.1
	90	0.002	0.007	0.034	0.296	5.406	337.0
Netzch (urea + catalyst)	99.9	0.007	0.025	0.122	0.977	16.16	874.9
	99.0	0.005	0.016	0.081	0.652	10.77	583.3
	90	0.002	0.008	0.041	0.326	5.386	291.6

The relevance of these results to steam reforming urea process design are however limited. To use them as a model for quantifying process design would require the assumption that these kinetic parameters apply throughout the whole decomposition up to at least 700 °C. This they undoubtedly do not, due to the deviation from linearity of plots of  $\ln(k)$  versus  $1/T$ , and from what is known about the complex mechanisms involved above ca. 185 °C at these slow heating rates. In the presence of water at  $T \geq 133$  °C, the HNCO-derived polymers that affect the reaction kinetics would not occur due to HNCO hydrolysis (R20), and not considering this reaction has ramifications on the elucidation of actual urea steam reforming kinetics. This is because HNCO hydrolysis, as has been previously reported in literature and in these EGA studies, would occur simultaneously with (R19). Its rapid hydrolysis kinetics would likely cause the reaction to be limited only by mass diffusion and water availability. The rate of (R20) is also increased by rapid heating, so the comparability of these TGA experiments to conditions prevalent in a flow reactor are very different and promote caution in the application of these derived kinetics. Finally, the temperature range over which these kinetics were calculated was significantly outside the range of this catalyst's activity,

and despite the inclusion of catalyst in the TGA experiments, no effect could be discerned due to the decomposition being complete prior to the minimum catalyst activity temperature of 500 °C (see Chapter 6). Overall, the values calculated here can be considered to provide a quantified “worst case scenario” for the reaction mechanism kinetic parameters involved in steam reforming of urea.

Supporting these conclusions, at the time of writing, experiments linked to the author’s and pursuant to the steam reforming experiments reported in Chapter 6 assessed the free energy associated with ammonia and water reforming<sup>†</sup>. It was found that the steam reforming of urea was also a more thermodynamically favourable reaction than ammonia cracking alone, indicating that the mechanism of H<sub>2</sub> production from urea and steam was indeed more active than just a sequence of decomposition to HNCO and NH<sub>3</sub>, followed by hydrolysis of HNCO and finally by ammonia cracking. This supported the assertion that the reaction (R25) could be defined on its own, as a global steam reforming mechanism.

#### 4.4 Conclusions

The maximum solubility of reagent urea in de-ionised water at room temperature was found to be S:C ≥ 3, with at most 30 minutes required for complete solvation. Cyanate ion concentration, evidential of urea isomerisation, was not observed above 0.5 ppm using chromatography in all samples up to one hour after preparation, supporting literature predictions for the same low levels of isomerisation with dilute urea solutions up to 5 hours after mixing. These results help to set parameters for experimental steam reforming and show that the nature of the fuel entering a steam reforming reactor will be, to significant proportions, almost totally urea in solution rather than any significant concentration of its isomer ammonium cyanate.

Evolved gas analyses by mass spectroscopy and FTIR were used in combination with thermogravimetric analyses (TGA, DTG, and DTA) of pure urea, aqueous urea (S:C = 7) solution and urea with nickel catalyst samples to expand on presently available literature in an attempt to further understand the nature of the aqueous urea fuel as it approaches and enters the catalyst bed in a urea steam reforming flow reactor as used and described in Chapters 5 and 6. These STA experiments also had the aim of verifying the mass balances used in experimentation by observation of species evolved

---

<sup>†</sup> See publication: Rollinson, A.N., Rickett, G.L., Lea-Langton, A., Dupont, V., Twigg, M.V. Hydrogen from urea-water and ammonia-water solutions. *Applied Catalysis B: Environmental*, 2011, **106** (3-4), pp. 304-315. The contribution of the author’s work to this publication is explicitly given on page ii of this thesis

during heating to ensure that all were accounted for. TGA was also used to calculate probable reaction kinetics of urea steam reforming.

Results of EGA supported previous literature reports that urea decomposition starts ca. 133 °C, though a previously unreported two stage evolution was detected by MS in the first episode of mass loss up to ca. 235 °C. HNCO was not detected in this first stage of mass loss by FTIR, though was inferred as present at higher temperatures by increases in ion intensity of  $m/z = 43$  with MS results.  $\text{NH}_3$  was found to predominate in first stage urea decomposition for all samples, evident with results from both MS and FTIR. With the samples that contained water, HNCO concentration was drastically reduced due to the availability of water and the consequent occurrence of HNCO hydrolysis. This was quantified by peak height ratios for  $\text{NH}_3$ :HNCO of 57:1 for dry urea and 1567:1 for urea solution. These results were significant in validating the exclusion of HNCO from experimental steam reforming material balances.

An unexpected detection of additional evolved species was observed by MS to accompany water evolution at temperatures from 80 °C. This was prior to the temperature necessary for decomposition of urea when dry urea alone was heated. The presence of species with mass/charge values of  $m/z = 28, 14$  could be attributed to dissolved  $\text{N}_2$  (from air) in the water vapour, however this would not account for the appearance of  $m/z = 2$  ( $\text{H}_2$ ). An alternative explanation is that when water and urea were combined, there occurred a simultaneous release at low temperature of some  $\text{NH}_3$  and  $\text{H}_2$ . Identification of  $\text{NH}_3$ ,  $\text{H}_2$ , and  $\text{N}_2$  could not be discerned from FTIR analyses, though CO could be discounted with certainty. The low temperature release of  $\text{H}_2$  from urea-water solutions, if feasible, would have major beneficial applications in energy technology systems, so the phenomenon constitutes an area for future work.

The catalyst used in this series of experiments had been shown in steam reforming to be effective only at temperatures  $\geq 500$  °C ([12] - see also Chapter 5 and 6). Therefore, the comparability of this methodology to flow reactor steam reforming and as a means of elucidating the nature of thermolysis was found to be limited by most of the urea decomposition having occurred prior to the catalyst's active temperature range. This was caused by the slow heating rate of the TGA programme and the sample being in an open reaction vessel under batch conditions rather than exposed to excess flowing steam. Furthermore, the evolution of water at low temperatures, prior to this catalytic activity temperature zone and prior to the temperature of urea decomposition also prohibits an appropriate analysis as it negates the availability of water for the important global urea reforming and HNCO hydrolysis reactions. Consequently, an assessment of the influence of nickel catalyst on urea thermolysis in a flow reactor with excess steam cannot be fully appraised. Therefore, observing the urea steam reforming reaction (R25)

predicted by modelling (Chapter 3) and supported by experimentation (Chapter 5 and 6) was not possible.

For the same reasons, the TGA method adopted in this series of experiments was found to be inadequate for elucidating the reaction kinetics of urea steam reforming. This was accentuated by an observed non-linear relation between temperature and urea decomposition above 185 °C. Despite these limitations, reaction kinetics for the first stage of thermal urea decomposition were determined and residence times calculated for variations in urea conversion. These provide a quantified “worst case scenario” for the reaction parameters and the residence times calculated for steam reforming of urea, with a predicted 99.9 % urea conversion within 0.5 seconds for the fuel prior to the reactor bed and any remaining urea predicted to be instantly decomposed upon contact with the catalyst bed at  $T \geq 550$  °C.



## 5 Steam Reforming: Quartz Upflow Reactor

### 5.1 Introduction

First attempts at extracting hydrogen from urea are described in this section. The aim of this research stage was to explore the practical feasibility of urea steam reforming, with the objectives of: attaining the steady state operation predicted by equilibrium modelling, acquiring knowledge of the particular behaviour of urea as a steam reforming feedstock, and assessing resultant product species. There were no previous reports of urea steam reforming available to use as a basis for process design. A bench-scale rig with ancillary equipment used previously for steam reforming of glycerol was adapted for these first experiments. A nickel catalyst also proven for steam reforming glycerol, methane and waste cooking oil was used. Nickel catalysts are economically attractive since they are cheap in addition to being sufficiently active at steam reforming [152]. Therefore these catalysts have long-term potential for practical application.

### 5.2 Method

A Nickel-based commercial steam reforming catalyst, containing 18 wt% NiO supported on Al<sub>2</sub>O<sub>3</sub> and manufactured by Johnson Matthey as 1.38 cm diameter pellets, 1.84 cm in length, with 0.38 cm perforations was used for all experimentation (see **Table 5-1**). The catalyst was crushed using a ceramic mortar and pestle and sieved to create a 0.66 – 1.70 mm particle size for the experiments.

**Table 5-1.** Urea steam reforming catalyst composition as supplied.

Component	wt%
NiO	18,
SiO <sub>2</sub>	<0.1,
SO <sub>3</sub>	<0.05
Al <sub>2</sub> O <sub>3</sub>	balance

Each experiment reported here used undiluted 15 grams of fresh (as supplied) catalyst occupying a volume of 7.9 cm<sup>3</sup> within the reactor tube supported on a stainless

steel circular mesh screen, though preliminary studies were done using a smaller quantity of catalyst.

The aims of these steam reforming experiments were to obtain hydrogen from urea, with an emphasis on maximum steam conversion and achieving equilibrium. The experiments were continuous flow and conducted in a brand new fixed-bed quartz tubular reactor under atmospheric pressure. A schematic diagram of the experimental system is shown in **Figure 5-1**, and a photograph of the experimental rig is shown in **Figure 5-2**.

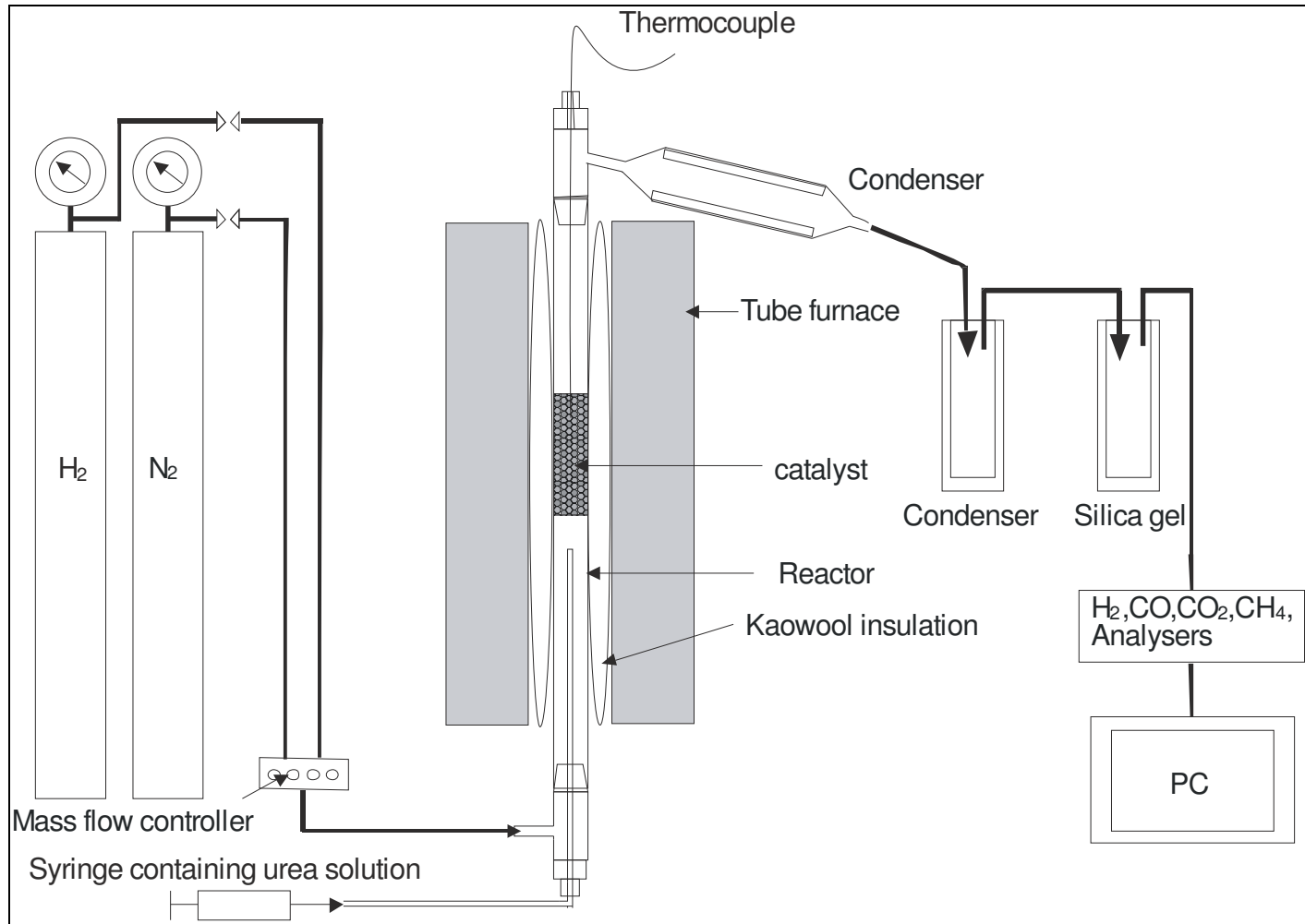


**Figure 5-1.** Schematic diagram of the atmospheric pressure quartz upflow urea steam reforming reactor system.

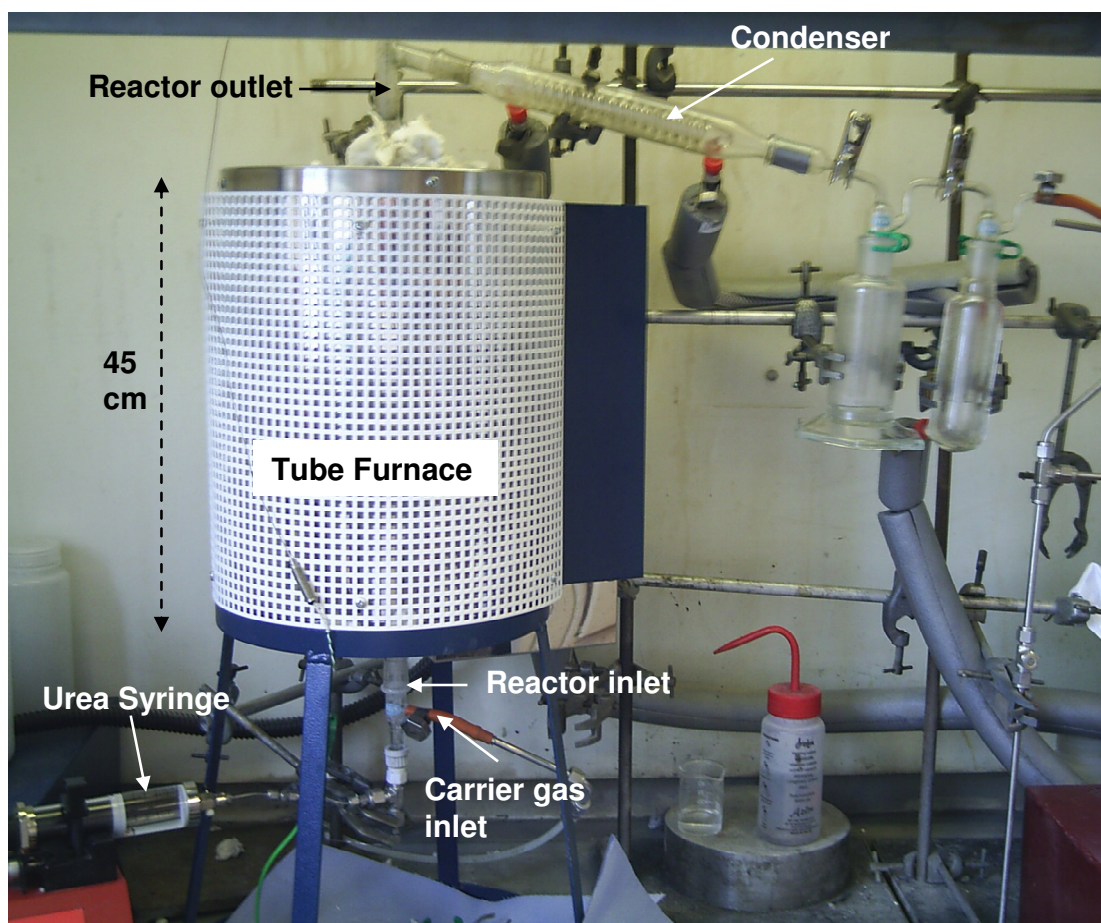


**Figure 5-2.** Photograph of the quartz upflow urea steam reforming reactor.

The reactor tube was 48 cm long with an internal diameter of 12 mm, connected at the top to a glass adaptor section and at the bottom to a glass inlet assembly creating a total vertical length of 70 cm. The glass inlet and outlet adapter sections were connected to the reactor tube by conically-tapered ground joints. The reactor was contained in, and heated by, a tube furnace with a programmable temperature controller operating via a thermocouple attached on the internal wall of the furnace. Kaowool insulation was packed into the 16 mm space between reactor tube and internal tube furnace walls along the full length of the reactor for stability. A K-type thermocouple inserted through the outlet assembly and into the reactor tube was used to measure the actual catalyst bed temperature. Inlet gases from BOC cylinders of > 99.99 % purity were regulated by MKS mass flow controllers. Steel tubing (30 mm long, 1 mm internal diameter) connected a syringe containing aqueous urea solution to the inlet assembly where a quartz tube (4 mm internal diameter, 27 cm long) connected this into the reactor tube. The syringe was connected to the feed tubing using an SGE Analytical NLL – 5/16, 4.5 cm needle attached to a Swagelok tube connector. Aqueous urea solutions of between  $4:1 \leq S:C \leq 7:1$  were injected into the reactor. Reactor temperature was set at 600 °C for all experiments.

Prior to steam reforming, the catalyst was reduced at 500 °C by a flow of 15 cm<sup>3</sup> min<sup>-1</sup> at standard temperature and pressure (STP) of H<sub>2</sub> in 300 cm<sup>3</sup> min<sup>-1</sup> (STP) of N<sub>2</sub> for 1 hour. Then, the reactor was purged for at least ten minutes with the same flow of N<sub>2</sub>. N<sub>2</sub> carrier gas was used in all steam reforming experiments with a flow of 300 cm<sup>3</sup> min<sup>-1</sup> (STP). This was fed separately into the inlet glassware and prior to the fuel-line outlet (see **Figure 5–1**). Reactor temperature was increased to 600 °C and steam reforming commenced with the introduction of aqueous urea solution into the reactor. This was dispensed via a micro-syringe pump (New Era Pump Systems). Fuel feed rates in the range of 3 ml hr<sup>-1</sup> to 20 ml hr<sup>-1</sup> (20 °C) were used. The reactor effluent was passed through two oil-cooled condensers and a silica gel trap containing 30 cm<sup>3</sup> silica gel (connected by ground glass conically-tapered joints and ball and socket joints), to remove moisture before being analysed. The dry gases were measured online with a series of ABB Advance Optima Analysers comprising a Uras 14 non-dispersive infrared module for CO, CO<sub>2</sub> and CH<sub>4</sub> analysis, and a Caldos 15 thermal conductivity module for H<sub>2</sub>.

Off-line gas chromatography was carried out by collecting product gas samples in a Tedlar bag. For hydrocarbons from C<sub>1</sub> to C<sub>4</sub>, a Varian 3380 gas chromatograph with a flame ionisation detector (GC/FID) was used with N<sub>2</sub> as a carrier gas and with a 2 m length by 2 mm diameter column packed with 80-100 mesh Haysep material. H<sub>2</sub>, CO, O<sub>2</sub>, N<sub>2</sub> and CO<sub>2</sub> were analysed by a Varian 3380 GC with two packed 2 m length by 2 mm diameter columns and with two thermal conductivity detectors (GC/TCD). H<sub>2</sub>, CO, O<sub>2</sub> and N<sub>2</sub> were analysed on a column packed with 60-80 molecular mesh sieve, with Ar as carrier gas. CO<sub>2</sub> was analysed on a column packed with 80-100 mesh Haysep.

On-line analysers were calibrated to zero and span prior to experimentation using pre-mixed (and therefore accurately known) concentrations of gas supplied by BOC cylinders. Mass flow controllers were calibrated to zero and span: for H<sub>2</sub> and air flow by using a bubble tube built in-house – where the gas volumetric flow rate was determined from timed measurements of a weak soap solution bubble traversing the known distance of tube length; and for N<sub>2</sub> by using an AGILENT ADM1000 gas hand-held gas flow meter. These values ( $\dot{V}_{measured}$ ) obtained at room temperature, were corrected to give a value for volume flow rate at STP ( $\dot{V}_{STP}$ ) to permit accurate operation of the mass flow controllers. This was accomplished using the formula:

$$\dot{V}_{STP} = \left( \frac{P_{measured}}{T_{measured}} \right) (\dot{V}_{measured}) \left( \frac{293.15K}{101.328kPa} \right) \quad (F16)$$

The values for room pressure ( $P_{measured}$ ) and temperature ( $T_{measured}$ ) were obtained from a barometer and thermometer located in an analytical laboratory in the same building as the experimental rig.

The experimental system was checked for gas-tight integrity prior to each steam reforming run and prior to each catalyst reduction stage to maintain accuracy by ensuring constant pressure and to protect against the occurrence of leakage from joints. This leak testing was achieved by connecting the AGILENT ADM1000 hand-held gas flow meter to the product outlet pipe with the system under carrier gas flow.

### 5.3 Data Analysis

Values of urea and steam conversion, species selectivity, and hydrogen gas yield were calculated with a mass and elemental balance spreadsheet using reactor exit concentrations of H<sub>2</sub>, CO, CO<sub>2</sub>, and CH<sub>4</sub> and the known inlet flows of aqueous urea and N<sub>2</sub>. The mass balance spreadsheet was formulated by Dr Valerie Dupont.

The possible presence of volatile hydrocarbons higher than CH<sub>4</sub> was eliminated by off-line GC analysis, and unmeasured products N<sub>2</sub> and H<sub>2</sub>O were predicted by calculation. Urea conversion was calculated from the carbon product concentrations and the urea feed rate, as in equation (E1), in which ‘ $\dot{n}$ ’ are the relevant flow rates (mol s<sup>-1</sup>), and ‘ $y$ ’, the gas mol fractions.

$$x_{urea} = \frac{\dot{n}_{urea,in} - \dot{n}_{urea,out}}{\dot{n}_{urea,in}} = \frac{(\dot{n}_{dry,out}) \left( \sum y_{c,out} \right)}{\dot{n}_{urea,in}} \quad (E1)$$

In (E1),  $\dot{n}_{dry,out}$  is the dry total molar flow of gaseous products, and  $\sum y_c$  refers to the sum of the mol fractions of the carbon species (CH<sub>4</sub>, CO<sub>2</sub> and CO).  $\dot{n}_{dry,out}$  was calculated from the nitrogen balance given in (E2):

$$\dot{n}_{dry,out} = \frac{\dot{n}_{N_2,in} + \dot{n}_{urea,in}}{y_{N_2,out}} = \frac{\dot{n}_{N_2,in} + \dot{n}_{urea,in}}{\left( 1 - \sum_{\text{all dry gas products}} y_i \right)} = \frac{\dot{n}_{N_2,in} + \dot{n}_{urea,in}}{\left( 1 - (y_{H_2} + y_{CO_2} + y_{CO} + y_{CH_4}) \right)} \quad (E2)$$

In (E2), the mol fraction of nitrogen leaving the reactor  $y_{N_2,out}$ , not measured online, was calculated from a balance to 1 from the sum of the measured dry gases H<sub>2</sub>, CO, CO<sub>2</sub> and CH<sub>4</sub>. The calculated  $\dot{n}_{dry,out}$  may be a minimum estimate because of the assumption that no products other than CO, H<sub>2</sub>, CO<sub>2</sub>, and CH<sub>4</sub> were formed from urea. As a result, the urea conversion  $x_{urea}$  calculated with (E1) may also be a minimum estimate.

The conversion of steam was then estimated from the hydrogen balance via equation (E3), where the molar rate of hydrogen input is that contained in the urea and steam flows, and the molar rate of hydrogen output is that in the product gases (H<sub>2</sub> and CH<sub>4</sub>), as well as in the unconverted urea and water.

$$x_{H_2O} = \frac{\dot{n}_{H_2O,in} - \dot{n}_{H_2O,out}}{\dot{n}_{H_2O,in}} = \frac{2\dot{n}_{H_2O,in} - [\dot{n}_{dry,out} (2y_{H_2} + 4y_{CH_4}) - 4(\dot{n}_{urea,in})(x_{urea})]}{2\dot{n}_{H_2O,in}} \quad (E3)$$

With both  $\dot{n}_{out,dry}$  and  $x_{urea}$  being minimum estimates,  $x_{H_2O}$  may either increase or decrease if any non-measured products were present.

Species selectivity (%) was calculated from the ratio of measured hydrogen or carbon species molar product flow to the known molar inflow of total hydrogen or carbon. Hydrogen selectivity (E4) assumed only the following product molecules: H<sub>2</sub>, H<sub>2</sub>O, CH<sub>4</sub>. No consideration was made for NH<sub>3</sub> or other nitrogenous-hydrogen molecules.

$$H_2, SEL(\%) = \frac{(y_{H_2})(\dot{n}_{out,dry})}{((y_{H_2} + 2y_{CH_4})(\dot{n}_{out,dry}) + \dot{n}_{H_2O,prod})} \times 100 \quad (E4)$$

Calculations of carbon selectivity assumed there were no carbon products other than CO, CO<sub>2</sub>, and CH<sub>4</sub> in the product gas and that no carbon deposits accumulated in the reactor. Because of this, and also from the fact that  $\dot{n}_{out,dry}$  is also at its minimum, the total carbon product (totalC) is a minimum.

$$totalC_{MIN} = \dot{n}_{out,dry} (y_{CO_2} + y_{CO} + y_{CH_4}) \quad (E5)$$

Selectivities of CO, CO<sub>2</sub> and CH<sub>4</sub> are estimates based on totalC<sub>MIN</sub>.

$$SEL_{CO,EST}(\%) = 100 \times \frac{y_{CO} \times \dot{n}_{out,dry}}{(totalC_{MIN})} \quad (E6)$$

$$SEL_{CO_2,EST}(\%) = 100 \times \frac{y_{CO_2} \times \dot{n}_{out,dry}}{(totalC_{MIN})} \quad (E7)$$

$$SEL_{CH_4,EST}(\%) = 100 \times \frac{y_{CH_4} \times \dot{n}_{out,dry}}{(totalC_{MIN})} \quad (E8)$$

Molar flow for the nitrogen carrier gas,  $\dot{n}_{N_2,in}$  was determined by (E9), where  $\dot{V}_{N_2}$  is the measured volume flow rate of N<sub>2</sub>, and STP refers to standard conditions of temperature and pressure:

$$\dot{n}_{N_2,in} = \frac{\dot{V}_{N_2}}{22.5 \times 10^{-3}} \left[ \frac{[m^3 s^{-1}]}{[m^3 mol^{-1} at STP]} \right] \text{ mol. s}^{-1} \quad (E9)$$

## 5.4 Results/Discussion

A syngas rich in hydrogen was produced for fuel mixtures of  $4:1 \leq S:C \leq 7:1$ . The syngas had a simple chemical composition, with hydrogen, nitrogen and carbon dioxide as the major products. Methane production was negligible. Experimental dry product gas concentrations as a function of time, representative of the set of experiments

conducted at S:C from 4 to 7, are displayed in **Figure 5-3** for S:C of 7 along with their respective equilibrium calculated values (shown as dashed lines). A detailed discussion of the calculated equilibrium values is given in Chapter 3.

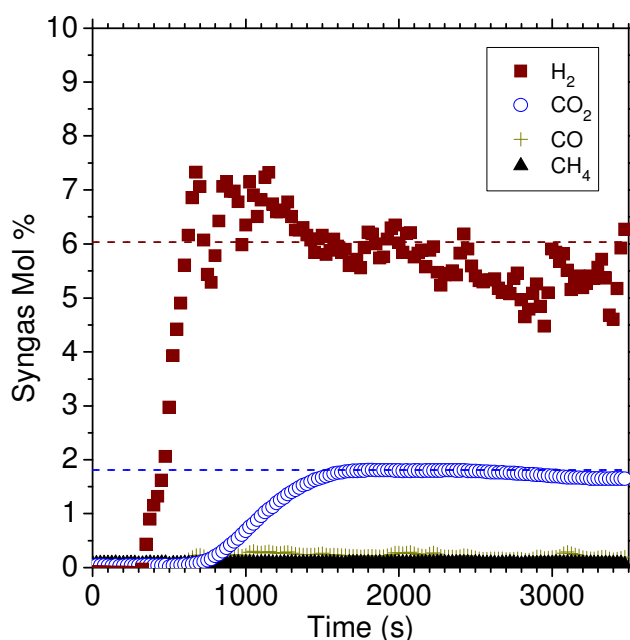


**Figure 5-3.** Dry product gas concentrations for S:C = 7 at 600 °C with a 4 ml hr<sup>-1</sup> fuel feed rate, and 300 cm<sup>3</sup> min<sup>-1</sup> carrier gas flow rate, shown as scatterpoints as a function of time using 20 % of datapoints for clarity. Also shown are calculated equilibrium values represented by dashed lines for H<sub>2</sub> and CO<sub>2</sub>.

The off-line GC analysis from a dry reformat gas sample taken immediately following steam reforming revealed no additional hydrocarbons. Results of this analysis are displayed in **Table 5-2** and represent ten minutes of dry gas capture at 4090 seconds (1 hour 8 minutes following a steam reforming experiment at 600 °C using S:C = 6 fuel dispensed at a rate of 4 ml hr<sup>-1</sup> with N<sub>2</sub> carrier gas flow at 150 cm<sup>3</sup> min<sup>-1</sup>. These results show the absence of any hydrocarbon greater than methane. No assessment to detect for the presence of NH<sub>3</sub> or other amide molecules was made during this analysis.



**Table 5-2.** GC analysis of dry reformat sample obtained immediately following on-line analysis of urea steam reforming with S:C = 6 fuel mixture fed at 4 ml hr<sup>-1</sup>, 600 °C reactor temperature, and 150 cm<sup>3</sup> min<sup>-1</sup> N<sub>2</sub> carrier gas flow.

Gas Species	Gas Concentration (Vol %)	Gas Species	Gas concentration (Vol %)
Carbon monoxide	0.8	Ethene	0.0
Hydrogen	13.0	Ethane	0.0
Oxygen	0.0	Propene	0.0
Nitrogen	82.2	Propane	0.0
Carbon dioxide	3.9	Butene & Butadiene	0.0
Methane	0.1	Butane	0.0

The concentration ratios of the dry gas species detected with offline GC analysis accord with those detected by the online analysers. **Figure 5-4** shows the dry syngas profile for the urea steam reforming experiment at 600 °C using S:C = 6 fuel dispensed at a rate of 4 ml hr<sup>-1</sup>. The difference between the actual concentration values in **Table 5-2** and **Figure 5-4** is due to the lower carrier gas flow rate used in the batch sample syngas capture for offline analysis (150 cm<sup>3</sup> min<sup>-1</sup>) compared to that used while the experiment was being analysed online (300 cm<sup>3</sup> min<sup>-1</sup>). The carrier gas flow was reduced because the minimum value necessary for accurate detection at the online analysers was considered too high to practically obtain a representative batch sample into the Tedlar bag.

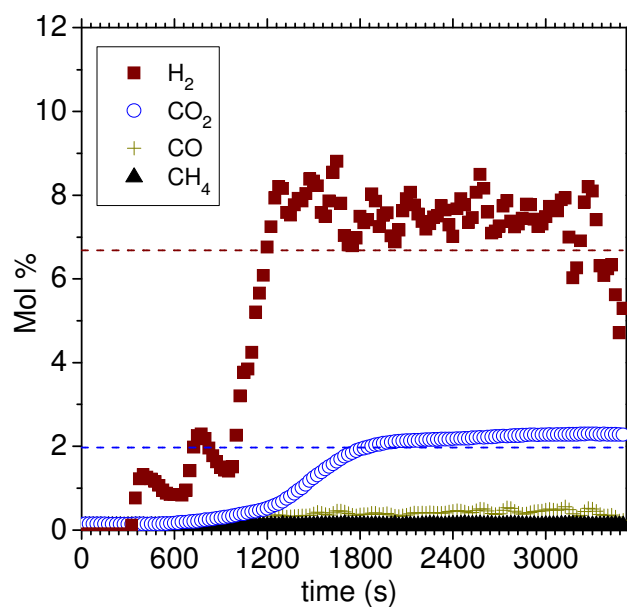


**Figure 5-4.** Dry product gas concentrations for S:C = 6, at 600 °C with 4 ml hr<sup>-1</sup> feed rate, and 300 cm<sup>3</sup> min<sup>-1</sup> carrier gas flow rate, shown as scatterpoints as a function of time, using 20 % of datapoints for clarity. Also shown are calculated equilibrium values represented by dashed lines.

A comparison between all the experimental urea and steam conversions using equations (E1) and (E3), and the products distribution at steady-state compared to their equilibrium calculated counterparts for  $4:1 \leq S:C \leq 7:1$  are shown in **Table 5-3**. See Chapter 3 for equilibrium calculations. These results quantify the closeness of the experimental profiles with the calculated equilibrium values and suggest that all significant products were measured.

**Table 5-3.** Mean experimental steady state (Exp), and calculated equilibrium (Eq.Calc) reactant conversions and product distribution at 600 °C with 4 ml hr<sup>-1</sup> fuel feed, and 300 cm<sup>3</sup> min<sup>-1</sup> carrier gas flow rate.

S:C		$x_{urea}$	$x_{H_2O}$	Selectivity			H <sub>2</sub> :CO <sub>2</sub>	H <sub>2</sub> :CO	Selectivity	
				C-products %						%
				CO <sub>2</sub>	CO	CH <sub>4</sub>				
4	Exp.	0.59	0.09	76.0	23.6	0.41	3.3:1	12:1	99.5	
	Eq.Calc	1.00	0.19	75.5	24.2	0.29	3.6:1	11:1	99.8	
5	Exp.	0.96	0.19	76.0	21.6	2.39	3.6:1	12:1	99.1	
	Eq.Calc	1.00	0.15	80.4	19.4	0.18	3.5:1	14:1	99.9	
6	Exp.	1.15	0.16	80.8	17.9	1.33	3.9:1	19:1	98.8	
	Eq.Calc	1.00	0.15	83.2	17.8	0.07	3.4:1	17:1	1.00	
7	Exp.	0.96	0.14	87.0	12.0	0.94	3.5:1	26:1	99.8	
	Eq.Calc	1.00	0.12	85.6	14.4	0.04	3.3:1	20:1	1.00	

The conditions close to equilibrium found in the experiments suggest that NH<sub>3</sub> would also have been close to equilibrium and therefore produced at very low concentrations (ca. 1-100 ppm). This could not be proven and the inability to measure product ammonia is considered a limitation of this experiment. The inability to measure other urea thermolysis species is not considered limiting due to TGA results and previous literature reporting complete urea decomposition (ultimately to CO<sub>2</sub> and NH<sub>3</sub>) prior to the reactor temperature of 600 °C (see section 2.6 and Chapter 4) in the presence of excess water.

Very slight blackening of the catalyst and interior of reactor tube outlet was observed post-experimentation and this was considered to be evidence of coke deposition. The spent catalyst was not subjected to further analysis during this stage of experimentation.

Some precipitation of the urea in the form of crystals in the water solution in the (colder) inlet part of the reactor was also evident being particularly prevalent in the urea-rich solutions tested. This was probably caused by the different boiling points of urea and water, resulting in two stage evaporation as the solution made a slow ascent up the reactor tube (see **Figure 5-5**). The temperature gradient encountered in this section of the reactor would have caused primarily water evolution and then supersaturation of the urea and so is a serious limitation of the process design.

Combined with the high prevalence of urea crystals observed, this supersaturation is also believed to be the cause of the lower urea conversion found for the S:C of 4 experiment (**Table 5-3**) and also in the overall instability of the online hydrogen gas

product that was a feature of all S:C runs. This instability in hydrogen output can be seen in the S:C = 6 dry syngas plot (**Figure 5-4**), also in the S:C = 4 dry syngas plot (**Figure 5-6**), and in many repeated experiments (not shown). Of note in **Figure 5-6**, in addition to the wide scatter of H<sub>2</sub> concentrations over time, is the lower than predicted hydrogen product fraction. This is indicative of the low urea conversion for this fuel mixture.

Occasionally, complete blockages of the inlet feed tube occurred, primarily identified by the syngas H<sub>2</sub> value dropping to zero. When the system was dismantled and inspected it was found that the blockages were caused by precipitate accumulation at the inlet and in particular inside the fuel feed tube. Only two runs at S:C = 4 and 5 could be obtained up to a duration of 1 hour without the feed tube blocking. S:C = 6 and 7 were less affected by precipitate blockages. A dry syngas plot for S:C = 5 at 600 °C with 4 ml hr<sup>-1</sup> fuel feed rate is shown in **Figure 5-7**. Of note is the instability in H<sub>2</sub> output, with particularly high peak of H<sub>2</sub> at the outset of detection. This feature was investigated and will be discussed in section **5.4.1**.

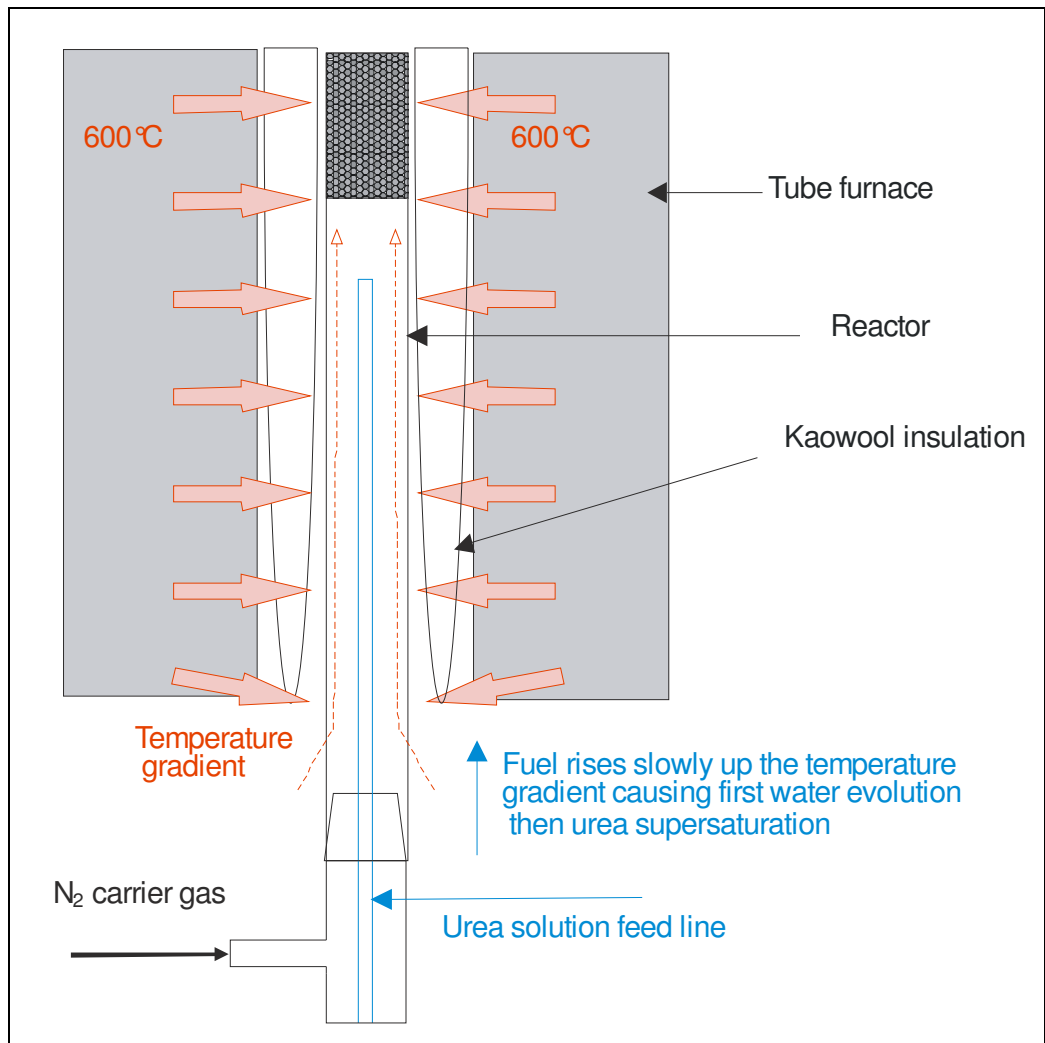


**Figure 5-5.** Schematic diagram of the fuel line, inlet and lower section of the upflow urea steam reforming reactor showing temperature gradient encountered by the urea solution.

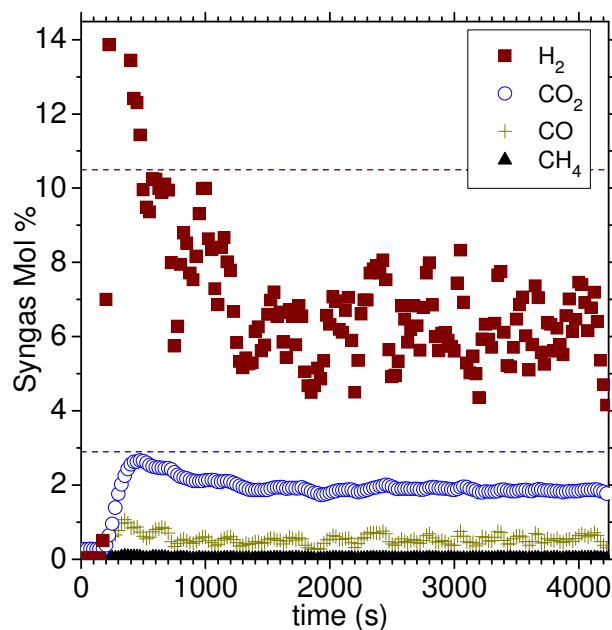


**Figure 5-6.** Dry product gas concentrations for S:C = 4, at 600 °C with 4 ml hr<sup>-1</sup> feed rate, and 300 cm<sup>3</sup> min<sup>-1</sup> carrier gas flow rate, shown as scatterpoints as a function of time, using 20 % of datapoints for clarity. Also shown are calculated equilibrium values represented by dashed lines.

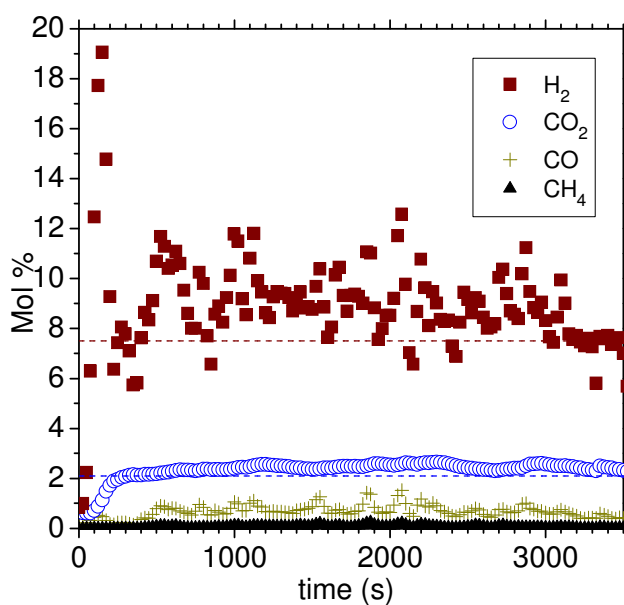


**Figure 5-7.** Dry product gas concentrations for S:C = 5, at 600 °C with 4 ml hr<sup>-1</sup> feed rate, and 300 cm<sup>3</sup> min<sup>-1</sup> carrier gas flow rate, shown as scatterpoints as a function of time, using 20 % of datapoints for clarity. Also shown are calculated equilibrium values represented by dashed lines.

Fuel feed rates higher than  $4\text{ml hr}^{-1}$  were found to flood the inlet, with the solution not vaporising at the feed line outlet and remaining in liquid state. This led to the solution pooling at the base of the inlet assembly. This is a second limitation of the upflow reactor design. Increased fuel would have increased the energy demand of the system with the greater energy demand to overcome the phase change enthalpy of increased quantities of water and urea per unit time, in addition to the enthalpy for reforming. It is possible that these endothermic phase changes may have resulted in a fall in reactor bed temperature that the response time of the tube furnace was not able to sustain. The endothermic demand of repeated injection of fuel combined with inertia of tube furnace response may also be an explanation for the output oscillations at steady state observed for the hydrogen product profiles. This theory is supported by the ubiquitous observance of oscillating hydrogen profiles as a function of time on-line with prior experimentation that used the same upflow design but with glycerol as a fuel [12]. The kaowool insulation inserted between reactor tube and tube furnace internal wall probably accentuated the reduced response time of the furnace.

## 5.4.1 Residence Times

### 5.4.1.1 Rationale

It was observed during the upflow reactor experiments that occasionally a peak of  $\text{H}_2$  occurred at the start of online analysis. This can be seen in the syngas profiles shown in **Figure 5-6** and **Figure 5-7**. Additionally, the  $\text{H}_2$  peak was less frequently seen to occur prior to the appearance of other species in the syngas online profiles (see **Figure 5-3**).

Due to the knowledge of when the fuel was dispensed, the known fuel feed rate, and by the known length of the feed line, the distance travelled by the fuel could be calculated and compared with the  $\text{H}_2$  breakthrough time detected at the analyser. These calculations revealed that the hydrogen peak recorded by the analysers had occurred prior to the fuel solution having reached the end of the feed line, and consequently prior to having entered the catalyst bed. Therefore, two hypotheses were formulated from this:

1. The  $\text{H}_2$  peak is an anomaly consequential of physical interactions in the reactor system, e.g. different residence times of gases en-route to the analyser.

2. A vapour with low boiling point was released at an early stage as the fuel ascended the temperature gradient into the reactor, and that this vapour was being steam reformed at the catalyst bed yielding a quantity of  $\text{H}_2$ . Since it is known that water evolution occurs first (at  $100\text{ }^\circ\text{C}$ ) with thermolysis of the urea solution, it led to the supposition that non-instantaneous vaporisation of the fuel was occurring, with

predominantly water vapour released into the reactor in the early stages. This would lead to hydrogen production from the gaseous urea-derived thermolysis products that were seen by the EGA experiments (Chapter 4) to be released with water evolution at ca. 100 °C. The possibility also existed that water splitting may be occurring at the catalyst bed:



This chemical reaction would have major industrial importance since creating H<sub>2</sub> from water is the ideal economic method of hydrogen production. Furthermore, NiO is widely acknowledged not to have catalytic activity for a number of steam reforming reactions, in particular steam methane reforming. As a result, commercial catalysts, although delivered mostly in oxidised state, are required to be fully reduced prior to steam reforming, which is carried out following a recommended ‘start-up’ procedure [152]. This reduction step is most often conducted in high excess of steam in order to prevent carbon deposition. While the presence of excess steam would seem beneficial to prevent catalyst deactivation by coking, the possibility of (R27) would instead cause deactivation by Ni oxidation.

A residence time experiment was undertaken to determine whether the phenomenon was due to the chemical reaction (R27) or due to the experimental residence time, i.e. different reactor bed interactions with the species or different speed of analysers’ response. Residence time of the fuel on the catalyst bed was also calculated for consideration with the values of residence times calculated from reaction kinetics (Chapter 4).

#### 5.4.1.2 Method

To test the hypotheses for the observed H<sub>2</sub> peak at syngas breakthrough, experiments were designed to assess residence time within the total system. High purity bottled calibration gases from BOC were used for the test gases. These were: H<sub>2</sub>:N<sub>2</sub> = 80:20 volume % pre-mixed, and CO<sub>2</sub>:N<sub>2</sub> = 25:75 mixed by the author from pre-supplied bottled gases of N<sub>2</sub> and CO<sub>2</sub> using calibrated mass flow controllers. A flow of 300 cm<sup>3</sup> min<sup>-1</sup> of nitrogen (the same rate as used in the urea steam reforming experiments) was switched to the calibration gases to introduce a step-change, and were passed over the same 15 g of (fully reduced) catalyst as in the steam reforming experiments using the experimental set-up. Conditions were set at 400 °C, to avoid the higher temperatures where the catalyst may have been chemically active.

For the residence time of the fuel on the catalyst bed, simple mean residence time was calculated. This assumed that the fuel was vaporised, and that particle density was constant:

$$\text{Mean residence time} = \text{Volume of catalyst/Fuel flow rate} \quad (\text{F17})$$



### 5.4.1.3 Results/Discussion

Residence times for the system with calibration gas compared against those from the urea steam reforming experiments under the same carrier gas flow rate are displayed in **Table 5-4**. As the calibration gases were released through the system at the inlet of the reactor, the time of detection at the analyser was recorded as follows:

$t_0$  = the time when the gases first appear at the analyser from the time of flow start.

$t_{50}$  = the time when 50% of the calibration value is reached (for calibration test) or when 50% of recorded maximum is reached (for experimental results).

$t_{90}$  = the time when 90% of the calibration value is reached (for calibration test) or when 50% of recorded maximum is reached (for experimental results).

**Table 5-4.** Calibration gases and experimental residence times through the upflow reactor system at a flow rate of  $300 \text{ cm}^3 \text{ min}^{-1}$ . Time (t) values are in seconds. See text for definition of  $t_0$ ,  $t_{50}$ , and  $t_{90}$ .

	H <sub>2</sub>			CO <sub>2</sub>			Difference		
	$t_0$	$t_{50}$	$t_{90}$	$t_0$	$t_{50}$	$t_{90}$	$t_0$	$t_{50}$	$t_{90}$
Calibration gas	130	195	270	90	255	470	-40	60	200
S:C = 7	330	515	835	600	1080	1450	270	565	615
S:C = 6	320	1105	1250	530	1470	1945	210	365	695
S:C = 5	0	90	125	0	160	995	0	70	870
S:C = 4	170	205	235	185	270	370	15	65	135

In the case of experimental S:C = 7, the initial measurement of CO<sub>2</sub> occurred approximately 330 seconds later than that of H<sub>2</sub>, time during which the syngas appeared to be free of carbon-containing products. The effect was slightly less severe for S:C = 6, and gradually reduced for the lower S:C ratios. For all the S:C range, the time at which CO<sub>2</sub> plateaued was always at least 200 s later than H<sub>2</sub>.

The intervals of time between the two species H<sub>2</sub> and CO<sub>2</sub> in the calibration gas were calculated to be  $t_0 = -40$ ,  $t_{50} = +60$ , and  $t_{90} = +200$  s respectively, based on 'CO<sub>2</sub> minus H<sub>2</sub>' times. By comparison, in the experiment S:C = 7, the intervals of time between H<sub>2</sub> and CO<sub>2</sub> were  $t_0 = +270$ ,  $t_{50} = +565$  and  $t_{90} = +615$  s respectively. This suggests that at the higher S:C ratios of 6 and 7, the detection of H<sub>2</sub> in the reactor products prior to that of CO<sub>2</sub> was indeed due to chemical reaction, but as the S:C was lowered to 4, with  $t_0 = +15$ ,  $t_{50} = +65$  and  $t_{90} = +135$  s respectively, it is more likely that physical interactions accentuated the observed lag in the two species measurements. These are significant findings and could be attributable to the fuel (S:C = 6 and S:C = 7)

being the water:urea eutectic mixture. The properties of this solution and the unique interaction between water and urea have previously been discussed [77].

To test (R27) outside the context of a steam reforming experiment, a pure de-ionised water feed solution was dispensed under experimental conditions with 15 g of freshly oxidised catalyst and at 600 °C temperature setting. Hydrogen production was not observed to occur with this pure water feed. The absence of hydrogen suggests that if (R27) occurred, then it was due to the presence of urea in the feed solution.

The high variation in residence times, particularly with the S:C = 5 experiment in comparison with the other results, reduce confidence in accepting either hypothesis about the cause of the H<sub>2</sub> peak. With certainty it has revealed that CO<sub>2</sub> had a longer residence time in the reactor system than H<sub>2</sub>. This could have been exacerbated by the quantity of silica gel in the moisture trap. The silica gel occupied an unknown volume in a 250 ml capacity Dreschel bottle; it was frequently changed and the capacity was not measured. Silica gel has been shown to retard CO<sub>2</sub> in a syngas flow [14] though in this publication no value of silica gel quantity was given by which to determine a relation and with which to compare results. The none uniform quantity of silica gel used in these residence times experiments and in the upflow reactor steam reforming of urea may account for the anomalously high S:C = 5 experimental residence times. Future experiments will operate with a reduced quantity of silica gel and the volume will remain fixed.

Two further limitations in the experimental method exist. Firstly, the temperatures were different between calibration tests and experimental runs. This may undermine accurate comparison between experimental and calibration gas results if chemical reactions were influencing the outputs. Secondly, in attributing times for t<sub>0</sub>, t<sub>50</sub>, and t<sub>90</sub>, maxima were not always clearly identifiable. For example, H<sub>2</sub> peaks were strong at the start for S:C = 4 and 5. With CO<sub>2</sub>, this species increased gradually over the experimental run time with S:C = 6 rather than plateauing.

The mean residence time of the vaporised fuel on the catalyst bed based on a carrier gas flow of 300 cm<sup>3</sup> min<sup>-1</sup>, and catalyst volume of 7.9 cm<sup>3</sup> was 1.58 seconds. Using the worst case scenario with the kinetic model devised in section 4.3.3.3, at T ≥ 500 °C this depth of catalyst would be more than adequate to achieve 99.9 % urea conversion.

## 5.5 Conclusions

The results of preliminary experimentation on steam reforming of urea reflect the tentative nature of extracting hydrogen using this novel approach. Hydrogen was detected in appreciable quantities in the dry output gas when compared with the other

gaseous constituents CO, CO<sub>2</sub>, and CH<sub>4</sub>, though oscillations in output values indicated some process instability. Concordance between experimental product values at steady state and modelled thermodynamic equilibrium values indicate that the process operated close to equilibrium. This leads to the conclusion that all significant gaseous species were likely to have been identified and measured; however a limitation is created by the inability to detect potential nitrogenous species, particularly ammonia, a factor that could undermine the accuracy of product calculations if this were present in significant quantity.

Work is needed to both stabilise output concentrations and optimise both urea and steam conversion, which was estimated as being slightly below expectations. The upflow design does not adequately permit the injection of urea in solution into the reactor due to the physical properties of this fuel and its ascent across a temperature gradient up to the catalyst bed. This limited the fuel flow rates to  $\leq 4 \text{ ml hr}^{-1}$  and led to multi-staged vaporisation with consequent supersaturation of the fuel.

An understanding of the practical requirements of using urea solution as a reactor fuel were revealed, and the design conditions necessary to maintain steady state and total fuel input have become apparent. This would involve, a balance between keeping the pre-reactor tube inlet temperature below 100 °C to avoid water evaporation from the fuel, and then a rapid entry to the catalyst bed to retain the urea in solution at time of vaporisation. Rapid delivery to the bed should not inhibit urea conversion based on previous kinetics evaluation and would also suppress the formation of unconverted urea-derived polymers.

An insight into the total process residence time for gases was provided for this urea steam reforming system. CO<sub>2</sub> was seen to exhibit a longer residence time than H<sub>2</sub>; a phenomenon to some extent attributable to the silica gel moisture trap. To identify whether the nickel catalyst was splitting water due to the presence of urea requires further detailed study which was considered to be outside the scope of this project. This significant hypothesis is an area for future work along with study into utilising the possible release of urea-derived products with water at ca. 100 °C.

## 6 Steam Reforming: Quartz Downflow Drop-feed Reactor

### 6.1 Introduction

In the work presented in Chapter 5, a hydrogen-rich synthesis gas was produced by urea steam reforming but a number of limitations were identified. To address these limitations and optimise the process, again with an emphasis on maximum steam conversion and stable proximity to equilibrium over time, the experimental system was redesigned as follows:

Ammonia product in gaseous and liquid phase would be measured to improve product analyses.

The inlet and fuel feed system would be redesigned to avoid fuel supersaturation prior to the reactor bed. The aim of this was to improve hydrogen product process stability as a function of time, to avoid fuel line blockages, and to maintain accuracy of product evaluation by ensuring that all urea remained in solution prior to instantaneous evaporation.

Post-reforming catalyst characterisation would be attempted to identify any changes to the catalyst following steam reforming such as coke formation. This was considered pertinent for identifying whether the integrity of the catalyst could be maintained for longer process running times. This work is presented in Chapter 7.

A full parametric study would be completed at a greater range of fuel S:C mixtures and reactor temperatures.

Syngas hydrogen concentration would be increased by using the lowest possible carrier gas dilution and a higher fuel feed rate.

### 6.2 Method

The same programmable tube furnace as described in section 5.2 was used to house the reactor and to supply controlled heat for the experiments. The quartz reactor tube (48 cm x 12 mm) described in section 5.2 was inverted inside the tube furnace, with carrier gas and fuel flow entering from a new design of glass inlet at the top. Inlet gases were from BOC cylinders of > 99.99 % purity and were regulated by MKS mass flow controllers.

Inlet and outlet ancillary glassware were connected to the reactor by conically-tapered ground glass joints. A schematic diagram of the experimental system is shown in **Figure 6-1**, and a photograph of the experimental rig is shown in **Figure 6-2**. Mass flow controllers were calibrated, and the experimental system checked to ensure constant pressure as described previously in section **5.2**.

Kaowool insulation was packed into the 16 mm space between reactor tube and tube furnace walls to a depth of 4 cm from the furnace's longitudinal extremities. This was to stop radiative heat transfer from the furnace to the inlet assembly and therefore to keep the feed line cool and avoid urea crystallisation. A photograph of the inlet assembly is shown in **Figure 6-3** showing the kaowool insulation between reactor tube and internal tube furnace walls. The central 40 cm longitudinal section between tube furnace internal wall and reactor tube was therefore uninsulated by kaowool with a space cavity created. This cavity was designed to try and improve heating response times of the tube furnace at the catalyst bed to possible decreases in temperature caused by endothermic demands of the reactants.

A K-type thermocouple embedded in the catalyst was used to measure the reactor bed temperature. This thermocouple was inserted through one end of a plastic Y-connector below the glass outlet component. A second K-type thermocouple was inserted into the cavity between reactor tube and tube furnace, adjacent to the reactor bed. This measured the outer reactor temperature. Reactor temperature was monitored and recorded manually.

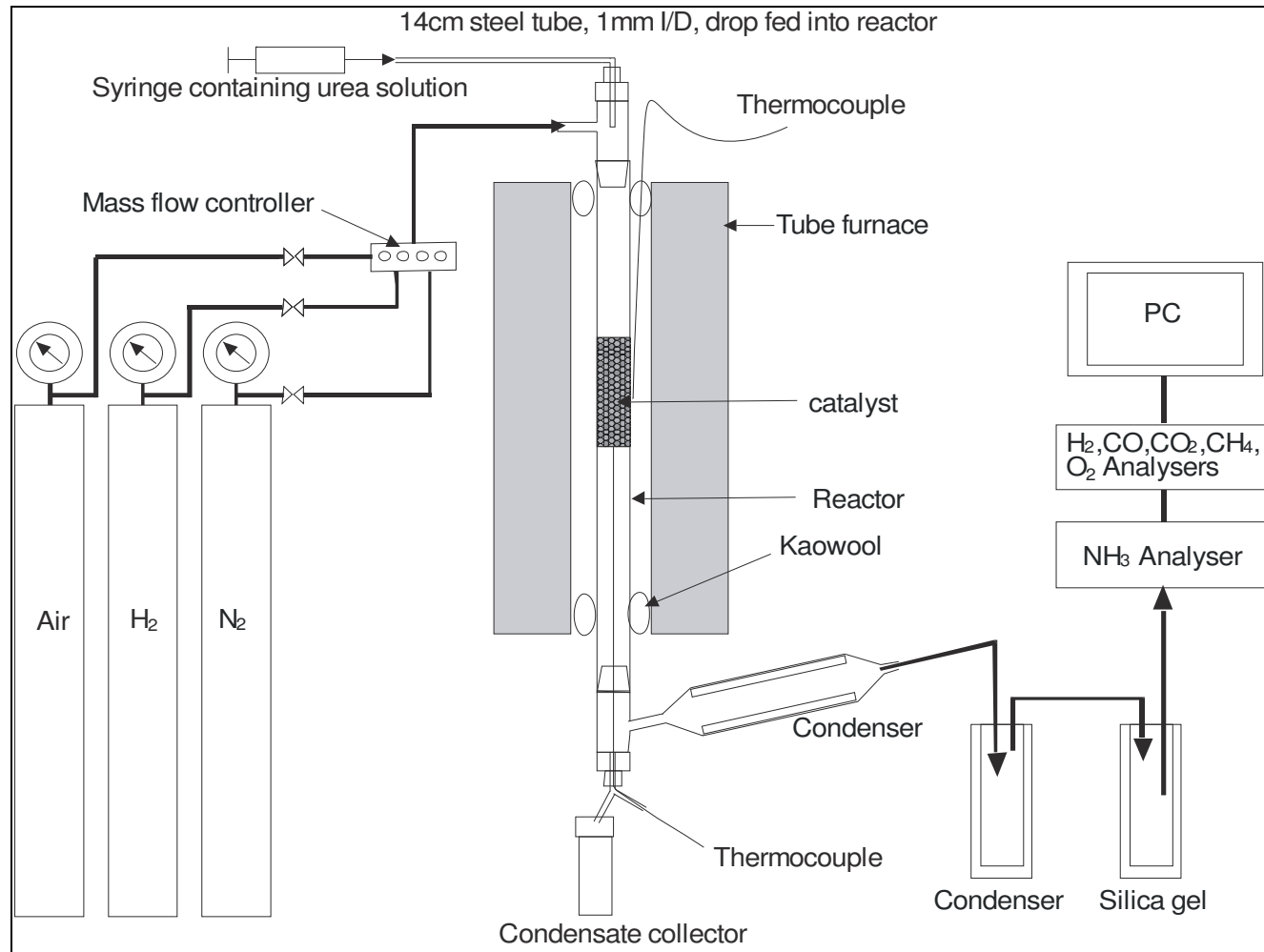


**Figure 6-1.** Schematic diagram of the experimental setup for atmospheric pressure quartz downflow drop-feed urea steam reforming reactor.

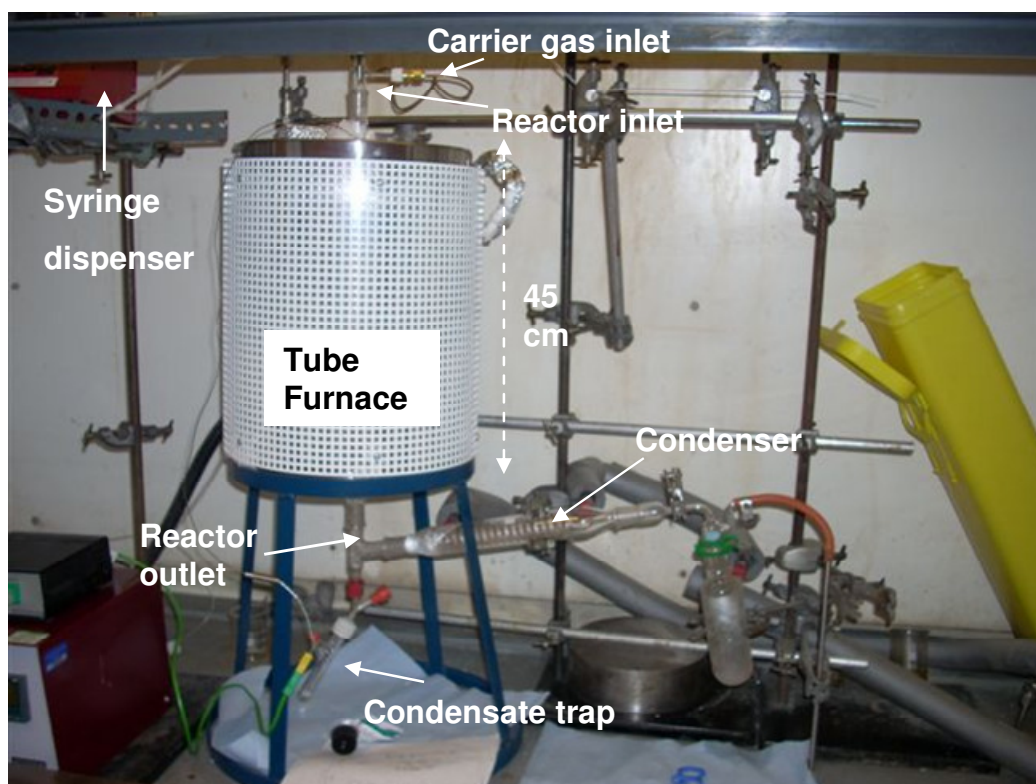


**Figure 6-2.** Photograph of the atmospheric pressure quartz downflow drop-feed urea steam reforming reactor.

The new inlet assembly (**Figure 6-3**) comprised steel tubing (14 cm long, 1 mm internal diameter) connected to a syringe pump via an SGE Analytical NLL – 5/16, 4.5 cm needle attached to a Swagelok tube connector. The feed line entered the top of the reactor through a 90° bend via Swagelok connector to a 2 mm I/D steel tube. This tube's outlet was situated centrally 2 cm above the reactor tube top and horizontally adjacent to the gas inlet. N<sub>2</sub> carrier gas was used in all of the experiments with a flow of 300 cm<sup>3</sup> min<sup>-1</sup> (STP), this being the minimum operating flow rate for the online analysers.

The system was at atmospheric pressure. Heightened pressure reforming was not attempted due to the unfavourable outputs predicted by thermodynamic modelling and by the limitations of the glass components for potential breakage.

The positioning of the carrier gas inlet was to both cool the inlet assembly to ensure that temperatures were kept < 100 °C and thereby avoid water evolution, and to promote the fuel drop dispensation. It was also considered that this design should inhibit convective heat transfer from the hottest zone of the reactor and thereby further help to keep the fuel line cool. When released, the drop of urea solution travelling under gravity and aided by the carrier gas flow, fell 20.5 cm to the top of the catalyst bed. This is shown in **Figure 6-3**. Its aim was to achieve rapid transport of the fuel along the temperature gradient prior to the catalyst bed and therefore permit instantaneous

vaporisation while the urea remained in solution. Thus, supersaturation of the fuel would be avoided and more urea would enter the reactor than with the upflow design.

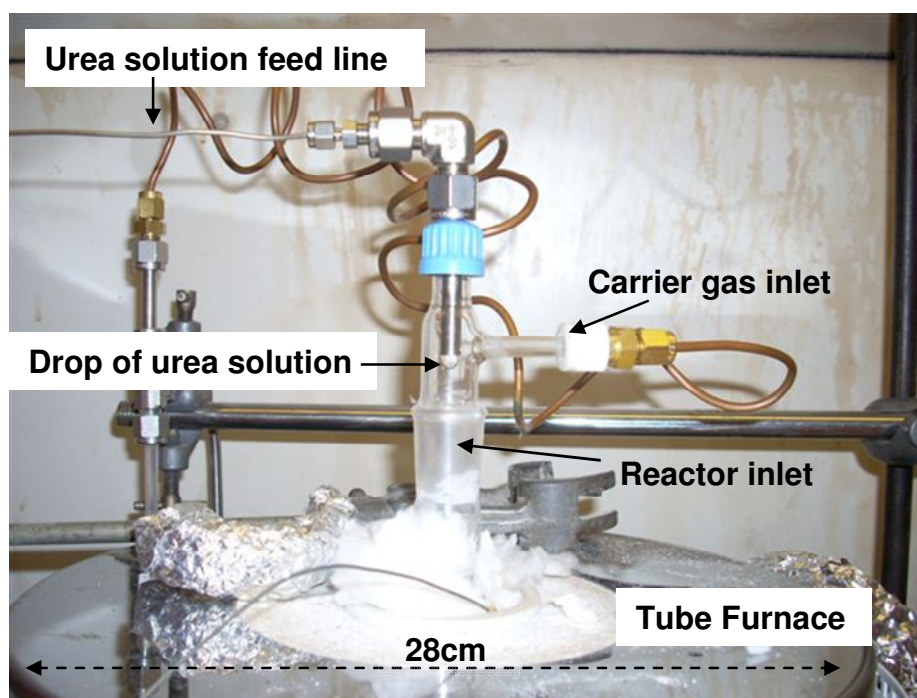


**Figure 6-3.** Inlet assembly of drop feed quartz urea steam reforming reactor during operation.

The gaseous effluent leaving the reactor was passed through two oil-cooled condensers to remove moisture before analysis. Condensate was collected in a glass flask at the base of the outlet assembly for determination of its ammonia content. The condensate collection system is shown in **Figure 6-4**.



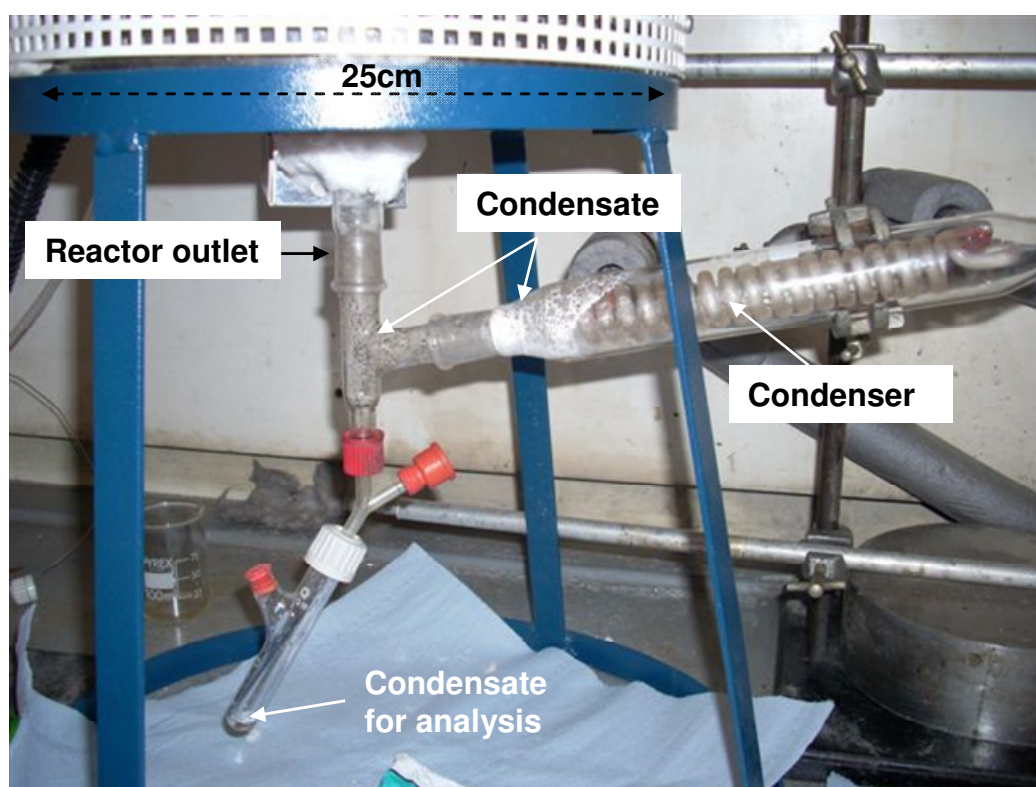


**Figure 6-4.** Condensate collection during steam reforming operation. Experiment shown is at 600 °C reactor temperature with an S:C = 6 fuel feed.

Preliminary experimentation was undertaken to optimise the process. A range of S:C mixtures, fuel feed rates and catalyst quantity were assessed to investigate maximum conversion of fuel at different mixtures of S:C rather than to elucidate reaction kinetics. From these preliminary experiments a parametric study was commenced using the following variables:

Steam reforming was performed on urea solutions of  $3:1 \geq \text{S:C} \geq 7:1$  at reactor temperatures of 500 °C, 550 °C, 600 °C, 650 °C, and 700 °C. Water enrichment of the S:C mixtures was limited to S:C = 7 due to the low conversions predicted at equilibrium (see Chapter 3). The following parameters were fixed:

Catalyst (**Table 5-1**) was prepared as described in section 5.2. Each experiment used 20 grams of undiluted catalyst occupying a volume of 10 cm<sup>3</sup> within the centre of the reactor tube, supported on a stainless steel mesh screen. Fresh catalyst was used, and this was fully replaced only three times during the parametric study of thirteen experiments. One quantity of catalyst was used for the five S:C = 7 experiments at the full range of temperatures, being regenerated each time. Similarly one quantity of catalyst was used for all five S:C = 6 experiments. One quantity of fresh catalyst was also used for the S:C = 5, S:C = 4, and S:C = 3 experiments at 600 °C. To regenerate the catalyst in-situ, following each steam reforming step, the system was purged with N<sub>2</sub> at

the same flow rate and temperature to remove any residual gases. Then, an air feed of  $1000 \text{ cm}^3 \text{ min}^{-1}$  (STP) maximum was applied at  $700 \text{ }^\circ\text{C}$ . This airflow step allowed for an assessment of possible coke build-up on the catalyst surface.

Prior to each steam reforming experiment, the catalyst was reduced for 1 hour at  $500 \text{ }^\circ\text{C}$  by a flow of  $30 \text{ cm}^3 \text{ min}^{-1}$  (STP) of  $\text{H}_2$  in  $400 \text{ cm}^3 \text{ min}^{-1}$  (STP) of  $\text{N}_2$ . The reactor was then purged for at least ten minutes with the same flow of  $\text{N}_2$  and the reactor temperature was programmed as desired for the steam reforming experiment. Urea solution fuel mixture was then prepared and inserted into the syringe (SGE 25 ml capacity with an I/D of 23 mm). Once inserted, the aqueous urea was then introduced at a rate of  $10 \text{ ml hr}^{-1}$  ( $20 \text{ }^\circ\text{C}$ ) into the reactor via a programmable micro-syringe pump (New Era Pump Systems). This capacity allowed a maximum operating period of 2.5 hours for a full syringe.

On-line analysers were calibrated to zero and span prior to experimentation using pre-mixed (and therefore accurately known) concentrations of gas for species  $\text{N}_2$ ,  $\text{CO}_2$ ,  $\text{CO}$ ,  $\text{NH}_3$ ,  $\text{CH}_4$ , and  $\text{H}_2$ , supplied by BOC cylinders. The system was leak tested prior to catalyst oxidation with an electronic flow meter inserted into the gaseous effluent line after the condensers and while carrier gas was supplied at the system inlet at a known flow rate.

## 6.3 Product Analysis

### 6.3.1 Dry Gases Online Analysis

The dry product gases were measured online with a series of (non sample-destructive) ABB Advance Optima Analysers comprising a Uras 14 non-dispersive infrared absorption module for  $\text{CO}$ ,  $\text{CO}_2$  and  $\text{CH}_4$  analysis, a Caldos 15 thermal conductivity analysis module for  $\text{H}_2$ , and a Limas 11 ultraviolet absorption module for  $\text{NH}_3$  analysis. Product concentration values were obtained every five seconds. During the air feed stage, oxygen was analysed at the end of the line using a Magnos 106 paramagnetic susceptibility module also by ABB Advance Optima.

### 6.3.2 Condensate Ion Chromatography

At cessation of the steam reforming step, condensate was collected immediately and stored in glass vials with screw-top lids (Bacto Laboratories T102/V2 and T1001/C7) and in dark refrigerated conditions. This condensate was then analysed using a Dionex DX-100 Ion Chromatograph at room temperature, with 0.02 mols methane sulphonic acid as eluent and Dionex polymeric packing (IONPAC CS12A), on a column  $4 \text{ mm} \times 250 \text{ mm}$ . Calibration samples were created by diluting a 1% ammonia nitrogen

standard (on a gravimetric basis) in deionised water to 1:100 and 1:200. A de-ionised water sample was run through the analyser to form a baseline.

Raw condensate samples were diluted (x625) with deionised water to fit within the detection range of the analytical technique and were analysed at room temperature. The pH of the diluted sample was measured using litmus paper after ion chromatography analysis.

Ion Chromatography results gave values for ammonium ( $\text{NH}_4^+$ ) concentration. This was corrected to  $\text{NH}_3$  by multiplication with the difference in  $M_r$  of  $\text{NH}_3/\text{NH}_4 = 17.031/18.031$ . To create these values, an inference was made that at steady-state, there was a uniform rate of solvation of the  $\text{NH}_3$  in unconverted  $\text{H}_2\text{O}$  leaving the reactor and therefore the ratio of  $\text{NH}_3:\text{H}_2\text{O}$  found in the condensate remained constant. Thus the values obtained in the condensate analysis are used to represent a time-averaged  $\text{NH}_3$  flow rate out of the reactor. This calculation is shown algebraically in section **6.4.1**.

## 6.4 Data Analysis

A new mass and elemental balance spreadsheet using reactor exit concentrations of  $\text{H}_2$ ,  $\text{CO}$ ,  $\text{CO}_2$ , and  $\text{CH}_4$  and the known inlet flows of aqueous urea and  $\text{N}_2$  was devised to incorporate gaseous and condensate  $\text{NH}_3$ . This provided values of urea and steam conversion, species selectivity, and hydrogen gas yield. The spreadsheet was formulated collaboratively by the author, Dr Valerie Dupont, and Dr Gavin Rickett.

The possible presence of volatile hydrocarbons higher than  $\text{CH}_4$  was eliminated by off-line GC analysis (**Table 5-2**), and unmeasured products  $\text{N}_2$  and  $\text{H}_2\text{O}$  were predicted by calculation. An assumption was made that all water and urea is vaporised prior to entering the reactor.

Species comprising the flow entering the reactor were  $\text{N}_2$  (considered inert),  $\text{H}_2\text{O}$ , and urea. In the following elemental balances, urea is  $C_nH_mO_kN_j$  with the subscripts being molar elemental composition of  $n$ ,  $m$ ,  $k$ , and  $j$  moles of C, H, O and N in the fuel, where  $n = 1$ ,  $m = 4$ ,  $k = 1$  and  $j = 2$ .

Elemental balances on carbon, hydrogen and nitrogen are given below, where:

$y_i$  = mol fraction of species  $i$  in the dry gas (known from online measurements).

*in*, and *out* subscripts denote relevant flows entering or leaving the reactor.

*dry* subscripts denote conditions after the condensate trap, prior to dry gas analyses.

$\dot{n}, \dot{n}_i$  = total molar flow rate and molar flow rate of species  $i$  ( $\text{mol s}^{-1}$ ).

### 6.4.1 Condensate

The condensate molar flow rates were determined to be constant at steady state:

$$\dot{n}_{cond} = \dot{n}_{H_2O,out} + \dot{n}_{NH_3,c,out} \quad (E10)$$

$$\dot{n}_{NH_3,c,out} = y'_{NH_3} \times \dot{n}_{cond} \quad (E11)$$

where:

$y'_{NH_3}$  = liquid mol fraction of  $NH_3$  in the condensate (known from ion chromatography analysis). Combining these equations gives a value for the molar flow rate of  $NH_3$  leaving the reactor in the condensate,  $\dot{n}_{NH_3,c,out}$ :

$$\dot{n}_{NH_3,c,out} = \left( \frac{y'_{NH_3}}{1 - y'_{NH_3}} \right) \dot{n}_{H_2O,out} \quad (E12)$$

The value  $\dot{n}_{H_2O,out}$  is an unknown and was determined from elemental balances.

### 6.4.2 Nitrogen balance

Nitrogen entering the system from urea and carrier gas flow is balanced by nitrogen leaving in the dry gas (as  $NH_3$  and  $N_2$ ) plus  $NH_3$  in the water condensate, and any unconverted urea. This balance, with the outputs on the left hand side and inputs on the right involves three unknowns,  $\dot{n}_{H_2O,out}$ ,  $\dot{n}_{out,dry}$  and  $\dot{n}_{CnHmOkNj,out}$ :

$$\begin{aligned} & \left( 2y_{N_2} + y_{NH_3} \right)_{out} \times \dot{n}_{out,dry} + \left( \frac{y'_{NH_3}}{1 - y'_{NH_3}} \right) \times \dot{n}_{H_2O,out} + j \times \dot{n}_{CnHmOkNj,out} \\ & = j \times \dot{n}_{CnHmOkNj,in} + 2\dot{n}_{N_2,in} \end{aligned} \quad (E13)$$

$y_{N_2}$  is the dry mol fraction of  $N_2$  leaving the reactor and was calculated by balance with 1 from the measured online dry gases:

$$y_{N_2} = 1 - (y_{CO} + y_{CO_2} + y_{CH_4} + y_{H_2} + y_{NH_3}) \quad (E14)$$

The molar flow of the  $N_2$  carrier gas,  $\dot{n}_{N_2,in}$  was calculated using (E9) (see section 5.3).

### 6.4.3 Carbon balance

The moles of carbon entering the system originate from the urea only (denoted by subscript  $n = 1$ ). Carbon leaving the system is contained in the measured dry gases. The accumulation of coke is assumed as zero in the carbon balance, shown in equation (E14)

here with outputs on the left hand side and inputs on the right. This balance contains two unknowns,  $\dot{n}_{out,dry}$  and  $\dot{n}_{CnHmOkNj,out}$  :

$$\left( (y_{CO} + y_{CO_2} + y_{CH_4}) \times \dot{n}_{out,dry} \right) + n \times \dot{n}_{CnHmOkNj,out} = \dot{n}_{CnHmOkNj,in} \quad (E15)$$

#### 6.4.4 Hydrogen balance

The hydrogen balance is shown in (E16). Hydrogen entering the system originates from water ( $2\dot{n}_{H_2O,in}$ ) and urea ( $m \times \dot{n}_{CnHmOkNj,in}$ ), where  $m = 4$ , representing the elemental hydrogen content of urea. These are shown on the right hand side of (E16). Hydrogen leaving the system (left hand side of (E16)) is that contained in measured dry gas molecules, and that contained in the condensate ( $2\dot{n}_{H_2O,out} + 3\dot{n}_{NH_3,c,out}$ ). It is assumed that there is no accumulation of hydrogen in the reactor. The hydrogen balance also contains the three unknowns  $\dot{n}_{H_2O,out}$ ,  $\dot{n}_{out,dry}$  and  $\dot{n}_{CnHmOkNj,out}$  :

$$\begin{aligned} & \left( 4y_{CH_4} + 2y_{H_2} + 3y_{NH_3} \right) \times \dot{n}_{out,dry} + \left( 2 + \frac{3y'_{NH_3}}{1 - y'_{NH_3}} \right) \times \dot{n}_{H_2O,out} + m \times \dot{n}_{CnHmOkNj,out} \\ & = m \times \dot{n}_{CnHmOkNj,in} + 2\dot{n}_{H_2O,in} \end{aligned} \quad (E16)$$

The three elemental balances form three simultaneous linear equations: (E13), (E15), and (E16). Since there are three common unknowns,  $\dot{n}_{H_2O,out}$ ,  $\dot{n}_{out,dry}$  and  $\dot{n}_{CnHmOkNj,out}$  the equations could be solved to provide values for these terms. This was achieved using the determinants method in an EXCEL spreadsheet.

#### 6.4.5 Products, Conversions, Selectivities, and Hydrogen Yield

Conversions for urea and water were obtained by:

$$x_{CnHmOkNj} = \frac{\dot{n}_{CnHmOkNj,in} - \dot{n}_{CnHmOkNj,out}}{\dot{n}_{CnHmOkNj,in}} \quad (E17)$$

$$x_{H_2O} = \frac{(\dot{n}_{H_2O,in} - \dot{n}_{H_2O,out})}{\dot{n}_{H_2O,in}} \quad (E18)$$

Rates of product evolution from the reformer in mol s<sup>-1</sup> were obtained by:

$$\dot{n}_{H_2,out} = y_{H_2} \times \dot{n}_{out,dry} \quad (E19)$$

$$\dot{n}_{CO_2,out} = y_{CO_2} \times \dot{n}_{out,dry} \quad (E20)$$

$$\dot{n}_{CO,out} = y_{CO} \times \dot{n}_{out,dry} \quad (E21)$$

$$\dot{n}_{CH_4,out} = y_{CH_4} \times \dot{n}_{out,dry} \quad (E22)$$

$$\dot{n}_{NH_3,out} = y_{NH_3} \times \dot{n}_{out,dry} + \left( \frac{y'_{NH_3}}{1 - y'_{NH_3}} \right) \times \dot{n}_{H_2O,out} \quad (E23)$$

The selectivity of hydrogen for the molecular species produced (in %) were obtained by:

$$SEL_{H_2} = 100 \times \frac{\dot{n}_{H_2,out}}{\dot{n}_{H_2,out} + \dot{n}_{NH_3,out} + \dot{n}_{CH_4,out}} \quad (E24)$$

$$SEL_{NH_3} = 100 \times \frac{\dot{n}_{NH_3,out}}{\dot{n}_{H_2,out} + \dot{n}_{NH_3,out} + \dot{n}_{CH_4,out}} \quad (E25)$$

$$SEL_{CH_4} = 100 \times \frac{\dot{n}_{CH_4,out}}{\dot{n}_{H_2,out} + \dot{n}_{NH_3,out} + \dot{n}_{CH_4,out}} \quad (E26)$$

The selectivity of carbon for the molecular species produced (in %) were obtained by:

$$SEL_{CO_2} = 100 \times \frac{\dot{n}_{CO_2,out}}{\dot{n}_{CO_2,out} + \dot{n}_{CO,out} + \dot{n}_{CH_4,out}} \quad (E27)$$

$$SEL_{CO} = 100 \times \frac{\dot{n}_{CO,out}}{\dot{n}_{CO_2,out} + \dot{n}_{CO,out} + \dot{n}_{CH_4,out}} \quad (E28)$$

$$SEL_{CH_4} = 100 \times \frac{\dot{n}_{CH_4,out}}{\dot{n}_{CO_2,out} + \dot{n}_{CO,out} + \dot{n}_{CH_4,out}} \quad (E29)$$

A value for hydrogen yield was obtained in mol s<sup>-1</sup> H<sub>2</sub> product per mol s<sup>-1</sup> of urea:

$$H_2 \text{ yield} = \frac{\dot{n}_{H_2,out}}{\dot{n}_{C_nH_mOkN_j,in}} \quad (E30)$$

## 6.5 Results/Discussion

### 6.5.1 Steam Reforming

Greater stability was achieved with the downflow drop-feed process than with the upflow design (Chapter 5). This allowed for an extended period of steam reforming limited only by the maximum period of operation attainable by the volumetric capacity of the fuel-feed syringe; suggesting also that longer-term operation should therefore be achievable. Process stability is evidenced by the dry syngas concentration as a function of time at 600 °C for S:C = 7 shown in **Figure 6-5**, and in sequential order over the full S:C range at 600 °C in **Figure 6-6** to **Figure 6-9**. All exhibited a rapid rise to a steady state and consisted of a dry syngas with hardly any of the undesired CH<sub>4</sub> and NH<sub>3</sub> by-products, little CO, and mainly the products CO<sub>2</sub> and H<sub>2</sub> (16 mol%). The remaining

composition of the syngas was  $N_2$  from both product and carrier gas. The closeness of these experimental profiles with the values predicted by thermodynamic modelling (Chapter 3) show that the conditions were very near equilibrium for the full duration of experimentation once steady state had been reached.

The output profiles in **Figure 6-5** to **Figure 6-9** show that the  $H_2$  detection at the analyser was seen to be concordant with the other syngas species at breakthrough, in contrast to the occasional discordant species breakthrough with the upflow reactor (section 5.4.1.3). This was probably due to a combination of an excessive quantity of silica gel volume in the moisture trap of the upflow system, and inability of the upflow inlet design to contain the urea fuel in solution prior to the reactor bed resulting in consequent distortion of the mixture's S:C ratio as previously discussed.

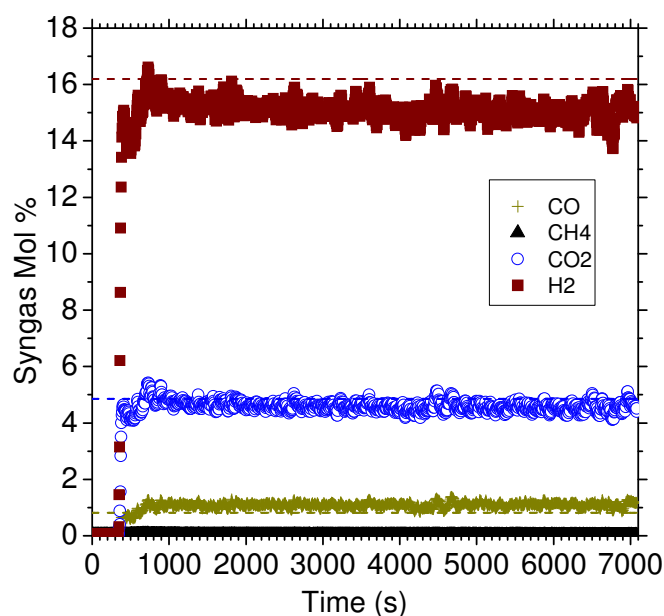


**Figure 6-5.** Dry product gas concentrations for S:C = 7, at 600 °C reactor temperature. 20 % datapoints are shown for clarity. Also shown is calculated equilibrium data displayed as dotted lines. Gaseous ammonia (< 0.00 %) at steady state omitted.

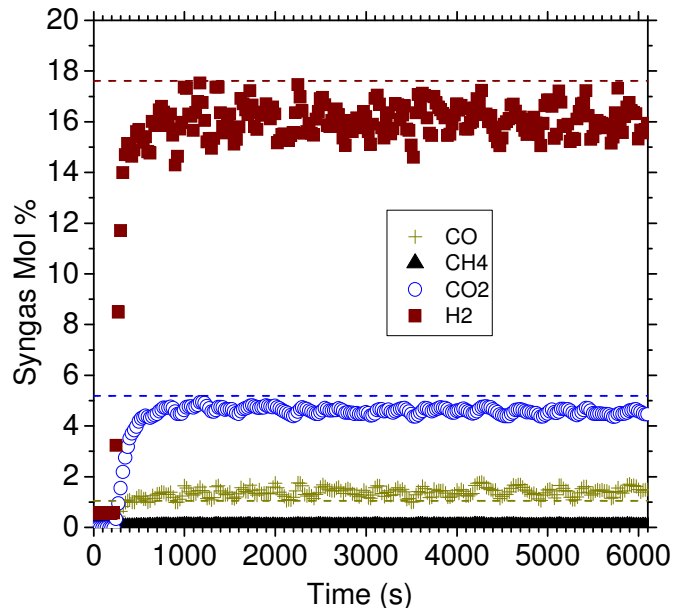


**Figure 6-6.** Dry product gas concentrations for S:C = 6, at 600 °C reactor temperature. 20 % datapoints are shown for clarity. Also shown is calculated equilibrium data displayed as dotted lines. Gaseous ammonia (< 0.00 %) at steady state omitted.

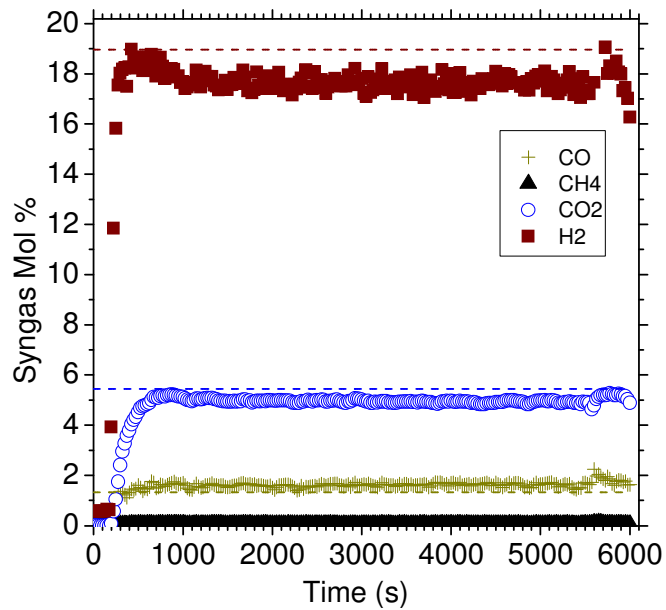


**Figure 6-7.** Dry product gas concentrations for S:C = 5, at 600 °C reactor temperature. 20 % datapoints are shown for clarity. Also shown is calculated equilibrium data displayed as dotted lines. Gaseous ammonia (< 0.00 %) at steady state omitted.



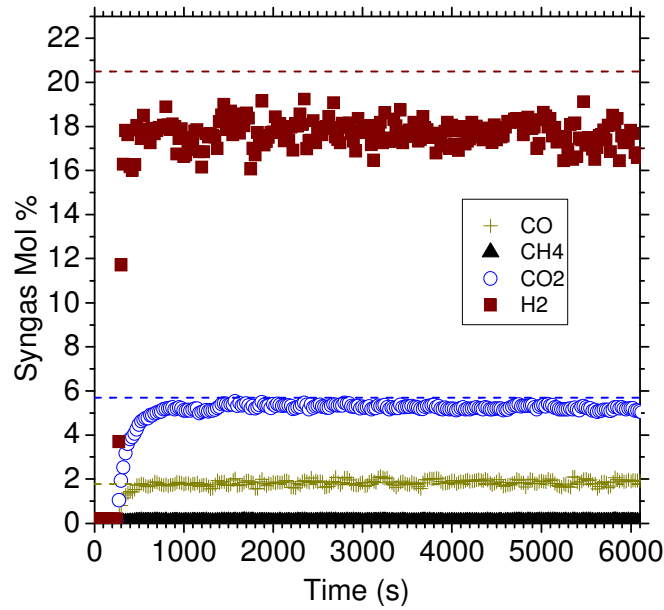


**Figure 6-8.** Dry product gas concentrations for S:C = 4, at 600 °C reactor temperature. 20 % datapoints are shown for clarity. Also shown is calculated equilibrium data displayed as dotted lines. Gaseous ammonia (< 0.00 %) at steady state omitted.

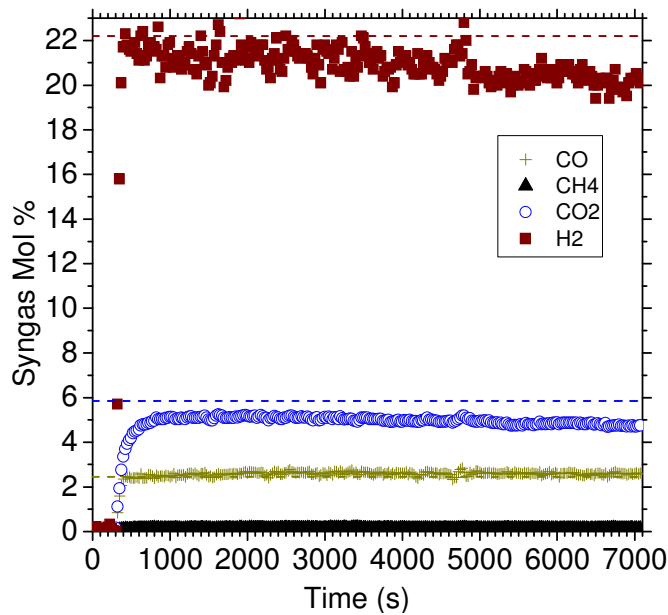


**Figure 6-9.** Dry product gas concentrations for S:C = 3, at 600 °C reactor temperature. 20 % datapoints are shown for clarity. Also shown is calculated equilibrium data displayed as dashed lines. Gaseous ammonia (< 0.00 %) at steady state omitted.

In terms of syngas purity (hydrogen concentration), the drop feed design permitted greater fuel feed rates. Consequently three times greater hydrogen content was obtained compared to identical operating S:C and reactor temperature settings used for the previous upflow reactor. Drop-rates were measured and the feed rate used in the

parametric study ( $10 \text{ ml hr}^{-1}$ ) corresponded to a drop being dispensed every 12-13 seconds. It is possible that this drop dispensation rate could be responsible for the slight oscillations in the profiles. The use of a controlled spray system in place of the tube and droplet design would be one way to assess this; however a spray injection system may pose extra problems because smaller injection apertures may accentuate the occurrence of urea precipitation and consequent fuel line blockages. Extended tests to increase the fuel flow rates and reduce the bore of the feed line would be another way to test whether the slight oscillations were caused by periodic fuel feed.

It is considered feasible that the syngas purity could be greatly increased. Attempts were made, prior to the parametric study, to test the maximum flow rates achievable and the system was pushed to failure. In this test a dry syngas hydrogen concentration of 55% was achieved for 10 minutes (see **Appendix A**). Since the objectives were for high steam conversion and process stability, optimisation of the reactor's ability to accommodate higher fuel feed rates were not pursued. Syngas purity could also be increased by reducing carrier gas flow dilution. The  $\text{N}_2$  flow rate used in this study ( $300 \text{ cm}^3 \text{ min}^{-1}$ ) was the minimum that could be accommodated by the online analysers, so was used purely for the purposes of analyses rather than as a necessity of the syngas production process.

The cavity design with kaowool inserted just 4 cm deep at the longitudinal extremities of the tube furnace/reactor tube may be a factor that led to an improvement in stability of the  $\text{H}_2$  profiles over time. Observations on the thermocouple readings and the reactor temperature readings during steam reforming revealed that they were stable throughout, with never more than  $2 \text{ }^\circ\text{C}$  difference between them. This indicates that any temperature changes that may have occurred due to endothermic energy demands inside the reactor were corrected rapidly by the thermostatic tube furnace control and that the design allowed the response time of the tube furnace to adequately maintain the set reactor temperature.

Crystallisation caused by fuel supersaturation was successfully overcome by this drop-feed process and by the method of passive cooling incorporated into the inlet design. The exterior of the inlet glassware was measured during reactor operation and found to maintain a temperature of  $35 \text{ }^\circ\text{C} \pm 5 \text{ }^\circ\text{C}$ . This was in the desired range. Though some slight crystallisation was observed for S:C = 3 and S:C = 4 on the fuel feed outlet at the region where the droplet formed prior to its release onto the reactor bed, this phenomenon was not observed to affect the product output values or the process stability. This is evidenced by the product gas profile for S:C = 3 (**Figure 6-9**) which shows the improvement (in terms of steady state  $\text{H}_2$  output stability and syngas composition with respect to time) when compared to the upflow process design at S:C =

4 at the same reactor temperature (**Figure 5-6**). Crystallisation was not observed for experimentation with  $5:1 \leq S:C \leq 7:1$  fuel mixtures.

Mixtures of  $S:C \geq 4:1$  were able to be fed directly into the reactor without any pre-heating. For  $S:C = 3:1$ , gentle heat was applied to the solution by a Bunsen burner for solvation; and a simmerstat controlled heating cord (Thermoscientific HC503) was applied to the syringe and feed line during operation. Pre-heating of the syringe and fuel feed line was aimed at maintaining a temperature of ca. 40 °C at the fuel prior to its release into the reactor. Great care was needed to keep the temperature within a narrow range as the maximum temperature tolerance of the syringe was 70 °C and overall a temperature of < 100 °C was necessary to avoid water evolution. Steam reforming with  $S:C \leq 2$  fuel mixtures could not be achieved as previously described (see Chapter 4). It would be advantageous to steam reform urea-rich mixtures of  $S:C \leq 2$  due to the higher hydrogen content and water conversion predicted (see section 3.3), however this would need further adaptations of this process design to achieve. Those adaptations would involve an accurately controllable heat resistant injection system and feed line tolerant of temperatures between  $40\text{ °C} \leq T \leq 100\text{ °C}$  and between  $60\text{ °C} \leq T \leq 100\text{ °C}$  for  $S:C = 1$  (see **Table 2-4**), or a pressurised system at reduced temperature. Lower than these temperatures, urea would not dissolve; higher than these temperatures, water would evolve and supersaturation would occur. Alternatively a separate water and fuel feed system might be suitable, thereby keeping the water and urea feeds apart prior to the reactor. This would however require a solid-fuel feed system for the urea. Pre-loading the reactor with urea reagent and then dispensing pure water into the system was considered, but not pursued since no means of accurately determining the reagent molar input ratios entering the reactor per unit time could be found. Though dry syngas concentrations would have been obtainable from the online analysers, the other product variables obtained from elemental calculations would not be as they depend on known molar input rates for each element.

**Table 6-1**, **Table 6-2**, and **Table 6-3** list all the experimental urea and steam conversion fractions derived from the elemental balances, and the products distribution at steady-state, compared to their equilibrium calculated counterparts. These outputs show a trend towards higher urea and lower steam conversions as  $S:C$  increased.  $S:C = 7$  is seen to give the best experimental results in terms of stability, urea conversion and closeness to predicted equilibrium values. This is advantageous for potential assimilation of technologies involving combustion, with the  $S:C = 7$  mixture corresponding to the eutectic mixture (32.5 wt%) presently employed in SCR systems for NO<sub>x</sub> removal [89]. The carbon products selectivity values were close to equilibrium and beneficially, in terms of its high greenhouse gas potential, CH<sub>4</sub> was not produced in significant amounts at any time. The decreasing selectivity of carbon for CO<sub>2</sub> and increasing selectivity for CO with increasing temperature can be explained by the

reverse WGS reaction (R24) becoming increasingly dominant as was predicted by the equilibrium modelling (section 3.3.1).

**Table 6-1.** Mean experimental (Exp) and calculated equilibrium (Eq.Calc) reactant conversions and product species distribution at 600 °C for a range of S:C fuel mixtures at steady state operation.

S:C		$x_{urea}$	$x_{H2O}$	Sel. H-products %			Sel. C-products %			H <sub>2</sub> Yield mol/mol
				H <sub>2</sub>	NH <sub>3</sub>	CH <sub>4</sub>	CO <sub>2</sub>	CO	CH <sub>4</sub>	
3	Exp	0.86	0.31	91.9	7.51	0.57	64.5	33.9	0.02	2.32
	Eq. Calc	1.00	0.22	99.0	0.05	0.92	69.1	28.5	2.43	2.62
4	Exp	0.88	0.15	95.3	4.38	0.32	73.8	25.4	0.01	2.17
	Eq. Calc	1.00	0.19	99.5	0.05	0.42	75.5	23.4	1.14	2.72
5	Exp	0.95	0.15	97.0	2.65	0.32	74.5	24.6	0.01	2.53
	Eq. Calc	1.00	0.16	99.8	0.05	0.20	80.1	19.4	0.56	2.78
6	Exp	0.93	0.13	96.6	3.24	0.18	76.3	23.2	0.01	2.50
	Eq. Calc	1.00	0.14	99.8	0.04	0.12	82.8	16.8	0.32	2.82
7	Exp	0.97	0.10	98.0	1.92	0.05	80.6	19.2	<0.01	2.57
	Eq. Calc	1.00	0.12	100	0.04	0.07	85.3	14.5	0.19	2.85

**Table 6-2.** Mean experimental (Exp) and calculated equilibrium (Eq.Calc) reactant conversions and product species distribution for S:C = 7 for a range of reactor bed temperatures at steady state operation.

Temp °C		$x_{urea}$	$x_{H2O}$	Sel. H-products %			Sel. C-products %		
				H <sub>2</sub>	NH <sub>3</sub>	CH <sub>4</sub>	CO <sub>2</sub>	CO	CH <sub>4</sub>
500	Exp	0.51	0.13	76.0	23.8	0.20	83.9	15.4	0.01
	Eq. Calc	1.00	0.12	98.2	0.10	1.68	87.9	7.43	4.69
550	Exp	0.76	0.08	97.1	2.60	0.25	83.8	15.5	0.01
	Eq. Calc	1.00	0.12	99.6	0.06	0.33	88.0	11.1	0.95
600	Exp	0.97	0.10	98.0	1.92	0.05	80.6	19.2	<0.01
	Eq. Calc	1.00	0.12	100	0.04	0.07	85.3	14.5	0.19
650	Exp	1.00	0.09	99.6	0.47	0	75.0	25.3	0
	Eq. Calc	1.00	0.12	100	0.03	0.01	81.9	18.0	0.04
700	Exp	1.00	0.08	99.9	0.19	0	70.1	30.2	0
	Eq. Calc	1.00	0.11	100	0.02	<0.01	78.5	21.5	0.01

**Table 6-3.** Mean experimental (Exp) and calculated equilibrium (Eq.Calc) reactant conversions and product species distribution for S:C = 6 for a range of reactor bed temperatures at steady state operation.

Temp °C		$x_{urea}$	$x_{H2O}$	Sel. H-products %			Sel. C-products %		
				H <sub>2</sub>	NH <sub>3</sub>	CH <sub>4</sub>	CO <sub>2</sub>	CO	CH <sub>4</sub>
500	Exp	0.53	0.16	79.4	20.1	0.40	81.2	17.4	1.39
	Eq. Calc	1.00	0.13	97.3	0.10	2.62	84.7	8.22	7.09
550	Exp	0.84	0.13	93.5	5.6	0.9	79.3	18.1	2.5
	Eq. Calc	1.00	0.14	99.4	0.07	0.57	85.6	12.8	1.6
600	Exp	0.94	0.13	96.6	3.2	0.2	76.3	23.2	0.5
	Eq. Calc	1.00	0.14	99.8	0.04	0.12	82.8	16.8	0.3
650	Exp	0.96	0.10	98.9	1.1	0.0	71.8	28.2	0.0
	Eq. Calc	1.00	0.13	1.00	0.03	0.03	79.2	20.7	0.07
700	Exp	0.98	0.09	99.5	0.5	0.0	67.9	32.2	0.0
	Eq. Calc	1.00	0.13	1.00	0.02	<0.01	75.5	24.5	0.02

The results of reforming across a range of temperatures for S:C = 6 and S:C = 7 fuel mixtures, as shown in **Table 6-2** and **Table 6-3** evidence that 600 °C is the optimum temperature for urea steam reforming in terms of steam conversion. Temperatures between 600 °C and 700 °C, are seen as favourable in terms of urea conversion close to 100 %, and experimental product selectivity close to predicted equilibrium values. Practically however, experimentation at temperatures above 600 °C would not be advantageous due to the predominance of the reverse water gas shift yielding higher relative concentrations of CO in the syngas. In commercial applications this would necessitate increased post-reforming process requirements to purify the syngas. Further support for 600 °C being an optimum process condition is found with an assessment of hydrogen yield as a function of temperature for S:C = 6 and S:C = 7 (**Figure 6-10**). Values of H<sub>2</sub> yield as functions of temperature reach maxima at 600 °C and then plateau when reactor temperatures are increased further. Thus no benefit in terms of hydrogen yield was obtained for the extra input of energy required.

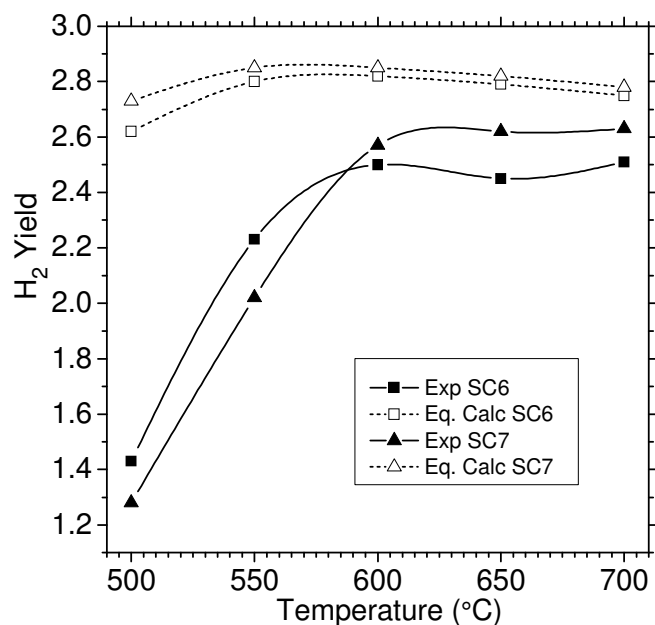


**Figure 6-10.** Mean experimental and calculated equilibrium hydrogen yield (mol H<sub>2</sub> produced per mol of urea in the feed) for S:C = 6 and S:C = 7 at a range of temperatures.

With consideration given to other criteria, urea steam reforming above 600 °C is not entirely disadvantageous. Maximum urea conversion was achieved (**Table 6-1** to **Table 6-3**) at temperatures of 650 °C and 700 °C. Furthermore, steady state profiles of the gaseous outputs (therefore also species selectivity and reagent conversions) were very stable over time at these heightened temperatures as shown in **Figure 6-11**. Though the ratio of CO<sub>2</sub>:CO decreased with increasing reactor temperature as previously discussed, CH<sub>4</sub> concentrations remained negligible. What was also noted as being favourable was that higher temperatures resulted in lower overall NH<sub>3</sub> production, a phenomenon that is discussed in greater detail in section **6.5.2**.

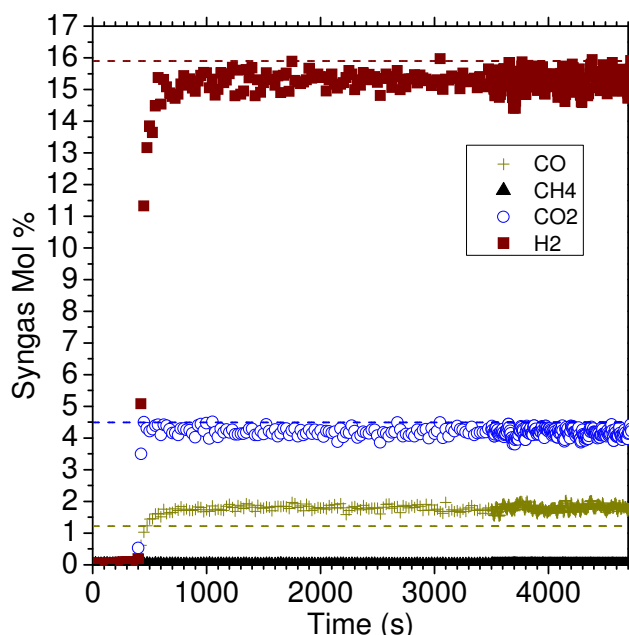


**Figure 6-11.** Dry product gas concentrations for S:C = 7, at 700 °C reactor temperature. 20 % datapoints are shown for clarity. Also shown is calculated equilibrium data displayed as dashed lines. Gaseous ammonia (< 0.00 %) at steady state omitted.

The effects of temperature in the range 500 °C to 700 °C are much larger than those observed when the S:C varied from 7 to 3 at 600 °C. Firstly, the fraction of urea converted reduced from near complete conversion at 600 °C to the poor value of 0.51 (for S:C = 7) and 0.53 (for S:C = 6) at 500 °C, with very significant drops between 600 °C and 550 °C, and again between 550 °C and 500 °C (**Table 6-2** and **Table 6-3**). This can be explained by a decrease in catalyst activity in the urea steam reforming reaction below 600 °C, as had been observed in previous studies using other feedstocks [12].

The importance of the catalyst for urea steam reforming was confirmed by a “blank run” experiment with no catalyst inside the reactor (not shown graphically). Alumina beads occupying the same volume as the catalyst bed were used instead, and the reactor set at a temperature of 600 °C. Using an S:C = 7 fuel mixture, fed at a rate of 10 ml hr<sup>-1</sup>, and an N<sub>2</sub> carrier gas flow rate of 300 cm<sup>3</sup> min<sup>-1</sup>, this experiment produced no hydrogen over the full duration of the run time (1 hour). The onset of steady state was identified at ca. 8 minutes, whence carbon species outputs were stable and concordant with both equilibrium predictions and previous catalytic steam reforming results at this temperature and fuel feed parameters. NH<sub>3</sub> outputs in the dry gas and in the condensate were also significantly higher than recorded with comparable catalytic reforming. A greater discussion of these NH<sub>3</sub> outputs is given in section 6.5.2.

A graph showing the gaseous product profiles measured online for S:C = 7 at 500 °C is provided in **Figure 6-12**. A comparison between **Figure 6-12** and plots of the

identical fuel feed rate at higher temperatures (cf. **Figure 6-5** and **Figure 6-11**) reveals how the  $\text{H}_2$  concentration has decreased well below that predicted at equilibrium and below that achieved by the comparable experiments at higher temperature. This is further evidence that the speed of catalytic activity reduces below  $600\text{ }^\circ\text{C}$ .

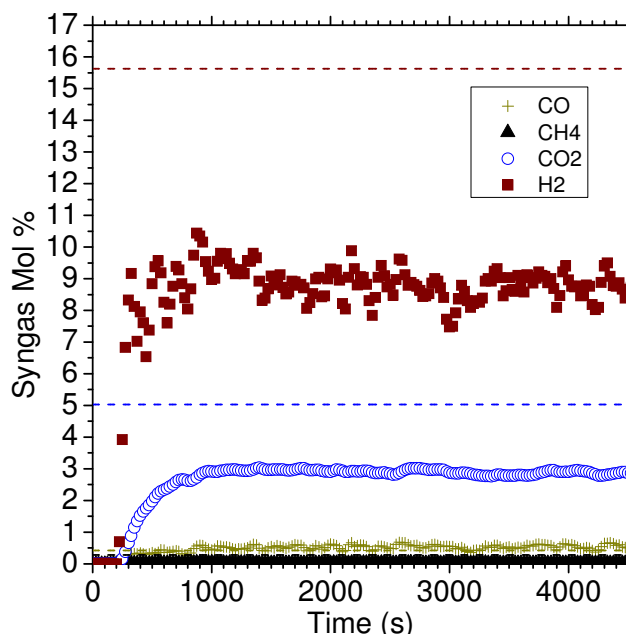


**Figure 6-12.** Dry product gas concentrations for S:C = 7, at  $500\text{ }^\circ\text{C}$  reactor temperature. 20 % datapoints are shown for clarity. Also shown is calculated equilibrium data displayed as dashed lines. Gaseous ammonia ( $< 0.00\%$ ) at steady state omitted.

Modelling had predicted that the S:C = 7 steam conversion was expected to slightly *increase* as temperature decreased from  $700\text{ }^\circ\text{C}$  to  $500\text{ }^\circ\text{C}$  (**Figure 3.2**). The general trend of the experiments did show a slight increase in steam conversion from 0.08 to 0.13 in the same temperature range (**Table 6-2**), although the experiment at  $550\text{ }^\circ\text{C}$  indicated a larger deviation from equilibrium with a poorer than expected steam conversion (0.08 instead of 0.12).

The temperature dependence of the selectivity of the H-containing products for S:C = 7 revealed that for  $\text{CH}_4$  this was insignificant (0 % to 0.2% with decreasing temperature). In contrast,  $\text{NH}_3$  selectivity increased significantly from 2.6% to 23.8% between  $550\text{ }^\circ\text{C}$  and  $500\text{ }^\circ\text{C}$ . The values, being a function of total urea entering the reactor rather than converted urea, suggest that the catalyst's ability to reform  $\text{NH}_3$  between  $550\text{ }^\circ\text{C}$  and  $500\text{ }^\circ\text{C}$  was influential. The larger  $\text{NH}_3$  selectivity adversely affected that of  $\text{H}_2$ , causing a corresponding large drop from 97.1% to 76% between  $550\text{ }^\circ\text{C}$  and  $500\text{ }^\circ\text{C}$ . Above  $550\text{ }^\circ\text{C}$  however, the selectivity to  $\text{H}_2$  remained very high, reaching above 99.6% from  $650\text{ }^\circ\text{C}$ .



Recall that HNCO is not expected in any appreciable amount, based both on literature evidence (that confirmed its ultimate decomposition via interaction with water and urea derivatives to  $\text{NH}_3$  and  $\text{CO}_2$  prior to ca. 500 °C), and on TGA experiments (see Chapter 4). The closeness of the carbon selectivity values to the calculated equilibrium predictions, for which the potential presence of HNCO would also have created discordance, provides confirmation that HNCO was not present as a significant product.

The maximum  $\text{H}_2$  yield per mol of urea in the fuel feed was found, as expected from the equilibrium trends (Chapter 3, **Figure 3-2**), for S:C of 7. This experimental yield maximum, as shown in **Figure 6-10**, had a value of 2.57 mol  $\text{H}_2$ /mol urea that corresponded to 90% of the equilibrium value. A cause for the decline in  $\text{H}_2$  yield with S:C mixtures  $\leq 5$  as shown in **Table 6-1** can be found in the significant decrease in urea conversion from S:C of 5 compared to S:C = 4 ( $x_{\text{urea}}$  of 0.95 and 0.88 respectively). Another contributing factor for this decline in  $\text{H}_2$  yield with S:C  $\leq 5$  was the increase in  $\text{NH}_3$  selectivity in the H-containing products (**Table 6-1**). These high values of  $\text{NH}_3$  come from the measured ammonium ion in the condensate. It can be observed that the only other H-containing by-product  $\text{CH}_4$  did not appear significantly dependent on the steam to carbon ratio, as predicted by the equilibrium calculations.

### 6.5.2 Condensate ion Chromatography

Ammonium ion detection was good in the condensate from the reforming experiments, with well defined peaks evident in all analyses. **Figure 6-13** shows an ion chromatogram produced by these experiments and representative of all samples analysed.

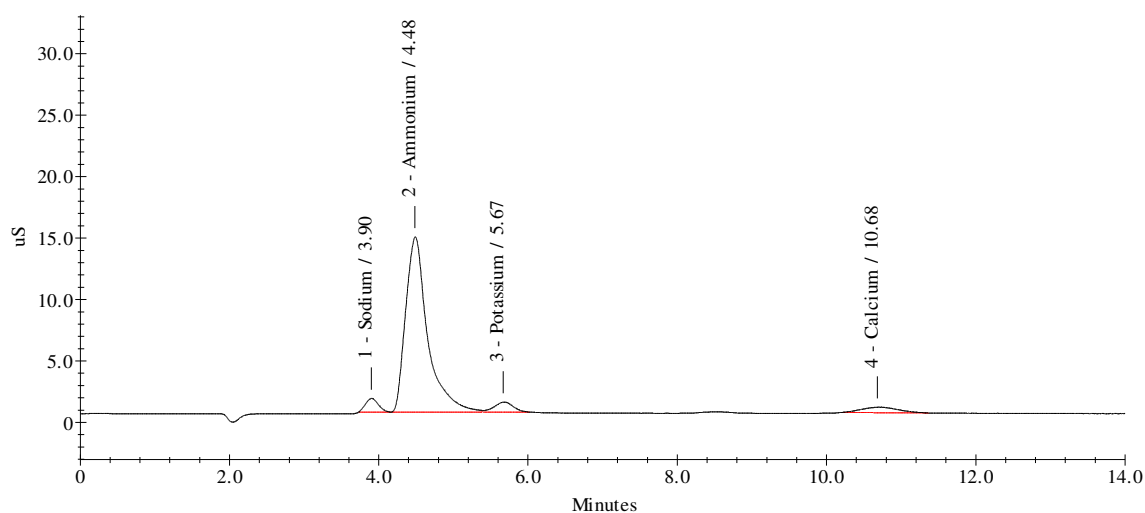


**Figure 6-13.** Ion chromatogram of condensate obtained during downflow reactor urea steam reforming experiment with S:C = 6 fuel at 550 °C reactor temperature.

The concentrations of NH<sub>3</sub> measured in the condensate from urea steam reforming experiments are shown in **Table 6-4**. All diluted samples had a neutral pH of 7. The acidity of the eluent was not tested but was expected to be only mildly acidic due to its low concentration. Therefore it was expected that eluted samples would have had a pH of 6 or 7 as they passed through the analytical column. Based on this assumption and from previous studies of the dependency of ammonia concentrations in solution to pH and temperature [153], it is expected that the results provided in **Table 6-4** are minimum values correct to + 0.02 - 0.5% relative uncertainty.

**Table 6-4.** NH<sub>3</sub> concentration in the urea steam reforming condensate in gravimetric parts per million (ppm).

Temperature	Steam:carbon (S:C) of fuel				
	7	6	5	4	3
700 °C	119	1588	-	-	-
650 °C	1221	3787	-	-	-
600 °C	6926	14396	14559	26557	85156
550 °C	7338	23621	-	-	-
500 °C	61564	66940	-	-	-

It can be seen from **Table 6-4** that the NH<sub>3</sub> produced with urea steam reforming increased with urea content in the feed solution as would be expected by the higher values of elemental nitrogen and hydrogen present. The increase in ammonia with decreasing reactor temperature is likely due to lower catalytic activity. Nickel catalysts have shown activity for splitting NH<sub>3</sub>, with conversion increased with higher temperature [32]. The activity of the catalyst for decomposing NH<sub>3</sub> is supported by the analysis of NH<sub>3</sub> from the blank run with alumina beads instead of catalyst (not shown in **Table 6-4**). This result showed that without the catalyst a value of 82788 ppm (8.27%) NH<sub>3</sub> was recorded, this being higher than all other samples analysed.

The condensate trap fed by a reflux condenser (shown during steam reforming experimentation in **Figure 6-4**) worked effectively at removing NH<sub>3</sub> from the product gas. In all but two experiments, the online dry gas concentrations of NH<sub>3</sub> were detected at < 10 ppm for the duration of steady state operation. The contribution of dry product NH<sub>3</sub> to the overall hydrogen selectivity was negligible with more than 99.3% of the NH<sub>3</sub> generated being collected in the condensate. This is highly advantageous process design as by utilising the unconverted water it is a cost-effective method of removing a component that is toxic to both humans and PEMFCs. During operation the condenser oil coolant remained within the temperature range of -5 °C ≤ T ≤ -20 °C.

The overall values obtained for experimental product  $\text{NH}_3$  showed an apparently exponential decay with increasing temperature and S:C, and were unexpectedly higher than those predicted by thermodynamic modelling, (**Figure 6-14** and **Figure 6-15**). This would indicate the difficulty of the catalyst to reform the ammonia at lower steam to carbon ratios and at lower temperatures. Tests on varying concentrations of  $\text{NH}_3$  decomposition in the presence of steam and  $\text{CO}_2$  would be one way to test this conjecture. This is an area for future study.

In **Table 6-1** the value for steam conversion with S:C = 3 is calculated as being slightly higher than that predicted by equilibrium modelling. Other steam conversion discrepancies appear with the higher than predicted (by equilibrium modelling) values at 500 °C for both S:C = 6 and S:C = 7. The S:C = 7 value only varies by one tenth and could be caused by averaging the data and by rounding errors created by placing the data to three significant figures. Interestingly, all these three steam conversion results correspond with a far higher than expected (by equilibrium modelling) estimation of the condensate  $\text{NH}_3$  concentration. This indicates that the discrepancy may be a result of either minor inaccuracies in the equilibrium model, errors caused by condensate calibration at the highest concentrations, or most likely an inability of the catalyst to actively decompose ammonia and bring the reaction close to equilibrium at these low temperatures, as discussed previously.

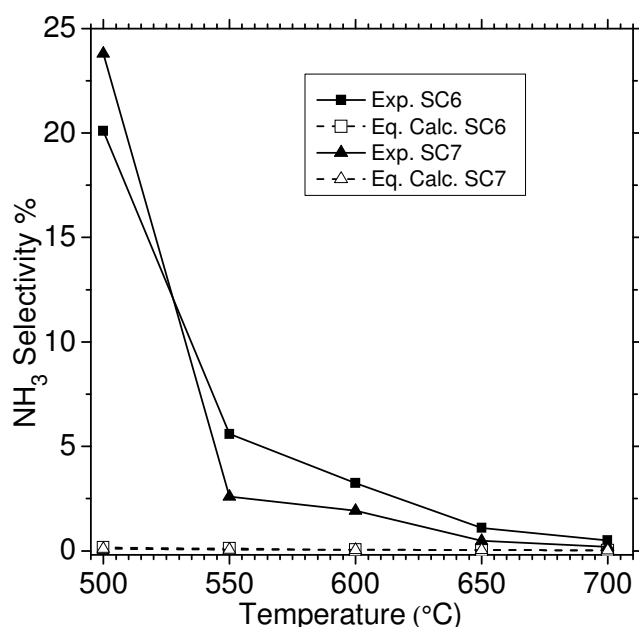


**Figure 6-14.** Mean experimental and calculated equilibrium hydrogen selectivity towards  $\text{NH}_3$  for a range of experimental temperatures. Experimental values are steady-state averages from 20 minutes after start of the experiment up to cessation.

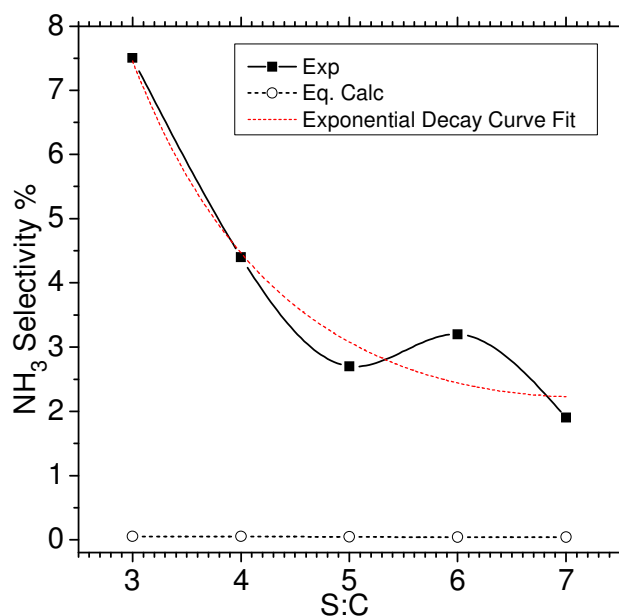


**Figure 6-15.** Mean experimental and calculated equilibrium hydrogen selectivity towards NH<sub>3</sub> for a range of S:C fuel mixtures at 600 °C reactor temperature. Experimental values are steady-state averages from 20 minutes after start of the experiment up to cessation. Exponential decay curve fit applied.

### 6.5.3 Coke Formation

In the experiments presented in section 6.5 there were several indications that coke formation was insignificant. These include: product outputs and calculations matching those at equilibrium, the absence of any degradation of catalyst activity over time, and no observed blackening at the reactor outlet and/or in the condensate. Black deposits (identified as coke) had been observed with preliminary experimentation using a glycerol feed (unpublished) following which carbonation was confirmed [12]. If coke formation had occurred with aqueous urea fuel, the post-steam reforming air-feed step was expected to create a rapid temperature rise inside the reactor and measurable carbon species detected at the gas analysers due to oxidation of any coke that had built up on the reactor bed:



It is also possible that slight increments in detected reactor temperature could be due to catalyst oxidation:



There was no recorded carbon species burn-off and no temperature increase detected by the in-situ reactor bed thermocouple following all S:C = 7 experiments at

the full range of temperatures, and following the S:C = 6, 700 °C steam reforming experiment. Short term and gradual increases in temperature were detected inside the reactor during the air feed step following other steam reforming experiments. The rise in temperature was small, between  $1\text{ °C} \leq T \leq 40\text{ °C}$  and was recorded over periods of  $1 \leq T \leq 5$  minutes. This occurred only when the air flow was increased to a maximum capacity of  $1000\text{ cm}^3\text{ min}^{-1}$ , thus evidencing that any oxidation was very small.

The catalyst can be inferred to be robust in terms of its ability to repeatedly regenerate under the air-feed (oxidation) then  $\text{N}_2\text{:H}_2$  (reduction) steps, which would also be further evidence that coke formation was negligible. With five stages of steam reforming for fuel mixtures of S:C = 6 and S:C = 7 for the full range of temperatures, no signs of degradation were observed, with its efficacy for urea steam reforming apparently maintained. No experiments were performed under completely identical operating parameters using a regenerated catalyst, thus making absolute conclusions about catalyst integrity under repeat cycling inappropriate. As has been previously described, there was clear evidence that the variables of temperature and fuel S:C mixture influenced the observed parameters that would also otherwise lead to an assessment of catalyst integrity following regeneration (such as urea conversion, steam conversion,  $\text{H}_2$  yield, syngas composition, and species selectivity). However, this postulation that the process remained robust and highly active for steam reforming can be qualified by a comparison of the results for the experiments in the high temperature range for both S:C = 6, and S:C = 7 which each used the same catalyst, and for the 600 °C experiments with fuel mixtures of  $3 \leq \text{S:C} \leq 5$ . This is seen in **Figure 6-10**, where for both S:C = 6 and S:C = 7 (which each used the same, regenerated catalyst), the  $\text{H}_2$  yield between 600 °C and 700 °C remains relatively constant and very close to the equilibrium predicted values. These same experimental results further support the process stability over repeated stages by comparison with the species selectivity and reagent conversion values shown in **Table 6-2** and **Table 6-3**. Here, particularly between the 650 °C and 700 °C experiments, values closely adhere to those predicted at equilibrium. **Figure 6-7**, **Figure 6-8**, and **Figure 6-9** also display results where the same regenerated catalyst had been used. From these output profiles no qualitative evidence of deterioration in gas concentration output with respect to equilibrium predicted values can be seen.

To provide more conclusive evidence on the status of the catalyst following regeneration and steam reforming experiments, used catalyst was left to cool in-situ and then saved in glass vials with screw-top lids (Bacto Laboratories T102/V2 and T1001/C7) in dark refrigerated conditions. This was then used for subsequent characterisation analysis. Results of this analysis will be discussed in Chapter 7.

## 6.6 Conclusions

A catalytic steam reforming reactor designed specifically for the physical properties of a urea in water solution fuel was tested in a parametric study at 600 °C over a range of fuel mixtures from  $3 \leq S:C \leq 7$ , and over a range of reactor temperatures from  $500 \text{ °C} \leq T \leq 700 \text{ °C}$  for  $S:C = 6$  and  $S:C = 7$ . Conditions were chosen to maximise the conversion of urea and steam and to maintain steady state operation close to equilibrium predicted values.

Results of outputs and output trends with respect to variations in temperature and S:C closely followed those predicted by equilibrium modelling. Greater stability in product outputs over time in comparison with the previous upflow method (Chapter 5) was achieved, with the process remaining close to equilibrium for the duration of the experiments. Longer operation times in excess of two hours were achieved, limited only by the volumetric capacity of the injection system, and suggesting that the process could effectively be increased in scale.

A new reactor inlet design successfully allowed a greater fuel input rate to be applied and successfully avoided supersaturation of the fuel prior to its release onto the reactor bed. The preservation of the urea solution fuel at below 100 °C is identified as essential for urea steam reforming. This was achieved by the experimental method, with the urea remaining in solution up to vaporisation at the catalyst bed by way of a novel drop-feed design. Inlet solution cooling was further enhanced by selective application of insulation and by the carrier gas inlet feed line supplying the point where the fuel drop was dispensed.

Selective insulation of the reactor tube also created a space cavity between reactor tube and furnace in an attempt to increase response times of the furnace to internal temperature changes. This was identified in previous experimentation as being one possible cause of oscillating H<sub>2</sub> product profiles. Small scale oscillations still occurred, but it is considered that this cavity design is favourable to the alternative full length insulation previously used (section 5.2) as no significant fluctuation in output was observed and thermocouple readings remained stable to  $\pm 2 \text{ °C}$ , matching those of the tube furnace temperature throughout.

A hydrogen rich syngas was produced with three times higher concentrations of hydrogen than had been achieved by earlier experiments with an upflow reactor design. The syngas was simple in composition, with minor products of CO<sub>2</sub> and CO only. CH<sub>4</sub> concentration was negligible. NH<sub>3</sub> was measured online in the dry gas and also offline by ion chromatography of the condensate leaving the reactor. A new design for condensate collection was implemented and was shown to be a cheap, simple and effective method of removing NH<sub>3</sub> from the gas stream due to its high solubility in the

unconverted water leaving the reactor. Dry gas  $\text{NH}_3$  concentrations were detected at < 10 ppm level. Thus the system effectively detoxified the syngas of  $\text{NH}_3$  making it attractive for fuel cell applications.

Fuel mixtures of S:C = 7 were considered to give the best experimental results in terms of stability, urea conversion, and closeness to predicted equilibrium values. Greater urea content in the fuel increased steam conversion and product  $\text{H}_2$  under the same conditions.

In terms of variation in reactor temperature, 600 °C was identified as the optimum, with  $\text{H}_2$  yield plateauing thereafter. With decreasing temperature, urea conversion and therefore  $\text{H}_2$  product decreased markedly; a phenomenon that can be attributed to lower catalytic activity below 600 °C. Analysis of the products revealed that the reverse water gas shift was affecting the carbon selectivity at higher temperature, and ammonia cracking was affecting the hydrogen selectivity at lower temperature. A trade-off in terms of water conversion and temperature was also identified, with greater temperature reducing the water conversion.

$\text{NH}_3$  values in the combined dry gas and condensate were seen to be greater than had been predicted by thermodynamic modelling at low temperatures. This contradiction requires further study to identify whether it is the presence of steam and  $\text{CO}_2$  that is causing the  $\text{NH}_3$  cracking reaction to be inhibited. It is speculated that urea decomposition to  $\text{NH}_3$  is rapid, but  $\text{NH}_3$  decomposition is the rate determining step and its conversion at temperatures < 550 °C is too slow to enable equilibrium conditions to be attained.

Urea steam reforming was seen to be a clean process. The nickel catalyst was found to remain effective at steam reforming over time without deactivation. Catalyst speed of reaction was seen to decrease below 600 °C. Coke formation was not identified by visible observation or by air-flow oxidation tests. Repeated regeneration of the catalyst allowed for steam reforming to be continued over five experiments without noticeable deterioration. This, combined with urea solution's safe and easy to handle properties meant that steam reforming experimentation could be undertaken and repeated with minimal intervention.

## 7 Catalyst Characterisation

### 7.1 Introduction

Catalyst characterisation provides a means to indirectly assess the underlying chemistry of the steam reforming reactions. It also gives information that can help assess the process for industrial applications, such as its influence on the catalyst's ability to remain active for long periods.

Reactor experiments had provided some qualitative characterisation on the 18 wt% nickel catalyst's ability to steam reform urea (Chapters 5 and 6); for example, a high purity syngas product and no apparent deactivation with repeated cycles of regeneration. Observations of phenomena apparent during experimentation also indicated that there was an absence of coke formation. Catalyst morphology, texture, and chemical composition, and any changes in these characteristics due to the various stages of the experimental steam reforming process could not be determined with the catalyst in-situ, due to the high temperatures and the enclosure of reactor and tube furnace prohibiting access. To investigate these parameters and give a comprehensive characterisation of catalyst function in the urea steam reforming process, alternative analytical techniques were necessary on the catalyst in its cooled state after extraction from the reactor.

There has been no prior published work on nickel catalyst characterisation following steam reforming of urea. Though this same catalyst had been used for steam reforming experiments with methane and sunflower oil [153], glycerol [12], and waste cooking oil [155], little ex-situ characterisation had been attempted. Dou analysed the catalyst in three states (oxidised, reduced, and post-reforming) using Scanning Electron Microscopy (SEM) and Energy Dispersive X-ray Spectroscopy (EDX) following steam reforming with an S:C = 3 fuel mixture [12]. A different morphology was described between the pre- and post-reforming catalyst, with carbon structures identified as entirely covering the catalyst surface, and larger crystallites previously seen in the reduced sample, were no longer visible post steam reforming. Knight also characterised the catalyst using SEM and EDX after methane steam reforming (S:C = 0.1), in comparison to catalyst in its oxidised and reduced states [153]. Carbon was present on the post-reforming catalyst and clearly visible on SEM images as abundant 1-100  $\mu\text{m}$  forms.



## 7.2 Method

The catalyst (composition given in **Table 5-1**) used in the urea steam reforming experimentation (Chapters 5 and 6) was analysed in three states:

1. Post-steam reforming (two samples).
2. As supplied (fresh and oxidised).
3. Fully reduced (pre-steam reforming).

The provenance of the catalyst samples used for characterisation is shown in **Table 7-1**. Sample 2 contained nickel in its oxidised (NiO) state. This sample had never been exposed to heightened temperature or the application of reagents post-manufacture. The fully reduced sample (3) was prepared by inserting the fresh as supplied catalyst inside the downflow steam reforming reactor (described in Chapter 6) and subjecting it to a flow of  $30 \text{ cm}^3 \text{ min}^{-1}$  (STP) of  $\text{H}_2$  in  $400 \text{ cm}^3 \text{ min}^{-1}$  (STP) of  $\text{N}_2$  for 1 hour at  $500 \text{ }^\circ\text{C}$ . It had not been subjected to steam reforming. Sample 1a had undergone five stages of steam reforming, with interstage air-oxidation and hydrogen-reduction; its maximum temperature exposure being  $700 \text{ }^\circ\text{C}$ , and its final stage being steam reforming at  $500 \text{ }^\circ\text{C}$ . Sample 1b had undergone three stages of steam reforming (with fuel mixtures of S:C = 5, S:C = 4, and lastly S:C = 3), all at  $600 \text{ }^\circ\text{C}$ , with interstage oxidation and reduction. The final stage of exposure for Sample 1b was reduction with a flow of  $30 \text{ cm}^3 \text{ min}^{-1}$  (STP) of  $\text{H}_2$  in  $400 \text{ cm}^3 \text{ min}^{-1}$  (STP) of  $\text{N}_2$  for 1 hour at  $500 \text{ }^\circ\text{C}$ .

After steam reforming, all samples were left to cool in-situ in the sealed reactor. Once cooled, the catalyst was placed in a glass vial with a screw top lid (Bacto Laboratories T102/V2 and T1001/C7) and stored in dark refrigerated conditions.

**Table 7-1.** Provenance of catalyst samples prior to characterisation analyses

Sample	S:C	Reactor temp	Times used for steam reforming	Condition	Experimental urea feed rate
1a	6	$700^\circ\text{C}$ to $500^\circ\text{C}$	Five	Post steam reforming	$10 \text{ ml hr}^{-1}$
1b	5, 4, 3	$600^\circ\text{C}$	Three	Post steam reforming, oxidation and reduction	$10 \text{ ml hr}^{-1}$
2	N/A	N/A	None	Fresh oxidised catalyst	N/A
3	N/A	$500^\circ\text{C}$	None	Reduced catalyst	N/A

Where catalyst was analysed that had never been used for steam reforming experiments (samples 2 and 3) it was prepared and stored in the same manner. All samples were therefore in the form of 0.66 – 1.70 mm particles having been crushed in a ceramic pestle and mortar. Further preparation was necessary for the TEM, EDX and XRD techniques, and a description of this method is given under the relevant sections.

### 7.2.1 Digital microscopy

High resolution digital microscopy images were obtained of catalyst samples post steam reforming (Sample 1a) and fresh as supplied catalyst (Sample 2) using a Keyence VHX-600 (GEN-2) digital microscope.

### 7.2.2 Scanning Electron Microscopy

Catalyst samples 1a, 2, and 3 (**Table 7-1**) were analysed. Each was sprinkled onto an individual 1.5 cm diameter platform containing tacky carbon cement. Pressurised air was blown onto the samples to remove dust, then they were sprayed with a platinum/palladium film 15 nm thick using an Agar high resolution sputter coater. The samples were placed in the SEM analyser (a Leo 1530 Field Emission Gun (FEG) SEM) and a vacuum was applied to evacuate pore spaces. Two point analyses and two wide region analyses were made on each catalyst sample. Images were saved in digital form using Smartsem v5 software.

### 7.2.3 BET Adsorption/Desorption

All catalyst samples in **Table 7-1** were analysed. A mass of catalyst (between  $0.210 \leq g \leq 0.400$ , correct to  $\pm 0.0005$  g) was weighed and inserted into a Quantachrome NOVA 2200e Surface and Pore Size Analyser. This was programmed to subject the sample to small incremental volumes of gas (adsorbate) in an evacuated isothermal chamber, to allow for the calculation of sample surface area using the Brunauer, Emmett and Teller (BET) method [156]. Samples were degassed at 120 °C under vacuum prior to analysis, and the final mass value obtained for use in the programming of the analyser. The Quantachrome NOVA 2200e was then run using helium as the carrier gas and nitrogen as the adsorbate for a range of N<sub>2</sub> partial pressures from 0.00 to 1.00, with 1 minute allowed for equilibration at each increment. High purity gases from BOC were used: CP grade He and zero grade N<sub>2</sub>. Sample temperature was maintained at -196 °C inside the analyser.

## 7.2.4 Transmission Electron Microscopy and Energy Dispersive X-ray

Catalyst samples 1a, 2, and 3 (**Table 7-1**) were analysed. Samples were finely ground in a ceramic pestle and mortar then mixed with distilled water in a ratio of ca. 1:8 by volume. The resulting suspension was sonicated then transferred by pipette drop-casting onto a holey carbon film supported on a gold (sample 1) or copper (samples 2 and 3) mesh grid. Samples were analysed on a FEI CM200 FEG Transmission Electron Microscope (TEM) running at 197 kV with an Oxford Instruments EDX Spectrometer and a Gatan Imaging Filter. The FEI Tecnai F20 microscope was fitted with an 80 mm<sup>2</sup> X-max SDD detector. Using an imaging filter, Fast Fourier Transform (FFT) power spectra (analogous to electron diffractograms) were taken at selected regions to examine visible repeating spatial frequencies (d-spacings). These d-spacings were used to identify compound-specific crystal lattice planar distances.

## 7.2.5 X-ray Diffraction

Samples 1a, 2, and 3 (**Table 7-1**) were subjected to analysis. Each sample was crushed to a fine powder using a pestle and mortar and packed flat (to minimise surface topography) into a 10 mm diameter cavity-type sample holding spinner stage (PW3064). The sample was then placed into an X:Pert Philips X-ray Diffractor (XRD) by PANalytical, with a 240 mm radius goniometer (PW3050/60). The system operated at a temperature of 25 °C. A copper anode x-ray generator set at 30 mA and 40 kV supplied radiation of K-Alpha1 = 1.54060 Å, K-Alpha2 = 1.54443 Å, K-Beta = 1.39225 Å, with a K-Alpha1/ K-Alpha2 ratio of 0.50000. The samples were scanned at 0.017° angle intervals from 5° ≤ θ ≤ 91° with a scan step time of 40.7 seconds. The incident beam passed through a fixed divergence slit of 1° and a receiving slit of 0.1° prior to entering the detector.

Spectra were analysed qualitatively by comparing peak intensities. Peak fitting and phase identification was made using Highscore Plus software.

## 7.3 Results and Discussion

### 7.3.1 Digital Microscopy

High resolution (54 million pixel) images were obtained. A topography profile was produced by taking slices at different resolutions to give a 3-D image. This “topography in focus” image of the catalyst post steam reforming (Sample 1a) is provided in **Figure 7-1**. The image shows a grain of catalyst at the size range obtained by crushing and sieving to 0.66 – 1.70 mm (see section **5.2**) with the cross sectional distance shown and marked as scale. The height distance between points b and c in

**Figure 7-1** is 1.2 mm. It can be seen from this that the catalyst surface did not apparently fracture along planes when crushed, but was left in the form of a smoothly undulating semi-cylindrical grain. A higher magnification image of the same catalyst sample, with the smaller scale topographical features discernible is shown in **Figure 7-2**. This shows the surface texture exhibiting a rough topography at  $\mu\text{m}$  scale, with 0.1 mm rounded features visible along with smaller particles not discernible at this magnification but appearing to be of a size  $\leq 1\mu\text{m}$ .

The catalyst appeared homogeneous, with no crystalline features evident or textures indicative of carbon. This relatively low magnification however does not give sufficient evidence to discount the presence of carbon.

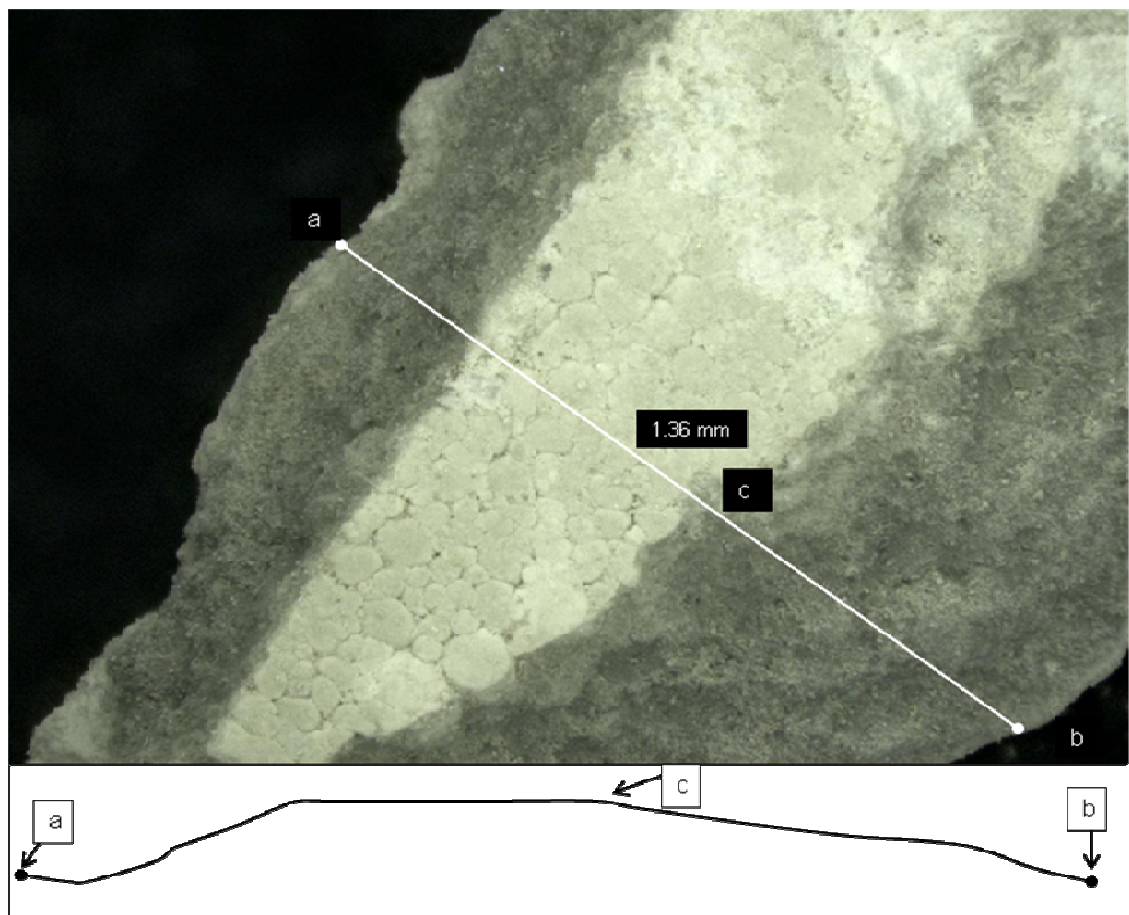


**Figure 7-1.** Digital microscopy image and topography of urea steam reforming catalyst crushed to size used in experiments (0.66 – 1.70 mm). Sample shown is post steam reforming catalyst 1a (see **Table 7-1**).

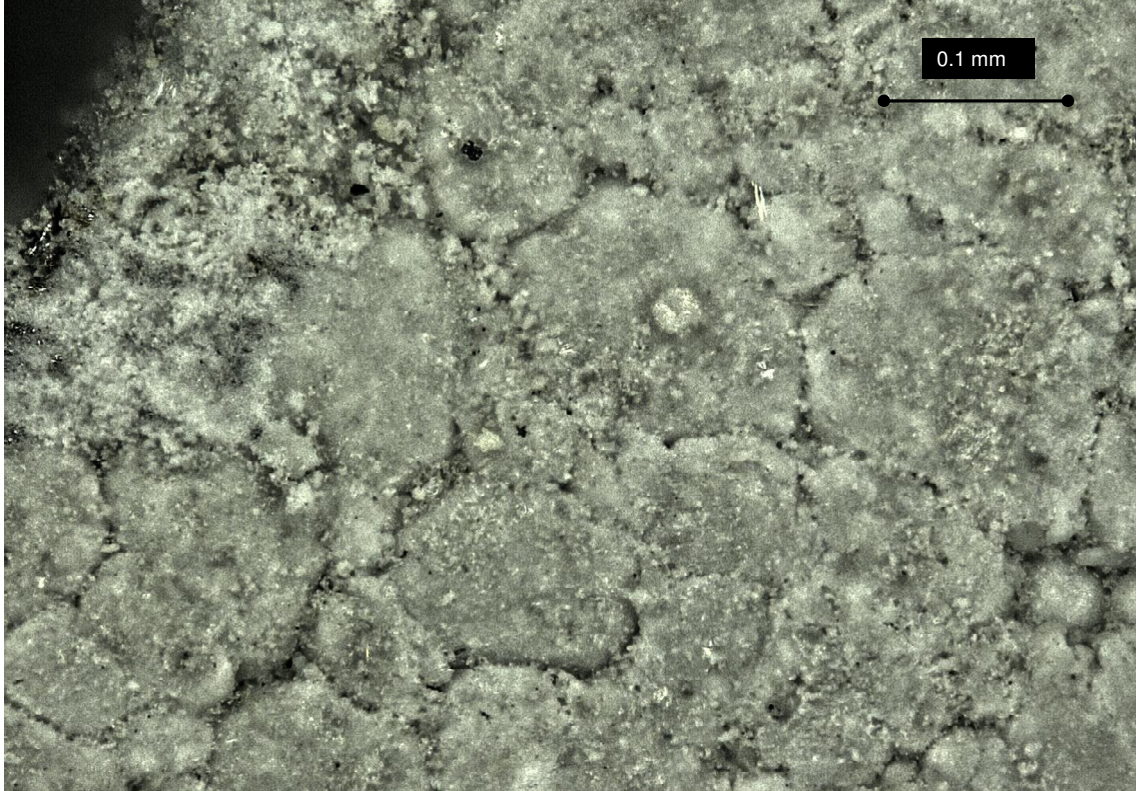


**Figure 7-2.** Digital microscopy image of urea steam reforming catalyst. Sample shown is post steam reforming catalyst 1a (see **Table 7-1**).

### 7.3.2 Scanning Electron Microscopy

A wide region image taken of the post steam reforming catalyst (sample 1a) shows the globular nature of the rough topography at  $\mu\text{m}$  scale (**Figure 7-3**). It can be seen that all crystallites appear to be sub-circular with larger particles having crystal faces, and smaller fragments with no crystal structure visible at this magnification.

Higher magnification images (**Figure 7-4** to **Figure 7-6**) showed more clearly the two types of particulate present in the catalyst, with the crystal faces visible on the larger particles and the smaller particles still revealing no long range crystal order. Based on known composition (18% Ni, 81.8%  $\text{Al}_2\text{O}_3$ ), the larger, more abundant crystals can be identified as alumina, with the smaller particles being nickel.

No evidence of carbon accumulation was identified in the post-steam reforming samples, easily seen as stringy/filamentous deposits (whisker carbon) and common to previous methane steam reforming work using the same catalyst and different fuels [12, 154]. This was particularly surprising considering that sample 1a had been exposed to the relatively adverse conditions of reforming at 500 °C where the urea conversion was lowest and  $\text{NH}_3$  production highest (see section 6.5) with high excess steam in the

reactor. The absence of observable differences in morphology between higher magnification images of the three catalyst samples suggest no significant carbon deposition and that urea steam reforming in the downflow reactor was therefore a clean process. Also, the similarity in morphology between the samples suggests that no sintering of the nickel had occurred. Sintering is known to take place at temperatures  $\geq 600$  °C, particularly in the presence of steam resulting in a loss of surface area and an increase in particle size [152]. As sintering and carbonation (along with poisoning) are two of the three phenomena that adversely affect catalyst performance [152], these findings establish that the process permitted the catalyst to remain apparently free of these events. Therefore the results are highly favourable in terms of the potential for prolonged process run time.

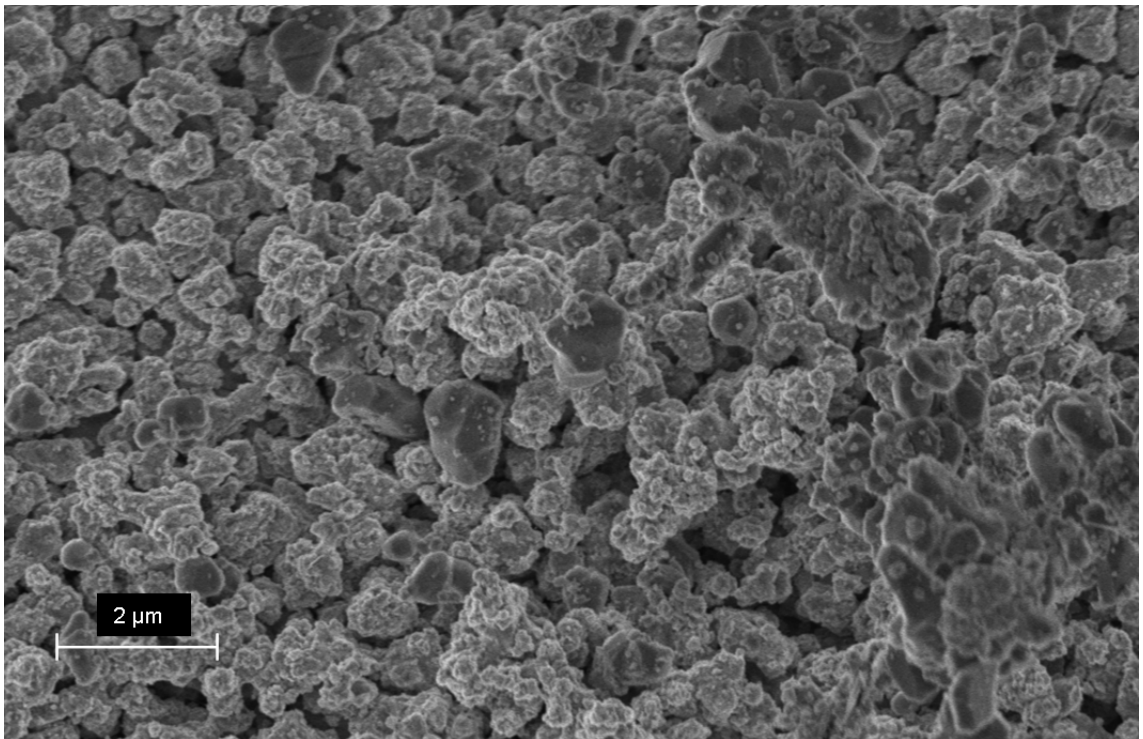


**Figure 7-3.** Low magnification SEM image of post steam reforming catalyst Sample 1a (see **Table 7-1** for sample provenance).

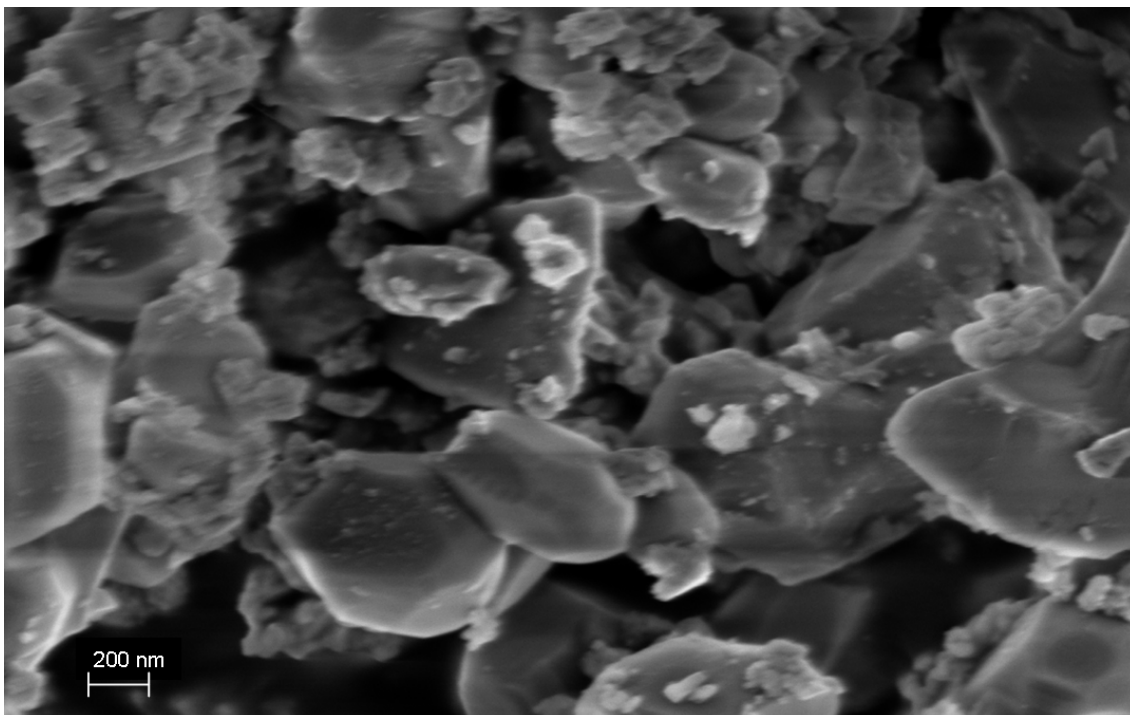


**Figure 7-4.** High magnification SEM image of the reduced catalyst Sample 3 (see **Table 7-1** for sample provenance).

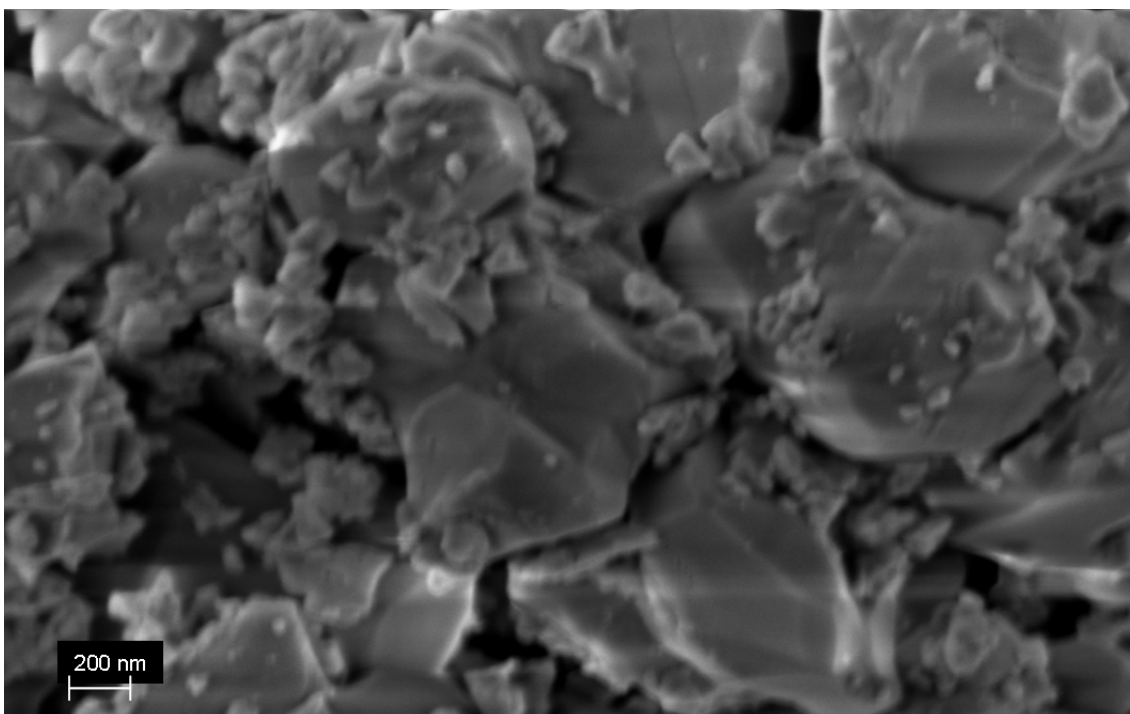


**Figure 7-5.** High magnification SEM image of fresh as supplied catalyst Sample 2 (see **Table 7-1** for sample provenance).

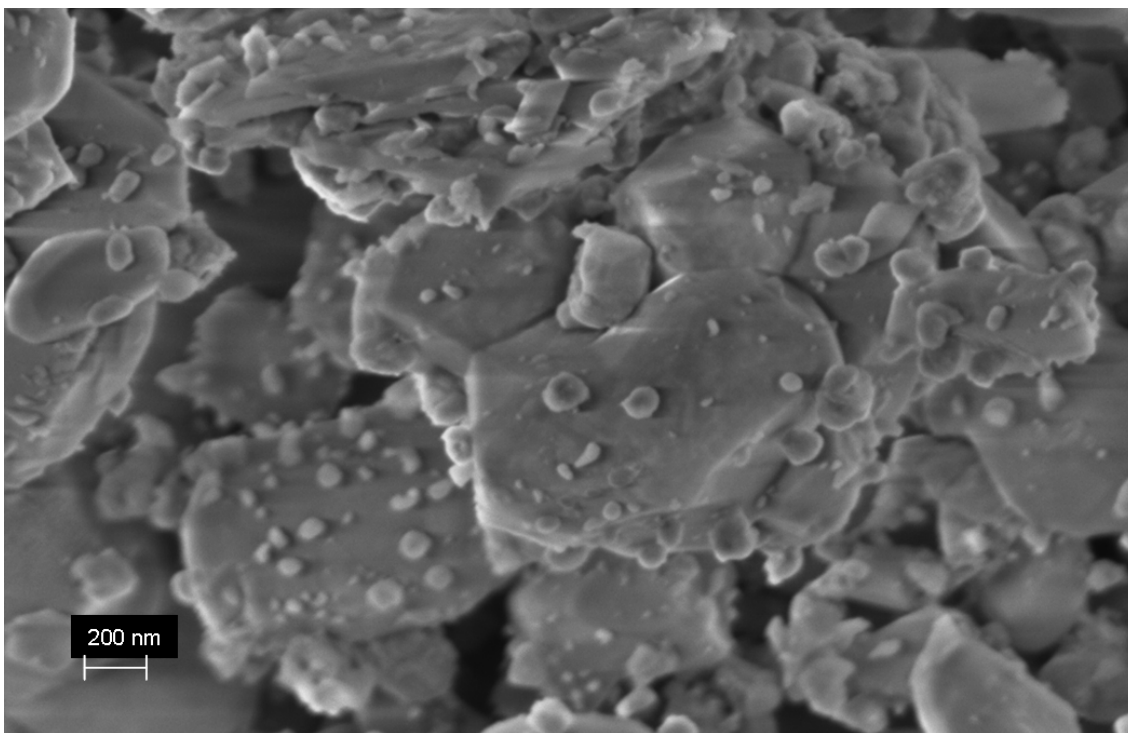


**Figure 7-6.** High magnification SEM of catalyst sample 1a post steam reforming (see **Table 7-1** for sample provenance).

### 7.3.3 BET Adsorption/Desorption

Results of the surface area analyses are displayed in **Table 7-2**. Values shown in column 3 of **Table 7-2** were obtained by the author, whereas values in column four were not and are marked with an asterisk. In terms of accuracy, repeatability appears poor (12 – 15 % error) between the two sets of experiments. Though the provenance of the column 4 samples were known, it was not known what methods in preparation or analyses they were subjected to. The differences appear to be due to systematic error, since column 4 values are always greater than those in column 3. The two sets of results however did show a concurrent pattern, with highest surface area recorded for both the Fresh Reduced samples, followed by next highest the Fresh Oxidised samples, then lowest surface area recorded for the Post Steam Reforming samples. This can be explained by the reduced samples acquiring an increased surface area during the reduction process: it is known that activation of catalyst by reduction with hydrogen at the temperatures used in these experiments reduces nickel crystallite size and therefore increases Ni surface area [152]. Lower surface area post-steam reforming, could be explained by sintering having occurred. Sintering is known to reduce surface area, and also to have a positive correlation with higher reactor temperatures and the presence of steam [152]. This would however conflict with the absence of any morphological evidence of sintering observed with the high magnification SEM analysis (section



7.3.2), unless the morphological changes were small and not visibly discernible by this technique.

**Table 7-2.** Results of catalyst surface area at different stages of the steam reforming process, obtained by BET adsorption/desorption method.

Sample	Condition	Surface Area	Replicated Surface Area* [157]	Mean Average
1a	Post steam reforming	2.971 m <sup>2</sup> /g	-	3.0 m <sup>2</sup> /g
1b	Post steam reforming, oxidation & reduction	2.775 m <sup>2</sup> /g	2.266 m <sup>2</sup> /g	2.5 m <sup>2</sup> /g ± 0.3
2	Fresh oxidised	3.262 m <sup>2</sup> /g	2.557 m <sup>2</sup> /g	2.9 m <sup>2</sup> /g ± 0.4
3	Fresh reduced	3.720 m <sup>2</sup> /g	2.798 m <sup>2</sup> /g	3.3 m <sup>2</sup> /g ± 0.5

The shape of the adsorption/desorption isotherms (not shown) approximated most closely to a Type 2 classification, associated with non-porous or macroporous solid (pore width > 50 nm) [158, 159]. This identification validates the reliability of the surface area results using the BET technique [158], but precludes analysis of pore structure [159]. This classification of a low porosity surface, is further corroborated by an absence of mesopores (2-50 nm) and micro-pores ( $\leq 2$  nm) seen with the SEM (section 7.3.2) and TEM analysis (section 7.3.4); a discussion of which follows.

#### 7.3.4 Transmission Electron Microscopy and Energy Dispersive X-ray

Magnification to  $\leq 1$  nm was achieved and a smooth surface texture observed with no pore structure evident. This accords with the results from SEM (section 7.3.2) and BET (section 7.3.3) analyses. The catalyst was seen to have an undulating  $\mu\text{m}$ -scale topography. The minimum size of structure observed was particles ca. 30 – 50 nm. An error of  $\pm 10\%$  can be applied to FFT d-spacing values for operator assignment.

Density contrasts within the sample, revealed by TEM, allowed for inferences to be made on the identification of crystallites/particulates. Denser areas within the sample had a greater inhibition for electron transmission and these were revealed as darker regions.

EDX provided only a qualitative identification of sample elemental composition. Electron's penetrated the subsurface of the sample to approximately 5 micrometres with error introduced by depth and latitude of penetration being a function of sample material, topography, and the relatively large field of analysis. With confidence, however, the content ratio of alumina and nickel in each sample could be affirmed and therefore comparisons could be made between sample compositions.

Relatively low magnification images from TEM analysis revealed the two different types of component present, the particle distribution of nickel on the alumina support, and also the crystal structure of alumina. An example from the fresh oxidised sample (sample 2) but representative of all samples analysed is provided in **Figure 7-7**. The nickel particles were seen to be occluded onto the closely packed and largely crystalline alumina. Common  $120^\circ$  angles between the alumina crystal faces identified the hexagonal crystalline form of  $\alpha$ -alumina [160].

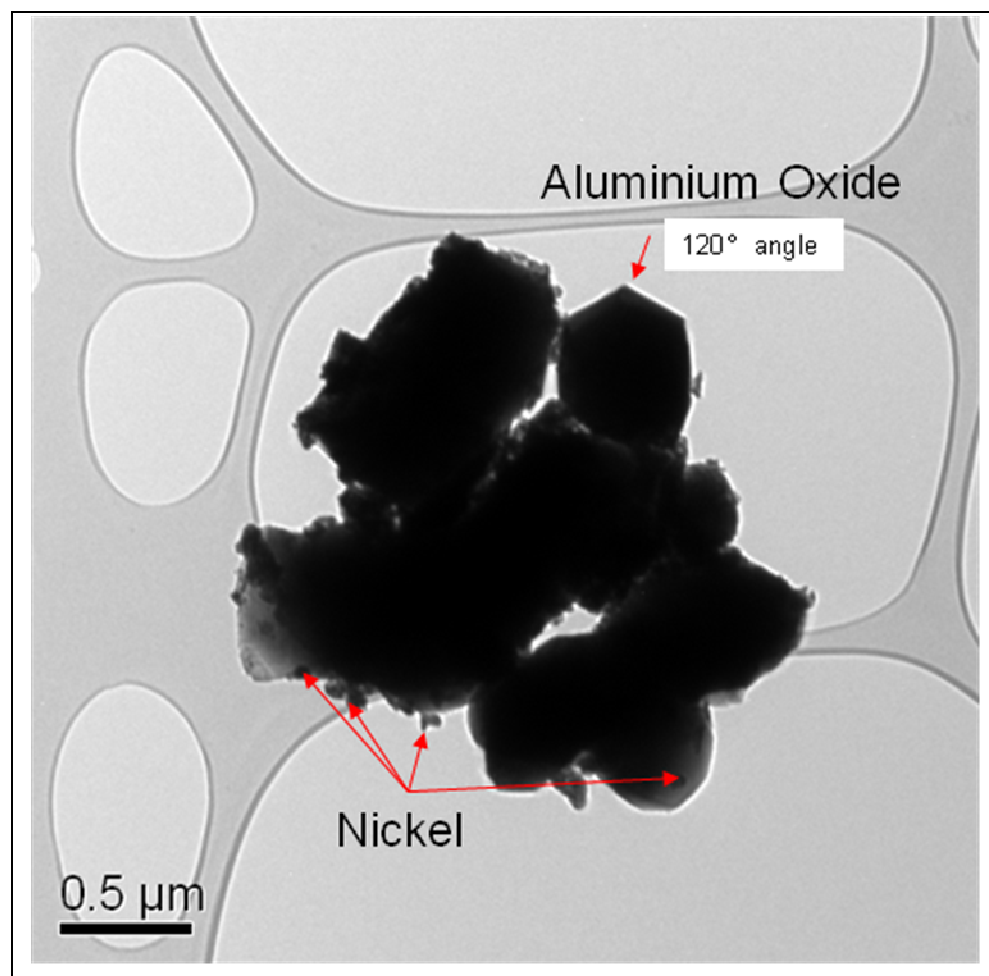


**Figure 7-7.** TEM image of fresh oxidised catalyst (Sample 2) showing differences in morphology between alumina and nickel..

#### 7.3.4.1 Sample 1a. Post Steam Reforming Catalyst

A high-magnification image representative of the full sample composition is shown in **Figure 7-8**. The light grey area to the left is taken from the large crystal face regions and further identified as aluminium oxide based on its  $3.4 \text{ \AA}$  FFT d-spacing. This spacing is unique to previously determined crystal lattice distances for alumina [161]. No EDX was done on this region. Other light grey sample regions were analysed

and found to have the same unique d-spacings as shown in **Figure 7-8**, and also to have observable striations attributable to long-range crystal order (see **Figure 7-10**).

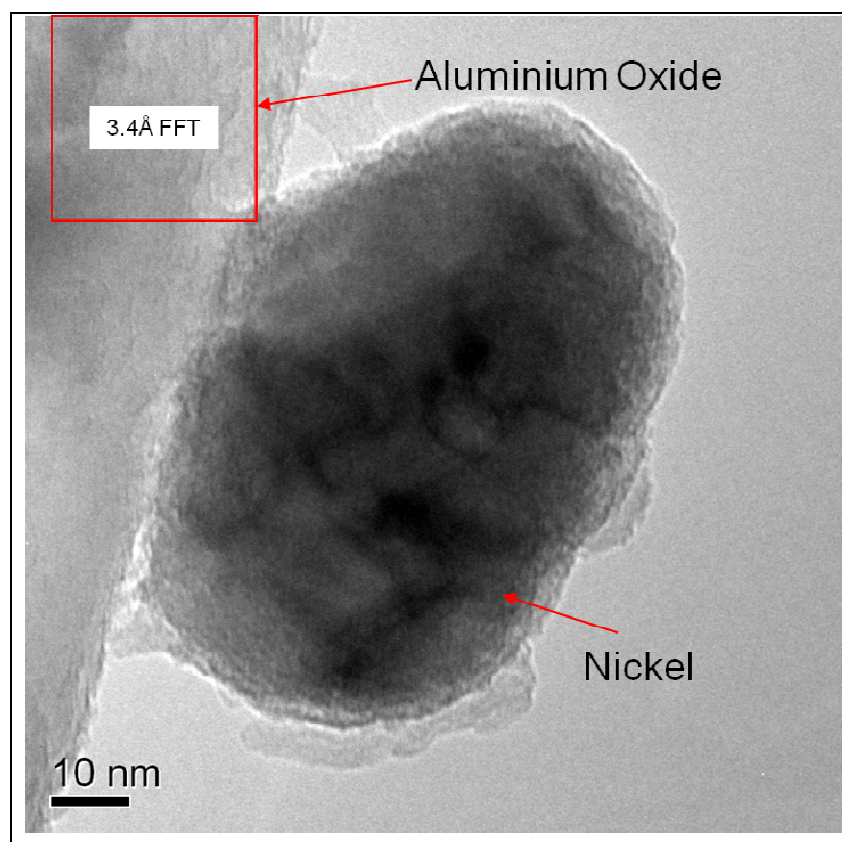


**Figure 7-8.** TEM image of post-steam reforming catalyst (Sample 1a) with FFT analysis in boxed region showing structural distances.

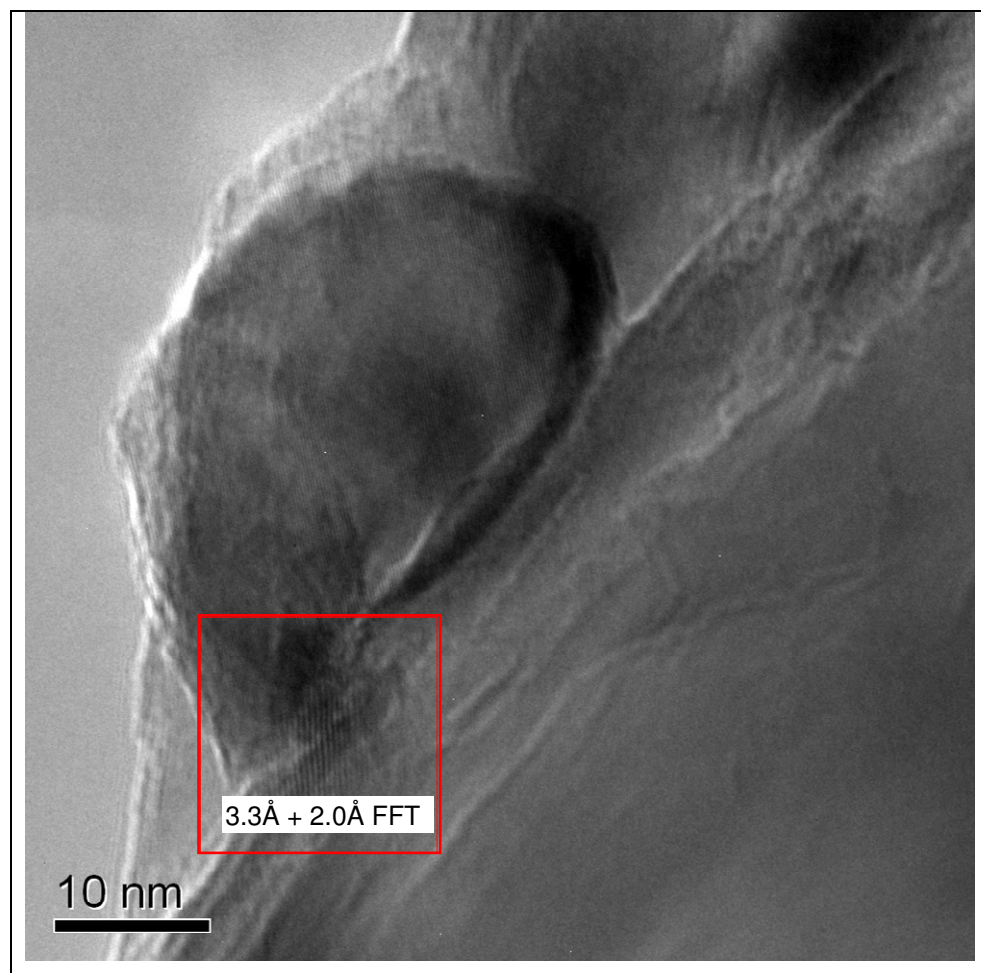


**Figure 7-9.** TEM image of post-steam reforming catalyst (Sample 1a) with FFT analysis in boxed region showing structural distances.

In contrast, the dark globular structure in the centre of **Figure 7-8** exhibited no nanoscale striations or d-spacings from FFT analysis and is labelled as “nickel”. These structures were seen throughout the sample and are representative of the relatively low (18 wt%) nickel component of the catalyst. That this structure is nickel-rich was confirmed by EDX analysis (**Figure 7-11**). The presence of gold in **Figure 7-11** can be attributed to the supporting grid material and not a feature of the catalyst sample. The very low concentration of oxygen in the EDX spectrum is evidence of nickel being in its reduced state. Small amounts of oxygen are considered to enter samples via contamination between sample and the oxygenated carbon support film, which is a possible explanation for its presence here. However, that the nickel in this sample was still in a reduced state despite steam reforming is established by comparison with the higher oxygen content of nickel regions in TEM analyses of the “as supplied catalyst” (**Figure 7-12**, cf. also reduced sample EDX – **Figure 7-13**). This is a very desirable outcome, since Ni rather than NiO is active for reforming of hydrocarbon fuels.

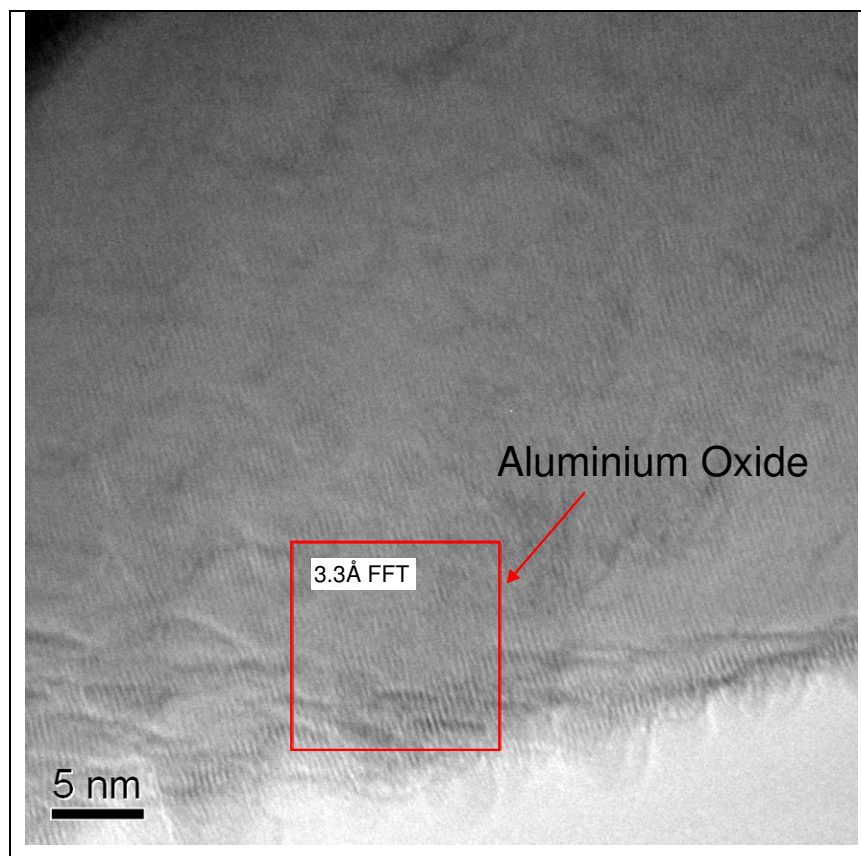


**Figure 7-10.** TEM image of post-steam reforming catalyst (Sample 1a) with FFT analysis in boxed region showing structural distances.

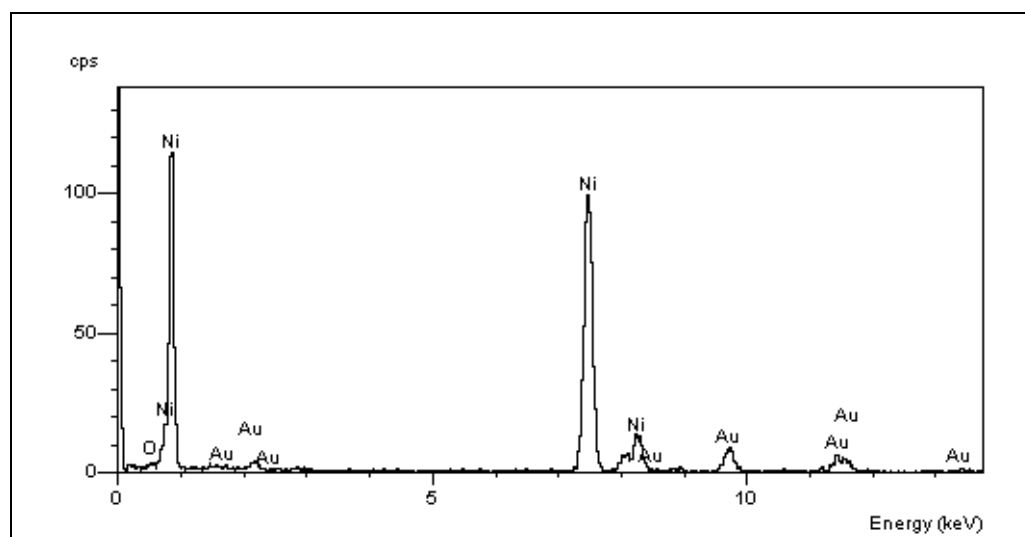


**Figure 7-11.** EDX of nickel in post steam reforming catalyst (Sample 1a) showing nickel is in its reduced state. Gold is from the support media, not the catalyst.

The presence of nickel-oxide in this sample or of long range crystal order in the nickel regions was not apparent. No visible lattice striations, no FFT detection, and no high-oxygen EDX results were found on any analyses of complete nickel regions,

indicating that the nickel lacked morphology and was in its reduced state. The only striations and FFT values found on regions containing nickel in this sample were where the detection range overlapped adjacent alumina. Since this technique involved the transmission of electrons through a sample region, detections from overlapping particles would create potentially spurious results. In **Figure 7-9**, such an overlapping region of the two different morphologies is shown. The FFT d-spacing value of 3.3 Å is uniquely identifiable of alumina, whereas 2.0 Å is a d-spacing that could be either alumina, nickel, or nickel-oxide [161]. Thus, a clear assignment of nickel cannot be made, and it is far more likely that the 2.0 Å d-spacing pertains to alumina, which had clearly revealed its structures and features elsewhere in the sample.

#### **7.3.4.2 Sample 2. Fresh Oxidised Catalyst**

Alumina and nickel regions could be clearly identified from their morphology and were seen to have concentrations and spatial distribution concordant with those found in sample 1a. Visible striations at higher magnification and FFT d-spacings repeatedly identified the higher-concentration light grey alumina regions. The nickel component, identified from EDX, shade gradation, and absence of FFT was again seen as ubiquitous dark low-concentration globules attached to the alumina matrix. Some poorly-defined edges could be seen on some of the nickel particles, but predominantly their shape was globular as per sample 1a, indicating that this morphology was not a symptom of reactor high-temperature induced sintering.

In contrast to sample 1a, definite oxygen content was revealed from EDX analyses of the nickel-regions (**Figure 7-12**), as would be expected of a catalyst that was known to be in its oxidised state. FFT analyses of the nickel regions were inconclusive with no d-spacings evident that could be definitely attributed to either nickel or nickel-oxide, in contrast to the alumina regions which were clearly identifiable from FFT. The further absence of visible lattice striations in the nickel regions also indicates that these were non-discernable crystallite or amorphous forms.

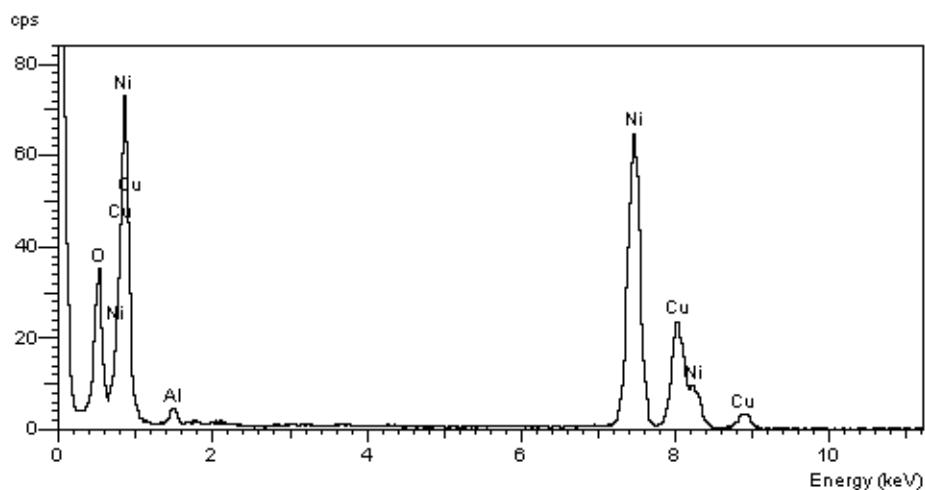


**Figure 7-12.** EDX of nickel in as supplied catalyst (Sample 2) showing the higher presence of oxygen indicative of nickel in its oxidised state. Copper is from the support media, not the catalyst.

#### 7.3.4.3 Sample 3. Reduced Catalyst

Alumina and nickel regions were again clearly identified by their concentrations and morphology being identical to Samples 1a and 2. EDX analyses of the nickel regions (**Figure 7-13**) showed an absence of oxygen-content similar to Sample 1a. This was as expected of a catalyst that had been subjected to a reducing  $\text{H}_2:\text{N}_2$  gas flow. All except one nickel-region showed no visible crystal lattice striations and would not yield FFT d-spacings, further evidencing its amorphology. One nickel region did have striations with two FFT-derived  $2.3 \text{ \AA}$  d-spacings, a value that can be attributed to either alumina or nickel-oxide, but not (reduced) nickel [161]. It is possible however that this region could have overlain an alumina area as the image clarity was poor.

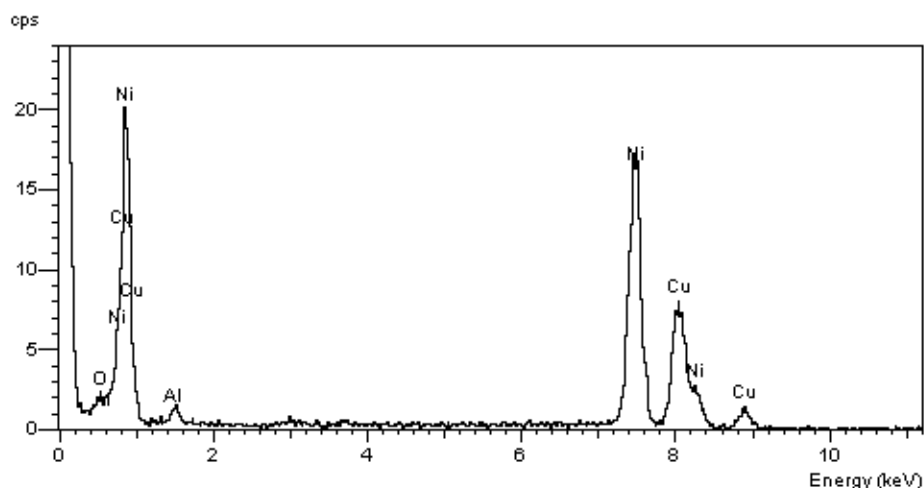


**Figure 7-13.** Reduced catalyst (Sample 3) EDX of nickel area. Copper comes from support grid

### 7.3.5 X-ray Diffraction

**Figure 7-14** to **Figure 7-16** show the presence in the catalyst samples of  $\text{Al}_2\text{O}_3$  (Red), NiO (Blue), and Ni (Green). The detection of nickel by XRD reveals that there was crystal order greater than 5 nm ( $50 \text{ \AA}$ ) – the limit of detection for XRD [162].

As expected, and as shown in **Figure 7-14**, the as supplied catalyst (Sample 2) was found to only contain nickel in its oxidised state (NiO). It can be seen from **Figure 7-15**, that also as expected, after reduction under a  $\text{H}_2:\text{N}_2$  flow, the catalyst sample (sample 3) exhibited nickel in its elemental (Ni) state. Interestingly, and of most importance, is the comparability between the fully reduced sample (**Figure 7-15**) and the spectra for sample 1 (**Figure 7-16**). This shows that after five stages of urea steam reforming the redox state of the nickel component in the catalyst appears to have been unaffected, with Ni still in its reduced state. These results support the findings of TEM and EDX analyses, that the catalyst was robust for the process and able to maintain its active state despite repeated and adverse operating conditions.



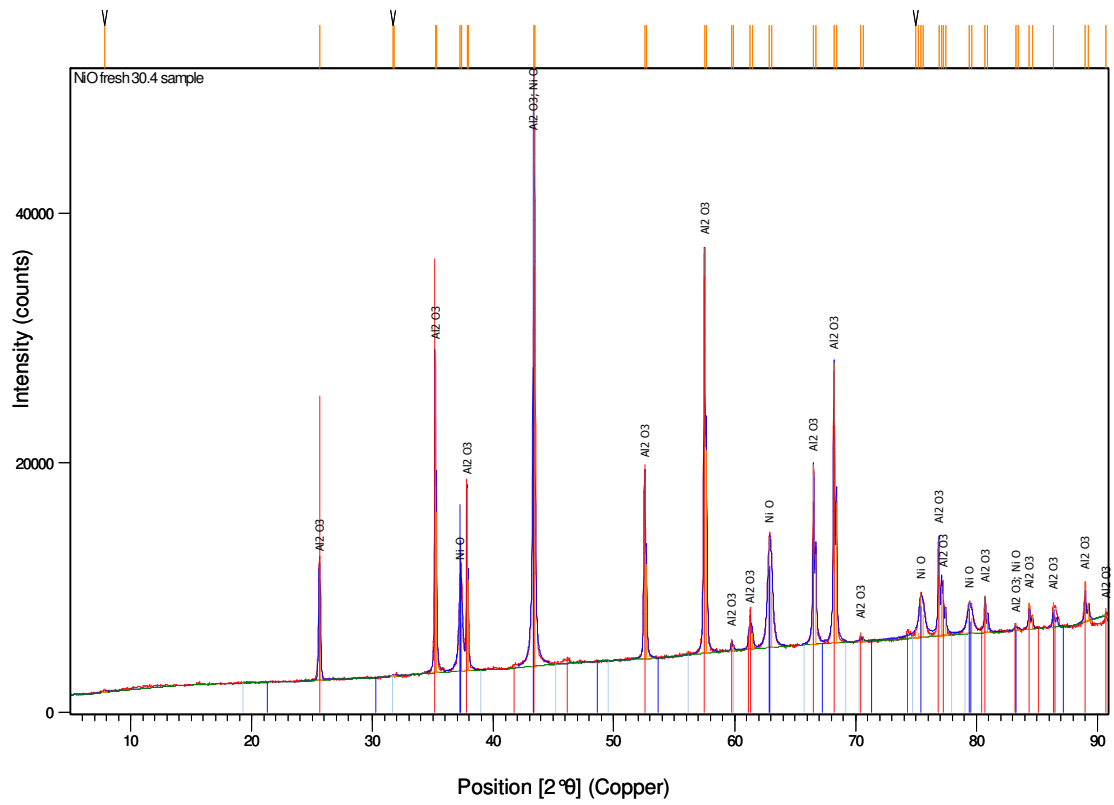


**Figure 7-14.** XRD spectrum of nickel in as supplied catalyst (Sample 2) revealing the presence of NiO and the absence of Ni peaks.

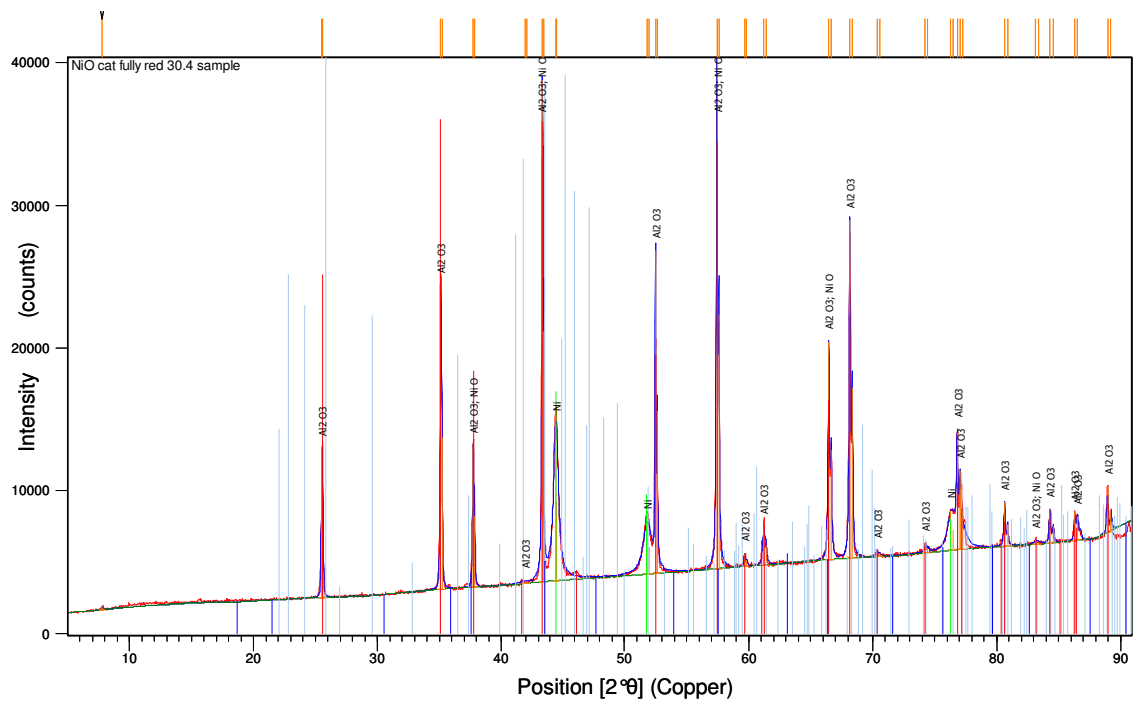


**Figure 7-15.** XRD spectrum of reduced nickel catalyst (Sample 3) revealing the presence of Ni peaks.



the inability to detect crystal plane spacing using FFT. Where FFT d-spacings of nickel-regions were detected, no unique values were apparent to allow substance identification, and these were coincident with the FFT/visible striations only being detected from regions suspected of overlapping with alumina.

XRD analysis was able to identify some crystallinity in the nickel constituents and, in combination with the results from EDX, gave corroborative affirmation of nickel in its reduced state (Ni) in the reduced catalyst and oxidised state (NiO) in the fresh as supplied catalyst. The post-steam reforming catalyst also revealed nickel to be in its reduced state despite being analysed immediately post-steam reforming and following five episodes of reforming activity. This was a surprising result and one which is highly favourable for long-term catalytic activity as it proves that the catalyst is robust for the urea steam reforming process.

The catalyst was also found to have emerged apparently unaffected in terms of morphology and carbonation following repeated steam reforming activity. The similarity between nickel particle morphology in the samples exposed to the high temperatures of steam reforming and reduction, and the as-supplied sample indicated that its globular form was not a product of in-reactor sintering. However, that some sintering may have occurred was suggested by the decrease in surface area of the post-steam reforming catalyst following BET analyses. If sintering had occurred it was therefore unobservable using these high magnification imaging techniques. The presence of carbon was not identified in any of the analyses on any of the catalyst samples, corroborating the in-situ experimental observations that coke formation had not occurred to any significance. This was despite relatively low temperatures, sometimes resulting in incomplete urea conversion and where the condition would favour carbonation.

The absence of changes in morphology observed by comparing catalyst samples using TEM, and SEM, and the analysis of qualitative elemental composition determined using EDX, support the results of in-situ experimental catalyst characterisation. Thus it can be concluded that the urea steam reforming process imposed little deleterious affect on the catalyst and that it remained active and robust throughout repeated steam reforming cycles. This resistance to coking, oxidation of Ni surface sites and sintering reveals the catalyst as being highly resistant and robust. It also establishes that urea steam reforming is a far cleaner process than has been reported for previously successful fuels.

## 8 Conclusions

This study has investigated the potential for using urea as a source of energy. A consideration has been made of urea's ability to release predominantly hydrogen, but also ammonia, since both these molecules can be used to generate energy when supplied to fuel cells. Steam reforming was the method used to produce hydrogen from urea.

Urea is as a non-toxic, safe and environmentally benign substance, setting it apart from other previously considered fuel cell energy carriers. A large and expanding commercial industry presently exists for urea manufacture from fossil fuels, creating a resource that is both readily available and relatively cheap; thus making urea advantageous for short term supply and rapid infrastructure implementation. This study has also identified that a large sustainable resource exists with the consequence being that urea is attractive as a long-term energy vector, with potential for global CO<sub>2</sub>-neutral power generation. It was discovered that the practicalities of extracting sustainably-sourced urea is lacking in research focus, despite the necessary technology being proven in other disciplines.

The feasibility of extracting hydrogen from urea was assessed by thermodynamic modelling. The results of these calculations were favourable, with complete urea conversion predicted over a wide range of temperatures. Predicted maximum steam conversion and H<sub>2</sub> yield coincided at mid-range temperatures of  $500\text{ }^{\circ}\text{C} \leq T \leq 700\text{ }^{\circ}\text{C}$  for aqueous urea reactant solutions attainable at room temperature ( $3:1 \leq \text{S:C} \leq 7:1$ ). The synthesis gas composition at optimum equilibrium conditions was ca. 60 % H<sub>2</sub>, 20 % N<sub>2</sub>, and 20 % CO<sub>2</sub>, as dry products. Dry syngas NH<sub>3</sub> concentrations were predicted to be in the  $10 \leq \text{ppm} \leq 100$  range at moderate ( $500\text{ }^{\circ}\text{C} \leq T \leq 600\text{ }^{\circ}\text{C}$ ) temperatures, with concentration decreasing as temperature was increased. Methane production was predicted to be negligible. Calculations were devised to determine the energy needed to produce H<sub>2</sub> from urea and steam. This was found to be slightly higher ( $55.5\% \pm 1.5\%$ ) than that for methane steam reforming, but still with a theoretical surplus when compared against the maximum possible energy content of the H<sub>2</sub> molecule.

Equilibrium calculations were also used to assess the performance of urea steam reforming experiments. Urea steam reforming was initially achieved in a bench scale reactor made of quartz, 70 cm long and 12 mm diameter, with a fixed-bed of nickel catalyst at its centre, supplied by a urea in aqueous solution ( $4:1 \leq \text{S:C} \leq 7:1$ ) fuel, and heated by an electrical tube furnace. Catalyst was proprietary 18 wt% nickel supported on alumina and crushed to a 0.66 – 1.70 mm particle size. Catalyst was primed by reduction under a H<sub>2</sub>:N<sub>2</sub> flow at 550 °C for one hour, and then the system flushed with N<sub>2</sub> prior to steam reforming. Fuel entered the system via a programmable syringe pump

and traversed the reactor in an upflow direction under an  $N_2$  carrier gas flow. The carrier gas flow enabled product analyses by material balance following species detection in a series of online analysers. Species monitored were  $H_2$  (by thermal conductivity),  $CH_4$ ,  $CO$ , and  $CO_2$  (by non-dispersive infrared).  $NH_3$  was not monitored in this first episode of experimentation. A greater range of hydrocarbon species were analysed by batch sample off-line gas chromatography. Moisture was removed from the synthesis gas in a series of post-reactor/pre-analyser condensers. At reactor temperatures of  $600\text{ }^\circ\text{C}$ , a synthesis gas rich in hydrogen was produced, with steady state outputs closely matching those predicted by the equilibrium model. No other hydrocarbons were identified by off-line analyses. Instability in output profiles over time was identified as a weakness of the reactor design and attributed to an incompatibility of the urea fuel with the slow ascent across a temperature gradient prior to vaporisation at the catalyst bed, thus creating a propensity for urea to supersaturate out of solution. Additional experiments were completed with this reactor system to assess species residence times for comparison with parallel investigations into reaction kinetics and to investigate an unexpected phenomenon of early (low temperature)  $H_2$  detection at the analysers. Results suggested that  $H_2$  production prior to the urea fuel having reached the catalyst bed was due to chemical reaction for fuels close to the urea eutectic mixture ( $S:C = 6$  and  $7$ ) rather than physical interaction.

Based on the knowledge acquired with preliminary urea steam reforming experiments, a new reactor system was designed that was specific to the requirements of aqueous urea fuel. The same quartz, fixed bed catalytic reactor was used, but inverted, with a new fuel inlet assembly designed and implemented to supply aqueous urea by a passively-cooled (to avoid supersaturation), drop feed (to avoid slow ascent across the temperature gradient and achieve a rapid approach to the catalyst bed) system. A parametric study assessed urea steam reforming at temperatures of  $500\text{ }^\circ\text{C} \leq T \leq 700\text{ }^\circ\text{C}$  and fuel mixtures of  $3:1 \leq S:C \leq 7:1$ ; parameters chosen with the intention of optimising steam conversion, and maintaining thermodynamic equilibrium. Twenty grams of undiluted catalyst was used and this was regenerated under airflow after steam reforming to assess for process recycle ability. In addition to the product gases measured in the previous upflow reactor, product  $NH_3$  was also monitored in both the online (post-condenser) gas and by off-line ion chromatography of the liquid collected in the post-reactor condensate trap. A new material balance was devised to incorporate the measurements of  $NH_3$ . Problems associated with fuel supersaturation were greatly overcome and improved stability was achieved with the new drop-feed reactor system, with the output products again matching those predicted by equilibrium and remaining close to steady state for the duration of the experiments: a period of two hours, which was limited by the volumetric capacity of the fuel dispenser. The new fuel input assembly permitted a lower ratio of fuel to carrier gas and consequently a three times

higher concentration of H<sub>2</sub> was produced. Yields calculated from the material balance and matching those at equilibrium indicated the existence of a global urea steam reforming reaction. Comparisons between material balance results and equilibrium modelling also strengthened the belief that all significant product species were measured. The condensate system was found to be highly effective at capturing NH<sub>3</sub>, a feature that is attractive for potential assimilation of technologies for direct supply of urea-derived syngas to fuel cells, particularly as the capture involved a simple passive trap using only the unconverted water leaving the reactor. NH<sub>3</sub> values in the condensate were however found to be higher than had been predicted by equilibrium modelling at the lower temperature operating range. This is an area that requires further study, but it is suspected that the cause is catalytic inability to rapidly decompose NH<sub>3</sub> at  $T \leq 550$  °C.

Preliminary laboratory experimentation had confirmed that the extent of urea solubility at room temperature was achievable for the mixtures  $3:1 \leq S:C \leq 7:1$ . Ion chromatography had confirmed that urea isomerisation prior to 5 hours after solvation could be discounted, with isomer products not detected above 0.5 ppm in all samples up to one hour after preparation. Simultaneous thermal and evolved gas analysis of aqueous urea and nickel catalyst using mass spectroscopy and FTIR identified that HNCO was hydrolysed rapidly when water was present with urea and that it would not evolve or be likely to occur in significant quantity under steam rich flow reactor conditions. These experiments also attempted to elucidate further the phenomenon of early (low temperature) H<sub>2</sub> release, first suggested by upflow reactor experiments. From 80 °C, STA results showed detections that could evidence both NH<sub>3</sub> and H<sub>2</sub> evolving from the urea solution samples, but not from pure (anhydrous) urea. This is an area for further study as it may provide a mechanism for low temperature H<sub>2</sub> production.

Though kinetic calculations could only determine a worst case scenario, based on the known parameters of rapid fuel entry, temperatures close to the considered optimum for steam reforming based on modelling and on the known activity range of this catalyst ( $T \geq 500$  °C), a 99.9 % conversion of urea was predicted in the experimental reactor within half a second. With the anticipated reactor settings of  $T \geq 550$  °C, any urea remaining would be instantly decomposed upon contact with the catalyst bed.

Post-reactor experimentation was completed using a variety of techniques (TEM, SEM, XRD, BET adsorption, digital microscopy) on post-steam reforming catalyst, fresh (as supplied catalyst), and fully reduced catalyst. This was used in combination with the in-situ experimental observations on coke formation, repeat cycling, and output performance over time to characterise the catalyst and assess its functionality. The nickel catalyst was found with experimentation to remain effective at steam reforming over repeated cycles of regeneration without deactivation. This was supported by observations from ex-situ analysis that the catalyst had retained its active Ni surface sites despite repeated steam reforming cycles. A resistance to coke formation and

sintering was also observed, establishing urea as a far cleaner fuel for steam reforming, more so than has been found with previous successful attempts at generating H<sub>2</sub> using the same catalyst but with alternative fuels.

## Appendix A: Downflow Reactor Maximum Fuel Feed Test

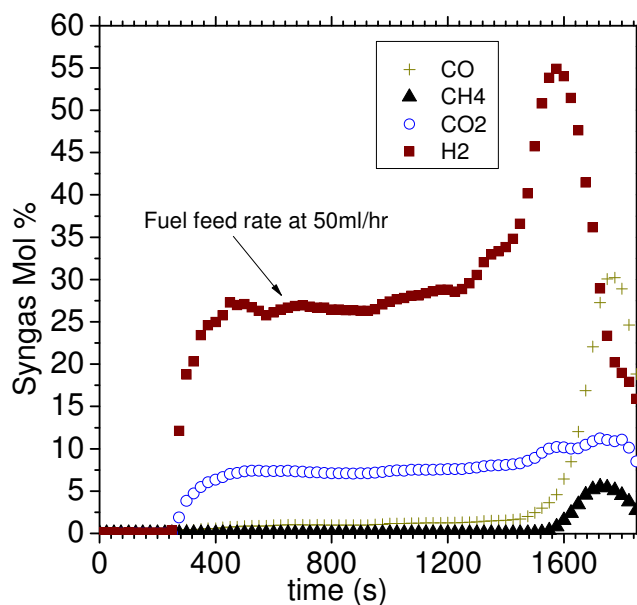


**Figure A.** Dry product gas concentrations for S:C = 7, at 600 °C with 350 cm<sup>3</sup> min<sup>-1</sup> carrier gas flow rate, shown as scatterpoints as a function of time, using 20 % of datapoints for clarity. Fuel feed rate varied, and increased to maximum during late stages of analysis time.

**Figure A** shows the online dry product gas results for a pre-parametric study using the downflow drop-feed urea steam reforming reactor described in Chapter 7. Fuel feed rate was started at 50 ml hr<sup>-1</sup> and then increased to maximum (999 ml hr<sup>-1</sup>). Stages of fuel feed rate increase were not measured, but where known, they are shown on **Figure A**. The test was aborted due to fuel flooding back along the carrier gas feed line. NH<sub>3</sub> measured at below 6 ppm for duration of experiment run time.

Parameters differ from study reported in Chapter 6 by carrier gas flow rate and fuel feed rate.



## Appendix B: Urea Wire Monolith Spray Reactor

### B.1 Introduction

Previous chapters have attempted to address the important considerations associated with using urea as a hydrogen carrier, to give a comprehensive appraisal of this novel energy source, and the feasibility of urea steam reforming as a realistic methodology for hydrogen extraction. The energy required to make the urea steam reforming reaction proceed in the process design reported in Chapters 6 and 7, and by the equilibrium modelling reported in Chapter 3 is however an unavoidable necessity of the mechanism. Though the obviation of this energy demand by using renewable energy systems such as solar concentrators is identified as attractive for future work, improvements in efficiency by reducing radiative and conductive heat losses, and by quickening the reaction rate kinetics by reducing fuel droplet size are other alternatives. This would require a new reactor system to the one used successfully in earlier chapters of this thesis. To reduce heat losses from the system, a more compact reactor with the application of concentrated and focused heating would be required.

A novel component was supplied by the industrial sponsor of this project with the requirement that it be built into a steam reforming reactor. There follows in this chapter a description of the construction of this reactor and fabrication of a process system around it specific to aqueous urea fuel. Though in many respects this could be considered merely an addendum to the research on “Hydrogen from Urea”, it does have relevance in describing an alternative, potentially optimised system for producing hydrogen from urea. The work involved in building this novel steam reforming system has also constituted a significant part of the time and effort involved in this project.

With the lessons learned about the utilisation of a urea fuel for steam reforming, the system was constructed with the following design objectives:

1. Durability, with long term operation and low operational maintenance.
2. A more reliable system of introducing larger flow rates of urea solution yet still protected against the risk of urea solution supersaturation prior to reactor.
3. Reduction in carrier gas dilution (obviated in a research sense by alternative on-line analysis tools that do not require minimum gas flow rates).
4. As will be seen with a description of the reactor, its relative small size, sturdiness and compactness appeared to have an advantage over the glass reactor system in which urea reforming was successfully achieved, for wider practical application. The

monolith reactor core was also considered to have potential for alleviating problems with pressure drop as may be encountered at high flow rate across a fixed catalyst bed. These attributes made it favourable for small-scale and lightweight applications as are envisaged to be the major benefit of a urea-derived energy supply, and also for scale-up to a larger industrial system. Creation of a prototype suitable for these practical applications was a fourth design objective.

This study concentrated on initial reactor design and fabrication of a urea spray system. Ancillary pre- and post-reactor process components were also incorporated into the design.

## B.2 Materials

A stainless steel encased reactor that contained a ceramic monolith (length = 75 mm, diameter = 30 mm) with 55 x 1.8 mm longitudinal holes was supplied. This is shown in **Figure B-1**. One single length of nickel-chromium (nichrome) wire was threaded through the monolith holes to function as both catalyst for the steam reforming reaction and as a heating coil. There was one vacant hole in the monolith.

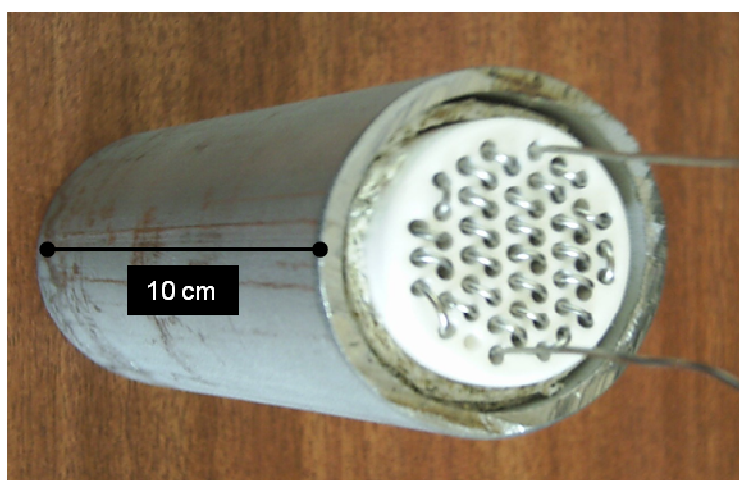


**Figure B-1.** Ceramic monolith in stainless steel casing with nichrome wire. See text for dimensions.

Seen separating the monolith from its temporary steel casing in **Figure B-1** is a quantity of 3M 100 EPP interam mat. This packing material (see **Table B-1** for composition) was unsecured within the steel casing, but was held in place by friction.

**Table B-1.** Insulating mat composition, used as packing in spray reactor. Purchased from 3M (100 EPP)

Product Specification	Composition (Wt %)
Vermiculite	50 - 65
Refractory ceramic fibres	25 - 40
Copolymer binder	1 - 10
Fibre bonding agent	0.1 - 5

A 316 stainless steel reactor casing was also supplied and is shown in **Figure B-2**. This casing was in two sections. The top of the casing was detachable and was secured to the main body by six bolts positioned along its circumference. A silicon o-ring was embedded between the two casing sections to create a gas-tight seal. The body section of the casing (point “a”) was the same dimensions as the casing shown in **Figure B-1**. Interam mat was fitted between monolith and the body of the casing. Each end of the nichrome wire exiting the monolith at the top, passed out through the steel casing via holes on either side of the reactor top insulated by PTFE sheaths.

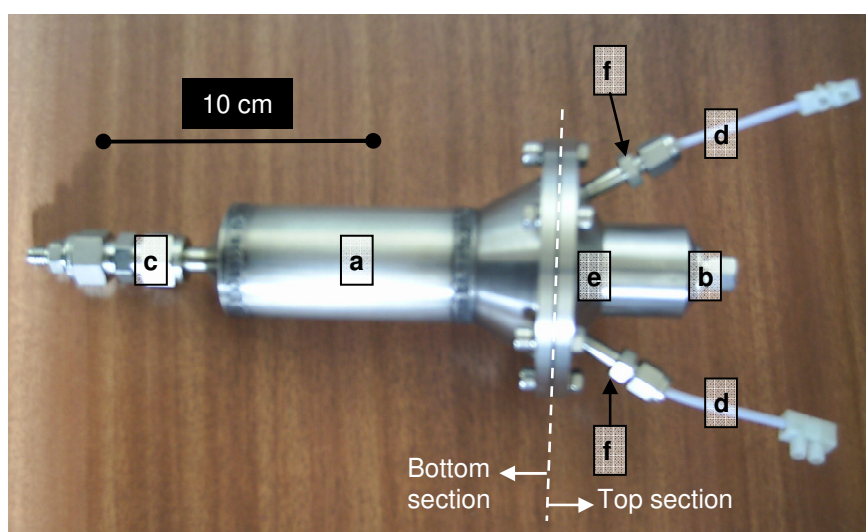


**Figure B-2.** Stainless steel casing supplied to house monolith as shown in **Figure B-1**.

Annotated areas “b” to “d” show components that were removed or replaced (see section **B.3**). Text refers to annotated areas “a”, “c”, “e”, and “f”.

A pressure spray nozzle was supplied with this reactor, permanently affixed (internally) to the casing top (at point “b” on **Figure B-2**) such that the nozzle was aligned axially with the top of the monolith. No details of the nichrome wire specifications were known.

### B.3 Reactor Design

The monolith reactor did not function within the casing supplied and shown in **Figure B-2**. The casing was re-designed, and ancillary equipment purchased to create a full process system. Sections of the reactor casing identified as areas “b” to “d” on **Figure B-2** were either removed, replaced or re-fabricated. Interam mat was packed between monolith and casing body. Two holes were drilled into the casing at the point marked “e” on **Figure B-2** 180° apart along the circumference of the casing top section. A lip of 3 mm high stainless steel was welded around these holes on the outside of the casing top. Through these holes, the two ends of nichrome wire exited the reactor. The nichrome wire was sheathed in 1.5 mm ceramic fishspine beads (by RS Components) along its full length outside of the monolith. This was to stop possible short-circuiting of the electric current onto the reactor casing during operation. The wire and sheath assembly was sealed to make the system gas tight by a combination of fire cement (by KOS) base layer and high temperature-tolerant epoxy resin (Optitec 5054) secondary layer. The nichrome wires were then connected to a Thurlby Thandar Instruments (TTI) QPX1200L DC power supply, and a power control unit with programmable temperature setting (built in-house). A schematic of the reactor system designed for urea steam reforming is provided in **Figure B-3**. The area marked “Reactor” on **Figure B-3** shows the monolith contained in the steel casing.

A K-type thermocouple was inserted into the vacant monolith hole to a depth of 30 mm. This exited the reactor casing top via a stainless steel Swagelok connector with PTFE ferrule through aperture “f” on **Figure B-2** and connected to the power control unit for manipulation as required of the reactor temperature settings. The other vacant aperture “f” was sealed with a Swagelok stainless steel plug.

An air atomiser nozzle by Delavan was connected at point “b” on **Figure B-2** using a Delavan stainless steel  $\frac{3}{4}$ ” screw thread mounting bracket. This was inserted centrally in the reactor top, 7 cm longitudinally above the monolith top-end face. The nozzle could be lowered or raised by the screw threads of its mounting to adjust its spray pattern onto the monolith top. The spray nozzle was 46 mm long and 25.7 mm wide. Various nozzle types with different apertures (creating different spray patterns) were available and this flexibility in design allowed for easy access to clean and repair, or to remove and replace the nozzle type. It was also a design that permits easy access for loading/unloading of additional catalyst into the reactor should that be considered necessary.

The spray nozzle had two 1/8” bsp screw threads for entry of atomising gas and fuel. Both were connected by Swagelok fittings. Atomising gas was > 99.99 % purity N<sub>2</sub> from BOC cylinders, supplied by a calibrated rotameter for flow rate control and

regulator-controlled gas cylinder via ¼" tubing and Swagelok fittings. The other feed line was urea solution via a syringe (SGE) and programmable micro-syringe pump (New Era Pump Systems) connected to the feed tubing using an SGE Analytical NLL – 5/16. 4.5cm needle attached to a Swagelok tube connector.

For operation, the reactor was pressurised to 1 atm. Pressure was monitored for safety and operational flow rate accuracy by a pressure gauge with a safety pressure relief valve inline, set at 2 atm.

The gaseous effluent leaving the reactor was passed through the same reflux condensate collection system that had been shown to be successful with quartz reactor experiments (Chapter 6) with two oil-cooled condensers to remove moisture before analysis, and condensate collected in a glass flask at the base of the outlet assembly for determination of its ammonia content.

The dry product gas line leaving the condenser system entered a (non sample-destructive) ABB Advance Optima Limas 11 ultraviolet absorption module for NH<sub>3</sub> analysis, then on to an AS-Series NH<sub>3</sub> scrubber, containing silicon orthophosphate combined with silicon pyrophosphate (99 Wt%) and quartz dust (1 Wt%). Following the NH<sub>3</sub> scrubber, a Varian CP-4900 micro GC supplied with argon carrier gas analysed the product composition of the syngas. Both micro GC and Limas 11 analysers were connected to a personal computer for collection of data.

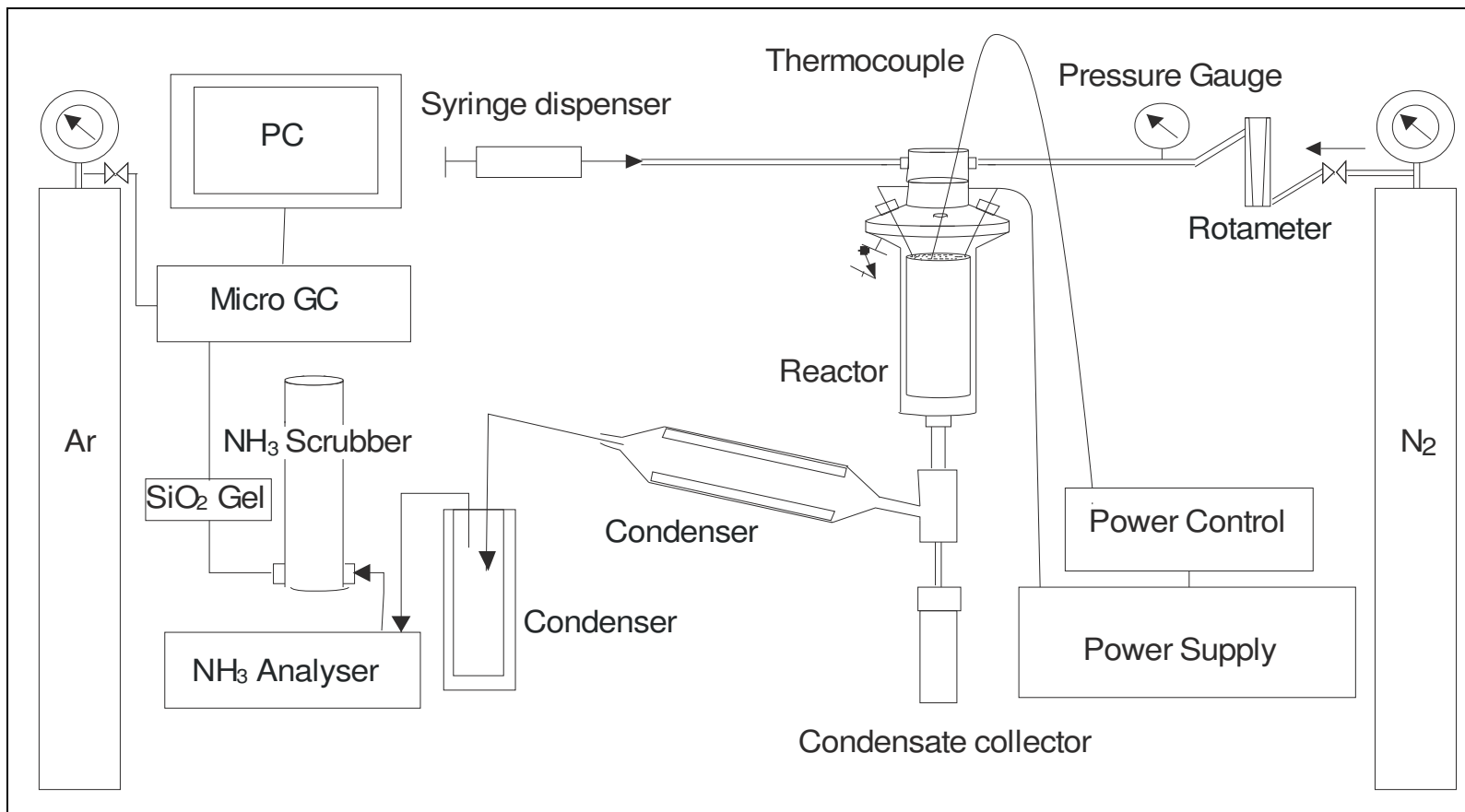


**Figure B-3.** Schematic of wire and monolith spray reactor

## B.4 System Tests

### B.4.1 Power Controller and Pyrometry

#### B.4.1.1 Method

A Fluke 62 Mini Infrared Pyrometer was used to calibrate the power settings necessary to heat the monolith. The monolith was inserted into the casing body section and connected to the power supply with a thermocouple inserted into the vacant hole of the ceramic reactor. For each programmed temperature, three measurements were taken at locations as shown in **Figure B-4** of:

- 1) The outer casing of the reactor.
- 2) The centre of the monolith face.
- 3) 5 mm in from the outer edge of the monolith face.

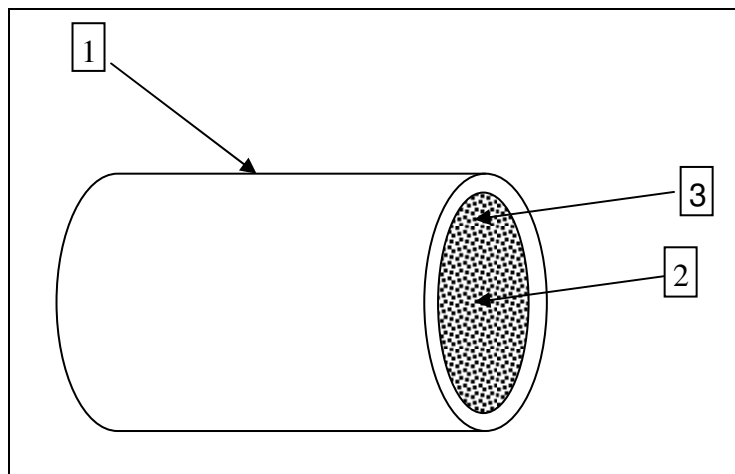


**Figure B-4.** Positions of pyrometer sampling on reactor outer metal casing

The pyrometer was activated for three seconds from 15 cm away from the source in all cases. The first measurement was recorded one minute after the temperature was stable (as shown by the thermocouple). Readings were taken at 50 °C intervals from 300 °C to a maximum of 500 °C (the limit range of the pyrometer). For each temperature setting, measurements were repeated three times at 1 minute, 3 minutes, and 5 minutes.

Tests with the encased reactor in-situ (as **Figure B-3**) were also done with the pyrometer to assess heat loss from areas on the casing body and for reasons of safety to monitor heat gain of the outer components. Using a multimeter, the interim packing was measured for its electrical resistance and heat resistance.

### B.4.1.2 Results and Discussion

Temperature measurements using the pyrometer on the ex-situ monolith and steel casing body are shown in **Table B-2**. These values are maxima: the default display setting of the pyrometer. Heating rate was found to be rapid, with stable temperatures achieved within 1 minute ( $\geq 97\%$  of final value) of power output.

**Table B-2.** Results of pyrometry test on reactor and power unit. T/C = thermocouple.

Temp setting (°C)	V	A	Outer Casing (1)			Monolith Centre (2)			Monolith Edge (3)		
			Temp (°C)			Temp (°C)			Temp (°C)		
			1min	3min	5min	1min	3min	5min	1min	3min	5min
300	36	4	59	55	55	225	231	239	202	211	210
350	36	4	69	68	68	273	280	278	225	240	243
400	36	4	77	79	78	338	329	347	314	292	311
450	36	4	87	88	92	354	358	358	324	349	324
500	36	4	98	102	103	391	390	401	346	333	345
550	36	4	111	111	111	413	435	449	390	352	408
600	36	4	124	122	123	449	443	467	414	407	394
650	40	5	N/K	N/K	N/K						
700			N/K	N/K	N/K						
750			N/K	N/K							

The observed disparity between pyrometer detected temperatures on the monolith and its casing and the desired temperature settings as shown in **Table B-2** can be confidently attributed to heat loss by radiative and convective air cooling. The reactor was just held on a bench in stand and clamp below an air extractor and therefore exposed to lab air temperature of 23 °C. The temperatures were very stable throughout the sampling period. When measuring the outer monolith edge temperature it was difficult to attain a steady “5 mm from edge” recording so operator error at this location of  $\pm 3$  mm is attributed.

Following the rapid heating of the monolith used in this method, cracks were observed in the ceramic. This was considered to be due to rapid heating. An identical replacement monolith and nichrome wire insert was used in all subsequent experiments.

With the reactor in its housing and connected as per **Figure B-3**, heat was applied gradually and temperatures were maintained for as long as desired up to a maximum test period of five hours. With the reactor operating temperature stable at 700 °C, different external sections of the outer components were measured with a thermocouple. It was



found that the maximum temperature recorded was for the ceramic beads at 126 °C. The nichrome wire and reactor casing top were recorded at 70 °C and 118 °C respectively. Without insulation, the outer case was seen to have a temperature of 250 °C. The interim mat was found to have poor heat insulating qualities. With kaowool insulation wrapped around the exterior of the reactor casing body, a significant reduction in outer temperature was seen with a value of 50 °C recorded. Not surprisingly, the kaowool insulation also significantly reduced the power output from the electricity supply unit.

The interim mat when dry, exhibited zero electrical resistance but it conducted electricity when wet. Testing with the multimeter showed 1M $\Omega$  resistance compared to the heating wire resistance of 8  $\Omega$ .

## **B.4.2 Spray System**

When tested, the fuel delivery nozzle provided with the casing was found to generate a spray pattern only under high pressure ( $\geq 5$  bar) and, according to manufacturer specifications, with a high fuel flow of  $\geq 1450$  ml hr<sup>-1</sup>. Both these state parameters were unsuitable due to the inability of the syringe dispenser to function at this pressure value and for the fuel flow rate being excessively high for this bench-scale system. It was therefore decided to choose an alternative air-atomising fuel delivery nozzle that could operate at atmospheric pressure. These chosen nozzles (see section **B.4.2.1**) were provided with guideline functional ranges with a pure water feed. Calibration tests were therefore required to determine their performance with a urea solution fuel.

### **B.4.2.1 Method**

Two types of nozzle were purchased and tested: an AL04 air atomiser - with an orifice of 0.088 mm, and an AL01 air atomiser - with an orifice of 0.040 mm). Both nozzles were made of 316 stainless steel. Tests were done with urea solution of S:C = 6.5 to determine conical spray pattern and distance required from the monolith top to produce this conical pattern. This ratio of mixture was chosen due to its closeness in concentration to the eutectic mixture and it being mid-range between the mixtures found to produce the best urea steam reforming results with the previously successful system (see Chapter 6) The rotameter used to control carrier gas flow rate, and the mass flow controllers used for fuel flow were calibrated using the bubble tube method as described in section 5.2. Extent of atomisation under different gas flow and fuel feed rates was also measured. The experiments were attempted using the final system set-up as described in section **B.3**, except that the reactor was removed and the spray pattern monitored as follows:

Initially droplet distribution was measured by putting a paper towel under the spray to assess the pattern. This was deemed inappropriate because the fluid soaked into the paper upon impact and spread out thus distorting the appearance of the actual droplet size and spray dispersion. An improved method for characterisation of spray distribution was employed by capturing the droplets in oil based on a design advocated by Ahmed [163]. Sunflower oil, 1-2 mm deep, was placed in a petri dish and inserted under the operating nozzle 2 - 4 cm axial distance from the nozzle orifice and held there for 1-2 seconds to capture droplets. This distance was chosen based on the diameter of the monolith end section (30 mm). For a 60° cone (bisecting two 30° angles from the vertical, the positioning of the nozzle aperture necessitated a position of  $15.00/\tan 30^\circ = 25.98$  mm away from the monolith.

Earlier tests had shown that the syringe pump dispensing capacity and system pressure were in the correct range for the nozzle to function but that atomising carrier gas flow was higher than desired. These tests were to formally assess the range of carrier gas flow and fuel feed rates that could achieve spray, commenting on the droplet sizes and the spray spread at a fixed distance from the nozzle aperture.

Initial tests had used  $4 \leq m \leq 10$  lengths of 4 mm I/D diameter tubing to supply N<sub>2</sub> from cylinder to nozzle. This was found to necessitate very high  $10 \text{ dm}^3 \text{ min}^{-1}$  (STP) N<sub>2</sub> flow rates to generate fuel atomisation. To reduce energy losses in the N<sub>2</sub> supply piping, a shorter length of 0.7 m of 4 mm I/D tubing was used and found to successfully permit a greatly reduced atomising gas flow rate.

For the AL04 (0.088 mm orifice) nozzle, N<sub>2</sub> gas flow was tested in the range  $3 \leq \text{dm}^3 \text{ min}^{-1} \leq 7$ . Pressure was tested in the range  $0.5 \leq \text{bar} \leq 2$ , and fuel flow was tested in the range of  $50 \leq \text{ml hr}^{-1} \leq 900$ . Based on these results and on the results of EQUIL modelling of anticipated urea steam reforming products at speculated fuel/N<sub>2</sub> mixtures, experiments with the smaller aperture, AL01 (0.040 mm orifice) nozzle, and N<sub>2</sub> carrier gas flow in the range of  $1.5 \leq \text{dm}^3 \text{ min}^{-1} \leq 2.5$ , were attempted. Pressure was tested at 1 bar, and fuel flow was tested in the range of  $100 \leq \text{ml hr}^{-1} \leq 500$ . This had the aim of reducing the syngas dilution by lowering the ratio of input N<sub>2</sub> to fuel.

#### **B.4.2.2 Results and Discussion**

A range of 11 different operating conditions were captured in sunflower oil and photographed. According to Ahmad [163], evaporation of droplets is reduced by this method as they are suspended just below the surface of the oil, and the droplets remain almost spherical as long as the density of the oil is only slightly less than the sprayed liquid. It was for this contrast in density that sunflower oil was chosen:

$$\text{Density of sunflower oil} = 0.92 \text{ kg m}^{-3}$$

Density of urea solution =  $1.1 \text{ kg m}^{-3}$

Potential errors associated with this method include, coalescence of the droplets (in flight or due to impact), shattering of the droplets on impact, and potentially, evaporation of the droplets in flight. None of these were considered likely to affect the visible appearance of the spray pattern breadth however.

With the larger aperture AL04 (0.088 mm orifice) nozzle, the  $\text{N}_2$  gas flow rate of  $4 \text{ dm}^3 \text{ min}^{-1}$  was found to be the minimum for liquid atomisation. At, and below this flow rate, no spray was formed, with the fluid just exiting the orifice as drips. Between  $\text{N}_2$  flows of  $3.75 \text{ dm}^3 \text{ min}^{-1}$  (where one single drip was emitted) and  $4 \text{ dm}^3 \text{ min}^{-1}$ , the drips were still clearly singular but began to spread out in a radial pattern. Selected images of the spray pattern produced by the AL04 nozzle at a range of carrier gas flow rates are shown in **Figure B-5** to **Figure B-7**. These images show how the droplet sizes increase with decreasing  $\text{N}_2$  flow, but that spray spread remains constant.

These  $\text{N}_2$  carrier gas flow rates with the AL04 (0.088 mm orifice) nozzle, though successful in dispensing the fuel in a conical spread, were higher than expected and outside the desired range. Though the  $4 \text{ dm}^3 \text{ min}^{-1}$  flow rate was within the capacity of the system, it would result in excessively high dilution of the syngas based on the limited 50 ml capacity of the dispensing syringe. It was not therefore considered practicable to choose this due to the short run time not giving adequate opportunity to assess whether the system reached equilibrium. The fuel rate could obviously be set at a lower rate and the syngas diluted, which may necessitate further post-reactor processing to increase purity. Alternatively, the fuel dispensing system could be replaced with a higher capacity vessel. Increasing the fuel flow rates to this extent would however affect the operating capacity of the reactor as a bench scale system would likely be unable to cope with the kinetics of reacting larger volumes of fuel.

Variations in  $\text{N}_2$  pressure had no discernible effect on the ability to spray or droplet size. Consequently all tests with the AL01 nozzle were performed at 1 bar pressure. Variations on liquid feed rate affected atomisation at the lowest range of  $\text{N}_2$  flows only, with increased liquid flow rate undermining spray formation and increasing droplet size. With the AL04 (0.088 mm orifice) nozzle, variations in fuel feed rate had no effect on atomisation at  $\geq 5 \text{ dm}^3 \text{ min}^{-1}$   $\text{N}_2$  gas flow. At the minimum  $\text{N}_2$  gas flow rate for the AL01 nozzle, atomisation only occurred for fuel flow rates of  $\leq 400 \text{ ml hr}^{-1}$ .

When spraying at higher fuel flow rates (of  $> 500 \text{ ml hr}^{-1}$ ) it was difficult to discern the droplet sizes visibly as the flow was so great. However, the oil capture method was found to be effective at recording and retaining each droplet. It is probable that there was some droplet coalescence and droplet shattering due to impacts with the oil at the close proximity to the nozzle orifice due to higher kinetic energy of the fuel flow. To compensate, the petri-dish was moved to the maximum distance of 35 to 40

mm away from nozzle aperture. Because of this the breadth of spray increased. Additionally, it was observed that the energy of droplet impact in the oil created movement of the oil, particularly at distances closer to the nozzle aperture. An operational error of  $\pm 5$  mm is assigned to the breadth of spray shown in **Figure B-5** to **Figure B-11**.

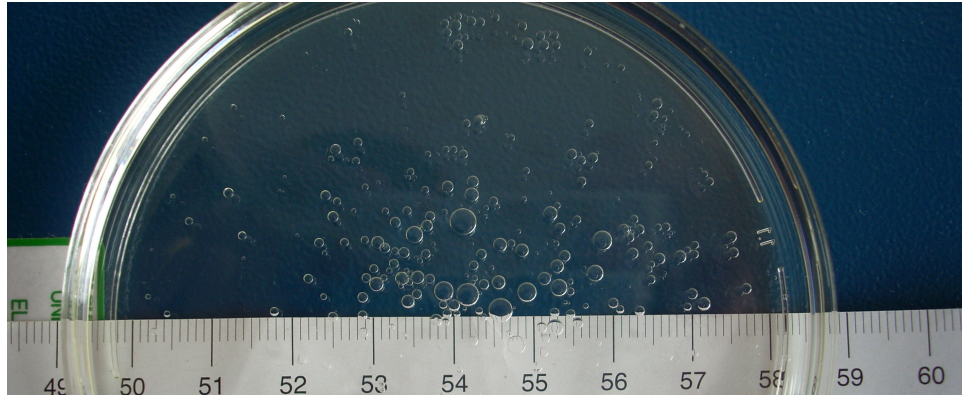


**Figure B-5.** AL04 (0.088 mm orifice) nozzle spray pattern with  $5 \text{ dm}^3 \text{ min}^{-1}$   $\text{N}_2$  flow at 3 – 4 cm from nozzle aperture and fuel flow of  $100 \text{ ml hr}^{-1}$ .

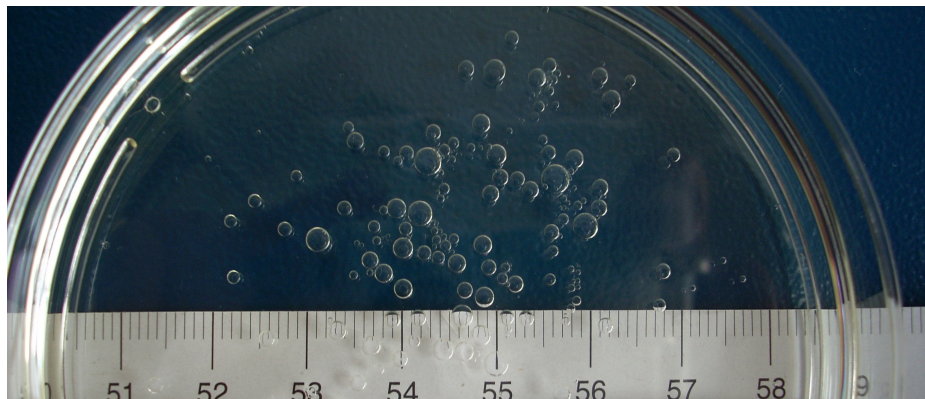


**Figure B-6.** AL04 (0.088 mm orifice) nozzle spray pattern with  $4.5 \text{ dm}^3 \text{ min}^{-1}$ ,  $\text{N}_2$  flow at 3 – 4 cm from nozzle aperture and fuel flow of  $200 \text{ ml hr}^{-1}$ .

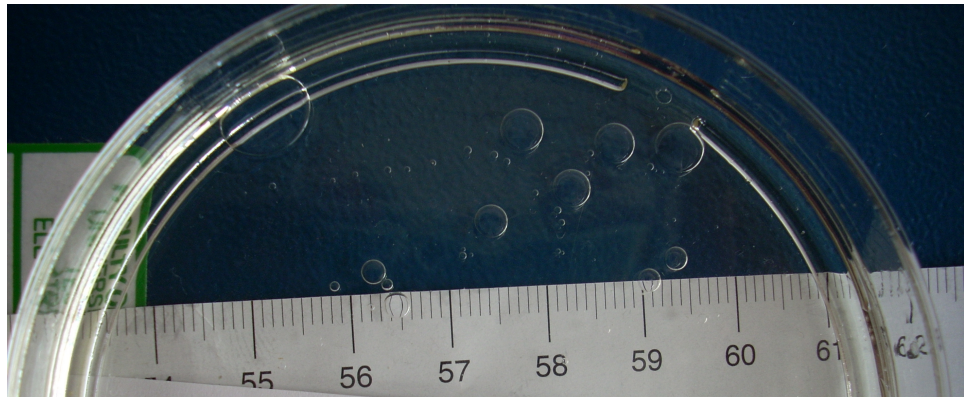


**Figure B-7.** AL04 (0.088 mm orifice) nozzle spray pattern with  $4 \text{ dm}^3 \text{ min}^{-1}$ ,  $\text{N}_2$  flow at 3 – 4 cm from nozzle aperture and fuel flow of  $200 \text{ ml hr}^{-1}$ .

The smaller aperture (0.040 mm orifice) AL01 air atomiser was capable of spraying the fuel at much lower  $\text{N}_2$  carrier gas flow rates, with  $1.5 \text{ dm}^3 \text{ min}^{-1}$  found to be the minimum. As with the larger aperture nozzle, at its lower limit of carrier gas flow, drops were emitted rather than small atomised droplets. The atomisation produced by this nozzle was however seen to be unaffected by fuel feed rate, in contrast to the AL04 nozzle. Not surprisingly, due to the smaller aperture, droplet size was in general smaller than with the AL04 nozzle. Photographic images of the spray patterns produced by the AL01 nozzle at a range of fuel feed rates and  $\text{N}_2$  carrier gas flows are provided in **Figure B-8** to **Figure B-11**.

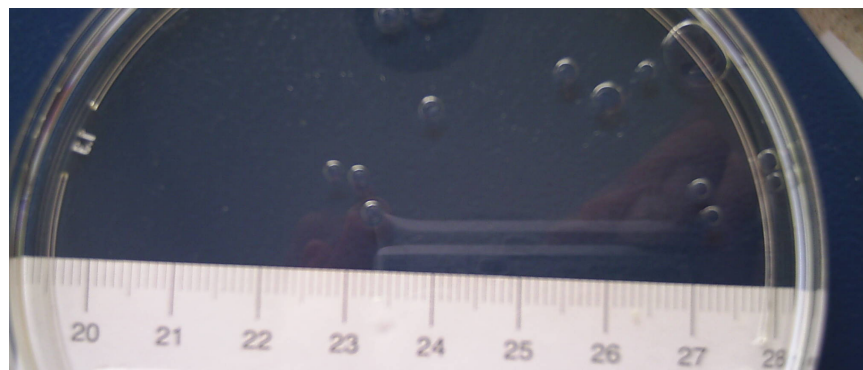


**Figure B-8.** AL01 (0.040 mm orifice) nozzle spray pattern with  $1.5 \text{ dm}^3 \text{ min}^{-1}$ ,  $\text{N}_2$  flow at 3 – 4 cm from nozzle aperture and fuel flow of  $200 \text{ ml hr}^{-1}$ .

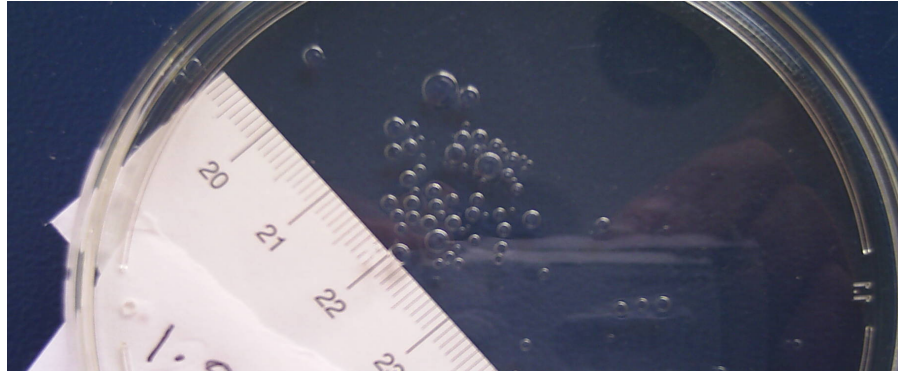


**Figure B-9.** AL01 (0.040 mm orifice) nozzle spray pattern with  $1.8 \text{ dm}^3 \text{ min}^{-1}$ ,  $\text{N}_2$  flow at 3 – 4 cm from nozzle aperture and fuel flow of  $100 \text{ ml hr}^{-1}$ .

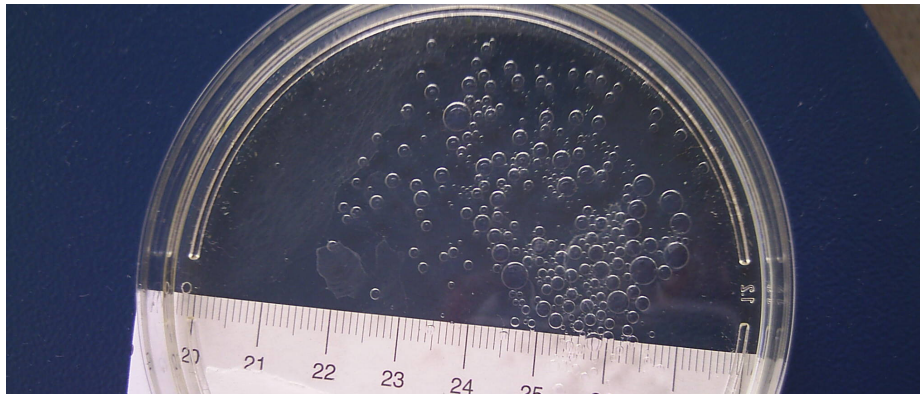


**Figure B-10.** AL01 (0.040 mm orifice) nozzle spray pattern with  $2.0 \text{ dm}^3 \text{ min}^{-1}$ ,  $\text{N}_2$  flow at 3 – 4 cm from nozzle aperture and fuel flow of  $500 \text{ ml hr}^{-1}$ .

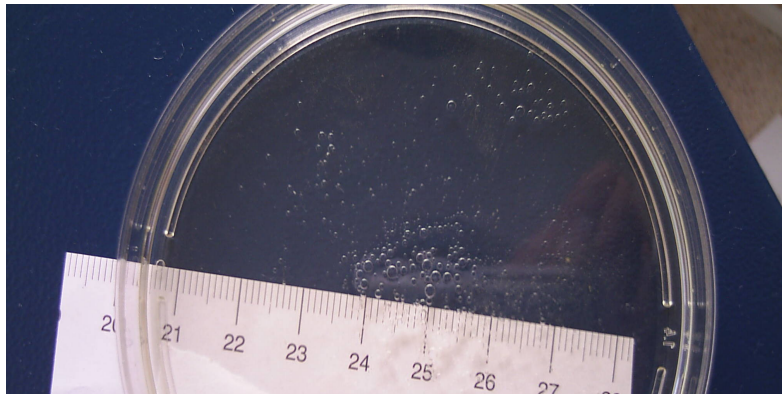


**Figure B-11.** AL01 (0.040 mm orifice) nozzle spray pattern with  $2.5 \text{ dm}^3 \text{ min}^{-1}$ ,  $\text{N}_2$  flow at 3 – 4 cm from nozzle aperture and fuel flow of  $500 \text{ ml hr}^{-1}$ .

In terms of spray achieved at lower atomising gas flow, the smaller aperture AL01 nozzle therefore performed better in these tests. This nozzle would permit a smaller ratio of carrier gas to fuel input resulting in a syngas greatly enriched with  $\text{H}_2$  by

comparison to the AL04 nozzle. With the lowest possible atomising gas flow for the AL01 nozzle of  $1.5 \text{ dm}^3 \text{ min}^{-1}$  this would, with a  $200 \text{ ml hr}^{-1}$  fuel feed rate, give a syngas dilution value of 28 %.

With such a lower dilution, a greater quantity of  $\text{H}_2$  in the syngas should be produced. This is not necessarily an improvement on the 63 % and 84 % dilution used in the Chapter 5 and Chapter 6 experimentation, since these carrier gas flow rates were required only for analytical purposes via online systems and material balance calculations. Both designs are therefore considered to have great flexibility for diluent range when used in practical applications. Though the spray system requires gas flow for atomisation, whereas the glass reactor system does not, the spray system could in theory be operated by a similar drop feed and therefore the carrier gas flow rate considerations made superfluous. Whether this may be possible would depend on the ability of the reactor to cope with the energy demands of both the steam reforming reactions and overcoming the latent heat phase transitions of water and urea as discussed in Chapter 3. Obviously, a period of experimentation with the system to establish optimised conditions for steady state operation is an area for future work. This was not possible as the system was made unavailable for further use once its construction was complete. The component having greatest novelty – the nichrome wire designed to act as both heating element and catalyst – still remains to be tested and assessed for efficacy.

With both nozzle types tested, no blockages occurred when using urea solution. This may not hold however when operating at steam reforming temperatures, with the preferred smaller aperture nozzle more likely to block. As has been shown previously with the quartz reactor the preservation of the aqueous urea at low temperature prior to reactor entry is a crucial consideration in using urea solution as a fuel due to its propensity for supersaturation above  $100 \text{ }^\circ\text{C}$ . The design of the spray reactor nozzle system with cooling  $\text{N}_2$  carrier gas flow mixed with fuel prior to release onto the monolith chamber was chosen to avoid crystal precipitation. The relatively high carrier gas flows required by these nozzles for atomisation, would accentuate the cooling effect and potentially decrease the risk of system failure from precipitate blockages. In addition to the experimentation for optimised operation of this reactor for actual steam reforming, computational fluid dynamics to model the reaction dynamics and kinetics of the spray system in comparison to a droplet fed system is an area for future work.

## **B.5 Conclusions**

A novel steam reforming spray reactor electrically powered and heated by catalytic nichrome wire was designed and fabricated. The full spray reactor system was tested and found to maintain integrity at  $\leq 10 \text{ bar}$  and  $\leq 700 \text{ }^\circ\text{C}$  for five hours, at which time

the test was ceased with the system still fully functional and gas tight. The reactor was able to be heated rapidly, within 1 minute, using low  $\leq 36$  Watts power, and  $\leq 5$  amps of current. The reactor was encased in stainless steel and heat losses from the casing body were minimised by the application of kaowool.

A gas-flow spray system was incorporated to supply the fuel at varying states of atomisation dependent on gas flow rate and to a lesser extent, fuel feed rate. The carrier gas was mixed with fuel within the nozzle to generate atomisation in the form of a conical spray pattern between  $2 \leq \text{cm} \leq 5$  beyond the nozzle aperture, this being the desired distance between nozzle aperture and reactor surface. The carrier gas flow would also cool the fuel prior to its rapid entry to the reactor, thereby reducing the propensity for urea solution to supersaturate and cause precipitate blockages. A reflux condensate trap and two-stage oil-filled condenser system was incorporated post-reactor, with an online non-destructive  $\text{NH}_3$  analyser,  $\text{NH}_3$  trap and online micro GC to monitor syngas composition.

Though all the components were seen to work independently as planned, the system remains to be tested for its overall ability to steam reform urea. In comparison with the previously successful quartz fixed-bed catalytic flow reactor system discussed in Chapters 5 and 6, the spray reactor is considered to have the advantage of being more sturdy and compact; aspects that make it attractive for both for scale-up and applications involving mobile and remote energy production to which it is envisaged that urea could hold great benefits as a hydrogen carrier. Possible problems that may be encountered with this reactor involve feed-line blockages due to urea fuel crystallisation if very small nozzle apertures are chosen. Flexibility of design allows different nozzles be inserted to overcome this issue, though increasing nozzle aperture size necessitates an increased atomising gas flow and therefore greater syngas dilution. This would not be a problem if the reactor were operated as a drop-feed, rather than spray, fuel inlet system. A determination of this could be made by future work involving steam reforming experimentation with the reactor and computational fluid dynamics at a range of spray parameters.

The main novelty of this new reactor was the dual functioning nichrome wire, designed to function as both heating element and catalyst. Though its efficacy for heating was shown, its ability to function as catalyst for steam reforming of urea was not tested. This is an area for future work.



## References

- [1] *Intergovernmental Panel on Climate Change. Climate Change 2007: Synthesis Report. Contribution of Working Groups I, II and III to the Fourth Assessment Report of the Intergovernmental Panel on Climate Change.* Geneva: IPCC, 2007, pp.104.
- [2] Stern, N. *Stern review on the economics of climate change* [online]. 2006 [Accessed 6<sup>th</sup> June 2007]. Available from: [http://www.hm-treasury.gov.uk/independent\\_reviews/stern\\_review\\_economics\\_climate\\_change/stern\\_review\\_report.cfm](http://www.hm-treasury.gov.uk/independent_reviews/stern_review_economics_climate_change/stern_review_report.cfm)
- [3] U.S. Environmental Protection Agency. *Future atmospheric changes in Greenhouse gas and aerosol concentrations* [online]. 2010 [Accessed 19<sup>th</sup> November 2010]. Available from: <http://www.epa.gov/climatechange/science/futureac.html>
- [4] International Energy Agency. *World Energy Outlook 2009.* Paris: IEA, 2009, p.696.
- [5] Rand, D.A.J., Dell, R.M. *Hydrogen energy, challenges and prospects.* Cambridge: RSC Publishing, 2008, pp.146-178.
- [6] Winter, C-J. Hydrogen energy – Abundant, efficient, clean: A debate over the energy-system-of-change. *International Journal of Hydrogen Energy*, **34** (14) Supplement 1, 2009, S1-S52.
- [7] Satyapal, S., Petrovic, J., Read, C., Thomas, G., Ordaz, G. The U.S Department of Energy's national hydrogen storage project: progress towards meeting hydrogen-powered vehicle requirements. *Catalysis Today*. 2007: **120**, pp.246-256.
- [8] *Explanations of FreedomCAR/DOE hydrogen storage technical targets* [online]. 2006 [Accessed 20<sup>th</sup> August 2008]. Available from: [http://www1.eere.energy.gov/hydrogenandfuelcells/pdfs/freedomcar\\_targets\\_explanations.pdf](http://www1.eere.energy.gov/hydrogenandfuelcells/pdfs/freedomcar_targets_explanations.pdf)
- [9] Navarro, R.M.; Peña, M.A.; Fierro, J.L.G. Hydrogen Production Reactions from Carbon Feedstocks: Fossil Fuels and Biomass. *Chemical Reviews*. 2007: **107**, pp.3952-3991.

[10] Barelli, L., Bidini, G., Gallorini, F., Servili, S., Hydrogen production through sorption-enhanced steam methane reforming and membrane technology: a review. 2008: *Energy*, **33**, pp.554-570.

[11] Ahmed, S., Krumpelt, M. Hydrogen from hydrocarbon fuels for fuel cells. *International Journal of Hydrogen Energy*, 2001: **26** (4), pp.291-301.

[12] Dou, B., Dupont, V., Rickett, G., Blakeman, N., Williams, P., Chen, H., Ding, Y., Ghadiri, M. Hydrogen production by sorption-enhanced steam reforming of glycerol. *Bioresource Technology*, 2009: **100** (14), pp.3540-3547.

[13] Lyon, R.K., Cole, J.A. Unmixed Combustion: An Alternative to Fire. *Combustion and Flame*: **108**, pp.249-261.

[14] Dupont, V., Ross, A.B., Knight, E., Hanley, I., Twigg, M.V. Production of hydrogen by unmixed steam reforming of methane. *Chemical Engineering Science*, 2008: **63** (11), pp.2966-2979.

[15] Ferng, Y.M., Tzang, Y.C., Pei, B.S, Sun, C.C., Su, A. Analytical and experimental investigations of a proton exchange membrane fuel cell. *International Journal of Hydrogen Energy*, 2004: **29** (4), pp.381-391.

[16] Ralph, T.R., Hogarth, M.P. Catalysis for low temperature fuel cells. Part II: the anode challenges. *Platinum Metals Review*, 2002: **46** (3), pp.117-135.

[17] David, E. An overview of advanced materials for hydrogen storage. *Journal of Materials Processing Technology*, 2005: **162-163**, pp.169-177.

[18] Hirscher, M., Becher, M., Haluska, M., von Zeppelin, F., Chen, X., Dettlaff-Weglikowska, U., Roth, S. Are carbon nanostructures an efficient hydrogen storage medium? *Journal of Alloys and Compounds*, 2003: **356-357**, pp.433-437.

[19] Vitillo, J.G., Ricchiardi, G., Spoto, G., Zecchina, A., Theoretical maximal storage of hydrogen in zeolitic frameworks. *Physical Chemistry Chemical Physics*, 2005: **7**, pp.3948-3954.

[20] Dincă, M., Long, J.R. Hydrogen storage in microporous metal-organic frameworks with exposed metal sites. *Angewandte Chemie International*, 2008: **47** (36), pp.6766-6779.

[21] Gallucci, F., Basile, A., Drioli, E. Methanol as an energy source and/or energy carrier in membrane processes. *Separation & Purification Reviews*, 2007, **36** (2), pp.175-202.

[22] Hamelink, C.N., Faaij, A.P.C. Future prospects for production of methanol and hydrogen from biomass. *Journal of Power Sources*, 2002: **111** (1), pp.1-22.

[23] Geissler, K., Newson, E., Vogel, F., Truong, T-B., Hottinger, P., Wokaun, A. Autothermal methanol reforming for hydrogen production in fuel cell applications. *Physical Chemistry Chemical Physics*, 2001: **3** (3), pp.289-293.

[24] Righelato, R., Spracklen, D.V. Carbon mitigation by biofuels or by saving and restoring forests. *Science*, 2007: **317** (5840), p.902.

[25] Ni, M., Leung, D.Y.C., Leung, M.K.H. A review on reforming bio-ethanol for hydrogen production. *International Journal of Hydrogen Energy*, 2007: **32** (15), pp.3238-3247.

[26] Vaidya, P.D., Rodrigues, A.E. Insight into steam reforming of ethanol to produce hydrogen for fuel cells. *Chemical Engineering Journal*, 2006: **117** (1), pp.39-49.

[27] Biniwale, R.B., Rayalu, S., Devotta, S., Ichikawa, M. Chemical hydrides: a solution to high capacity hydrogen storage and supply. *International Journal of Hydrogen Energy*, 2008: **33** (1), pp.360-365.

[28] Asazawa, K., Yamada, K., Tanaka, H., Oka, A., Taniguchi, M., Kobayashi, T. A platinum-free zero-carbon-emission easy fuelling direct hydrazine fuel cell for vehicles. *Angewandte Chemie*, 2007: **46** (42), pp.8024-8027.

[29] Christensen, C.H., Johannessen, T., Sørensen, R.Z., Nørskov, J.K. Towards an ammonia-mediated hydrogen economy? *Catalysis Today*, 2006: **111** (1-2), pp.140-144.

[30] Thomas, G., Parks, G. *Potential roles of ammonia in a hydrogen economy: a study of issues related to the use of ammonia for on-board vehicular hydrogen storage*. Washington DC: U.S. Department of Energy, 2006.

[31] Zamfirescu, C., Dincer, I. Using ammonia as a sustainable fuel. *Journal of Power Sources*, 2008: **185** (1), pp.459-465.

[32] Gay, S.E., Ehsani, M. Ammonia hydrogen carrier for fuel cell based transportation. *S.A.E International Special Publication*, 2003: **112** (3), pp.1748-1773.

[33] Klerke, A., Christensen, C.H., Nørskov, J.K., Vegge, T. Ammonia for hydrogen storage: challenges and opportunities. *Journal of Materials Chemistry*, 2008: **18**, pp.2304-2310.

[34] Fournier, G.G.M., Cumming, I.W., Hellgardt, K. High performance direct ammonia solid oxide fuel cell. *Journal of Power Sources*, 2006: **162** (1), pp.198-206.

[35] Hejze, T., Besenhard, J.O., Kordesch, K., Cifrain, M., Aronsson, R.R. Current status of combined systems using alkaline fuel cells and ammonia as a hydrogen carrier. *Journal of Power Sources*, 2008: **176** (2), pp.490-493.

[36] Halseid, R., Vie, P.J.S., Tunold, R. Effect of Ammonia on the Performance of Polymer Electrolyte Membrane Fuel Cells. *Journal of Power Sources*, 2006: **154** (2), pp.343-350.

[37] Halseid, R., Heinen, M., Jusys, Z., Behm, R.J. The effect of ammonium ions on oxygen reduction and hydrogen peroxide formation on polycrystalline Pt electrodes. *Journal of Power Sources*, 2008: **176** (2), pp.435-443.

[38] Sørensen, R.Z., Hummelshøj, J.S., Klerke, A., Reves, J.B., Vegge, T., Nørskov, J.K., Christensen, C.H. Indirect, reversible high-density hydrogen storage in compact metal ammine salts. *Journal of the American Chemical Society*, 2008: **130** (27), pp.8660-8668.

[39] Barney, B.M., Lee, H-I., Dos Santos, P.C., Hoffman, B.M., Dean, D.R., Seefeldt, L.C. Breaking the N<sub>2</sub> triple bond: insights into the nitrogenase mechanism. *Dalton Transactions*, 2006: **19**, pp.2277-2284.

[40] International Programme on Chemical Safety ICIS [online]. [accessed 26<sup>th</sup> October 2010]:

Urea [1997]. Available from:

<http://www.inchem.org/documents/icsc/icsc/eics0595.htm>

Ethanol [2000]. Available from:

<http://www.inchem.org/documents/icsc/icsc/eics0044.htm>

Methanol [2000]. Available from;

<http://www.inchem.org/documents/icsc/icsc/eics0057.html>

Ammonia [1998]. Available from:

<http://www.inchem.org/documents/icsc/icsc/eics0215.htm>

Methylcyclohexane [1997]. Available from:

<http://www.inchem.org/documents/icsc/icsc/eics0923.htm>

Hydrazine [1995]. Available from:

<http://www.inchem.org/documents/icsc/icsc/eics0281.htm>

Cyclohexane [2008]. Available from:

<http://www.inchem.org/documents/icsc/icsc/eics0242.htm>

[41] Kurzer, F., and Sanderson, P.M. Urea in the History of Organic Chemistry. *Journal of Chemical Education*, 1956: **33** (9), pp.452-459.

[42] Werner, E.A. *The chemistry of urea*. Longmans, Green, & Co: London, 1923.

[43] Cohen, P.S., Cohen, S.M. Wöhler's synthesis of urea: how do the textbooks report it? *Journal of Chemical Education*, 1996: **73** (9), pp.883-886.

[44] Shorter, J. The conversion of ammonium cyanate into urea – a saga in reaction mechanisms. *Chemical Society Review*, 1978: **7**, pp.1-14.

[45] Dunitz, J.D., Harris, K.D.M., Johnston, R.L., Kariuki, B.M., MacLean, E.J., Psallidas, K., Schweizer, W.B., Tykwinski, R.R. New light on an old story: the solid-state transformation of ammonium cyanate into urea. *Journal of the American Chemical Society*, 1998: **120** (50), pp.13274-13275.

[46] MacLean, E.J., Harris, K.D.M., Kariuki, B.M., Kitchen, S.J., Tykwinski, R.R., Swainson, I.P., Dunitz, J.D. Ammonium cyanate shows N–H•••N hydrogen bonding, not N–H•••O. *Journal of the American Chemical Society*, 2003: **125** (47), pp.14449-14451.

[47] Kroschowitz, J.I. (ed). *Kirk-Othmer encyclopedia of chemical technology*, 4<sup>th</sup> ed: **13**, New York, Chichester: John Wiley & Sons Ltd. 1998. pp.838 -894.

[48] Schaber, P.M., Colson, J., Higgins, S., Thielen, D., Anspach, B., Brauer, J. Thermal decomposition (pyrolysis) of urea in an open reaction vessel. *Thermochimica Acta*, 2004: **424** (1), pp.131-142.

[49] Meessen, J., and Petersen, H. Urea. *In: Elvers, B., and Hawkins, S., (eds). Ullman's encyclopedia of industrial chemistry. 5<sup>th</sup> edn. A27 thorium and thorium compounds to vitamins.* Weinheim: VCH, 1996. pp.333-365.

[50] Singer, M.A. Do mammals, birds, reptiles and fish have similar nitrogen conserving systems? *Comparative Biochemistry and Physiology Part B*, 2003: **134**, pp.543-558.

[51] Thirkildsen, M.S., King, G.M., Lomstein, B.A. Urea production and turnover following the addition of AMP, CMP, RNA and a protein mixture to a marine sediment. *Aquatic Microbial Ecology*, 1996: **10**, pp.173-179.

[52] Chadwick, T.D., Wright, P.A. Nitrogen excretion and expression of urea cycle enzymes in the Atlantic cod (*Gadus morhua* L.): a comparison of early life stages with adults. *Journal of Experimental Biology*, 1999: **19**, pp.2653–2662.

[53] Walsh, P.J., Heitz, M.J., Campbell, C.E., Cooper, G., Medina, M., Wang, Y., Goss, G., Vincek, V., Wood, C. and Smith, C. Molecular characterization of a urea transporter in the gill of the Gulf Toadfish (*Opsanus beta*). *Journal of Experimental Biology*, 2000: **203** (15), pp.2357–2364.

[54] Vogels, G.D., Van Der Drift, C. Degradation of purines and pyrimidines by microorganisms. *Bacteriological Reviews*, 1976: **40** (2), pp.403-468.

[55] Kojima, S., Bohner, A., Von Wirén, N. Molecular mechanism of urea transport in plants. *Journal of Membrane Biology*, 2006: **212**, pp.83-91.

[56] Alexandrova, A.N., Jorgensen, W.L. Why urea eliminates ammonia rather than hydrolyzes in aqueous solution. *Journal of Physical Chemistry B*, 2007: **111** (4), pp.720-730.

[57] Carp, O. Considerations on the thermal decomposition of urea. *Revue Roumaine de Chimie*, 2001: **46** (7), pp.735-740.

[58] Jacox, M.E., Milligan, D.E. Low-temperature infrared study and intermediates in the photolysis of HNCO and DNCO. *The Journal of Chemical Physics*, 1964: **40** (9), pp.2457-2460.

[59] Bogan, D.J., Hand, C.W. Mass spectrum of isocyanic acid. *The Journal of Physical Chemistry*, 1971: **75** (10), pp.1532-1536.

[60] SciFinder Scholar. RN 57-13-6 (urea); RN 108-19-0 (biuret); RN 556-99-0 (triuret); RN 645-93-2 (ammelide); RN 645-92-1 (ammelina); RN 108-78-1 (melamine); RN 75-13-8 (isocyanic acid); RN 420-05-3 (cyanic acid); RN 108-80-5 (cyanuric acid); RN 1111-78-0 (ammonium carbamate); RN 22981-32-4 (ammonium cyanate). Columbus: Chemical Abstracts Service, 2010.

[61] Stradella, L., Argentero, M. A study of the thermal decomposition of urea, of related compounds and thiourea using DSC and TG-EGA. *Thermochimica Acta*, 1993: **219** (1-2), pp.315-323.

[62] Birkhold, F., Meingast, U., Wassermann, P., Deutschmann, O. Modeling and simulation of the injection of urea-water-solution for automotive SCR DeNO<sub>x</sub>-systems. *Applied Catalysis B:Environmental*, 2007: **70** (1-4), pp.119-127.

[63] Thagard, S.M., Mihalcioiu, A., Takashima, K., and Mizuno, A. Analysis of the By-Products in the Ammonia Production From Urea by Dielectric Barrier Discharge. *IEEE Transactions on Plasma Science*, 2009: **37** (3), pp.444-448.

[64] Elkanzi, E.M. The effect of side reactions on urea production. *Research and Industry*, 1991: **36** (4), pp.254-259.

[65] Zanoelo, E.F. A lumped model for thermal decomposition of urea. Uncertainties analysis and selective non-catalytic reduction of NO. *Chemical Engineering Science*, 2009: **64**, pp.1075-1084.

[66] Mahilik, K., Sahu, J.N., Patwardhan, A.V., Meikap, B.C. Kinetic studies of urea in a semi-batch reactor at atmospheric pressure for safe use of ammonia in a power plant for flue gas conditioning. *Journal of Hazardous Materials*, 2010: **175**, pp.629-637

[67] Lundström, A., Andersson, B., Olsson, L. Urea thermolysis studied under flow reactor conditions using DSC and FT-IR. *Chemical Engineering Journal*, 2009: **150** (2-3), pp.544-550.

[68] Koebel, M., Strutz, E.O. Thermal and hydrolytic decomposition of urea for automotive selective catalytic reduction systems: thermochemical and practical aspects. *Industrial and Engineering Chemistry Research*, 2003: **42** (10), pp.2093-2100.

[69] Yim, S.D., Kim, S.J., Biak, J.H., Nam, I-S., Mok, Y.S., Lee, J-H., Cho, B.K., Oh, S.H. Decomposition of urea into  $\text{NH}_3$  for the SCR process. *Industrial and Engineering Chemistry Research*, 2004: **43** (16), pp.4856-4863.

[70] Kleemann, M., Elsener, M., Koebel, M., Wokaun, A. Hydrolysis of isocyanic acid on SCR catalysts. *Industrial and Engineering Chemistry Research*, 2000: **39** (11), pp.4120-4126.

[71] Yang, W., Chen, Z., Zhou, J., Huang, Z., Cen, K. Catalytic performance of zeolites on urea thermolysis and isocyanic acid hydrolysis. *Industrial and Engineering Chemistry Research*, 2011: **50** (13), pp.7990-7997.

[72] Kröcher, O., Elsener, M. Materials for thermohydrolysis of urea in a fluidised bed. *Chemical Engineering Journal*, 2009: **152** (1), pp.167-176.

[73] Keuleers, R., Desseyn, H.O., Rousseau, B., Van Alsenoy, C. Vibrational analysis of urea. *The Journal of Physical Chemistry A*, 1999: **103** (24), pp.4621-4630.

[74] Koebel, M., Elsener, M., Kleemann, M. Urea-SCR: a promising technique to reduce  $\text{NO}_x$  emissions from automotive diesel engines. *Catalysis Today*, 2000: **59** (3-4), pp.335-345.

[75] Callahan, B.P., Yuan, Y., Wolfenden, R. The burden borne by urease. *Journal of the American Chemical Society*, 2003: **127** (31), pp.10828-10829.

[76] Estiu, G., Mertz, K.M. The hydrolysis of urea and the proficiency of urease. *Journal of the American Chemical Society*, 2004: **126** (22), pp.6932-6944.

[77] Stumpe, M.C., Grubmüller, H. Aqueous urea solutions: structure, energetics, and urea aggregation. *Journal of Physical Chemistry B*, 2007: **111** (22), pp.6220-6228.



[78] Couch, H.T., Birbara, P.J., Grin, W. Steam gasification and reformation of spacecraft wastes. *SAE Transactions*, 1997: **106** (1), pp.467-477.

[79] Boggs, B.K.; King, R.L.; Botte, G.G. Urea electrolysis: direct hydrogen production from urine. *Chemical Communications*, 2009: **32**, pp.4859-4861.

[80] Lan, R., Tao, S., Irvine, T.S. A direct urea fuel cell – power from fertiliser and waste. *Energy and Environmental Science*, 2010: **3**, pp.438-441.

[81] Rahimpour, M.R., Mottaghi, H.R., Barmaki, M.M. Hydrogen production from urea wastewater using a combination of urea thermal hydrolyser-desorber loop and a hydrogen-permaselective membrane reactor. *Fuel Processing Technology*, 2010: **91** (6), pp.600-612.

[82] Hamidipour, M. Modelling the synthesis section of an industrial urea plant. *Chemical Engineering Journal*, 2005: **106** (3), pp.249-260.

[83] European Fertilizer Manufacturers Association. *Best available techniques for pollution prevention and control in the European fertilizer industry. Booklet No 5 of 8. Production of urea and urea ammonium*. Brussels: European Fertilizer Manufacturer's Association, 2000.

[84] Fable, S; Kamakaté, F; Venkatesh, S. *Selective catalytic reduction urea infrastructure study 2002. NREL/SR-540-32689*. California: National Renewable Energy Laboratory, 2002.

[85] Prud'homme, M., and Heffer, P. International Fertilizer Industry Association 78<sup>th</sup> annual conference, Paris (France) 31st May – 2<sup>nd</sup> June 2010. *Fertilizer Outlook 2010-2014*. Paris: IFA 2010.

[86] Aholou, C. *Re: United Kingdom IFA question*, 10<sup>th</sup> July 2008 [Accessed 10<sup>th</sup> July 2008]. Message to Andrew Rollinson. Personal communication.

[87] Smil V. Detonator of the population explosion. *Nature*, 1999: **400**, p.415.

[88] European Fertilizer Manufacturers Association. *European Fertilizer Manufacturers Association. World nitrogen fertilizer consumption by product 2006* [online]. 2008 [Accessed 28<sup>th</sup> August 2008]. Available from:

[http://cms.efma.org/EPUB/easnet.dll/ExecReq/Page?eas:template\\_im=00105B&eas:dat\\_im=00105B](http://cms.efma.org/EPUB/easnet.dll/ExecReq/Page?eas:template_im=00105B&eas:dat_im=00105B)

[89] Salanta, G., Zheng, G., Kotrba, A., Rampazzo, R. Optimization of a urea SCR system for on-highway truck applications. *SAE International Technical Papers*, 2010: p.2010-01-1938.

[90] Akhavan, J. *The chemistry of explosives*. Cambridge: Royal Society of Chemistry, 2004, pp.149-164.

[91] Fredriksson, T. Urea creams in the treatment of dry skin and hand dermatitis. *International Journal of Dermatology*, 1975: **14** (6), pp.442-444.

[92] Campuzano-Maya, G. An optimized <sup>13</sup>C-urea breath test for the diagnosis of H pylori infection. *World Journal of Gastroenterology*, 2007: **13** (41), pp.5454-5464.

[93] Leng, R.A., Preston, T.R., Sansoucy, R. Kunju, G.P.J. Multinutrient blocks as a strategic supplement for ruminants. *World Animal Review*, 1991: **67**, pp.11-19.

[94] Pizzi, A. *Advanced wood adhesives technology*. New York: Marcel Decker, 1994.

[95] Thorén, A-K., Legrand, C., Hermann, J. Transport and transformation of de-icing urea from airport runways in a constructed wetland system. *Water Science and Technology*, 2003: **48** (5), pp.283-290.

[96] Salvador, A., and Chisvert, A. *Analysis of cosmetic products*. Amsterdam: Elsevier, Amsterdam, 2007.

[97] Dennis, A.S. *Weather modification by cloud seeding*. New York, London: Academic Press, 1980.

[98] Cote, A. (ed). *Fire protection handbook*. Quincy: National Fire Protection Association, 1997.

[99] Sulieman, M., MacDonald E., Rees JS., Newcombe RG., Addy M. Tooth bleaching by different concentrations of carbamide peroxide and hydrogen peroxide whitening strips: an in vitro study. *Journal of Esthetic and Restorative Dentistry*, 2006: **18** (2), pp.93-100.

[100] Moss, S.J. Carbamide and food – a review of the literature. *FDI World*, 1999: **3**, pp.9-14.

[101] Burdock, G.A. *Encyclopaedia of Food and Colour Additives*. V.3. London: CRC Press, 1997.

[102] Bragg, J.R., Prince, R.C., Harner, E. J., Atlas, R.M. Effectiveness of bioremediation for the Exxon Valdez oil spill. *Nature*, 1994: **368** (6470), pp.413-418.

[103] Pritchard, P.H., Costa, C.F. EPA's Alaska oil spill bioremediation project. Part 5. *Environmental Science and Technology*, 1991: **25** (3), pp.372-379.

[104] Bergueiro-López, J.R., Moreno-García-Luengo, S., Serra-Sociás, F., Fuertes-Pérez, A., Pérez-Navarro-Gómez, A., Morales-Correas, N., Domínguez-Laseca, F. Biodegradation of hydrocarbon residuals by biological activators in the presence of INIPOL EAP 22. *Spill Science & Technology Bulletin*, 1996: **3** (4), pp.273-276.

[105] Nash, M. ICIS pricing urea sample report [online]. 2010 [Accessed 26<sup>th</sup> October 2010]. Available from:

[http://www.icispricing.com/il\\_shared/Samples/SubPage76.asp](http://www.icispricing.com/il_shared/Samples/SubPage76.asp)

[106] United Nations Environment Programme. United Nations international register of potentially toxic chemicals organisation for co-operation and development screening dataset. Urea 57-13-6 [online]. 1994 [Accessed 16<sup>th</sup> July 2008]. Available from: [www.chem.unep.ch](http://www.chem.unep.ch)

[107] Miller, C.A., Glibert, P.M. Nitrogen excretion by the calanoid copepod *Acartia tonsa*: results of mesocosm experiments. *Journal of Plankton Research*, 1998: **20** (9), pp.1767-1780.

[108] Erisman, J.W., Bleeker, A., Galloway, J., Sutton, M.S., Reduced nitrogen in Ecology and the Environment. *Environmental Pollution*, 2007: **150**, pp.140-149.

[109] Glibert, P.M., Harrison, J., Heil, C., Seitzinger, S. Escalating worldwide use of urea – a global change contributing to coastal eutrophication. *Biogeochemistry*, 2006: **77**, pp.441-463.

[110] Howarth, R.W., Anderson, D., Cloern, J., Elfring, C., Hopkinson, C., Lapointe, B., Malone, T., Marcus, T., Marcus, N., McGlathery, K., Sharpley, A.,

Walker, D. Nutrient pollution of coastal rivers, bays, and seas, *Issues in Ecology*, 2000: **7**, pp.1-15.

[111] Galloway, J.N., Aber, J.D., Erisman, J.W., Seitzinger, S.P., Howarth, R.W., Cowling, E.B., Cosby, B.J. The nitrogen cascade. *Bioscience*, 2003: **53** (4). pp.341-356.

[112] Turley, C.M. *The distribution and biodegradation of urea in coastal waters*. Ph.D thesis, University of Wales, 1980.

[113] Macpherson, G. *Black's student medical dictionary*. London: A.C.Black. 2004. pp.647-648.

[114] Maurer, M., Muncke, J., Larsen, T.A. Technologies for Nitrogen recovery and reuse. In: Lens, P., Pol, L.H., Wilderer, P., Asano, T. (Eds). *Water Recycling and Resource Recovery in Industry*. London: IWA Publishing, 2002. pp.491-510.

[115] Maurer, M., Pronk, W., Larsen, T.A. Treatment processes for source-separated urine. *Water Research*, 2006: **40**, pp.3153-3166.

[116] Udert, K.M., Larsen, T.A., Biebow, M., Gujer, W. Urea hydrolysis and precipitation dynamics in a urine-collecting system. *Water Research*, 2003: **37**, pp.2571-2582.

[117] Nielsen, D.W. The method and system for treating waste matter from animals containing urea. International Patent. WO 2005/009925 A1. 3<sup>rd</sup> February 2005.

[118] Mobley, H.L.T., and Hausinger, R.P. Microbial ureases: significance, regulation, and molecular characterization. *Microbiological Reviews*, 1989: **53** (1). pp.85-108.

[119] Hellström, D., Johansson, E., Grennberg, K. Storage of human urine: acidification as a method to inhibit decomposition of urea. *Ecological Engineering*, 1999: **12**, pp.253-269.

[120] Hanæus, J., Hellstrom, D., Johanson, E. A study of urine separation in an ecological village in northern Sweden. *Water Science and Technology*, 1997: **35** (9), pp.153-160.

[121] Marsden, R.F., Thomassen, J.R., Vial, D., Binot, R.A. The proposal for the completely closed system in the Columbus Space Station. *Desalination*, 1991: **83** (1-3), pp.123-136.

[122] Pronk, W., Palmquist, H., Biebow, M., Boller, M. Nanofiltration for the separation of pharmaceuticals from nutrients in source-separated urine. *Water Research*, 2006: **40**, pp.1405-1412.

[123] Jenkinson, C.P., Grody, W.W., Cederbaum, S.D. Comparative properties of arginases. *Comparative Biochemistry and Physiology. Part B, Biochemistry & molecular biology*, **114** (1), p.107-132, May 1996.

[124] Meijer, A.J., Lamers, W.H., Chamuleau, R.A.F.M. Nitrogen metabolism and ornithine cycle function. *Physiological Reviews*, 1990: **70**, pp.701-748.

[125] Cunin, R., Glansdorff, N., Pierard, A., Stalon, V. Biosynthesis and metabolism of arginine in bacteria. *Microbiological Reviews*, 1986: **50** (3), pp.314-352.

[126] Albanese, A.A., Irby, V., Frankston, J.E. The utilization of D-amino acids by man. III. Arginine. *Journal of Biological Chemistry*, 1945: **160**, pp.25-30.

[127] Allen, M.A., Weathers, P.J. Structure and composition of cyanophycin granules in the cyanobacterium *Aphanocapsa* 6308. *Journal of Bacteriology*, 1980: **141** (2), pp.959-962.

[128] Lawry, N.H., Simon, R.D. The normal and induced occurrence of cyanophycin inclusion bodies in several blue-green algae. *Journal of Phycology*, 1982: **18** (3), pp.391-399

[129] Krehenbrink, M., Oppermann-Sanio, FB., Steinbüchel, A. Evaluation of non-cyanobacterial genome sequences for occurrence of genes encoding proteins homologous to cyanophycin synthetase and cloning of an active cyanophycin synthetase from *Acinebacter* sp. Strain DSM587. *Archives of Microbiology*, 2002: **177** (5), pp.371-380.

[130] Elbahloul, Y., Frey, K., Sanders, J., Steinbüchel, A. Protamylasse, a residual compound of industrial starch production, provides a suitable medium for large-scale

cyanophycin production. *Applied and Environmental Biotechnology*, 2005: **71** (12), pp.7759-7767.

[131] Elbahloul, Y., Sanders, J.P.M., Scott, E.L., Weusthuis, R., Mooibroek, H., Obst, M., Steinbüchel, A. *Cyanophycin production from nitrogen containing chemicals obtained from biomass*. International patent. W02006093411. 8<sup>th</sup> September 2006.

[132] Sanders, J., Scott, E., Weusthuis, R., Mooibroek, H. Bio-refinery as the bio-inspired process to bulk chemicals. *Molecular Bioscience*, 2007: **7** (2), pp.105-117.

[133] Scott, E., Francisc, P., and Sanders, J. Biomass in the manufacture of industrial products – the use of proteins and amino acids. *Applied Microbiology and Biotechnology*, 2007: **75** (4), pp.751-762.

[134] Ikeda, T., Yasunaga, T. Kinetic behaviour of l-arginine in the interlamellar layer of montmorillonite in aqueous suspension. *Journal of Physical Chemistry*, 1984: **88** (6), pp.1253-1257.

[135] Lutz, A.E.; Rupley, F.M.; Kee, R.J. *EQUIL: a Program for Computing Chemical Equilibria*. *CHEMKIN Collection, Release 3.5*. Reaction Design, Inc: SanDiego, 1999; pp.2-20.

[136] Reynolds, W.C., *The Element Potential method for Chemical Equilibrium Analysis: Implementation in the Interactive Program STANJAN*. Department of Mechanical Engineering, Stanford University. 1986, pp.1-48.

[137] *NIST Chemistry WebBook* [online]. 2011 [Accessed 18<sup>th</sup> October 2011]. Available from:

<http://webbook.nist.gov/>

[138] Rock, P.A. *Chemical Thermodynamics*. California: Oxford University Press, 1983. pp.185-231.

[139] Burcat, A., Ruscic, B. *Third millennium ideal gas and condensed phase thermochemical database for combustion with updates from active thermochemical tables* [online]. Undated [Accessed 20<sup>th</sup> February 2009]. Available from: <http://garfield.chem.elte.hu/Burcat/THERM.DAT>

[140] Kim, S.; Shimpalee, J.W.; Van Zee, J.W. The effect of reservoirs and fuel dilution on the dynamic behaviour of a PEMFC. *Journal of Power Sources*, 2004: **137** (1): pp.43-52.

[141] Rollinson, A.N., Rickett, G.L., Dupont, V., Twigg, M.V. *Hydrogen Production by Catalytic Steam Reforming of Urea*. 5th International Ege Energy Symposium and Exhibition (IEESE-5): 27-30 June 2010, Pamukkale University, Denizli, Turkey.

[142] Baade, W.F., Parekh, U.N., Raman, V.S. *Hydrogen*. In: *Kirk-Othmer encyclopedia of chemical technology* [online]. 2001 [Accessed 18<sup>th</sup> July 2011]. Available from:  
<http://onlinelibrary.wiley.com/doi/10.1002/0471238961.0825041803262116.a01.pub2/full>

[143] Hagel, P., Gerding, J.J.T., Fieggen, W., Bloemendal, H. Cyanate formation in solutions of urea. I. Calculation of cyanate concentrations at different temperature and pH. *Biochimica et Biophysica Acta*, 1971: **243**, pp.366-373.

[144] Lin, M-F., Williams, C., Murray, M.V., Conn, G., Ropp, P.A. Ion chromatographic quantification of cyanate in urea solutions: estimation of the efficiency of cyanate scavengers for use in recombinant protein manufacturing. *Journal of Chromatography B*, 2004: **803** (2), pp.353-362

[145] Welles, H.L., Giaquinto, A.R., Lindstrom, R.E. Degradation of urea in concentrated aqueous solution, *Journal of Pharmaceutical Sciences*. 1971: **60** (8), pp.1212-1215.

[146] Saddawi, A., Jones, J.M., Williams, A., Wojtowicz, M.A. Kinetics of the thermal decomposition of biomass. *Energy and Fuels*, 2010: **24**, pp.1274-1282.

[147] Fischer, G., Geith, J., Klapötke, T.M., Krumm, B. Synthesis, properties and dimerization study of isocyanic acid. *Zeitschrift fur Naturforschung*, 2001: **57b**, pp.19-24.

[148] Pretsch, E., Bühlmann, P., Badertscher, M. *Structure Determination of Organic Compounds (4<sup>th</sup> ed)*. Berlin, Heidelberg: Springer-Verlag, 2009, pp.3-303.

[149] Herzberg, G., Reid, C. Infra-red spectrum and structure of the HNCO molecule. *Discussions of the Faraday Society*, 1950: **9**, pp.92-99.

[150] Maiella, P.G, Brill, T.B. Spectroscopy of hydrothermal reactions III: the water-gas reaction, “hot spots”, and formation of volatile salts of  $\text{NCO}^-$  from aqueous  $[\text{NH}_3(\text{CH}_2)_n\text{NH}_3]\text{NO}_3$  ( $n = 2, 3$ ) at 720 K and 276 bar by T-jump/FT-IR spectroscopy. *Applied Spectroscopy*, 1996: **50** (7), pp.829-835.

[151] Khandpour, R.S. *Handbook of Analytical Instruments*. New Dehli: Tata-McGraw-Hill, 2006, p.242.

[152] Twigg, M.V (ed). *Catalyst handbook (2<sup>nd</sup> ed)*. London: Manson, 1996, pp.17-282.

[153] Radojevic, M. 1999. *Practical Environmental Analysis*. Cambridge: Royal Society of Chemistry. p 219.

[154] Knight, E.H., *Optimisation of unmixed steam reforming*. PhD thesis, University of Leeds, 2009.

[155] Pimenidou, P., Rickett, G., Dupont, V., Twigg, M.V. Chemical looping reforming of waste cooking oil in a packed bed reactor. *Bioresource Technology*, 2010: **101** (16), pp.3540-3547.

[156] Brunauer, S., Emmett, P.H., Teller, E. Adsorption of gases in multimolecular layers. *Journal of the American Chemical Society*, 1938: **60** (2), pp.309-319.

[157] Medina, C.H. *Steam reforming of urea for hydrogen production*. M.Sc research project, University of Leeds, 2010.

[158] Anderson, J.R., Pratt, K.C. *Introduction to Characterization and Testing of Catalysts*. North Ryde: Academic Press Australia, 1985, pp.1-54.

[159] Lowell, S., Shields, J.E. *Power Surface Area and Porosity (2<sup>nd</sup> ed)*. Bristol: J.W.Arrowsmith Ltd, 1984, pp. 54-71.

[160] Wefers, K., Misra, C. *Oxides and Hydroxides of Aluminum, Alcoa Technical Paper Number 19, Revised*. Alcoa Laboratories, 1987, pp.1-19.



[161] International Centre for Diffraction Data. *Power Diffraction File: 00-010-0173 (Alumin), 00-044-1159 (Nickel oxide), 00-047-1049 (Nickel oxide), 00-004-0850 (Nickel)* [online]. 2010 [Accessed 12th June 2010]. Available from:

[www.icdd.com](http://www.icdd.com)

[162] Medina, F., Salagre, P., Sueires, J.E. Characterisation and catalytic properties of several potassium-doped iron-nickel catalysts. *Applied Catalysis A: General*, 1992: **92** (2), pp.131-141.

[163] Ahmad, A. *Characterisation of spray distribution from hollow cone swirl nozzles*. M.Sc research project, University of Leeds, 1993.